INFORMATION TO USERS

This manuscript has been reproduced from the microfilm master. UMI films the text directly from the original or copy submitted. Thus, some thesis and dissertation copies are in typewriter face, while others may be from any type of computer printer.

The quality of this reproduction is dependent upon the quality of the copy submitted. Broken or indistinct print, colored or poor quality illustrations and photographs, print bleedthrough, substandard margins, and improper alignment can adversely affect reproduction.

In the unlikely event that the author did not send UMI a complete manuscript and there are missing pages, these will be noted. Also, if unauthorized copyright material had to be removed, a note will indicate the deletion.

Oversize materials (e.g., maps, drawings, charts) are reproduced by sectioning the original, beginning at the upper left-hand corner and continuing from left to right in equal sections with small overlaps. Each original is also photographed in one exposure and is included in reduced form at the back of the book.

Photographs included in the original manuscript have been reproduced xerographically in this copy. Higher quality 6" x 9" black and white photographic prints are available for any photographs or illustrations appearing in this copy for an additional charge. Contact UMI directly to order.

UMI

A Bell & Howell Information Company
300 North Zeeb Road, Ann Arbor MI 48106-1346 USA
313/761-4700 800/521-0600

A STANDARD MATERIAL FOR LIBERATION ANALYSES AND EXAMINATION OF THE ROBUSTNESS OF STEREOLOGICAL CORRECTION PROCEDURES

David Lin

A thesis submitted to the
Faculty of Graduate Studies and Research
in partial fulfilment of the requirements
for the degree of Doctor of Philosophy

Department of Mining and Metallurgical Engineering
McGill University, Montreal
February, 1997

ABSTRACT

In this work, an artificial standard material was developed and used to examine the robustness of various different stereological correction procedures. The four correction procedures that were examined were: large-sections correction, Hill's fast approximation, Barbery's correction and PARGEN correction.

There were three steps to this work:

1) refinement of the standard material - certain modifications were made to make the standard material (developed as an M.Eng. project) more versatile and easier to use.
2) sectioning and correction of computer-generated spheres - different liberation distributions of single-capped spheres were computer-generated and sectioned. The four correction procedures were used to correct the stereological bias in the sectioning data. The corrected liberation distributions were compared with the true liberation distributions.
3) sectioning and correction of standard material particles - the standard material was used to re-create the same distributions that were computer-generated. The particles were mounted, sectioned and the sectioning data measured with an electron microscope and image analyzer. The data were corrected using the correction procedures and the corrected and true distributions were compared.

A two-phase (glass/lead borate) standard material was successfully developed. This standard material can be made to exhibit granular, layered or simple locking.

The correction of the sectioning of the computer-generated spheres and standard material particles yielded similar observations about the different correction procedures.

The large-sections correction provided a simple, uncorrupted correction. It performed better in the sphere cases than in the standard material cases.

Hill's fast approximation performed well except in the cases of narrow liberation distributions. The sectioning data of the standard material cases appeared to support the

assumption in this correction that the locked section and locked particle distributions are identical.

Barbery's correction performed better in the standard material cases than in the sphere cases. The correction had problems in situations where an incomplete beta function could not be fitted to the true liberation distribution.

The PARGEN correction was able to provide a good estimate of the true amount of free material, but it had difficulty estimating the locked particle distribution.

RÉSUMÉ

Dans cette étude, un matériau artificiel a été développé et utilisé afin d'examiner la robustesse de différentes procédures de correction stéréologique. Les quatre procédures de correction qui ont été examinées étaient: la correction à larges sections, l'approximation rapide de Hill, la correction de Barbery et la correction PARGEN.

Les trois étapes de ce travail étaient:

1) Le raffinement du matériau standard - certaines modifications ont été faites afin de rendre le matériau standard (développé comme projet de M.Eng) plus versatile et facile à utiliser.

2) Le sectionnement et la correction de sphères générées par ordinateur - différentes distributions de libération de sphères à simple recouvrement ont été générées par ordinateur et sectionnées. Les quatre procédures de correction ont été utilisées afin de corriger le biais stéréologique dans les données de sectionnement. Les distributions de libération corrigées ont été comparées avec les véritables distributions de libération.

3) Le sectionnement et la correction des particules de matériau standard - le matériau standard a été utilisé pour recréer les mêmes distributions que celles générées par ordinateur. Les particules ont été assemblées, sectionnées et l'information sur le sectionnement mesurée à l'aide d'un microscope électronique et d'un analyseur d'image. Les données ont été corrigées en utilisant les procédures de correction et les distributions corrigées et véritables ont été comparées.

Un matériau standard à deux phases (verre, borate de plomb) a été développé avec succès. Ce matériau standard peut être fabriqué afin d'exhiber un emprisonnement granulaire, étagé et simple.

La correction du sectionnement des sphères générées par ordinateur et des particules de matériau standard a produit des observations similaires au sujet des différentes procédures de correction.

Les corrections à larges sections ont permis une correction simple et non-corrompue. La performance a été supérieure dans les cas des sphères que dans les cas du matériau standard.

L'approximation rapide de Hill a donné de bons résultats à l'exception des cas de distributions de libération étroite. Les données du sectionnement du matériau standard ont semblé supporter l'hypothèse de cette correction que la section emprisonnée et les distributions de particules emprisonnées sont identiques.

La correction de Barbery s'est mieux comportée dans les cas du matériau standard que dans les cas des sphères. La correction a eu des problèmes dans les situations où une fonction beta incomplète n'a pu être ajustée à la véritable distribution de libération.

La correction PARGEN a pu fournir un bon estimé de la véritable quantité de matériau libre, mais a eu des difficultés à estimer la distribution de particules emprisonnées.

CONTRIBUTIONS TO ORIGINAL KNOWLEDGE

1) A method was developed (based on work performed in M.Eng. research) for the creation of a standard material (i.e. a material of known particle composition and locking characteristics) consisting of two phases: glass and lead borate. This standard material is quite versatile. Particles with granular and layered locking were created. Simple-locked particles were also successfully created. The standard material has many applications:

   i) It can be used to test the robustness of stereological correction procedures (as was done in this thesis).

   ii) Due to the strong bonding between the glass and lead borate, it can be used to assess the accuracy of so-called "size reduction" liberation models. These models attempt to predict liberation using the assumption that there is negligible breakage along the phase interfaces.

   iii) The standard material can be used as the basis for a stereological correction procedure. Composition fractions of the standard material can be sectioned to provide a series of kernel matrices for use in the correction of sectioning data.

2) The robustness of four stereological correction procedures, large-sections correction, Hill's fast approximation, Barbery's correction and PARGEN correction, was determined. These correction procedures were tested firstly, by applying them to the sectioning data of known liberation distributions of computer-generated, single-capped spheres and then applying them to the sectioning data of standard material particles having the same distributions. The distributions that were simulated ranged from those commonly encountered in mineral processing to very irregular ones.

3) A batch magnetogravimetric separator that permitted density separations of up to 5.0 g/ml was created. The separations are performed in a magnetic fluid which is subjected to a magnetic field supplied by a modified Frantz isodynamic magnetic separator. By varying the current to the Frantz, the magnetic fluid can be made to have different effective densities.

ACKNOWLEDGEMENTS

First and foremost, I wish to acknowledge the sure-handed guidance of my supervisor, Professor J.A. Finch. Without his help, support and enthusiasm, none of this would have been possible.

I would like to thank Dr. C.O. Gomez and Michel Leroux for their insight and help into my work. Thanks also to Prof. A.R. Laplante and other members of the mineral processing group for their useful advice and suggestions.

The liberation analyses of the standard material were performed by Dr. Rolando Lastra with the facilities at CANMET and his help in this matter is greatly appreciated.

The software programs POLYKING and BOOKING were developed at Laval University, Sainte-Foy, Québec, by Professor Gilles Barbery and graduate student Robin Pelletier through research funded by le Groupe de Recherche sur les Applications de l'Informatique à l'Industrie Minérale. They were loaned to McGill University by Laval University following a joint agreement between the respective departments of Mining and Metallurgical Engineering. The loan is gratefully acknowledged.

Thanks are also due to Professor R.P. King for the loan of the software program, Stereological Reconstruction of Linear and Areal Grade Distributions.

Funding for this research was provided by Inco Ltd. and the Natural Sciences and Engineering Research Council of Canada through the Inco-NSERC Chair in Mineral Processing and the Department of Energy, Mines and Resources, Canada.

TABLE OF CONTENTS

GLOSSARY

Backscattered electrons (BSE): Backscattered electrons are the result of elastic collisions between the electrons of an electron beam and the electrons of the sample. The yield of backscattered electrons is proportional to the average atomic number of the sample. Thus, an image based on backscattered electrons supplies compositional information about the sample.

Complexity (of the locking): the number of interfaces between the phases in a locked particle (see **simple locking** and **complex locking**).

Complex locking: locking such that there is more than one interface between the phases in a locked particle.

Composite particle: a locked particle.

Corrected (or reconstructed) liberation distribution: the liberation distribution that is obtained by applying a stereological correction procedure to the sectioned liberation distribution.

Diluent (or filler) material: particles of a material deliberately introduced into a sample (to be mounted in resin) to reduce the incidence of contact between the sample particles and to support the particles in space thus reducing preferential settling.

Dispersion density (dd): the number of grains per particle.

Energy dispersive spectroscopy (EDS) analysis: The interaction of an electron beam with a sample may cause an inner shell electron of a sample atom to be ejected. An outer shell electron will fill the vacancy resulting in the emission of an X-ray. Since the energy of such X-rays are characteristic of the atom from which it originated, the elements in the sample can be determined from X-ray energy spectra.

Exclusion criterion: The size (in terms of area) below which a section is excluded from a liberation analysis when the large-sections correction is applied.

False free section: a free section generated by a locked particle.

Free (or liberated) particle: a particle consisting of one phase only. (In reference to the production and separation of the standard material, the term, free particle, refers to a particle containing >5 or <95 vol. % of one phase while the term, true free particle, refers to a particle consisting of one phase only.)

Grain: a discrete feature in the (ore or particle) matrix.

Granular locking: locking such that one phase occurs as grains inside the other phase(s).

Halo: the variation in the grey level around the interfaces of features in an electron microscope image caused by the averaging of the signals in the interaction volume. Halos make phase boundaries difficult to discriminate.

Interaction volume: the part of the sample which produces signals when excited by an electron beam.

Kernel (or sectioning) matrix (or function): a matrix (or function) which characterizes the sectioning behaviour of locked particles in a given system by describing the sectioned (or observed) liberation distribution for all volumetric particle compositions.

Layered locking: locking such that the phases occur in layers parallel to each other.

Liberation: the phase composition of individual particles.

Liberation distribution: the amount (volume or mass) of material at each particle composition for a given phase.

Locked particle: a particle consisting of more than one phase.

Matrix: the material which surrounds the (mineral) grains before comminution.

Mounting medium: the material (usually resin) in which particles are embedded so that they can be sectioned and examined by microscope.

Particle: a fragment of material resulting from comminution.

Preferential breakage: the higher breakage rate of a given phase in an ore compared to the other phase(s).

Preferential orientation: if there are significant differences in density between the phases in the locked particles in a sample to be mounted for microscopic examination, then preferential orientation may occur. The locked particles may settle in the mounting

medium in one alignment (usually with the densest phase facing downwards). This may result in an unrepresentative polished surface.

Preferential settling: if there are significant differences in density between the particles in a sample to be mounted for microscopic examination, then preferential settling may occur. The denser particles will settle in the mounting medium to the bottom of the mold faster than the less dense particles. This may result in an unrepresentative polished surface.

Resolution: the ability of a microscope to accurately discriminate small features in a sample.

Secondary electrons (SE): Secondary electrons are the result of inelastic collisions between the electrons of an electron beam and weakly-bound electrons of the sample near the surface. An image based on secondary electrons supplies topographic information about the sample.

Sectioned (or observed) liberation distribution: the liberation distribution that is obtained from an examination of particle sections.

Silicate-containing borate: lead borate which has been in contact with glass in the furnace.

Simple locking: locking such that there is only one interface between the phases in a locked particle.

Single-capped sphere: a sphere exhibiting simple locking with a planar interface.

Standard material: a material of known particle composition and locking characteristics.

Stereological bias: a bias caused by the measurement of liberation using linear or areal sections. This bias creates an overestimation of free particles. It also affects locked particles since a given locked particle can produce a wide distribution of locked sections.

Stereological correction: a procedure devised to reduce or eliminate the stereological bias in liberation sectioning data; a procedure which transforms one- or two- dimensional sectioning data to three dimensions.

True free particle: see **free particle.**

True liberation distribution: the actual assemblage of particle compositions.

Wavelength dispersive spectroscopy (WDS): similar to **energy dispersive spectroscopy** except that the wavelength rather than the energy of the X-rays is measured. WDS provides more accurate quantitative information than EDS since there are fewer overlaps between the peaks.

LIST OF FIGURES

LIST OF TABLES

CHAPTER 1: INTRODUCTION

1.1 General introduction

The mineral composition of individual particles, or liberation, is an important variable in the physical processing of minerals. Liberation will determine how particles behave in subsequent separation stages. It is the distribution of the liberation of an ore that determines the ultimate separation that can be achieved. The main purpose of the comminution of the ore is to achieve a sufficient level of liberated particles so that the valuable mineral can be physically separated from the non-valuables. An insufficient amount of comminution may result in the production of many locked (composite) particles which would result in a poor grade in the final product(s). A high level of comminution may produce a high degree of liberation, but at the expense of producing a large number of fine particles which may create problems in separation. Also, comminution is a very cost intensive process. Comminution should cease once an acceptable compromise between liberation and the degree of fineness has been obtained.

The standard procedure to measure liberation distributions is by the microscopic examination of cross-sections of particles. The first step in a liberation analysis is size classification. The sample particles are usually screened so that they are the same size (i.e. within one Tyler size class). Liberation analyses are generally performed on a size-by-size basis so that the variation of liberation with size can be determined. The sample particles are then randomly dispersed in a mounting medium (usually a resin in liquid form) in a mold. The resin is solidified with the addition of heat and/or a catalyst to produce a pellet with the particles supported in space by the resin. This pellet is cut and polished to expose the particles in section. Finally, the polished surface is examined with an optical or electron microscope and the liberation measured by determining the percentage of the relevant mineral in the different particle sections on an areal or linear

basis. Note that for liberation analyses, only two phases ("0" and "1") need be considered. Since an analysis is performed one phase at a time, the other phases can be collectively considered to be a second phase.

Originally, liberation was measured using visual inspection, but the advent of computerized image analyzers has greatly increased the speed of gathering liberation data and the precision of the data. The image of the polished surface from the microscope is digitized and sent to the image analyzer which is simply a software package designed to identify the features in the image and make measurements such as section shape, size, liberation, etc. (Fig. 1.1).

Image analysis has made the measurement of the liberation distribution much more precise than before, but not necessarily more accurate. There are several errors that are inherently associated with the measurement of the liberation distribution:

1) sample preparation - The particles must be randomly embedded in the mounting medium so that a polished surface will reveal random sections. If there is preferential settling or orientation of the particles, the resulting polished surface may be unrepresentative of the sample. Preferential settling will occur if there are significant differences in density between the particles in the sample. The denser particles will settle in the mounting medium to the bottom of the mold faster than the less dense particles. When the mounting medium has hardened and a polished surface created, the denser particles (or the lighter particles depending on how much polishing is done) will be over-represented on the surface. Preferential orientation will occur if there are significant differences in density between the phases in the locked particles. If this is the case, then the locked particles may settle in the mounting medium in one alignment (usually with the densest phase facing downwards). Again, this may result in an unrepresentative polished surface. It should also be noted that the process of polishing itself is important. The polished surface should be free from topographic features which may be misinterpreted by the image analyzer to be a phase or a section.

2) image analysis processing - The digitized image of the polished surface must be processed using filters to "clean" the image to help the image analyzer distinguish between the different features and phases in the sample. The filters should be carefully applied so that there is no distortion of the information contained in the original image.

3) sampling - A sufficient number of sections must be analyzed to make the data statistically valid.

4) stereology - Liberation measurements on polished surfaces are biased because the information that is collected is one or two-dimensional while liberation is, of course, a three-dimensional variable.

This work will mainly deal with the problems posed by stereology. Correction procedures proposed to deal with stereological bias will be examined and the production procedure for a standard material (i.e. a material of known particle composition and locking characteristics) will be developed. This material will be used to test the effectiveness of the correction procedures.

1.2 Electron microscopy

In this work, electron microscopy was used extensively, not only for generating the images for liberation analysis, but also for examining the materials used in the creation of the standard material. The standard material in this work was developed specifically for use with electron microscopy.

The principles of electron microscopy are quite straightforward. A beam of electrons is focused onto a sample. The interaction of the beam with the sample surface yields several signals that are collected by various detectors. An image can be generated using the three main types of signals:

1) Secondary electrons. These electrons are the result of inelastic collisions between the electrons of the electron beam and the weakly-bound electrons of the sample near the surface. An image based on secondary electrons supplies topographic information about the sample.

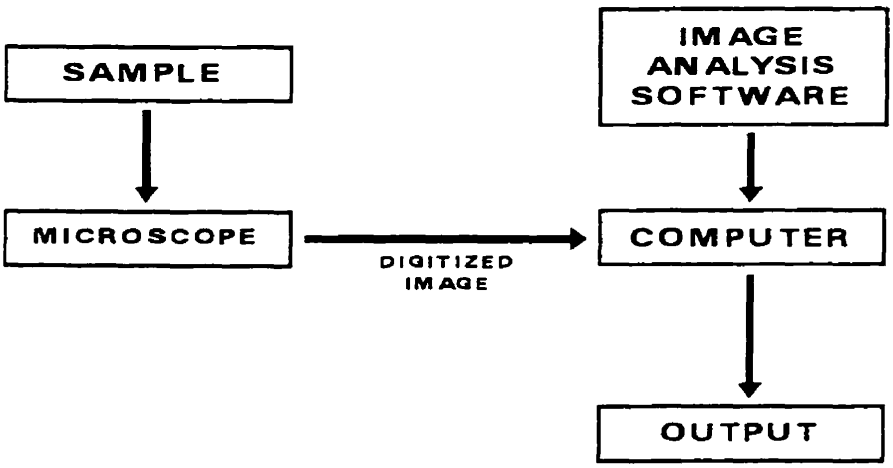

Fig. 1.1: Conceptual illustration of liberation measurement. A polished surface of the sample is examined with a microscope from which digitized images are produced. These images are sent to the image analyzer which measures the composition of each individual particle section.

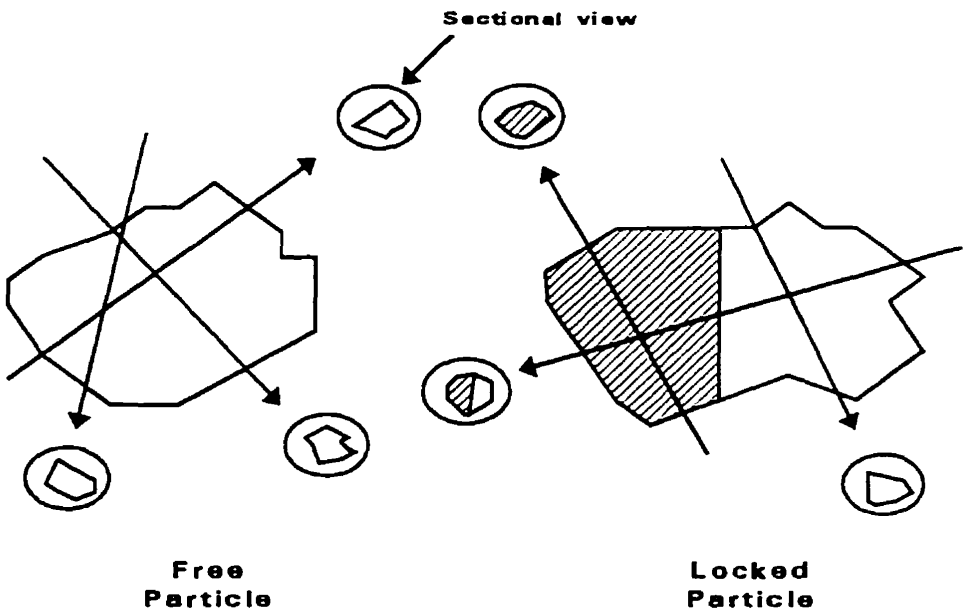

Fig. 1.2: The effect of stereological bias on liberation information.

2) Backscattered electrons. These electrons are the result of elastic collisions between the beam electrons and the sample electrons. The yield of backscattered electrons is proportional to the average atomic number of the sample. An image based on backscattered electrons provides compositional information about the sample.

3) Characteristic X-rays. The interaction of a beam electron with a sample atom may cause an inner shell electron of the atom to be ejected. An outer shell electron will fill the vacancy and emit an X-ray having an energy and wavelength characteristic of the atom from which it originated. Using EDS (energy dispersive spectroscopy) analysis [1,2], X-ray energy spectra of the sample permit the identification of the specific elements.

Backscattered electron imaging is primarily used in liberation analyses since images can be generated quickly and compositional information about the sample is available. Secondary electron imaging provides only topographic information and X-ray images are too time-consuming to generate and generally have poorer resolution than either backscattered or secondary electron images.

Backscattered electron imaging provides a grey level image of the sample: low atomic number materials appear dark while high atomic number materials appear bright. If the grey levels of two phases are difficult to distinguish then EDS analysis may be used to provide elemental information to differentiate the two. The QEM*SEM system [3,4] makes extensive use of both backscattered electron and X-ray imaging. In one QEM*SEM machine, four X-ray detectors are used to speed up the measurement of X-rays.

1.3 Stereology

The error created in sectioning data by stereology, or stereological bias, is demonstrated in Fig. 1.2. Free particles (particles consisting of only one phase) when sectioned will always yield free sections, but locked particles (particles consisting of more than one phase) when sectioned can produce either free or locked sections [5].

As a result of this, free particles will always be over-estimated when measured from a polished surface due to these false free sections. This bias also affects the measurement of locked particles since a given locked particle can produce a wide distribution of locked sections. Stereological bias can be quite significant. Its magnitude varies depending upon the particle locking texture and the particle shape.

Liberation distributions can be measured from using linear sections (i.e. intercepts) or areal sections. This thesis deals with areal sectioning only since areal sectioning is less stereologically biased than linear sectioning [6(pp.56-64)] and is more commonly used to gather liberation data.

1.4 Stereological correction

There have been many procedures developed to correct stereological bias, but their accuracy has not been fully determined. The different correction procedures are described below.

1.4.1 Use of the sectioned distribution

This technically is not a correction procedure at all. The assumption is simply that the sectioned liberation distribution is an adequate measure of the true liberation distribution. In many liberation studies, this approach is taken - the data are not corrected and are presented in their raw form. Sometimes the assumption that the sectioned and true distributions are the same is stated; other times, it is implicit.

This "correction" is only effective in the following cases:

1) There is a large proportion of free particles. If there are few locked particles then few false free sections will be generated.
2) The particle size is much larger than the grain size (particle size refers to the size of the broken material; grain size refers the size of the discrete features of the phase of interest in the ore before breakage). This produces a large number of locked particles whose texture is fine-grained. A section through such a particle is likely to cross an interface and yield a locked section thus reducing the stereological bias.

3) A combination of the above.

An advantage of using this procedure (apart from its obvious simplicity) is that the data cannot be corrupted as no mathematical transformations are performed. The disadvantage is that the data remain biased and there are many situations where the true and sectioned distributions are markedly different.

1.4.2 Large-sections correction

This procedure is practised to a certain degree in all liberation analyses. Small sections are difficult to resolve with a microscope. Consequently, sections below a certain size are usually excluded from the analysis. There is a benefit to excluding small sections: small sections are more stereologically biased than large sections. For material in a narrow size range, large sections are more likely to go through the centre of particles and thus be more representative. They are also more likely to cross an interface and yield locking information (Fig. 1.3). The large-sections correction takes advantage of this by considering only the largest sections of a liberation analysis.

This procedure has three advantages. Firstly, it is very simple to apply. All that need be done is to instruct the image analyzer not to analyze particles below a certain size. Secondly, the correction is independent of particle shape and locking texture which makes it generally applicable. The elimination of small sections provides an improvement in the sectioning data without the chance of corrupting it (i.e., the corrected liberation distribution will nearly always be in the range between the true and sectioned liberation distributions). The degree of improvement depends on the exclusion criterion (the size, in terms of area, below which a section is excluded from the liberation analysis). Thirdly, small features are not only more stereologically biased, but they are also more likely to be artifacts. With the large-sections correction, even if an artifact survives the image analysis filtering procedure, it will not be considered.

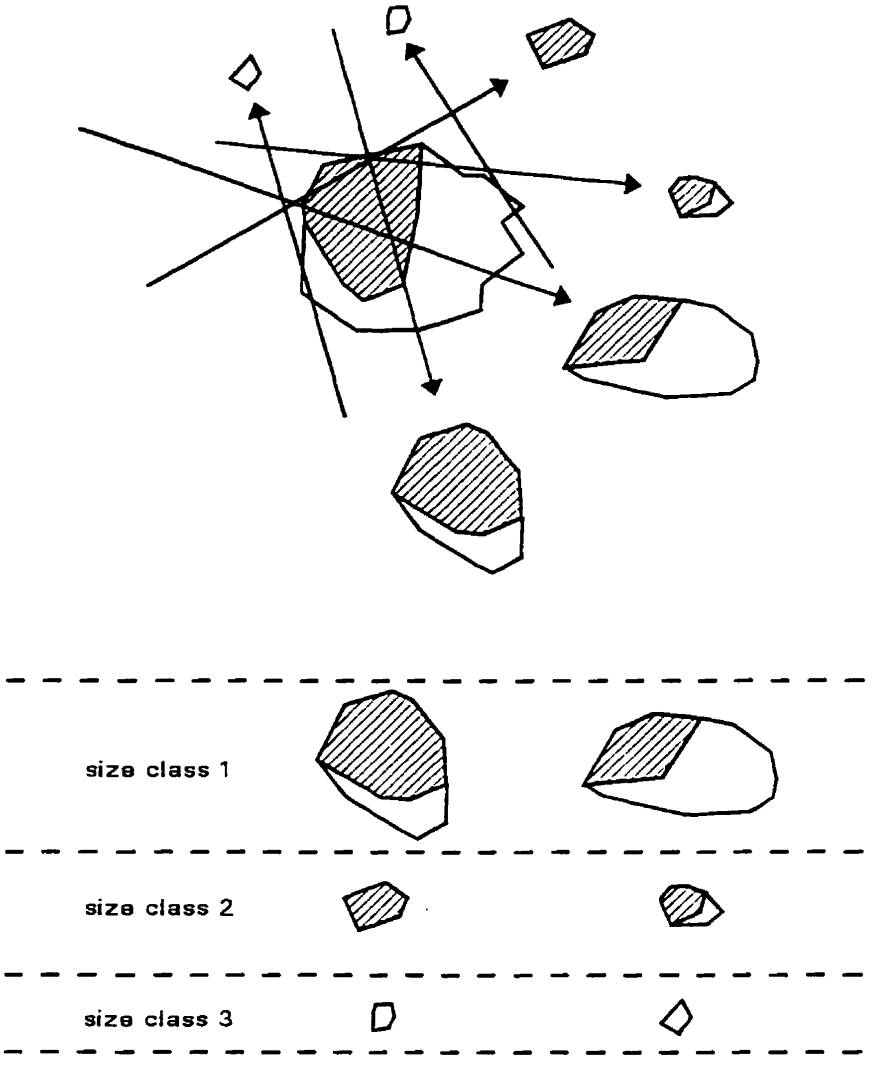

Fig. 1.3: Sections of particles can be size classified (ex. using a Tyler progression). The large-sections correction excludes small sections and considers only large sections which are more representative of the original particles.

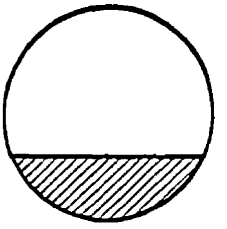

Fig. 1.4: Single-capped sphere.

The disadvantage of this procedure is that many sections may have to be examined in order to maintain statistical validity since a large fraction of the sections may be excluded. Also, there is an upper limit on the effectiveness of this correction. Even if only sections that cut through the centre of particles are considered, false free sections may still be observed. Although this procedure can reduce the stereological bias, the true distribution could never be completely reconstructed. (An apparent disadvantage is that the grade calculated using only large sections is biased. However, the bias in the grade does not affect textural information. An accurate measure of the grade can be obtained using all the data in a separate exercise.)

1.4.3 Hill's fast approximation

Hill et al. [7,8] performed extensive analyses using computer-generated, single-capped spheres (Fig. 1.4) to represent ore particles. (Single-capped spheres are simple-locked spheres with planar interfaces. Simple locking is locking such that there is only one interface between the phases in a locked particle.) They observed that in many cases the locked section distribution was similar to the locked particle distribution. If it is assumed that they are identical, stereological correction is simplified to the process of eliminating false free sections. Hill's fast approximation is a correction procedure that employs this assumption. It uses an empirical relationship between the sphere composition and the amount of free sections produced to predict the amount of false free sections generated in a sample.

Hill determined that the relationship between $\mathcal{L}_0$, the area fraction of false free phase "0" sections expected as the result of sectioning, and c_1, the volumetric sphere composition (volume fraction phase "1"), was:

$$\mathcal{L}_0 = \frac{10^{(-2c_1)}}{2} \qquad (1.1)$$

The relationship between $\mathcal{L}_1$, the area fraction of false free phase "1" sections expected as the result of sectioning, and c_1 was determined to be:

$$\mathcal{L}_1 = \frac{10^{(2c_1 - 2)}}{2} \qquad (1.2)$$

Once the areas of all the false free sections are calculated, they are subtracted from the area of the observed free sections and the locked section distribution is linearly scaled-up. Hill [7(pp.172-83)] has demonstrated the effectiveness of his fast approximation on different distributions of single-capped spheres.

Barbery and Pelletier [9] claimed that the results of Hill's sectioning of spheres did not match the theoretical results, but Finch et. al. [10] have subsequently verified Hill's sectioning procedure.

The advantages of this procedure are speed and simplicity. The disadvantage is that for real mineral particles there is no evidence that the locked section and locked particle distributions are similar and that the sphere model can be used to predict the occurrence of false free sections.

1.4.4 Correction using simple geometric shapes

The relationship between the linear or areal liberation distribution and the volumetric liberation distribution [11] can be expressed thus :

$$O(c_{obs}) = \int_0^1 S(c_{obs}, c)\, T(c)\, dc \qquad (1.3)$$

where c = volumetric particle composition

c_{obs} = linear or areal particle composition

$O(c_{obs})$ = observed (or sectioned) liberation distribution

$S(c_{obs},c)$ = kernel (or sectioning) function - this function characterizes the sectioning behaviour of locked particles in a given system by describing the sectioned liberation distribution for all volumetric particle compositions.

$T(c)$ = true (or volumetric) liberation distribution

A straightforward method of correcting the sectioned liberation distribution uses the assumption that the particle shape and the particle locking texture are constant. The shape is assumed to be a simple geometric shape such as a sphere or a cube [5,7,8,12,13,14]. The locking texture is simplified as well. In most cases, it is assumed that there is a single, planar interface dividing the two phases although parabolic interfaces [13] and multiple planar interfaces [12,15] have also been studied. By analysing two-phase (binary) systems of such shapes, a kernel matrix can be generated and used for stereological correction. Equation 1.3 can be simplified to:

$$O = S \times T \tag{1.4}$$

where O = (m×1) matrix representing the observed (sectioned) liberation distribution

S = (m×m) kernel (or sectioning) matrix characterizing the behaviour of the sectioning of a specific geometric locked particle for all volumetric particle compositions

T = (m×1) matrix representing the true liberation distribution

m = the number of intervals (particle composition fractions) into which the distribution has been discretized.

The O matrix represents the sectioning data from the image analyzer. The S matrix can be constructed using numerical integration (in the case of single-capped spheres) or analytically by computer generating particle shapes with different particle compositions and randomly sectioning them on a linear or areal basis. With O and S known, T can be solved thus:

$$T = S^{-1} \times O \tag{1.5}$$

An example of a kernel matrix is shown in Table 1.1.

Table 1.1: Kernel matrix for single-capped spheres.

		ACTUAL PARTICLE COMPOSITION											
		0%	0-10%	10-20%	20-30%	30-40%	40-50%	50-60%	60-70%	70-80%	80-90%	90-100%	100%
	0%	100.00	39.44	23.44	15.62	10.65	7.17	4.66	2.82	1.52	0.62	0.10	0.00
O	0-10%	0.00	48.01	16.90	9.91	6.28	4.04	2.53	1.50	0.78	0.31	0.05	0.00
B	10-20%	0.00	9.51	33.59	12.76	7.40	4.55	2.77	1.60	0.82	0.33	0.05	0.00
S	20-30%	0.00	1.62	16.23	31.19	12.30	6.89	4.01	2.26	1.14	0.44	0.07	0.00
E	30-40%	0.00	0.59	4.42	15.89	30.83	12.58	6.61	3.54	1.72	0.66	0.10	0.00
R	40-50%	0.00	0.29	1.98	5.73	14.52	30.83	13.35	6.30	2.92	1.07	0.16	0.00
V	50-60%	0.00	0.16	1.07	2.92	6.30	13.35	30.83	14.52	5.73	1.98	0.29	0.00
E	60-70%	0.00	0.10	0.66	1.72	3.54	6.61	12.58	30.83	15.89	4.42	0.59	0.00
D	70-80%	0.00	0.07	0.44	1.14	2.26	4.01	6.89	12.30	31.19	16.23	1.62	0.00
	80-90%	0.00	0.05	0.33	0.82	1.60	2.77	4.55	7.40	12.76	33.59	9.51	0.00
	90-100%	0.00	0.05	0.31	0.78	1.50	2.53	4.04	6.28	9.91	16.90	48.01	0.00
	100%	0.00	0.10	0.62	1.52	2.82	4.66	7.17	10.65	15.62	23.44	39.44	100.00

The main advantage of using geometric shapes for stereological correction is its relative simplicity. The kernel matrix is easily generated.

The disadvantage is that real particles are never spherical or cubical and they are never all the same shape. Also, the locking texture is never constant and rarely conforms to a simple geometric definition. Another difficulty is that the kernel matrix is not unique; it varies depending on the particle shape and locking texture.

Hill et al. [8] have observed that the use of simple geometry tends to overcorrect the sectioning data (i.e. reduce the free occurrences too much). They suggested that the corrected distribution be used as an estimation of one of the limits of the stereological error; the other limit would be the sectioned distribution itself. The true distribution should lie somewhere between these limits.

1.4.5 PARGEN correction

The PARGEN stereological correction is similar to correction using simple geometric shapes except that in this case, irregularly-shaped particles are used. The PARGEN computer software [16,17] generates randomly-shaped, ellipsoidal particles in which grains of another phase are grown inside to produce locking. These locked particles are sectioned to create the kernel matrices. Barbery and Pelletier [9]

claimed that the sectioning of the PARGEN particles was not performed randomly, but Lin, Miller and King [18] have subsequently validated the sectioning procedure.

The effect of the following parameters on the sectioning behaviour of PARGEN particles has been investigated [19]:

1) dispersion density (dd), number of grains per particle
2) particle shape
3) grain size distribution.

The effect of particle shape was examined by simulating and sectioning four ellipsoidal shapes: spheres, ellipsoids, oblate/prolate and flattened ellipsoids. The effect of the grain size distribution was examined by simulating four types of distributions: uniform, exponential, normal and Weibull. The dispersion density was examined by simulating values ranging from 1 to 50. Of these three parameters, only the dispersion density was judged to have a significant effect on the sectioned distribution. Thus, a family of kernel matrices was generated by varying only the dispersion density.

These kernel matrices can be used to transform the sectioning data to three dimensions using Equation 1.5, but Lin, Miller and Herbst [20] and Schneider et al. [21] observed that direct inversion of the kernel matrices is not practical because they are ill-conditioned and $\boldsymbol{O}$ is not error-free. Direct inversion may lead to negative values or values exceeding 100 % in composition fractions of $\boldsymbol{T}$. Equation 1.5 is more correctly expressed as:

$$\boldsymbol{T} = \boldsymbol{S}^{-1} \times (\boldsymbol{O} + \epsilon) \tag{1.6}$$

where ϵ = experimental error in the measurement of $\boldsymbol{O}$.

Lin, Miller and Herbst suggested the use of the Philips-Twomey inversion to overcome this instability. Schneider et al. suggested the use of the constrained Rosenbrock Hillclimb Procedure with an objective function. They claim that this method

is more robust than the Philips-Twomey inversion and is more appropriate in the cases where T is not smooth or continuous.

In this thesis, a computer program developed at the University of Utah, Stereological Reconstruction of Linear and Areal Grade Distributions, was used to perform the PARGEN correction. The constrained Rosenbrock Hillclimb Procedure was used in this software. The data that this program requires are:

1) the observed (linear or areal) liberation distribution discretized into composition fractions of 0, 0-10, 10-20,...,90-100, 100%
2) the grade (as measured from image analysis).

Bole et al. [22] examined the performance of the PARGEN procedure with real mineral particles. They used ore particles from two binary systems (sphalerite/dolomite and iron-oxide/silicate). The composition of the particles was determined by density fractionation. The particles were sectioned on both a linear and areal basis and the sectioning data were corrected using the PARGEN procedure. They showed that there was good agreement between the true liberation distributions of the ore and the PARGEN-corrected liberation distributions.

Since the PARGEN particles have a granular locking texture, in the PARGEN correction, one phase must be designated the grain phase and the other, the matrix phase. In most cases, this selection is straightforward: an examination of the unbroken ore (or in some cases, the particles alone) will reveal which phase is the granular phase (if the texture is granular). This determination must be done with care since reversing the phase labels will result in different corrected liberation distributions. An inspection of the PARGEN kernel matrices reveals that they are not symmetric.

The advantages of the PARGEN procedure are that the particles and grains are randomly shaped and that it allows the selection of the dispersion density to correspond with the occurrence of mineral grains inside the real particles. PARGEN particles are certainly more realistic than simple geometric shapes.

The disadvantages of this correction are that it assumes that the particle shape is ellipsoidal and the locking texture is granular. Although this is a common situation, it

may not necessarily always be the case. Also, the selection of the dispersion density has not yet been clearly resolved. It can be based on the observed occurrence of grains in the particle sections, but this number would be subject to stereological bias. Also, it would be difficult to select a single dispersion density if there is a wide distribution in the number of grains per particle.

1.4.6 Barbery's correction

Barbery's correction procedure [6,23,24,25] makes use of geometric probability and thus requires only a few assumptions be made with regard to particle shape and ore texture (the interlocking of the phases before breakage). This correction is the result of the coupling of an ore texture model and a breakage model.

Barbery suggested that the ore texture be represented by a covariance function, $C(L)$:

$$C(L) = E([h(z) - p_1][h(z+L) - p_1]) \tag{1.7}$$

where z = a random point in a texture consisting of two phases ("0" and "1")

$h(z)$ = the texture indicating function ($h(z) = 1$ if z is in phase "1" and $h(z) = 0$ if z is in phase "0")

L = distance

p_1 = the fractional grade of phase "1" in the ore.

$C(L)$ corresponds to the normalized probability that z and $z+L$ are both in phase "1".

Barbery further suggested that the ore texture be modelled using either a Poisson polyhedra texture or a boolean texture with primary Poisson grains. The Poisson polyhedra texture is constructed by dividing space into polygons with random uniform isotropic planes. The probability that a given polygon consists of phase "1" is p_1. The boolean texture with primary Poisson grains is constructed by selecting points randomly and isotropically in space where a Poisson polygon is implanted independent of the presence of other polygons. Barbery describes these two textures and their covariance functions in detail [6(pp.42-9)]. The covariance function of these textures can be

described using two parameters: the grade and a size descriptor. Both of these can be calculated from sectioning data.

Breakage is accomplished by applying random uniform isotropic fragmentation (RUIF) (i.e. random breakage independent of the phases in the ore and of phase interfaces) to the ore texture. Barbery suggested that particle shape be characterized by:

$$P(L) = 1 - \frac{L}{\alpha D} \exp\left(1 - \frac{L}{\alpha D}\right) \qquad (1.8)$$

for $0 \leq L \leq \alpha D$; $P(L) = 0$, otherwise.

where $P(L)$ = the probability that two points separated by a distance L will be in the same particle for all pairs of points (with at least one point in the particle) for all orientations

α = 1.2 (as suggested by King [26])

D = particle mesh size.

The corresponding intercept length density distribution, $i(L)$, for random intercepts through particles with a mesh size D is:

$$i(L) = \frac{1}{\alpha D}\left(2 - \frac{L}{\alpha D}\right) \exp\left(-\frac{L}{\alpha D}\right) \qquad (1.9)$$

for $0 \leq L \leq \alpha D$; $i(L) = 0$, otherwise.

King [26,27] has shown the agreement between Equation 1.9 and experimental data. Particles described by this equation are generally referred to as King particles.

By defining the ore texture and particle shape in this manner, the breakage simulation of Barbery's procedure is reduced to a sampling problem. Since both the particle shape and ore texture are modelled as probability functions, RUIF is easily simulated by "sampling" the shape from the texture. The corrected liberation distribution is represented by an incomplete beta function described by four parameters: the amount of free phase "0" and "1" and the mean and variance of the liberation distribution. In the corrected distribution, the material that contained -5 or +95 vol. % of the phase of interest was considered free [28].

This correction can be performed either on an linear or areal basis. In this thesis, a boolean texture with primary Poisson grains was used to model the ore texture. Barbery [6(p.197)] has claimed that the use of either boolean or Poisson polyhedra texture does not affect the correction results. The computer program, BOOKING, developed by G. Barbery and R. Pelletier, was used to perform this correction. The program requires the following data:

1) the grade (as measured from image analysis)
2) the upper and lower particle sizes
3) E(S), the expected value of the section area
4) Var(S), the variation in section area
5) $E(S^2)$, the expected value of the square of the section area
6) $E(S_0S_1)$, the expected value of the product of the section area of phase "0" and the section area of phase "1" of each section.

All these parameters can be readily calculated from the sectioning data.

The robustness of the Barbery's correction as applied to distributions of single-capped spheres has been examined previously by the author [29]. The results are included and expanded upon in this work.

The advantage of this procedure is that it expresses the ore texture and particle shape as probability functions rather than as pre-defined geometric forms. This provides the correction with more flexibility than a correction using fixed shapes or textures.

The disadvantage of this procedure is that it may have difficulties in the following situations:

1) the occurrence of a large degree of preferential breakage in the ore
2) the sample was concentrated or resulted from the mixing of streams as occurs in a mineral processing plant [15(p.370)].

Either of these may lead to a poor estimation of the size descriptor of the texture model and a poor estimation of the variance of the liberation distribution.

Gay [15(p.113)] has observed that preferential breakage may not be a problem if a phenomenon he calls virtual non-preferential breakage takes place. Preferential breakage inevitably occurs to some degree since the phases in an ore will possess

different hardnesses, but the harder phases in an ore will be subject to more breakage depending on the design of the grinding circuit. In most circuits, there is a size classification step (such as hydrocyclones) which determines if the particles are too large and should be recycled to the grinding mill. For example, if two phases, one hard and one soft, are subject to the same amount of breakage, one would expect the harder phase to produce larger particles, but if the particles of the harder phase are continually recycled and broken, the end result would be that the particles of the harder phase would be the roughly the same size as those of the softer phase.

An apparent disadvantage of Barbery's correction is the use of a boolean or Poisson polyhedra texture to model the ore texture. These models are used only as a mathematical representation of the original ore texture; the only necessary condition for the reconstructed texture is that its breakage result in particles similar to those that were sectioned. It must be remembered that the reconstructed texture is based on parameters derived from sectioning data. Barbery has performed some tests examining the effect of the use of the different texture models on the correction procedure, but a more complete study into this matter should be conducted.

1.4.7 Gay's correction

A correction procedure recently developed by Gay [15,30,31] has shown considerable promise. In his correction, a series of geometric probability equations are defined that estimate a number of statistical parameters of the volumetric liberation distribution. These equations are independent of particle shape and locking texture. A sorting algorithm is used to allocate the particle sections to different "bins" (particle composition fractions) until the objective function, a weighted sum of squares of deviations of the probability equations, is minimized. As of writing, further details regarding this procedure are in press and software is being prepared.

The advantage of this procedure lies in its general approach; there are no assumptions made about particle shape, locking texture or breakage. The disadvantage is that it requires extensive computation and an analysis of the pixel information of each section. In all other correction procedures, the data that were necessary (and were

measured) were the size and composition of each section. For Gay's correction, a series of geometric measurements must be performed on each individual section shape. Image analysis systems are not designed to perform these measurements so the pixel information must be downloaded onto a microcomputer where the measurements can be made.

1.4.8 Rules of thumb

The complexity inherent in some correction procedures has led to the development of simple corrections or so-called rules of thumb which are based upon experience or upon a simplification of some of the above-mentioned corrections. A review of these has been presented by Barbery [6(pp.172-5)]. Most of these procedures provide only a correction to the amount of free material; the locked distribution is not considered.

1.5 Thesis objective and outline

The objective of this thesis is two-fold:

1) Development of a standard material.

   Although a method has been previously established to create a standard material, this work refines the approach so that the standard material can be made to possess different locking textures and is easier to use. Chapter 2 discusses the development of such a standard material. Chapter 3 discusses the density fractionation techniques that were used to determine the composition of the particles (particle density and composition are directly related since the standard material is two-phase).

2) Examination of the robustness of four different stereological correction procedures: large-sections correction, Hill's fast approximation, Barbery's correction and PARGEN correction.

   Two sets of tests were performed. In Chapter 4, various distributions of single-capped spheres were computer-generated and sectioned. The correction procedures were used to correct the sectioning data and the corrected distributions were compared with the true distributions. In Chapter 5, the same distributions were re-created using standard material particles developed in this work. These

particles were mounted, sectioned and a liberation analysis was performed with an electron microscope and image analyzer. The correction procedures were used to correct the sectioning data and the results again compared with the true distributions. These two sets of tests provided information about the strengths, weaknesses and applicability of the correction procedures.

CHAPTER 2: STANDARD MATERIAL

2.1 Overview

A standard material for liberation analysis would consist of particles of known composition and locking characteristics. A two-phase (binary) standard material is all that is required because liberation, as mentioned earlier, is measured one phase at a time: while the liberation of one mineral phase is being measured, the rest of the mineral phases in the sample can simply be grouped together as the second phase. A true two-phase material is essential if density fractionation of the particles is performed to provide the independent and true measure of the particle composition. If there are more than two phases, there will not be a direct correlation between the particle density and particle composition. Obviously, a significant density difference between the two phases is necessary to provide good resolution to the density splits. A near-perfect separation such as that obtained using heavy liquids is desired to ensure the precision of the splits.

There must be a method of distinguishing the two phases from each other. If optical microscopy is used, the two phases must be different colours or have some other differentiating feature. If electron microscopy is used, the two phases must have different grey levels when viewed with backscattered electron imaging. With electron microscopy, it is desirable that there is a large density difference between the phases because the backscattered grey level of a phase is directly related to its average atomic number (a low atomic number material will appear dark and a high atomic number material will appear bright). In this work, the standard material was designed for use with electron microscopy.

It is desirable that the standard material be able to exhibit simple locking (locking such that there is only one interface between the phases in the particle). Simple locking is probably the most important of all locking types in mineral processing following the

argument that since comminution is aimed at creating free particles, the mineral which fails to be liberated is most likely concentrated in the next simplest class - the simple-locked particle class. Simple locking also creates the most severe stereological bias and is, therefore, a severe test of any stereological correction procedure.

The standard material should also be flexible enough to simulate various different types of locking textures. Although a correction procedure may be effective with one type of locking texture, it may not be as effective with others.

Since the liberation distribution of the standard material is known, it can be used as a check on the effectiveness of stereological correction procedures (provided the other components of liberation analysis - sample preparation and image processing - are performed correctly). The known true liberation distribution can be compared with the corrected data. In more general terms, a standard material would enable the whole procedure (not just stereological correction) to be tested, although the source of error may be difficult to isolate. In this regard, a standard material is superior to using computer-generated particles since it involves all the steps of a liberation analysis.

Several attempts have been made at creating standard materials. There are two categories of standard materials: naturally-occurring and artificial.

2.1.1 Naturally-occurring standard materials

Naturally-occurring standard materials are created from naturally-occurring two-phase ores. The ore is broken, screened and the composition of the particles measured by density fractionation. There have been several efforts to develop a standard material from natural sources, but there are difficulties in finding a two-phase ore whose phases are homogenous and free from impurities. Also, the use of a naturally-occurring standard material is limited because the locking texture cannot be controlled. Work performed in this area is described below.

1) Stewart and Jones [32] used a siliceous iron ore. The ore consisted of grains of iron oxides (hematite with magnetite and minor amounts of goethite and limonite) in a siliceous matrix (quartz with minor amounts of other silicates). The ore was crushed to 90% -1.0 mm and screened. The particles were

separated based on density using heavy liquids (for densities below 3.32 g/ml) and a fluidized bed (for densities above 3.32 g/ml). The siliceous material was estimated to have a density of 2.65 g/ml and the iron oxide to have a density of 5.06 g/ml. There were two problems with this standard material: there may have been significant porosity in the ore [15(p.118)] and there was some variation in the density of the iron minerals.

2) Bole et al. [22] examined two binary ores: an iron-oxide/silicate sample and a sphalerite/dolomite sample. Both ores were crushed and screened to 417-595 μm. The iron-oxide/silicate particles were fractionated using heavy liquids. The densities of the iron oxide and silicate phases were 5.10 and 2.72 g/ml, respectively. The sphalerite/dolomite particles were density fractionated using the Magstream separator (a centrifugal magnetogravimetric separator described in Section 3.3). The density of the dolomite was 2.85 g/ml and that of the sphalerite, 4.00 g/ml.

3) Miller and Lin [19] used a unique approach to determining the true liberation of mineral particles. They used serial sectioning to determine the liberation of an iron ore (middlings stream of an iron ore processing plant) and a copper ore (ball mill discharge of a pilot plant). These particles were screened to 74-105 μm and mounted in resin. By polishing this pellet down by intervals of 18 μm, a series of parallel sections was gathered for each particle. The composition of each particle was reconstructed based on its sections. Although serial sectioning does provide an unbiased measure of the true liberation distribution, it is too tedious and expensive to use in regular liberation analyses.

2.1.2 Artificial standard materials

A general procedure to create an artificial standard material has been previously developed by several researchers. The production procedure for locked particles is summarized in Fig. 2.1.

1. Embedding of monosize grains into a matrix.

2. Grinding the grain-matrix blocks.

3. Size classification of the particles.

4. Density classification.

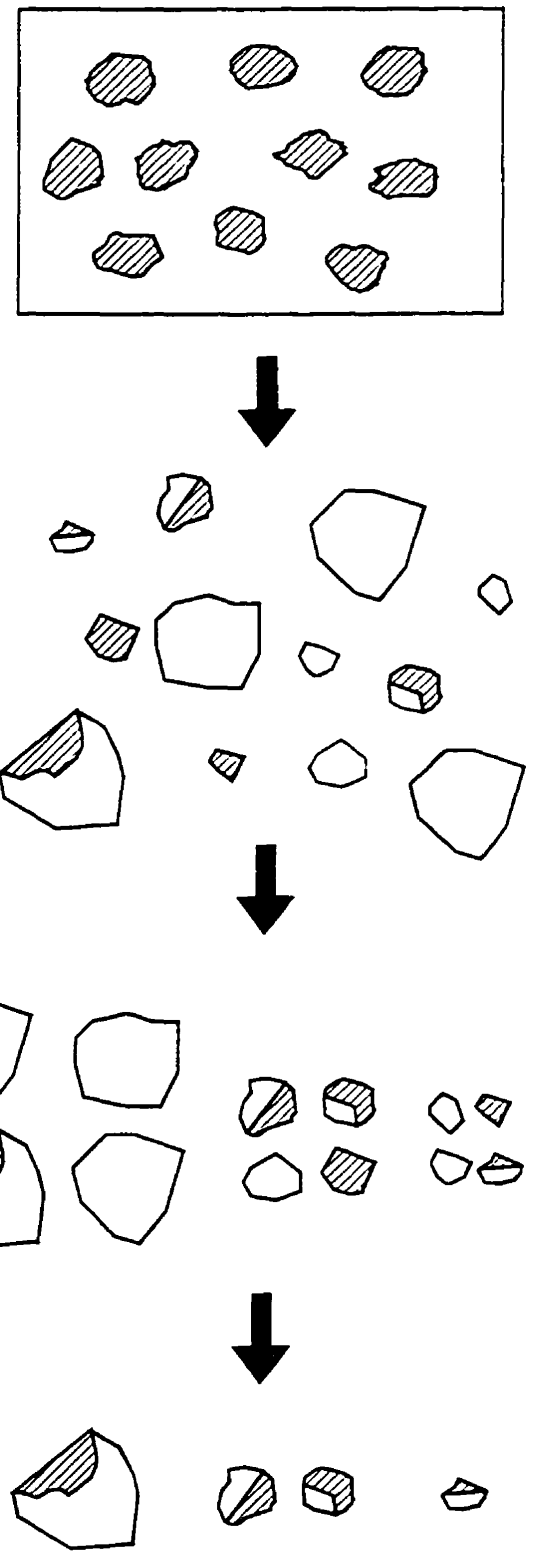

Fig. 2.1: Locked particle production; conceptual procedure.

Monosize grains of one phase are embedded into a matrix which acts as the second phase. The matrix phase is usually a plastic or resin in liquid form. When the plastic hardens, a two-phase block is formed. The blocks are then ground producing free and locked particles. These particles are screened into different size classes and a density fractionation is performed. This procedure allows the manipulation of parameters such as the grain and particle size so that there is some control over the locking texture.

Work that has been done in this area is described below:

1) Bagga [33] created a standard material using 600-710 μm pyrite as the grain material and polystyrene as the matrix material. The locked blocks were crushed after treatment with liquid nitrogen to make the polystyrene more brittle. Several particle sizes were screened out and a density fractionation was done using heavy liquids of $CaCl_2$ and $ZnCl_2$. A complete density fractionation could not be done since the highest density that could be reached using these liquids is 2.00 g/ml and the density of pyrite is 5.00 g/ml.

2) Woollacott and Valenta [34] created a standard material by embedding grains of a polyester resin which had been doped with lead oxide powder and black dye into a matrix of the same polyester resin in liquid form, doped with white dye. The lead oxide powder increased the density of the grain material to allow density fractionation and the dyes provide optical differentiation between the grain and matrix phases; this material was designed for optical microscopy. When the matrix resin had hardened, the locked blocks were broken and screened to 2.5-4.0 mm. The separations were performed using a heavy liquid (zinc chloride solution). The densities of the grain and matrix phases were 1.756 and 1.219 g/ml, respectively.

3) Lin et al. [35,36] created their standard material by embedding grains of silica in a matrix of epoxy resin. The silica density was 2.62 g/ml and the resin density was 1.22 g/ml. The particles were separated using a water-soluble heavy liquid (sodium polytungstate (SPT)). The particle size was 75-106 μm. Because these particles were designed for electron microscopy, they had to be mounted in a resin doped with iodoform powder so that the mounting medium could be

distinguished from the epoxy resin that was the matrix phase of the standard material.

4) Gay [15] created a standard material in much the same way as Woollacott and Valenta. Grains of a polyester resin doped with zinc oxide powder and a coloured dye were embedded in a polyester resin doped with a different concentration of zinc oxide and a different coloured dye. The densities of the two phases were 1.36 and 1.62 g/ml. Two particles sizes, 3.35-4.00 mm and 2.36-2.80 mm, were screened out and separated using a zinc chloride solution.

2.2 Refinement of the standard material

In this work, an artificial standard material was refined and used because with naturally-occurring standard materials there is no control over impurities or porosity. If there are significant quantities of either of these in the particles then determination of the particle composition from particle density measurements is not accurate. Similarly, this would be a problem if there were variations in the density of either of the two phases. Also, with a naturally-occurring standard material, there is no control over the locking texture.

Although an artificial standard material had been established in previous work by the author [35,36], it became apparent that certain improvements were needed to make it easier to use. The problems with this standard material that needed to be addressed were the following:

1) There was a large degree of breakage along the interfaces probably due to poor adhesion between the resin and the silica. This greatly reduced the amount of locked particles produced. In the tests in which the particle and grain sizes were equal, only $\approx$ 30 wt.% of the broken material became locked particles. When the particle size was one size class below the grain size, the amount of locked dropped to $\approx$ 10 wt.%.

2) There was a large difference in brittleness between the resin and silica. The silica was significantly more brittle than the resin. The edges of some free resin sections were rough and contained uneven gouges indicating that abrasion, not

brittle fracture, had taken place. This occurred even when the resin had been submerged in liquid nitrogen prior to breakage.

3) It was difficult to produce locked particles containing minor amounts of silica. The locked particles were mostly concentrated in the intermediate or high vol. % silica composition fractions. There were significantly fewer particles that contained <35 vol. % silica.

4) Only a granular locking texture could be created. In many particles, the matrix phase partially (or completely) surrounded the grain phase. This was the most common type of locking probably because it reflected the strongest bonding between the phases.

5) The standard material had to be mounted in doped resin. This made it slightly inconvenient to use since other researchers would have to create the same doped resin for them to use the standard material.

There are several variables that can be changed to enhance the quality and the quantity of the artificial standard material. The standard material could be improved by:

1) strengthening the bond between the grain and matrix material. By producing a strong bond between the two phases, there would be a decrease in breakage along the interfaces and an increase in the amount of locked particles. The amount of locked particles produced should be substantial enough that large amounts of grain and matrix material do not have to be processed. If a two-phase material could be created in which there was little breakage along the interfaces then this material could also be used in the assessment of liberation models (which usually assume negligible breakage along grain boundaries) in the prediction of the occurrence of free particles, for example.

2) varying the grain size. Decreasing the grain size would result in an increase in the interfacial area between the two phases which would increase the probability of forming locked particles. Unfortunately, there is a constraint on decreasing the grain size: if the grain size is much smaller than the particle size, then the occurrence of complex locking (locking such that there is more than one interface

between the phases in the particle) will increase. As mentioned earlier, simple locking is desired for the standard material. Increasing the grain size would increase the amount of simple locking, but decrease the amount of locked particles produced.

3) varying the particle size. If the particle size is increased, this would have two benefits: it would make the heavy liquid determination of particle composition more accurate (large particles are easier to separate by density) and it would reduce the amount of grinding which would induce less stress at the phase interfaces and thus produce more locked particles. Unfortunately, increasing the particle size will cause an increase in complex locking. It will also reduce the number of sections visible per polished surface. With some microscopes, the size of the sample that can be placed on the stage is limited. Therefore, many polished surfaces may have to be prepared to produce enough sections to satisfy statistical requirements.

4) changing the grain and/or matrix material. The ideal materials for the standard material should be brittle and possess good polishing properties (which enhances the quality of the image). The two materials should be significantly different in density. The greater the difference in density, the greater the resolution of the density separations. However, the density of the denser of the two phases should not exceed the upper limit of the separation method.

5) creating other locking textures. With the current procedure for producing locked particles, only granular locking can be created. While this may reflect the situation in most ores, this is not necessarily always the case. For instance, particles with a layered locking texture (a texture consisting of alternating layers of different phases) may result if an ore with a sedimentary structure was broken.

6) developing a strategy for producing only simple-locked particles. With the current procedure for manufacturing locked particles, simple locking is produced only when the particle size is significantly smaller than the grain size, but as mentioned earlier this may seriously reduce the amount of locked particles produced. In any case, it is very difficult to control the amount of simple locking

due to the granular nature of the texture: unless the grains are perfectly dispersed in the matrix, grains that touch each other will almost inevitably create complex locking. This is complicated by the fact that it is impossible to measure the degree of simple locking since stereological bias affects the measurement of the locking texture. Complex-locked particles can produce simple-locked sections and simple-locked particles can produce free sections.

In this work, most of the above suggested improvements were acted upon.

2.3 Experimental development of an improved standard material

2.3.1 Production of simple-locked, glass/resin particles

A method was developed for creating particles with only simple locking. If alternating layers of two materials could be bonded to each other, a layered texture is created. Simple-locked particles with planar interfaces would result if blocks of this material were crushed to a size below the thickness of the layers (Fig. 2.2).

A series of tests were conducted to examine this idea. Long glass slides (75 mm x 25 mm x 1 mm) alternated with short glass slides (25 mm x 25 mm x 1 mm) were clamped together at one end. This permitted the long glass slides to be parallel to each other and separated by a gap of exactly 1 mm. The slides were placed in a bath of liquid resin so that only the lower portion of the long slides were in contact with the resin; the short glass slides and the clamp itself were clear of the bath. The slides and resin were centrifuged together to ensure that there were no air bubbles and that the resin completely wetted the slides. After the resin had hardened, this produced a block of material consisting of alternating 1 mm layers of glass and resin. The clamp and the short glass slides were removed and the block was cut into smaller pieces with a diamond saw and crushed.

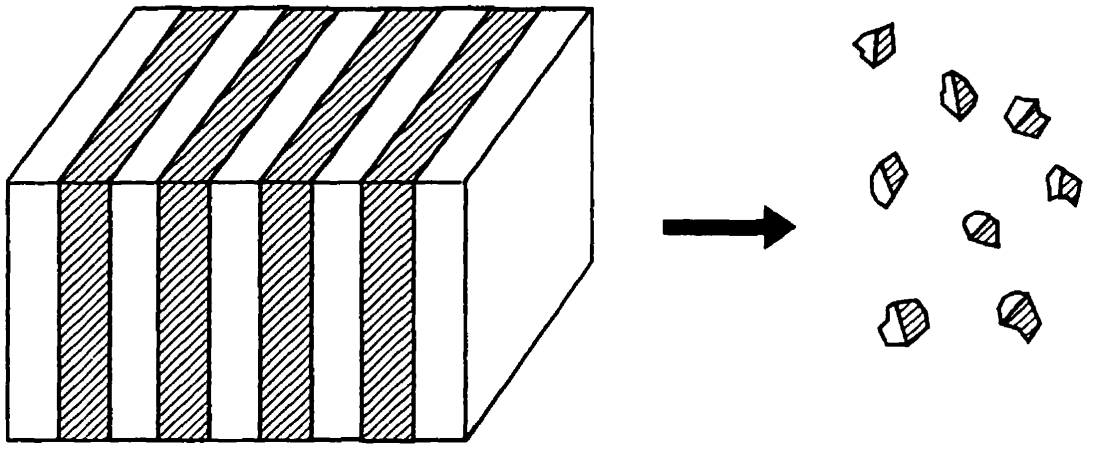

Fig. 2.2: Simple-locked particles can be created if a layered-texture block of material is crushed so that the particle size is smaller than the layer thickness.

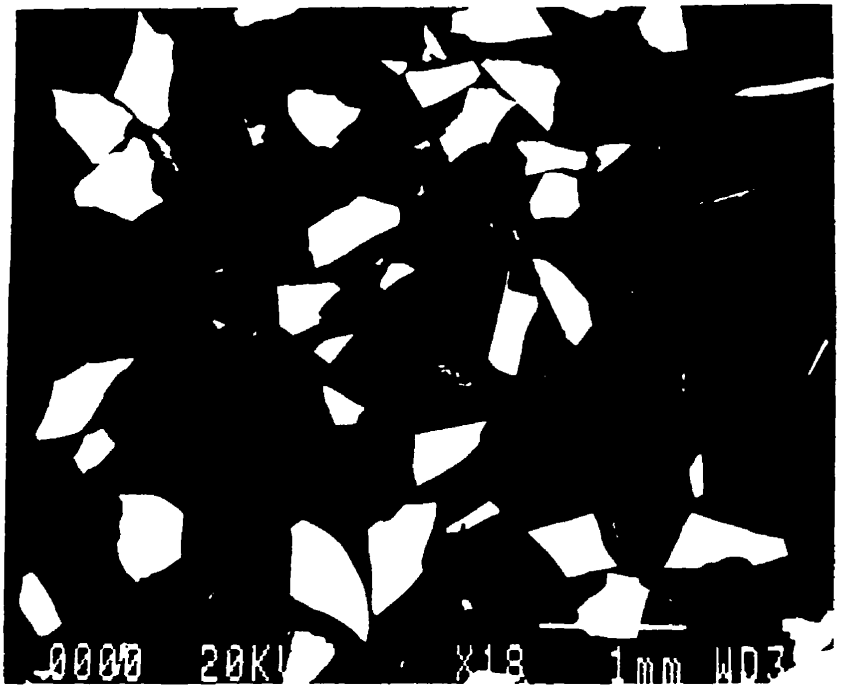

Fig. 2.3: SEM backscattered electron micrograph of simple-locked, glass/resin particles (light phase is glass; grey phase is resin; dark phase is mounting medium).

In preliminary tests, the material was exposed to liquid nitrogen before crushing to make the resin more brittle, but the liquid nitrogen appeared to greatly weaken the bond between the resin and the glass which led to excessive breakage along the interfaces. Liquid nitrogen was not used in subsequent tests, but it was still observed that the different layers of material readily separated from each other in the crushing process. After breakage, the 600-850 μm fraction was screened out, mounted and examined with a JEOL 840A scanning electron microscope (SEM). Prior heavy liquid separations were not performed so free particles were present as well as locked particles. Five different types of resin were tested:

1) Epotuf 37-200 cured with Epotuf 37-624 (Reichold Chemical Inc.)
2) Epi-Rez 510 & Heloxy 5063 (Rhone-Poulenc Inc.) cured with HMPA (hexahydro-4-methylphthalic anhydride) (Aldrich Inc.)
3) Epi-Rez 5163 & Epi-Rez 510 (Rhone-Poulenc Inc.) cured with HMPA
4) Epofix cold-mounting resin (Struers Inc.)
5) ERL-4221 (Union Carbide Inc.) cured with HMPA.

The first three resins contained high levels of bromine. This facilitated the differentiation of the matrix resin from the mounting medium resin with SEM backscattered electron imaging. The material created with the other two resins had to be mounted in a doped resin.

The SEM examination of all five samples revealed that very few locked particles were created. The vast majority of the sections were free, but the locked sections that were observed did exhibit simple locking with planar interfaces as expected (Fig. 2.3). The low amount of locking indicated that there was a large amount of breakage along the interfaces. Had there been no breakage along the interfaces, nearly all the particles would have been locked since the particle size was only slightly smaller than the thickness of the layers of glass and resin.

The excessive breakage along the interfaces is due to weak bonding between the glass and resin. The interface between the phases was flat and this certainly contributed to the poor adhesion between them. An attempt was made to increase the adhesion

between the resin and glass by roughening the surface of the glass slides. Two tests were performed: one using glass slides which were manually roughened with 60 grit (250 μm) silicon carbide grinding paper and another roughened with 120 grit (125 μm) grinding paper. Again, the slides were clamped parallel to each other with a 1 mm gap and then placed in ERL-4221 resin cured with HMPA. The material was crushed and the 600-850 μm particles screen out. A heavy liquid separation was performed at 1.40 g/ml and 2.20 g/ml using sodium polytungstate (SPT). This effectively removes the free particles; the glass density is 2.50 g/ml and the ERL-4221 density is 1.22 g/ml. The results are summarized in Table 2.1.

Table 2.1: Amount of locked material (1.40-2.20 g/ml) generated by the breakage of blocks of ERL-4221 resin and glass slides roughened with silicon carbide grinding paper.

Density range (g/ml)	120 grit SiC paper		60 grit SiC paper	
	Weight (g)	Weight %	Weight (g)	Weight %
-1.40	2.51	55.3	4.67	56.4
1.40-2.20	0.18	4.0	0.31	3.7
+2.20	1.85	40.7	3.30	39.9
Total:	4.54	100.0	8.28	100.0

The data indicate that there was still a large degree of breakage along the interfaces. In both tests, most of the particles were either free resin or free glass. There was only a small amount ($\approx$ 4 wt.%) of locked material (i.e. 1.40-2.20 g/ml). It is desirable that $\approx$ 30 wt.% or greater of the broken material should be locked so that the production of the standard material is not too time-consuming [36]. The locked particles that were created were mounted and examined by SEM. All the locked sections exhibited simple locking. One problem with the simple-locked particles was that some exhibited partial breakage along the interface. Parts of one phase (usually the glass) would break off from the interface at one or more points (Fig. 2.4). A close

examination of the interface revealed that the scratches in the glass were not very deep (10 to 20 μm), even though the particles of the grinding paper were considerably coarser.

A test was performed to see if the amount of locking could be increased by using glass slides with very rough surfaces. Glass slides (75 mm x 25 mm x 3 mm) were sandblasted with 100 grit (150 μm) particles. The thickness of the glass had to be increased to 3 mm because 1 mm slides shattered under this treatment. The slides were immersed parallel to each other separated by a gap of 1 mm in ERL-4221 resin. After the resin had hardened, the material was crushed and the 600-850 μm particles screened out. As before, heavy liquid separations at 1.40 g/ml and 2.20 g/ml were performed. The results are shown in Table 2.2.

Table 2.2: Amount of locked material generated by the breakage of blocks of ERL-4221 resin and sandblasted glass slides.

Density range (g/ml)	Weight (g)	Weight %
-1.40	4.03	33.1
1.40-2.20	0.06	0.5
+2.20	8.08	66.4
Total:	12.17	100.0

Again, the results indicated that few locked particles were produced (in fact, fewer than in the previous tests with roughened glass). The increased thickness of the glass slides caused an increase in free glass particles, but even taking this into account, the amount of locking produced was very low. A SEM examination of these locked particles showed that most of the sections were locked and that all the locking was simple (Fig. 2.5). There were some particles exhibiting partial breakage along the interface. An examination of the interface showed that the scratches in the glass were deeper than in the previous tests, but were still only 30 to 40 μm.

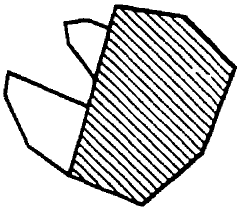

Fig. 2.4: Partial breakage along the interface.

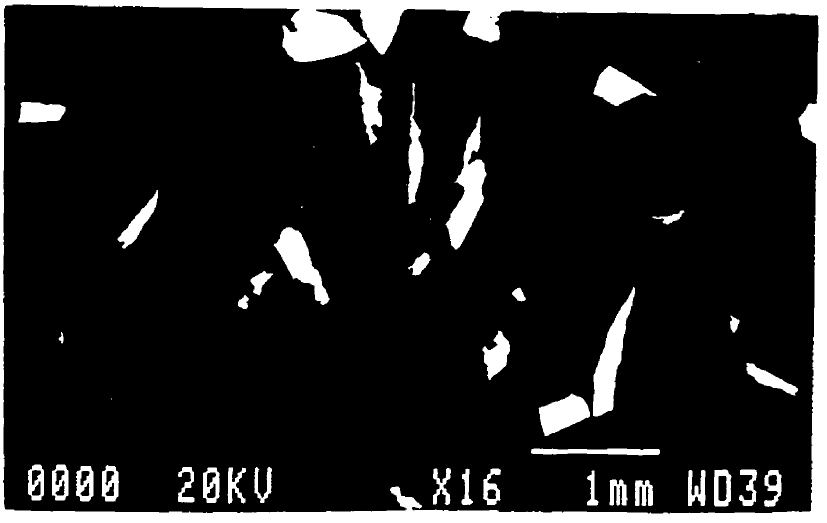

Fig. 2.5: SEM backscattered electron micrograph of simple-locked, glass/resin particles created using sandblasted glass slides (light phase is glass; dark phase is ERL-4221 resin; grey phase is mounting medium).

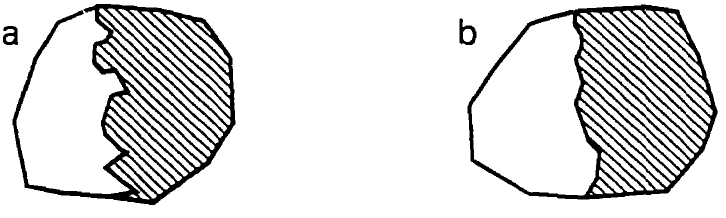

Fig. 2.6: A sharp, pitted interface (a) provides better resistance to breakage along the interface than a gently sloping interface (b).

The small amount of locked particles produced in all the experiments using roughened glass surfaces can be explained by considering the sharpness of the scratches on the glass surfaces. In all the tests, the scratches, regardless of depth, were gently sloping. They were not sharply pitted as desired (Fig. 2.6). Deep, sharp pits on the glass surface would have provided the best resistance to the shear force caused by breakage. Due to the lack of locking, it was decided to abandon using epoxy resin as the matrix material.

2.3.2 Titanium dioxide/silica tests

It was discovered in high temperature experiments to separate titanium dioxide (TiO_2) from silica in Norway [37] that the TiO_2 formed discrete well-dispersed droplets in the silica matrix. After cooling, the TiO_2 remained as discrete droplets in the silica and when this material was crushed, most of the resulting particles were locked. A material such as this would be ideal for the standard material. Experiments were carried out to explore this possibility. This material could prove to be superior to the glass/resin standard material by possessing a stronger bond between the phases thus limiting breakage along the interfaces. Also, TiO_2 is significantly more brittle than resin and has fracture qualities similar to silica.

In the first test, particles of TiO_2 (75-106 μm) from QIT (Quebec Iron and Titanium Co.) and fine silica (-45 μm) were mixed together at 60 vol. % silica. This mixture was pressed into a disk (3 cm diameter, 1 cm thick) with a hand press. The melting point of TiO_2 is 1830-1850°C [38(p.B-160)] and the melting point of silica is 1610°C [38(p.B-143)]. The disk was placed in a tube furnace (maximum temperature = 1700°C) set to 1550°C. The furnace required 8 hours to reach 1550°C and was left at this temperature for half an hour before the power was shut off. The disk was removed the following day. A visual inspection of the disk showed that the silica had melted and formed a continuous phase around the TiO_2. The disk was cut with a diamond saw and a surface polished and examined by SEM. It revealed that although the silica had softened and formed a continuous phase around the TiO_2, the silica

contained many voids (10-100 μm) and the TiO_2 remained as grains and did not become discrete droplets.

Two further tests were conducted with the tube furnace. Two disks were created: the first consisted of 75-106 μm TiO_2 and -45 μm silica at 60 vol. % silica and the second consisted of 75-106 μm TiO_2 and -38 μm glass from White Glass Inc. (henceforth simply referred to as glass) at 60 vol. % glass. Both disks were placed in the furnace and the temperature was set to 1600°C. The furnace required 10 hours to reach this temperature. This temperature was maintained for 45 minutes before the furnace was shut off. The disks were removed the following day. It was discovered that the glass in the second disk had become completely non-viscous and had leaked into the bottom of the crucible. The first disk, though, had become quite compact. It was cut, polished and examined by SEM. The examination revealed that the silica had formed a continuous, nearly non-porous matrix around the TiO_2 and the TiO_2 grains had started to fragment into droplets and diffuse into the silica (Fig. 2.7). Unfortunately, these droplets were very small (-10 μm). This is not desirable because this material would produce a large amount of complex locking and very little simple locking unless the particle size was much smaller than 10 μm.

Due to the fragmentation of the TiO_2 into very small droplets, the use of silica as the matrix material was abandoned. The glass though, due to its low viscosity, appeared to be a promising matrix material.

2.3.3 Glass matrix tests

Tests were performed to examine the possibility of using glass as the matrix material. In a previous test, it was observed that glass at 1600°C became extremely non-viscous. Glass has a lower melting point than silica due to the fluxing agents that are added during its production. If glass is used as the matrix material then these tests should be performed at the lowest possible temperature because it is preferable in this case that the grain material retain its original shape and not fragment into droplets. The ideal temperature to create the standard material is at the point where the glass becomes

sufficiently non-viscous that air bubbles can escape and where the grain material becomes slightly non-viscous so that upon cooling it forms a strong bond with the glass.

In the first test, 300-425 μm TiO_2 particles were mixed with glass powder (-38 μm) at 50 vol. % glass and placed in a refractory crucible. The material was not pressed into a disk. This mixture was heated to 1000°C (which required 6 hours) and maintained at this temperature for 4 hours. The resulting block of material was cut with a diamond saw into smaller pieces and crushed. Four fractions (425-600 μm, 300-425 μm, 212-300 μm and 150-212 μm) were screened out, mounted and polished. A SEM examination of the fractions revealed that many locked particles were formed (Fig. 2.8). There were voids (25-100 μm) in the glass and most of the particles were complex-locked, but there was no fragmentation of the TiO_2 into droplets and the large amount of locking seemed to indicate that there was a good bond between the two phases. Even at the smaller particle sizes, there was still a substantial amount of locking. This method of producing locked particles appeared to be quite promising so a series of tests were performed using glass as the matrix material with various different grain materials.

The ideal grain material should have the following qualities:

1) homogeneous - There should be little variation in the density of the grain material.
2) low porosity - Excessive porosity may cause variation in the density.
3) similar breakage characteristics to glass - This would prevent excessive preferential breakage.
4) high melting point - The grain material must be able to maintain its original shape and not fragment into droplets.
5) available in large sizes - The grain size must be sufficiently large so that if the locked block is crushed to several size classes below the grain size (in an attempt to increase the amount of simple locking), the resulting particles would still be large enough to permit accurate density separations.

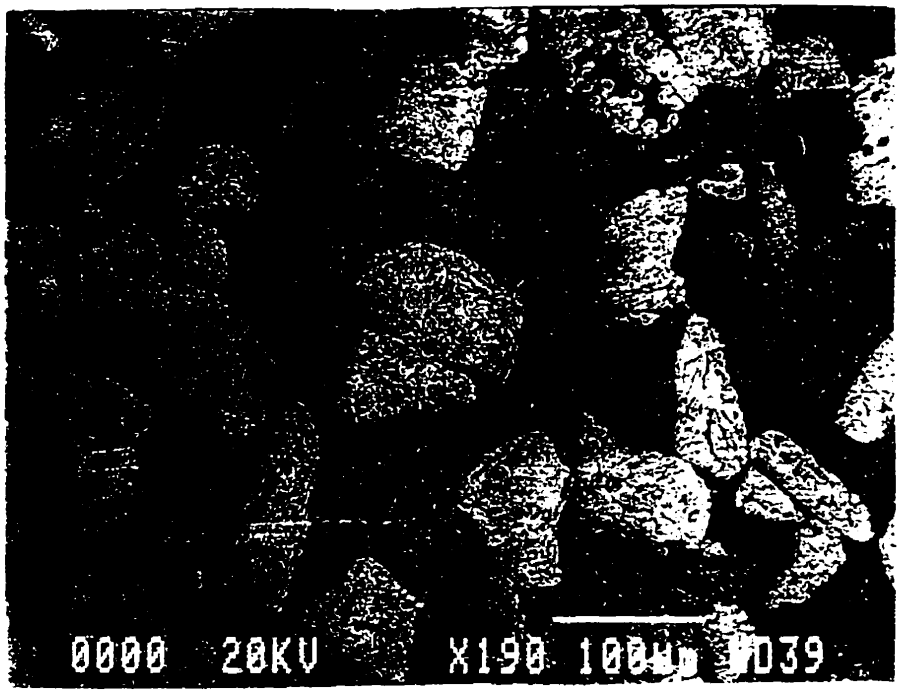

Fig. 2.7: SEM secondary electron micrograph of TiO2 grains in a silica matrix (light phase is TiO2; grey phase is silica; dark patches are voids).

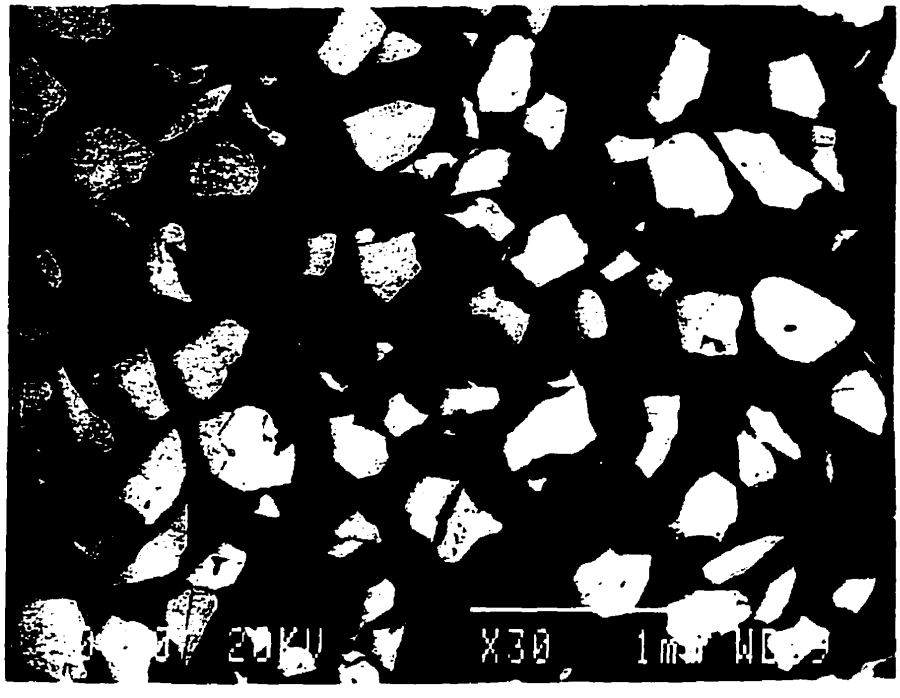

Fig. 2.8: SEM backscattered electron micrograph of 300-425 um TiO2/glass locked particles (light phase is TiO2; grey phase is glass; dark phase is mounting medium).

6) possess a significantly higher density than glass - The larger the density difference between the two phases, the more accurate the density fractionation. Also, a large density difference would make the differentiation of the phases easier with SEM backscattered electron imaging.

7) possess a density which is low enough to allow density fractionation - The density of the grain material should not exceed the upper limit of the separation method if a complete density fractionation is desired.

8) non-magnetic - This is only necessary if magnetogravimetric separation is used for density fractionation.

Several prospective candidates for the grain material were examined:

1) fayalite pellets, 106-300 μm
2) MgO, 2 mm particles
3) Nb_2O_5, 99.8% pure, 1-3 mm (Aldrich Inc.)
4) TiO_2 tablets, 99.5-99.9% pure, various sizes (Cerac Inc.)
5) VO_2, 150 μm (Cerac Inc.)
6) ZrO_2, 99.7% pure, 3-12 mm sintered tablets (Cerac Inc.)
7) TiO, 99.9% pure, 1-3 mm pieces (Cerac Inc.)
8) TiO_2, $D_{80} \approx 150$ μm (Continental Minerals Inc.)
9) $ZrSiO_4$, 200 μm (Continental Minerals Inc.)
10) unchlorinated TiO_2, 1 mm (QIT)
11) Al_2O_3 (tabular alumina), 3 mm
12) ZrO_2 (naturally-occurring), 95% -212 μm (Zirconia Sales Inc.)
13) ZrO_2 (synthetic), 5 mm (Norton Zirconia Inc.).

These materials were mounted in resin, polished and examined by SEM. The problem with the majority of these materials was that there was a trade-off between porosity and homogeneity. The naturally-occurring materials were available at large sizes, but in most cases, they contained an unacceptably large amount of impurities. The artificial materials, generated using a fusion or sintering process, were of high-purity, but in most

cases, they contained an unacceptably large number of voids. Besides the TiO_2 (from QIT) that was tested earlier, only three of the materials listed above were found to be acceptable: unchlorinated TiO_2, Al_2O_3 and ZrO_2 (both naturally-occurring and synthetic). The densities of TiO_2, unchlorinated TiO_2, Al_2O_3 and ZrO_2 were measured to be 3.96 g/ml, 3.98 g/ml, 3.97 g/ml and 5.80 g/ml, respectively. Using these materials as the grain material, a series of tests were performed under different conditions:

1) two matrix materials were tested: glass and borosilicate glass (a low melting point glass)
2) two volumetric proportions of matrix material: 60% and 80%
3) different furnaces and crucibles
4) different particle/grain size relationships
5) different strategies were employed to prevent the occurrence of voids in the glass:
   a) increased temperature - by increasing the furnace temperature, the viscosity of the glass may be reduced to the point where the air bubbles rise and leave the glass
   b) use of a vacuum furnace - by applying a vacuum during heating, the air bubbles may be drawn out
   c) pressing the mixture into a pellet before heating - by forcing the fine glass particles closer together, the initial void space would be reduced.

The results of these tests are in Appendix 1. A summary of the results follows.

Borosilicate glass (2.48 g/ml) had a lower melting point than glass. This was borne out in the first tests and thus, it was used in a majority of the subsequent tests.

The results using different grain materials were as follows:

1) TiO_2 - Although TiO_2 grains had small voids (1-2 μm), they were evenly distributed throughout the grains and thus provided a constant density. Unfortunately, these voids were infiltrated by glass in these tests and there was a tendency for the TiO_2 to begin to fragment into small pieces at approximately 1200°C. Another problem with the TiO_2 was that it contained deep cracks that

were up to 10 μm wide. Glass infiltrated these cracks and this greatly increased the instances of complex locking.

2) unchlorinated TiO_2 - This material was much less porous than the TiO_2 and as a result there was less glass infiltration. Although it, too, started to fragment at higher temperatures, it did so to a lesser degree than with TiO_2. It also appeared to contain fewer cracks than TiO_2.

3) Al_2O_3 - The Al_2O_3 was non-porous and did not exhibit any fragmentation, but it was very difficult to crush due to its hardness. When the Al_2O_3/borosilicate glass blocks were crushed, the borosilicate glass broke preferentially. As a result, the locked particles contained a high vol.% Al_2O_3. Most of the borosilicate glass became fine, free particles.

4) ZrO_2 - Naturally-occurring ZrO_2 (Zirconia Sales Inc.) grains had low porosity and did not exhibit any fragmentation, but they were not available at a high purity at a sufficiently large size. Synthetic ZrO_2 (Norton Zirconia Inc.) grains proved to be very hard. As with the use of Al_2O_3, this led to the preferential breakage of the borosilicate glass.

Temperatures ranging from 800 to 1500°C were tested. It was found that the borosilicate glass required a temperature of 1200°C or higher to make it sufficiently non-viscous so that air bubbles could escape and the excessive occurrence of voids avoided.

Different furnaces produced varying results:

1) gas furnace - The maximum temperature that could be reached was approximately 1100°C. The temperature was difficult to control with fluctuations of up to 30°C.

2) vacuum furnace - The use of a vacuum while heating did not prove to be effective in preventing voids.

3) induction furnace - This type of furnace was easy to use and control. It was used in a majority of the tests.

Two types of crucibles were tested: slip-cast alumina and refractory (A.P. Green Refractories Ltd.). The alumina crucibles were fragile and sometimes cracked, spilling the sample, but otherwise, the sample was easy to remove from the crucibles after heating. The refractory crucibles proved more durable, but since they were quite porous, the glass infiltrated the pores and this made the sample difficult to remove. In either case, the crucible had to be broken to remove the sample. In most of the tests, refractory crucibles were used due to their durability and lower cost.

Pressing the mixture into a pellet before heating failed to reduce the number of voids in the samples. The borosilicate glass became so non-viscous that all the pellets collapsed at approximately 900°C.

At 60 vol.% matrix material, with the particle and grain sizes equal, a large amount of locked particles was produced, although most were complex-locked. At 80 vol.% matrix material, slightly fewer locked particles were produced, but there was a slight increase in simple locking. In both cases, a significant amount of locking was produced. The particle/grain size relationship was found to have a much greater impact on the amount and texture of the locking than the vol.% matrix material.

In all the tests, the bonding between the grain and matrix phases was quite strong and many locked sections were observed even when the particle size was several Tyler size classes below the grain size. In general, when the particle size was one size class below the grain size, a majority of the locked sections were complex-locked. When the particle size was two size classes below the grain size, roughly equal amounts of complex and simple-locked sections were observed. As the particle size decreased, the amount of simple locking increased and the complexity (the number of interfaces between the two phases) of the complex-locked sections decreased (i.e. there were fewer interfaces). Of course, the stereological bias has to be taken into consideration in any microscopic examination of locking texture, but there is no method of accurately determining the amount of simple locking.

Of all the tests, the best results were achieved under the following conditions:

1) 300-425 μm unchlorinated TiO_2
2) 80 vol.% borosilicate glass (-38 μm)

3) refractory crucible
4) 40 minutes at 1200°C in an induction furnace
5) particle size of 150-212 μm (i.e. 2 Tyler size classes below the grain size).

There were still some problems with the standard material created under these conditions:

1) Although there was not a large amount of fragmentation, there were still some areas where small fragments of unchlorinated TiO_2 had moved from a grain into the glass matrix. Also, small (≈ 1 μm) fragments of material yielding a sharp iron peak were observed in the borosilicate glass using SEM EDS analysis; the most likely source of this contaminant is the unchlorinated TiO_2 (which contains minor amounts of iron).
2) Using SEM EDS analysis, a small amount of titanium was observed in the borosilicate glass near its interface with the unchlorinated TiO_2. This may indicate that a small amount of TiO_2 diffused into the borosilicate glass. This could be a problem if the diffusion altered the density of the borosilicate glass.
3) Although it was possible to reduce the incidence of voids in the borosilicate glass by increasing the temperature, they could not be completely eliminated. Approximately 3% of the borosilicate glass sections contained small (< 10 μm) voids.

2.3.4 Hot press test

The fragmentation and diffusion of the grain material into the matrix material was caused by the high temperatures used to prevent the occurrence of voids in the matrix. The use of a hot press may provide the solution to this problem.

If pressure is applied to the sample while it is heated, the voids may be eliminated. Pressing could be performed at a temperature lower than that used in the induction furnace since the pressure can be applied as soon as the borosilicate glass is soft; a very low viscosity is not necessary. It was expected that the lower temperature would prevent fragmentation or diffusion of the grain material.

The use of pressure in the creation of the standard material should also promote simple locking. Since the borosilicate glass could be pressed at a lower temperature, it would be more viscous. The higher borosilicate glass viscosity should help support the grains and prevent their contacting each other. The reduction in the incidence of touching grains would reduce the chance of particles containing parts of two grains, thus increasing the chance of simple locking.

A test was performed using the McGill University hot press with 300-425 μm unchlorinated TiO_2 and borosilicate glass at 80 vol.% glass. The sample was placed in a 1.5" graphite mold and the temperature was set to 800°C at a heating rate of 10°C/min. Once the furnace reached 800°C, the temperature was maintained for 0.5 hour and a 2 tonne load was applied. The cooling rate was 14°C/min. and the load was maintained until the temperature dropped to 600°C.

The resulting sample was a thin, compact, cylindrical disk. It had fused with the graphite mold and had to be cut off. The disk was crushed and the 150-212 μm fraction was screened out. SEM examination of the particles revealed many locked sections. The borosilicate glass sections did not contain any voids and the unchlorinated TiO_2 showed no signs of fragmentation. Also, SEM EDS analysis revealed that there was no diffusion of unchlorinated TiO_2 into the borosilicate glass near the interface and there were no fine (1 μm) iron fragments in the glass. This was the best standard material produced up to this point. There were, however, two drawbacks to this method:

1) It would be difficult to produce large quantities of this material due to the small size of the mold that can fit in the hot press and the fact that each test requires a day to complete.
2) The hot press is difficult and expensive to operate.

2.3.5 TiO hot press tests

There were two weaknesses to the unchlorinated TiO_2/borosilicate glass standard material:

1) The density of unchlorinated TiO_2 (3.98 g/ml) is relatively low and close to that of the borosilicate glass (2.48 g/ml). A higher density grain material would provide better resolution in density separations.
2) There is no method of creating layered locking or simple locking using unchlorinated TiO_2 as the grain material. The method of alternating layers cannot be used since unchlorinated TiO_2 is not available in thin, flat layers.

Due to the limitations of using unchlorinated TiO_2 as the grain material, other materials were examined. As discussed earlier, a suitable grain material was hard to find since few materials met all the necessary requirements. Very pure materials could be found, but were only available at small particle sizes. Large particles of a given material could be found, but these particles were either naturally-occurring materials which contained impurities or a fused or sintered material which contained voids. The concern over the purity and porosity of the grain material of the standard material may seem to be over-stressed, but it is legitimate. These variables affect the density of the grain material. Care should be taken to make sure that the density of the phases is constant so that the density separations are as accurate as possible. Also, impurities and voids create unpredictable results when image analysis is performed. They may be interpreted to be part of the matrix phase or part of the mounting medium.

Since large particles of a pure material could not be found, an attempt was made to create large particles by hot pressing a powder. The maximum temperature that could be reached with the hot press was 1800°C; consequently, only those materials which softened sufficiently below this temperature could be considered. Pure ZrO_2 (5.60 g/ml) has a melting point of 2715°C [38(p.B-254)] and thus could not be used. Pure TiO_2 has only a slightly higher density (4.26 g/ml in rutile structure) than the unchlorinated TiO_2 and a relatively high melting point of 1825°C [38(p.B-254)], but pure titanium monoxide (TiO) has a significantly lower melting point, 991°C [38(p.B-254)], and the advantage of a higher density, 4.93 g/ml [38(p.B-160)] and thus TiO was selected for hot press tests.

If the TiO could be successfully pressed into a compact block, then it could be broken into particles for use as the grain material of the standard material. If this was possible then tests could be conducted examining the possibility of pressing TiO into thin, compact layers. These layers could then be pressed with alternating layers of borosilicate glass powder to form a block possessing layered locking. If the block was broken below the thickness of the layers, simple-locked particles would be produced.

TiO from Cerac Inc. (99.9 % pure; -38 μm) was hot pressed under different conditions using the Ottawa CANMET (Canadian Centre for Minerals and Energy Technology) and McGill University hot presses. The resulting block of TiO was cut, polished and examined by SEM. The results are summarized in Table 2.3. The CANMET hot press was larger than McGill's and could accommodate a larger volume of material. This was not taken advantage of during these tests since they were performed only to examine the possibility of creating a compact block.

The results indicate that the hot press was only successful in reducing the size of the voids in the TiO down to $\approx$ 5 μm. This is not sufficient since previous tests have indicated that glass will infiltrate such voids. Another problem was that the voids were unevenly distributed throughout the sample. The area near the top or bottom surface of the sample (i.e. the areas that were in contact with the graphite piston) contained fewer and smaller voids than the rest of the sample. If voids are to be tolerated in the grain material, they must not only be small, but evenly distributed, otherwise this will create variations in the material density. In some of the tests, contamination was observed. A SEM EDS analysis of these small occurrences indicated that they were composed of titanium, iron and copper. The source of this contamination is unknown, but it is suspected that it may originate from the grinding medium (the TiO was ground at McGill using a pulverizer with a puck and ring configuration). One test was conducted using TiO_2 powder, but it was not successful.

Table 2.3: Results of the hot pressing of TiO under different conditions.

Hot press	Mass TiO (g)	Temp. (°C)	Time at temp. (min.)	Pressure† (MPa)	Comments from SEM examination of TiO polished surface
McGill test 4-184	30	1550	0	17.2	10-30 μm voids
CANMET test 6-224	30	1700	30	19.0	10 μm voids
McGill test 6-104	30	1750	60	17.2	5-10 μm voids
McGill test 9-024	25	1750	180	17.2	5 μm voids; there were 1 μm contaminants
McGill test 7-194	21 (TiO_2 powder)	1750	60	17.2	20-30 μm voids
CANMET test 8-294	25	1800	180	16-18	2-5 μm voids; there were 1-5 μm contaminants

† The pressure was applied as soon as the material softened.

An X-ray diffraction (XRD) analysis was performed on the TiO before and after hot pressing. There were some differences between the spectra of the two samples, indicating that there was some structural change. Other titanium oxide phases may have been formed in the hot press.

Due to these difficulties, the attempt to create a grain material using the hot press was abandoned. Due to the difficulty of finding or creating a suitable grain material, this whole approach to generating the standard material was abandoned.

2.3.6 Leaded glass additives tests

A new approach to creating the standard material was developed. Tests were conducted using leaded glass additives as the matrix material and glass particles as the grain material. Leaded glass additives are more commonly used as a source of lead for glass melts or ceramic glazes, but in this work they will be used by themselves as one of the phases of the standard material. These additives have a low melting point and a high density.

Three leaded glass additives (Hammond Lead Inc.) were tested:

1) lead borate ($2PbO \bullet B_2O_3$) (melting point = 490-510°C; ρ = 6.98 g/ml)
2) lead monosilicate ($PbO \bullet 0.67SiO_2$) (melting point = 700-748°C; ρ = 6.55 g/ml)
3) tribasic lead silicate ($PbO \bullet 0.33SiO_2$) (melting point = 705-733°C; ρ = 7.60 g/ml).

In a series of preliminary tests, each additive (in powder or fine granular form) was placed in a refractory crucible along with 850-1700 μm glass particles. Since the glass had a lower density than the additives, it was expected that the glass would float to the top of the additives. In the crucibles, the glass was placed at the bottom and the additive was placed on top so that the additive would wet the surface of the glass as it rose to the top. The material was heated to 50°C above the melting point of the additive for 30 minutes in an induction furnace. After cooling, the samples were removed and crushed to 600-850 μm. The leaded glass additives were as brittle as the glass and the sample broke easily. The particles were mounted and examined by SEM.

The tribasic lead silicate did not become very non-viscous and as a result, the glass stayed at the bottom of the crucible and did not embed in the silicate. Both the lead borate and the lead monosilicate, however, produced promising results. Both additives bonded well with the glass and many locked sections were observed. There were only a few small (<10 μm) voids present in the additives. There was no evidence of fragmentation of the glass. Of these two additives, lead borate (henceforth simply referred to as borate) appeared to be the most suitable for the standard material because it possessed the lowest melting temperature, highest density and lowest viscosity.

A SEM micrograph of a polished surface of glass grains embedded in a borate matrix before breakage is shown in Fig. 2.9. The borate forms a continuous matrix around the glass grains. Although there were some large (>50 μm) voids in the borate, the subsequent breakage of the block eliminated them.

Two parameters had to be determined: the particle/grain size relationship and the method of density fractionation. These parameters depended upon the density of the borate.

In this work, density was measured with a water displacement technique [66] using a pycnometer bottle (25 or 100 ml depending upon the volume of the sample). A pycnometer bottle is a glass bottle fitted with a glass stopper that contains a small length-wise hole through which excess water can escape. With the stopper in place, the bottle is designed to hold a constant volume.

The density is calculated thus:

$$\rho = \frac{(M - P)}{W + (M - P) - F} \qquad (2.1)$$

where P = mass of dry, empty pycnometer bottle

M = mass of dry bottle with the sample in the bottle

F = mass of bottle with the sample in the bottle filled with water

W = mass of bottle full of water only.

Air bubbles in the water were removed by placing the bottle in an ultrasonic bath. For optimum results, the sample should occupy approximately 30-40 vol.% of the pycnometer bottle.

Using a 100 ml pycnometer bottle, the density of the borate was measured to be 6.833 g/ml ($\pm$0.006) (this is slightly different from the density quoted by the manufacturers (6.98 g/ml)). Due to high density of the borate, conventional heavy liquids could not be used to fractionate this standard material so a decision was made to use the Magstream separator, a centrifugal magnetogravimetric separator (described in Section 3.3).

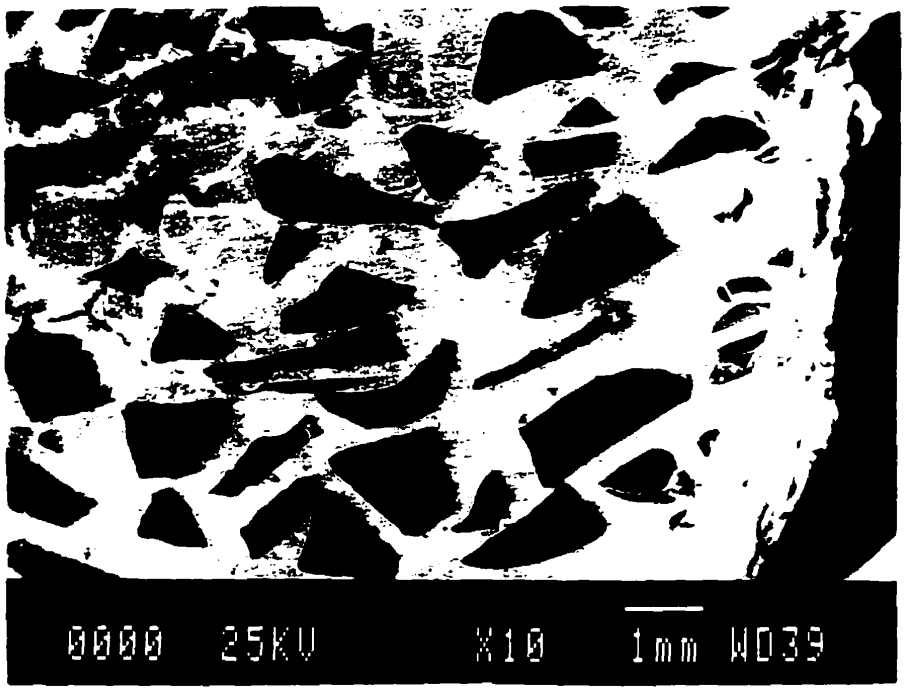

Fig. 2.9: SEM secondary electron micrograph of glass grains in a lead borate matrix (light phase is lead borate; grey grains are glass).

The decision to use the Magstream meant that the particle size would have to be 425-600 μm since this is the largest particle size that the Magstream Model 100 can accommodate and since the Magstream splits are more accurate with larger particles. The grain size was set to 1180-1700 μm which is three Tyler size classes larger than the particle size. This should provide a significant amount of simple locking.

Glass rather than borosilicate glass was used as the grain material. This was done because it is desirable that the grain material have a high melting point to prevent it from diffusing into the borate. Silica (which has a significantly higher melting point than either glass or borosilicate glass) was considered as the grain material, but the use of glass rather than silica allows greater control over the locking texture: with silica, it would be impossible to perform the tests using alternating layers of material to produce layered and simple locking. Also, there is always the chance of impurities when using naturally-occurring materials. The density of the glass was measured to be 2.502 g/ml ($\pm$0.001) using a 100 ml pycnometer bottle.

2.3.7 Crucible selection

The initial tests with the glass/borate standard material were performed in refractory crucibles, but the borate was sufficiently fluid that it infiltrated the pores of the crucible and made it difficult to remove. The crucible had to be broken and the sample chipped out. This was a very laborious process and raised the possibility that pieces of the crucible might contaminate the standard material. Different types of crucibles were tested to solve this problem:

1) graphite crucible - These crucibles were similar to the ones that were used in the hot press tests. The problem with the use of this type of crucible is that the borate became fluid enough to leak out of the crack between the cylinder and piston at the bottom of the crucible. Also, the sample could not be removed without having to break them. This is not desirable since graphite crucibles are quite expensive.

2) slip-cast alumina crucible - The sample was very difficult to remove from alumina crucibles even when a lubricant (graphite coating) was applied because the alumina and borate bonded together very strongly.

3) porcelain crucible (Fisher Scientific Inc.) - Although these crucibles had to be broken to remove the sample, the sample was easily removed and came out in one piece. These crucibles were relatively inexpensive and became the crucible of choice in the creation of the standard material.

2.3.8 Production of glass/lead borate standard material particles

The procedure for the creation of the glass/borate standard material was as follows:

1) 30 g of 1180-1700 μm glass particles were placed in a 40 ml porcelain crucible
2) 60 g of powdered borate was placed on top
3) the crucible and sample were placed in an induction furnace pre-heated to 600°C and this temperature was maintained for 30 minutes
4) the power was shut off to the furnace and the crucible was allowed to cool to room temperature
5) the sample was removed from the crucible, crushed and wet-screened to remove the fines
6) the 425-600 μm fraction was screened out.

SEM backscattered electron micrographs of this material are shown in Fig. 2.10. There were a few voids in the borate sections, but they were small (< 10 μm) and were present in approximately only 1% of the borate sections. It appeared that there were slightly more simple-locked sections than complex-locked sections. The complexity of the complex-locked sections was low; most of the complex-locked sections contained only two interfaces.

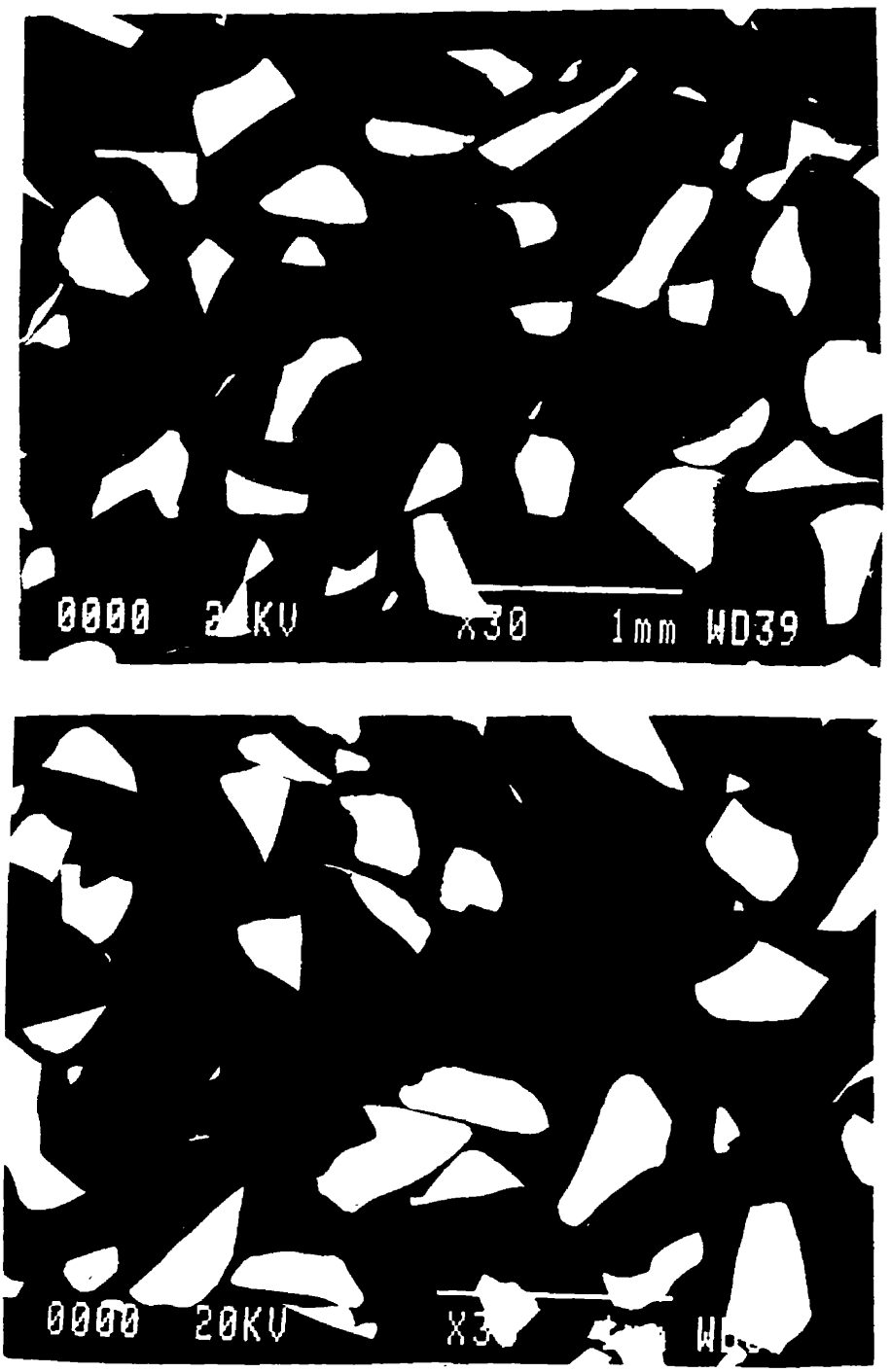

Fig. 2.10: SEM backscattered electron micrographs of 425-600 um glass/borate standard material particles (light phase is lead borate; grey phase is glass; dark phase is mounting medium).

A SEM EDS analysis was performed to determine if there was diffusion of one phase into the other. The glass sections yielded peaks corresponding to silicon, aluminum and calcium; no lead peak was observed indicating that there was no borate in the glass. The borate sections yielded a peak corresponding to lead and an unidentified peak. This unidentified peak was near the area where a peak for silicon or tungsten would occur. The sample was analyzed on a microprobe, but it still could not be identified. (A later full microprobe analysis of the sample revealed that there was significant diffusion of glass into the borate. The resolution of that problem is described in the next chapter.)

The production procedure created blocks containing 42 % borate by volume. Tests using different proportions of glass and borate (27-52 vol. % borate) were performed. There were changes in the quality of the standard material only at the extremes. At a very high vol. % borate, there was excess borate resulting in an increase in the number of free borate sections. At a very low vol. % borate, there was insufficient borate to fill the voids between the glass grains and the borate became very porous.

A test was performed at 700°C to determine if the borate could be made more fluid and thus eliminate all the voids. SEM examination of this sample revealed that there appeared to be the same number of voids as at 600°C. A further increase in temperature was not attempted since this could lead to diffusion of one phase into the other.

The density fractionation of the standard material (discussed in the next chapter) creates several locked particle composition fractions. The material that was -5 vol. % borate or +95 vol. % borate was considered to be free. Although some particles in these fractions are locked, they are, for practical purposes, free. The creation of the true free material (i.e. material containing 100 % of one phase only) for the standard material is straightforward. True free glass was created simply by crushing glass to 425-600 μm. True free borate was created by placing borate powder alone in porcelain crucibles and heating it to 600°C for 30 min. After the borate had cooled and solidified, it was removed from the crucible and crushed to 425-600 μm.

2.3.9 Production of simple-locked, glass/lead borate standard material particles

Tests were conducted to examine the possibility of creating simple locking using the method of alternating layers described earlier. Ten glass slides (75 x 25 mm) with a thickness of 1 mm were placed parallel to each other, separated by a gap of 1 mm, into a crucible containing 250 g of borate powder. A series of these samples was placed in the furnace at 600°C for different time periods. The material was allowed to cool to room temperature and was crushed. The 425-600 μm fraction was screened out, mounted in resin, polished and examined by SEM. The results are summarized in Table 2.4.

The optimum time period in the furnace appeared to be 45 minutes. A SEM micrograph of these simple-locked particles is shown in Fig. 2.11. In tests using a shorter time period, the glass and borate did not have sufficient time to bond, resulting in excessive breakage along the interface and few locked particles. In tests using a longer time period, the slides became soft and began to bend causing the 1 mm gap between the slides to narrow. This resulted in complex locking.

Tests were performed in an attempt to prevent the bending of the slides. It was thought that the cause of the bending was due to the glass slides collapsing under their own weight. The solution to this was to suspend the glass slides in the bath of borate so that they did not touch the bottom of the crucible. The tests at longer time periods (i.e. > 45 minutes) were repeated, but it was found that this did not make any noticeable difference; the slides still became bent.

With a time period of 45 minutes, approximately 16% of the particles were observed to be locked, but this number is stereologically biased; the actual amount of locking should be greater than this. The true amount of locking can be roughly estimated by assuming the particles are single-capped spheres (i.e. spheres exhibiting simple locking with planar interfaces). Using a simple rule-of-thumb correction (Gateau and Broussaud [14]), it was estimated that 21% of the particles were locked. This is a relatively low amount of locking (compared to the amount of locking generated by the breakage of granular-texture blocks), but it should supply a sufficient amount of locking so that the creation of locked particles is not too tedious.

Table 2.4: Results of the simple-locked, glass/borate particles tests.

Time in furnace at 600°C (min.)	Observational frequency (%) of simple-locked particles	Comments
†0	< 1	Excessive breakage along the interfaces occurred.
15	< 1	Excessive breakage along the interfaces occurred.
30	9	Some breakage along the interfaces occurred, but a significant amount of locked particles was observed. All the locking was simple locking with planar interfaces. There were only a few instances of partial breakage along the interfaces observed.
45	16	Same comments as the 30 minute test.
60	26	The slides began to bend. This caused a narrowing of the gap between the slides. Only the part of the block of material where the slides did not bend was crushed. Many simple-locked particles with planar interfaces were observed.
> 60	-	In tests using a time period above 60 minutes, the slides became bent (so much so in some cases that they touched). As a result, complex-locked particles were observed.

† In this test, the borate alone was placed in the furnace until it became a liquid. It was then removed from the furnace and the glass slides inserted.

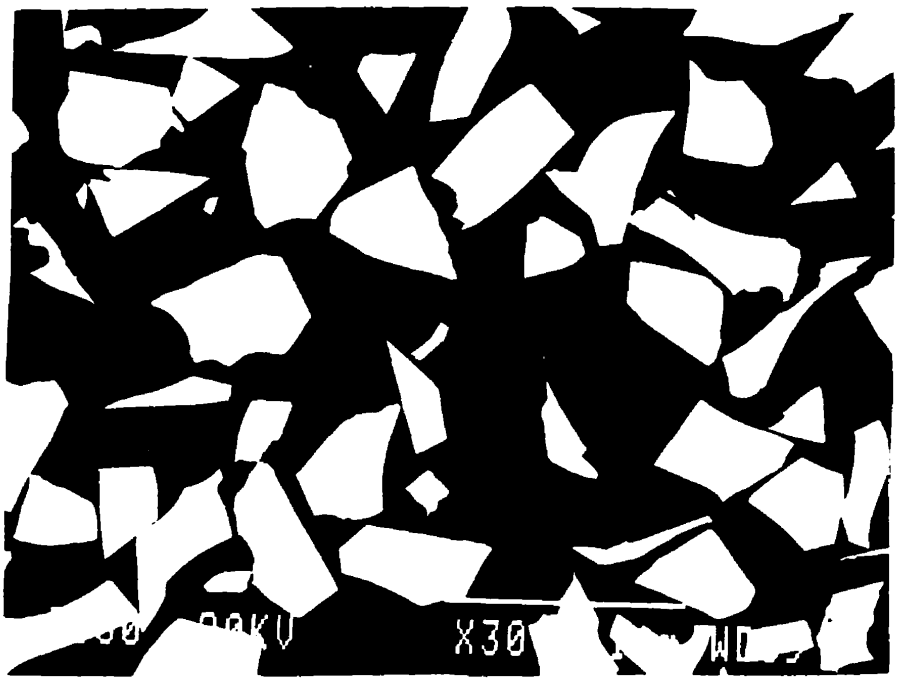

Fig. 2.11: SEM backscattered electron micrograph of 425-600 um simple-locked, glass/borate standard material particles (light phase is borate; grey phase is glass; dark phase is mounting medium).

One method of increasing the locking would be to use glass slides with a thickness of 600 μm. This would increase the chance that a particle would break across an interface since the particle size was 425-600 μm. Slides with a thickness of 1 mm were used in these tests because they were easily obtained; this is the standard thickness of glass microscope slides. Glass slides with a different thickness would have to be special-ordered.

The particle size of the simple-locked particles was chosen to be 425-600 μm because the granular-texture standard material was this size. If the simple-locked and the granular-texture standard materials were to be combined to form a liberation distribution, the particles would have to be the same size.

Although simple-locked particles with planar interfaces were successfully created, they were not density fractionated since it was decided at this point to test the stereological correction procedures using the granular-texture standard material particles only.

Simple-locked and layered-texture particles are a useful supplement to the granular-texture standard material. In future work, they could be used to test the correction procedures by themselves or combined with granular-texture particles.

CHAPTER 3: SEPARATION PROCEDURES AND RESULTS

Since the density of the glass/lead borate standard material ranged from 2.502 to 6.833 g/ml, it was necessary to find a density separation procedure that could cover this range. Three density separation procedures were evaluated:

1) use of a suspension of tungsten carbide (WC) particles in sodium polytungstate (SPT)
2) magnetogravimetric separation
3) Magstream separation (centrifugal magnetogravimetric separation).

3.1 WC-SPT suspensions

The range of conventional heavy liquids can be expanded by the addition of fine particles of a heavy, inert material to create a suspension [39,40]. By adjusting the concentration of the particles or the density of the heavy liquid, the density of the suspension can be controlled. The inert material should be fine enough so that it remains suspended while the separation occurs. For suspensions, the larger the feed particles, the quicker and more accurate the separation.

Sodium polytungstate (SPT), an inorganic, water-soluble heavy liquid, appeared to be a good candidate for this type of work since it is relatively fluid at high densities and non-toxic and thus easy to work with. The density of SPT can be easily adjusted by adding or evaporating water. The highest density possible with SPT alone is 3.1 g/ml.

Tests were conducted by Rhodes et al. [41] to increase the range of SPT up to 4.18 g/ml using fine ($<38\ \mu m$) ferrosilicon particles. They fractionated a lead ore using this suspension and although the separations were quite accurate, the particles that were separated were quite coarse (4-8 mm). In their work, there was no attempt to determine the minimum particle size that could be separated, but there could be difficulties

separating smaller particles using this type of suspension since mixing was necessary to keep the ferrosilicon particles in suspension during the separation.

Sometu Inc., the manufacturers of SPT, have reported [42] that the density of a SPT solution could be increased through the addition of fine (0.8 μm) particles of tungsten carbide (WC). WC was recommended for this application because it is inert and has a high density (15.6 g/ml [38(p.B-160)]). Sometu Inc. suggested that the density of the SPT be raised up 3.1 g/ml and then WC particles added according to Fig. 3.1.

In this work, WC particles (Osram Sylvania Inc., 99.97% pure) in the size range 0.50 to 0.65 μm were used. The suspension density was measured with a 100 ml pycnometer bottle.

The preparation procedure suggested by Sometu Inc. was followed, but several problems were encountered. The WC did not disperse well in the SPT and as a result, the WC-SPT suspension had to be placed in an ultrasonic bath to break up agglomerates of WC. Although the WC did eventually disperse, this required several hours and during this time, the SPT started to crystallize and water had to be added to prevent the suspension from solidifying. It also was discovered that Fig. 3.1 incorrectly predicted the density of the suspension. The pycnometer-measured density of the suspension was higher than the value obtained from the graph for a given vol. % WC.

The solution to the crystallization of the SPT was to start with a SPT solution of approximately 2.65 g/ml and then add the appropriate amount of WC to generate the desired suspension density. The amount of WC to be added can be calculated using the following equation:

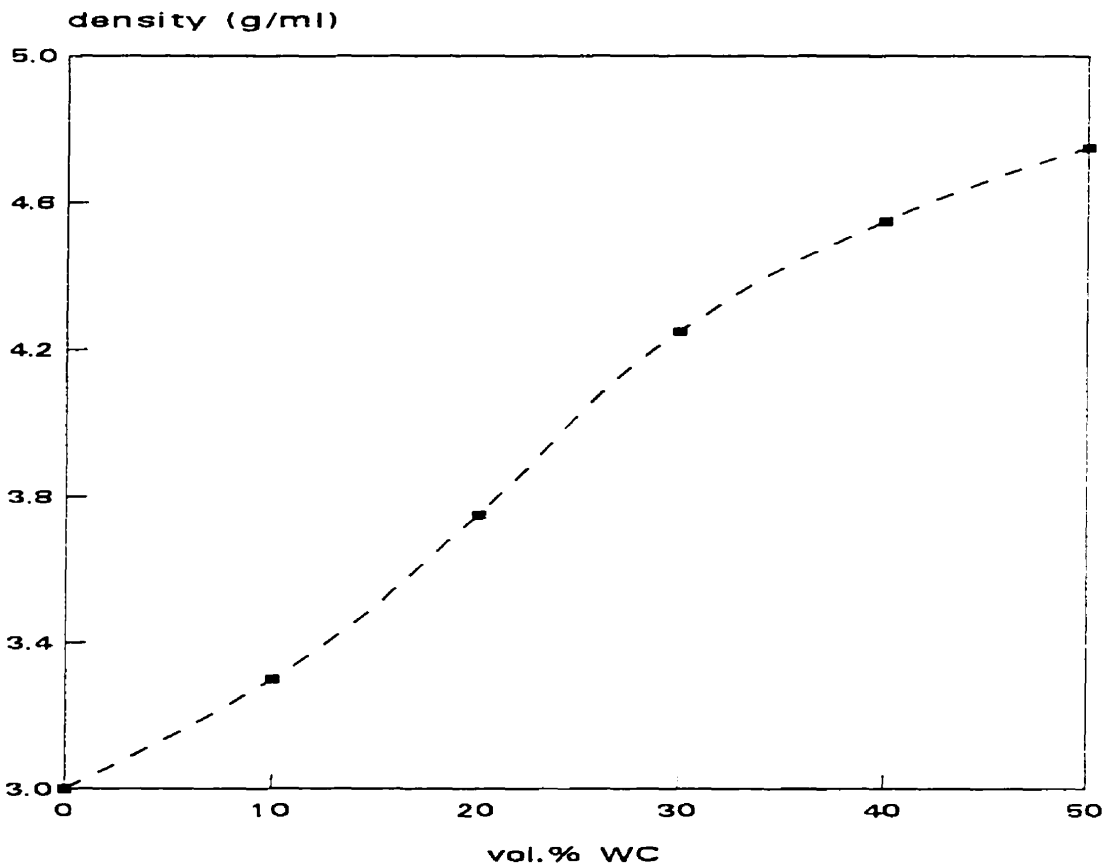

Fig. 3.1: Graph of the relationship between the vol.% WC in the SPT and the suspension density [Sometu Inc.].

$$W_{WC} = \frac{1 - \frac{\rho_S}{\rho_{SPT}}}{\frac{\rho_S}{\rho_{WC}} - 1} \times W_{SPT} \qquad (3.1)$$

where W_{WC} = weight of WC particles to be added (g)

W_{SPT} = weight of SPT (g)

ρ_S = desired suspension density (g/ml)

ρ_{WC} = WC density (g/ml)

ρ_{SPT} = SPT density (g/ml).

If the suspension is not exactly at the desired density, fine adjustments can be made by adding or evaporating small amounts of water.

3.1.1 WC-SPT suspension stability

A WC-SPT suspension with a low density, 3.31 g/ml, was prepared and placed in a 100 ml graduated cylinder. A solid-liquid interface eventually formed and the WC began to settle out. The WC settled at a rate of about 2 ml per 15 minutes which corresponds to 0.25 mm/min.

The stability of the WC-SPT suspension was tested by preparing 110 ml of WC-SPT at a density of 3.27 g/ml ($\pm$0.02). After thorough mixing, the WC-SPT was placed in a 120 ml beaker. After 15 minutes, 25 ml of the WC-SPT was drawn off near the surface with a syringe. The density of this 25 ml was measured with a 25 ml pycnometer bottle to be 3.29 g/ml which is within experimental error. This appeared to indicate that the density of the suspension was uniform even in the top portion of the suspension where it would be most likely to be affected by settling. The WC-SPT suspension is stable for at least 15 minutes at 3.27 g/ml. This stability test was performed at a low WC-SPT density as this is where settling will most likely be a

problem. At higher densities, more WC particles would have to be added to the SPT, resulting in hindered settling which should reduce the settling rate.

3.1.2 Low density ($\rho < 3.5$ g/ml) WC-SPT suspension separations

A WC-SPT suspension with a density of 3.40 g/ml was prepared and a mixture of 2.00 g of 150-212 μm borosilicate glass (2.48 g/ml) and 1.00 g of 150-212 μm unchlorinated TiO_2 (3.98 g/ml) was placed with the suspension into a separatory funnel. The funnel was agitated manually and the particles were allowed to settle for 30 minutes. The heavies and lights were then removed, filtered and visually examined (silica is a translucent white; the unchlorinated TiO_2 is black). The heavies consisted only of unchlorinated TiO_2, but the lights were a mixture of both borosilicate glass and unchlorinated TiO_2. The separation should have been much sharper. The poor separation could be attributed to three factors: small particle size, high suspension viscosity and insufficient settling time. Since the viscosity could not be altered and the settling time could not be lengthened without the WC settling to some extent, the particle size was increased.

A mixture of 2.00 g of 600-850 μm silica (2.65 g/ml) and 3.00 g of 600-850 μm unchlorinated TiO_2 was placed in WC-SPT having a density of 3.30 g/ml. The separation was performed in a modified separatory funnel. (A 250 ml separatory funnel was modified by removing the stopcock arrangement and replacing it with a piece of tubing with a hose clamp. This had to be done since the 600-850 μm particles plugged the stopcock of regular separatory funnels.) The funnel was manually agitated and the particles were allowed to settle for 10 minutes. The heavies were removed and then the cylinder was shaken again and the particles allowed to settle for a further 10 minutes. Afterwards, the heavies and lights were removed and filtered. The mass of the lights (-3.30 g/ml) was 2.01 g and the mass of the heavies (+3.30 g/ml) was 2.99 g. A visual inspection of the products revealed that there were no silica particles in the heavies and only a few unchlorinated TiO_2 particles in the lights; the separation worked well.

The WC-SPT suspension was used to perform a fractionation on 425-600 μm unchlorinated TiO_2/borosilicate glass locked particles (Appendix 1: Test 2-14-4). A 3.00

g sample of this material was separated at 3.08 g/ml (40 vol. % unchlorinated TiO_2) and at 3.27 g/ml (53 vol. % unchlorinated TiO_2). The particles were placed in the suspension for 10 minutes. The products were filtered and weighed. The results are shown in Table 3.1.

Table 3.1: Density fractionation of 425-600 μm unchlorinated TiO_2/borosilicate glass locked material.

Composition fraction (vol. % unchlorinated TiO_2)	Density range (g/ml)	Mass (g)
-40	-3.08	2.23
40-53	3.08-3.27	0.24
+53	+3.27	0.58

These three fractions add up to 3.05 g which is greater than the feed mass. This increase in mass may be attributed to infiltration of the cracks of this material by WC. The three fractions were mounted and examined by SEM. As suspected, WC was observed in the cracks of the particle sections. Immersion in an ultrasonic bath after separation should remove the WC from the feed. A visual inspection of the particle sections revealed that they appeared to belong in their respective composition fractions (although it is difficult to identify misplaced particles due to stereological bias). The -3.08 g/ml material was mostly free glass or high vol. % glass; the +3.27 g/ml material was mostly free or high vol. % unchlorinated TiO_2; and the 3.08-3.27 material consisted mostly of locked sections.

3.1.3 High density ($\rho > 3.5$ g/ml) WC-SPT suspension separations

Tests were done examining the performance of the WC-SPT suspensions at higher densities. A suspension with a density of 4.44 g/ml was prepared. Due to the high concentration of WC, it was quite viscous. A mixture of 2.00 g of 425-600 μm TiO (4.8

g/ml) and 2.00 g of 425-600 μm unchlorinated TiO_2 was placed in this suspension for 15 minutes. The heavies were removed and then the separatory funnel was manually agitated and the separation was allowed to continue for another 15 minutes. The heavies and lights were removed, filtered and weighed. The mass of the lights (-4.44 g/ml) was 3.47 g and the mass of the heavies (+4.44 g/ml) was 0.63 g. Visual inspection of the products (TiO is brass coloured) revealed a poor separation; both heavies and lights appeared to be a mix of TiO and unchlorinated TiO_2. The TiO particles should have reported to the heavies and the unchlorinated TiO_2 should have reported to the lights. It was suspected that the high suspension viscosity was the main cause of the poor separation.

Another test was performed using a WC-SPT suspension at a high density. In an effort to overcome the suspension viscosity, a longer residence time was used. A suspension with a density of 3.75 g/ml was created and a mixture of 2.00 g of 600-850 μm unchlorinated TiO_2 and 2.00 g of 600-850 μm silica was separated. The particles were left in the suspension for 2 hours. The mass of the lights (-3.75 g/ml) was 3.66 g and the mass of the heavies (+3.75 g/ml) was 0.34 g. Again, the separation did not work well. The unchlorinated TiO_2 should have reported to the heavies and the silica to the lights. A visual inspection of the products revealed that although the heavies contained mostly unchlorinated TiO_2, the lights were a mix of the two. The long residence time did not improve the separation.

One final separation using a high density WC-SPT suspension was attempted; this time, very coarse particles were separated. A suspension with a density of 3.58 g/ml was prepared. A separation was performed in a 200 ml beaker on a mixture of 1.00 g of 1700-2360 μm silica and 2.00 g of 1700-2360 μm pyrite (5.02 g/ml). The particles were placed into the WC-SPT suspension and left for 5 minutes. The separation appeared to take place quickly; the silica floated to the top nearly instantly. The lights were removed with a scoop. The separation was perfect (i.e. all the silica reported to the lights and all the pyrite to the heavies), but the particle size was very large in this test. It would not be practical to have standard material particles this size (large standard

material particles would require that many polished surfaces be prepared in order to produce enough sections to satisfy statistical requirements).

3.1.4 Summary of WC-SPT suspension separations

The WC-SPT suspension separations appeared to be effective only in situations where the suspension viscosity, and thus density, is low or the particle size is very large ($> 1700\ \mu m$). Due to these restrictions, it was decided to abandon further study into this separation method.

3.2 Magnetogravimetric separations

Due to the ineffectiveness of WC-SPT suspension separations at high densities, magnetogravimetric separations were examined. Magnetogravimetric separations are based on the fact that a magnetic fluid can be made to behave like a heavy liquid when a magnetic field is applied [43,44,45]. Over the past three decades, the behaviour of magnetic fluids in magnetic fields has been extensively studied [46,47,48,49,50,51]. These magnetic fluids are either paramagnetic salt solutions or stabilized suspensions of colloidal ferromagnetic particles. Magnetic fluids have a Newtonian nature and retain their fluidity in the presence of a magnetic field.

Consider the net force, F_t, acting on a magnetic fluid, in a magnetic field. If the gravitational force, F_g, and magnetic force, F_m, are acting in the same direction then:

$$F_t = F_g + F_m \tag{3.2}$$

The gravitational force on a volume of the magnetic fluid, V, is:

$$F_g = V \rho_f g \tag{3.3}$$

where ρ_f is the fluid density and g is gravitational acceleration. The magnetic force on the fluid is:

$$F_m = V \kappa_f \left(\frac{B}{\mu_o}\right) \frac{dB}{dx} \tag{3.4}$$

where κ_f = magnetic susceptibility of the fluid (dimensionless in SI units)

μ_o = permeability of free space ($4\pi \times 10^{-7}$ Tesla•metre/Ampere)

B = magnetic flux density (Tesla)

x = distance perpendicular to the lines of flux of the magnetic field (metre).

Thus, the net force on the fluid is:

$$F_t = V \rho_{fa} g = V \rho_f g + V \kappa_f \left(\frac{B}{\mu_o}\right) \frac{dB}{dx} \tag{3.5}$$

where ρ_{fa} = apparent density of the fluid.

The apparent density can be solved for and expressed as:

$$\rho_{fa} = \rho_f + \frac{\kappa_f}{g} \left(\frac{B}{\mu_o}\right) \frac{dB}{dx} \tag{3.6}$$

Note that the apparent density is a function of $B \bullet dB/dx$, the force factor, which can be adjusted by changing B or dB/dx, the latter being a function of magnet geometry.

3.2.1 CRM magnetogravimetric separator

Le Centre de Recherches Minérales (CRM) devised a continuous magnetogravimetric separator [52] using a modified Frantz isodynamic magnetic separator. The Frantz was modified by rotating the magnetic coils until the gap between the pole pieces was facing upwards and replacing the isodynamic pole pieces with trapezoidal-shaped ones. This yielded a V-shaped notch in which a cell containing magnetic fluid could be placed. Different densities were simulated by varying the current that was supplied to the coils. The separator was calibrated using density floats (Cargille Inc.). The lights were removed by overflowing a chute at the top of the cell and the heavies exited via a chute at the bottom.

A test of the CRM separator was performed by separating a sample of locked particles and then verifying the separation using a heavy liquid. The feed was 150-212 μm ZrO_2/borosilicate glass locked particles (Appendix 1: Test 2-11-4). It was fractionated with the CRM separator into the following density fractions: <2.75, 2.75-3.50, 3.50-4.10, 4.10-5.00 and >5.00 g/ml which corresponds to <8, 8-31, 31-49, 49-76 and >76 vol.% ZrO_2, respectively. The different fractions were mounted in epoxy resin and examined by SEM; the composition of the sections seemed to correspond with their composition fractions, but of course, stereological bias makes the actual particle composition indeterminate. The accuracy of one of the separations was examined using a heavy liquid. Three grams of the 2.75-3.50 g/ml fraction were placed into a SPT solution (no WC particles) at a density of 2.73 g/ml for 40 minutes. The products were filtered, dried and weighed. The mass of the lights was 2.95 g while the mass of the heavies was 0.04 g. This result indicated that there was a great discrepancy between the two separation methods; most of the material that sank at 2.75 g/ml in the CRM separator should have sunk in the SPT solution. None of the higher split-points could be tested since the maximum density of the SPT solution is 3.1 g/ml.

The inaccuracy of the CRM separation may be attributable to several causes:

1) continuous operation - The CRM separator was designed to be continuous, but the cell was small (15 cm long) and the residence time correspondingly short. Short circuiting will result if the particles are not given sufficient time to report to the proper product stream.
2) small particle size - The particles that were separated were relatively small. Small particles are more difficult to separate accurately than larger ones.
3) lack of proper mixing - There is a possibility that particles adhere to the sides of the cell and agitation of the magnetic fluid may be necessary to free the particles so that they can separate.

These problems can be solved by:

1) modifying the cell so that the separation can be done in batch mode
2) increasing the particle size so that the separations are quicker and more accurate

3) agitating the magnetic fluid after the particles have been placed in the cell.

3.2.2 Batch magnetogravimetric separator

A batch magnetogravimetric separator was developed based on the design of the CRM separator. The separator is described in detail in the published paper "Batch magnetohydrostatic separations with a modified Frantz separator" [53] which is included in Appendix 2. It functioned well, but unfortunately, this separator could only attain an upper density of 5.00 g/ml and the requirement was 6.833 g/ml (the density of the borate). In order to reach a higher density, the pole pieces would have to be moved closer together, but this would greatly lessen the capacity of the separator. Due to this limitation, it was decided to abandon further study of this separation method.

3.3 Magstream separator

A decision was made to use the Magstream separator (developed by Intermagnetics General Corporation (IGC)) to separate the standard material particles into density fractions. This was done because no other method could be found to separate material up to 6.833 g/ml. The Magstream is a centrifugal magnetogravimetric separator. Its principles have been described previously by Walker, Devernoe and co-workers [54,55,56,57], but a short description of the separator follows.

3.3.1 Magstream operating principles

The Magstream separator utilizes centrifugal, magnetic and gravimetric forces to separate particles based on density. A schematic representation of the Magstream is shown in Fig. 3.2. The material to be separated is introduced at the top of a cylinder containing magnetic fluid. An annular fixed magnet around the rotating cylinder produces a constant magnetic field within the cylinder. As the particles descend in the cylinder, they are subjected to two opposing, radial forces: the outward centrifugal force, F_c, and the inward buoyant force of the magnetic fluid, F_{mb} (the magnetic field creates an outward attraction of the fluid which pushes the particles inwards). This creates a

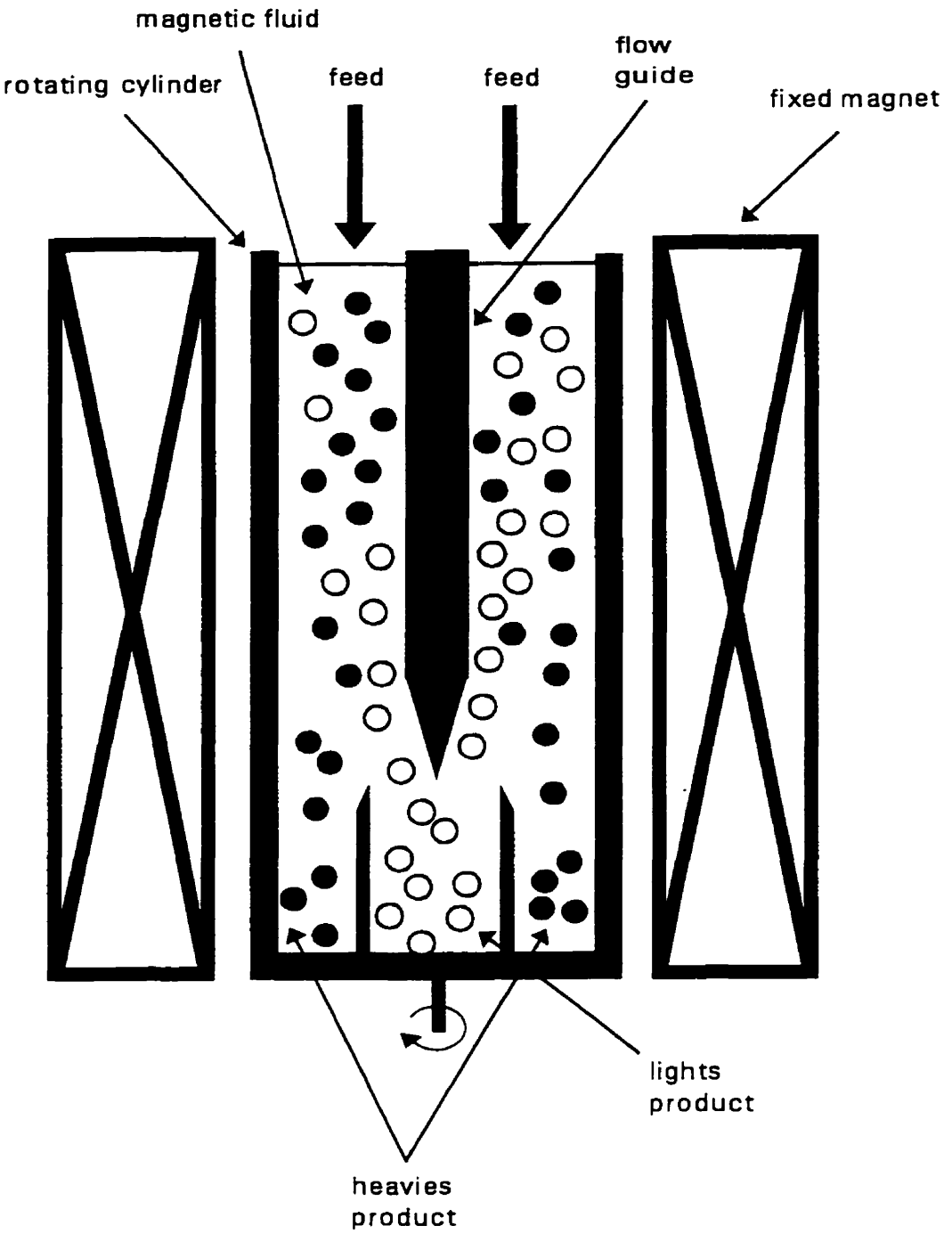

Fig. 3.2: Conceptual representation of the Magstream separator.

situation where the particles are segregated by density. Heavier particles are forced outward and lighter particles are forced inwards. A divider at the bottom of the cylinder separates the particles into two products. F_c is given by:

$$F_c = V(\rho_p - \rho_f)\,\omega^2 r \tag{3.7}$$

where V = particle volume, ρ_p = particle density, ρ_f = magnetic fluid density

ω = rotational velocity of the fluid, r = radial position.

In the Magstream, the pattern of the magnetic field is designed such that the gradient of the field is linearly related to the radial position. Thus, F_{mb} is given by:

$$F_{mb} = V M_f k r \tag{3.8}$$

where M_f = magnetic fluid magnetization, k = constant related to separator geometry. The net radial force, F_r, is equal to F_c - F_{mb}, or:

$$F_r = V(\rho_p - \rho_f)\,\omega^2 r - V M_f k r \tag{3.9}$$

At equilibrium, $F_r = 0$. The split-point density, ρ_{sp}, can be determined from Equation 3.9:

$$\rho_{sp} = \rho_f + \frac{k M_f}{\omega^2} \tag{3.10}$$

Thus, the split-point density can be adjusted simply by changing the rotating speed of the cylinder of magnetic fluid.

The advantage of the Magstream separator over heavy liquids is that it permits separations at high densities. Heavy liquids are toxic and difficult to work with at densities >3.0 g/ml.

The disadvantage of the Magstream is that it is not a perfect separator. In order to ensure the accuracy of the separations, the heavies and lights products of the separation have to be re-processed (cleaned). Also, Bunge and Fuerstenau [58,59,60] have observed that the accuracy of Magstream separations decreases with particle size. A recent theoretical study by Svoboda [61] suggests that the effect

of hydrodynamic drag on the particles to be separated should also be taken into consideration (Walker, Devernoe and co-workers considered the drag to be negligible). He found that if the drag was factored into the equations, the performance of the Magstream became strongly dependent upon the particle size. Based on this, he cautions against the use of separating fine particles in the Magstream. In this work, the Magstream Model 100, a batch machine, was used. The largest recommended particle size for this machine is 425-600 μm [62] which is the size of the standard material particles. The performance of the Magstream Model 100 was examined (in the next section) by calibrating the machine with homogeneous materials of known density.

The Magstream separation is based on density alone provided the particles are non-magnetic; otherwise, the particles themselves would be affected by the magnetic field. The standard material should be non-magnetic because it consists of glass and lead borate, but to verify this, the magnetic susceptibility of the two phases of the standard material was measured using a Frantz isodynamic magnetic separator [63]. As expected, both the glass and lead borate had very low magnetic susceptibilities ($\kappa_{glass} <$ 5.32 x 10^{-5} SI units and $\kappa_{lead\ borate} <$ 1.95 x 10^{-5} SI units; for comparison, $\kappa_{chalcopyrite} \approx$ 4 x 10^{-4} SI units). Their diamagnetic properties were also measured. Both materials showed no measurable diamagnetism.

3.3.2 Magstream calibration and operation

For the Magstream Model 100, the relationship [62] between the rotating speed of the cylinder and the desired separation density is:

$$N = 370 \sqrt{\frac{M_f}{\rho_{sp} - \rho_f}} \qquad (3.11)$$

where N = rotating speed (rpm)

M_f = magnetization per unit volume of the magnetic fluid (emu/cm^3)

ρ_{sp} = desired separation density (g/ml)

ρ_f = magnetic fluid density (g/ml).

The magnetic fluid density was measured with a hydrometer. There is a linear relationship between the magnetic fluid density and its magnetization, but this relationship is different for different batches of magnetic fluid. Each batch, therefore, must be calibrated. The calibration of the magnetization of the magnetic fluid [62] is performed using a homogenous material of known density and the following equation:

$$M_f = \frac{(N_{50/50})^2 (\rho_p - \rho_f)}{136\ 827} \tag{3.12}$$

where $N_{50/50}$ = rotating speed (rpm) at which the homogeneous material reports equally to the lights and heavies.

ρ_p = density of the homogeneous material (g/ml).

The homogenous material is split with the Magstream at different values of N until an approximate $N_{50/50}$ is found. An accurate $N_{50/50}$ can be calculated by interpolation [62]:

$$N_{50/50} = \sqrt{N_1^2 + \left[\frac{(X-50)(N_2^2-N_1^2)}{(X-Y)}\right]} \tag{3.13}$$

where N_1 = rotating speed (rpm) that places X% (between 50 and 85%) of the sample in the heavies

N_2 = rotating speed (rpm) that places Y% (between 15 and 50%) of the sample in the heavies.

After the M_f which corresponds to the $N_{50/50}$ is calculated, the graph of the relationship between M_f and ρ_f can be constructed by drawing a line through this M_f and ρ_f and the point M_f = 0 emu/cm^3 and ρ_f = 1.00 g/ml.

In this work, the Magstream was calibrated using three materials: glass, pyrite and borate. These three materials span the full range of density of the standard material. The particle size of all these materials was 425-600 μm.

The pyrite (Wards's Natural Science Ltd.) was obtained as crystals and only crystals that did not have any visible impurities were used. After the pyrite was crushed and screened, it was passed through a Frantz isodynamic magnetic separator to ensure

that it was non-magnetic; its susceptibility was in the same range as the glass and borate. The pyrite density was measured to be 5.024 g/ml (using a 100 ml pycnometer) which is very close to the density of pure pyrite [38].

The magnetic fluid (Magfluid, IGC) was available only in concentrated form and had to be diluted. The initial density was 1.16 g/ml and the fluid was diluted with distilled water to two different density levels: a low and high density fluid. The low density fluid had a density of 1.11 g/ml and was used in separations up to 5.00 g/ml. The high density fluid had a density of 1.14 g/ml and was used in separations above 5.00 g/ml. The reason for this division is that the use of a low density fluid in high density separations resulted in poor results. Borate particles were separated using a low density magnetic fluid at densities ranging from 5.7 to 6.7 g/ml. The results are shown in Fig. 3.3. All the particles should have reported to the heavies in these separations, but in each case, there was a significant amount of misplaced particles. Bunge and Fuerstenau [60] also observed in tests with the Magstream that sharper separations were obtained with high density magnetic fluids. Separations at high densities using the high density fluid yielded markedly superior results. IGC does not recommend the use of high density fluids, but Carpco Inc., its distributors, have reported no problems from researchers that have used high density fluids. The calibration curves of the low density fluid with glass and pyrite are shown in Figs. 3.4 and 3.5, respectively. The calibration curves of the high density fluid with pyrite and borate are shown in Figs. 3.6 and 3.7, respectively. A similar calibration was performed on a second batch of magnetic fluid that was used in later separations.

In the Magstream Model 100, the heavies and lights report to different cups at the bottom of the cylinder. The capacity of this machine is limited by the volume of the cups: the lights cup can accommodate 85 ml and the heavies cup, 47 ml. To ensure that neither cup overflowed, the volume of the feed was always kept below 30 ml.

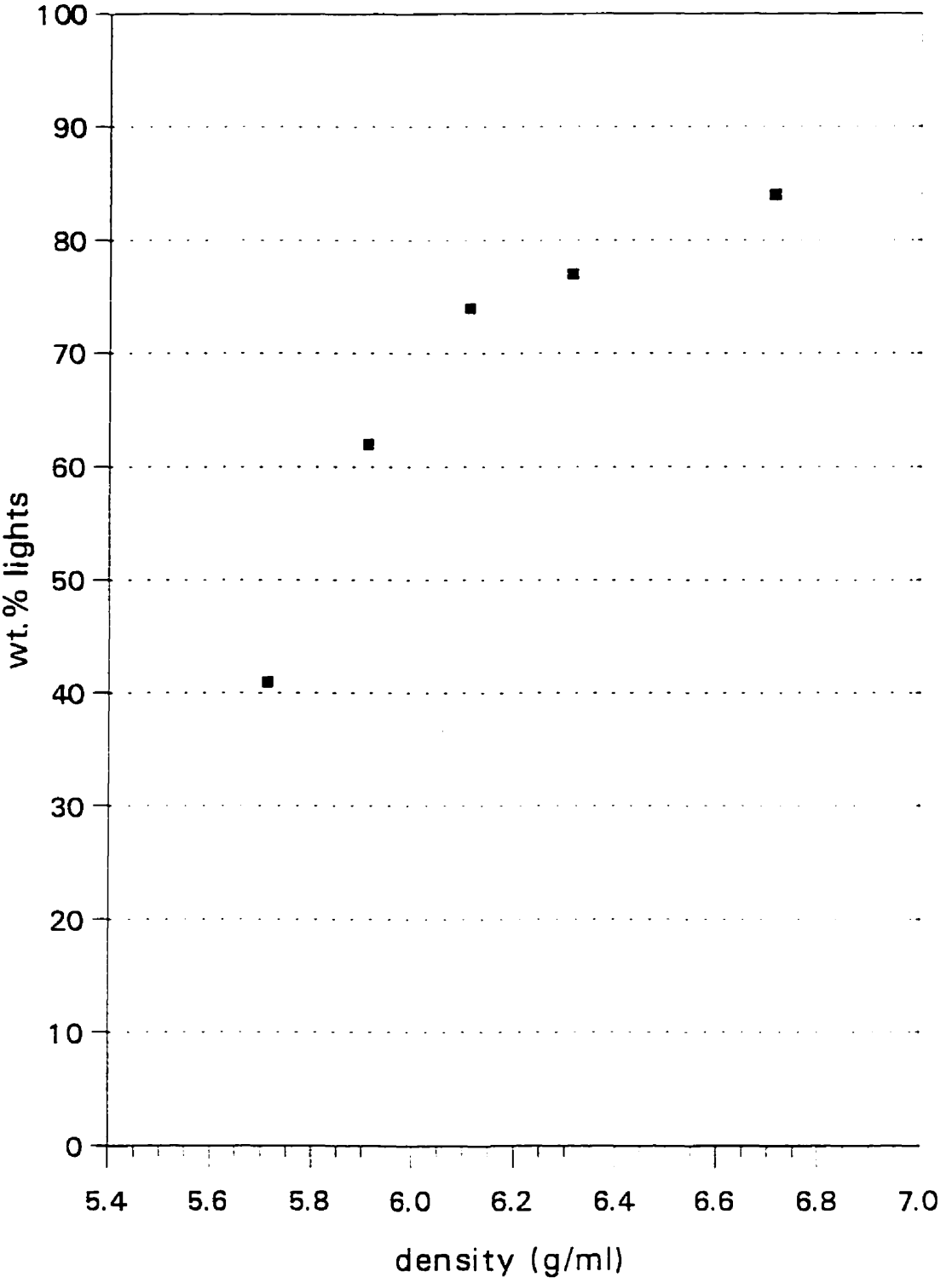

Fig. 3.3: Magstream separations of lead borate using a low density magnetic fluid.

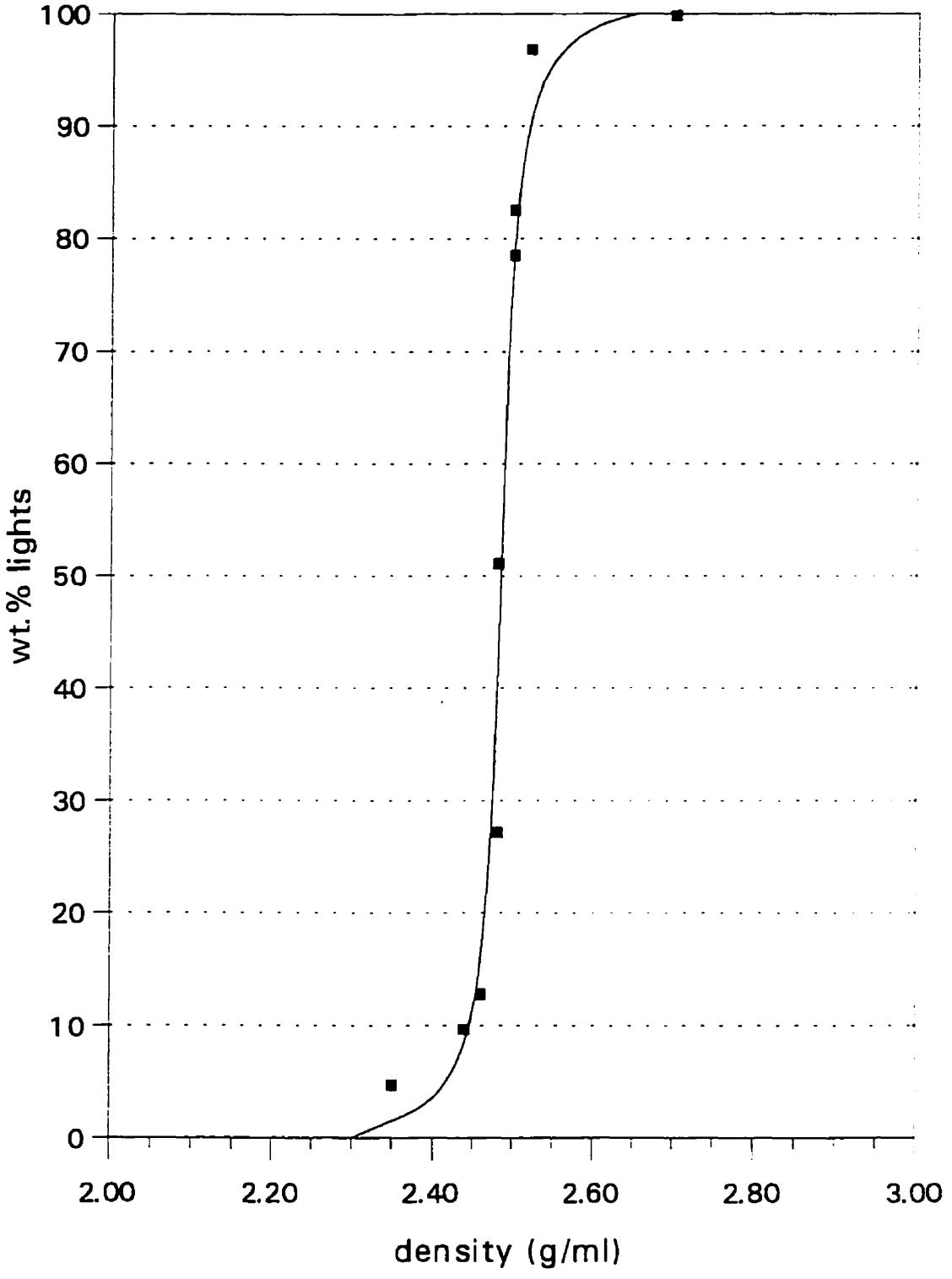

Fig. 3.4: Magstream calibration with glass using a low density magnetic fluid.

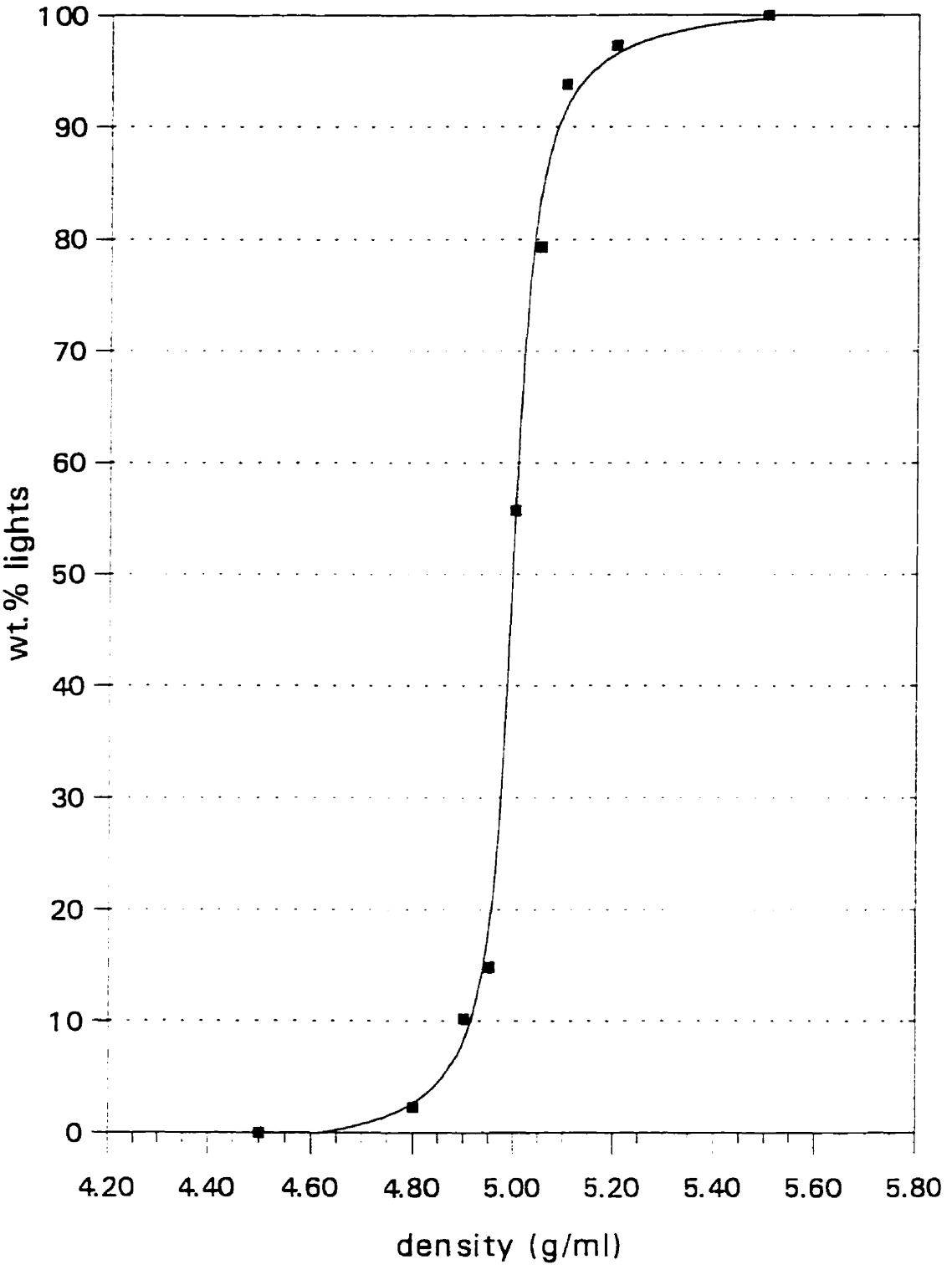

Fig. 3.5: Magstream calibration with pyrite using a low density magnetic fluid.

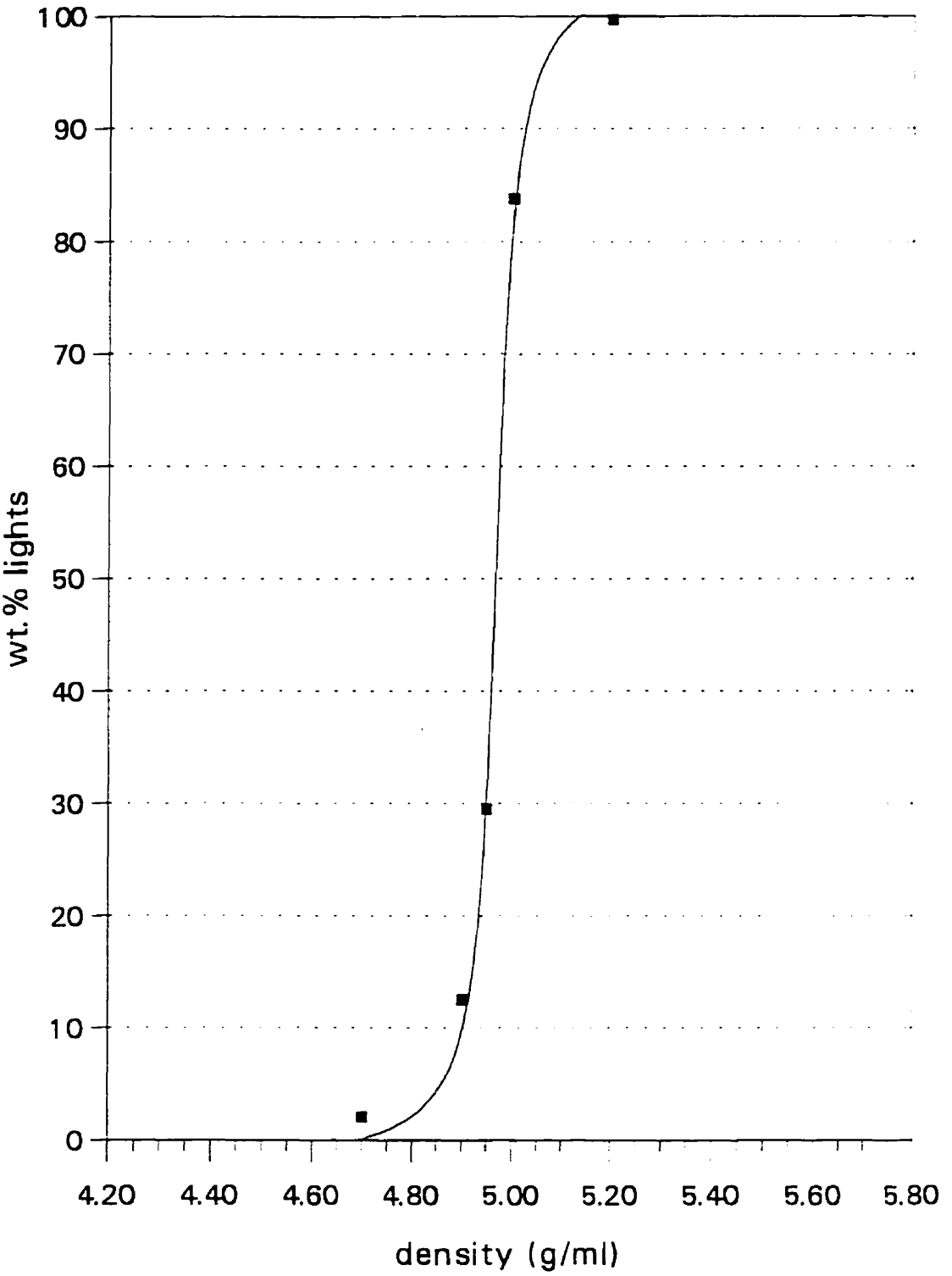

Fig. 3.6: Magstream calibration with pyrite using a high density magnetic fluid.

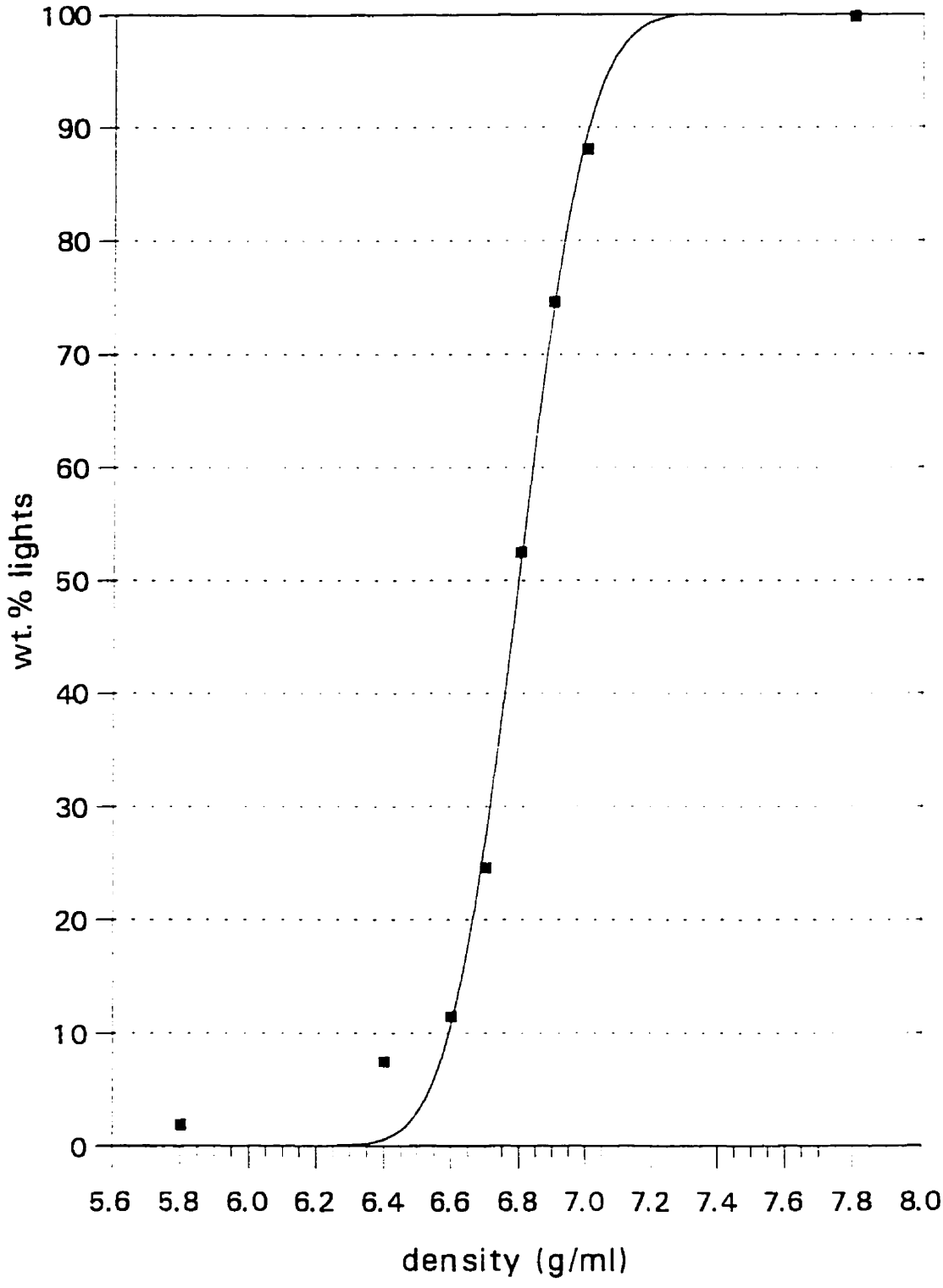

Fig. 3.7: Magstream calibration with lead borate using a high density magnetic fluid.

The separation must be performed carefully to prevent particles from being misplaced. In some cases, the force on the particles may be so great that they may become pinned to the flow guide (the short cylinder at the top which guides the feed downwards) or the interior wall of the cylinder. When the power is shut off and the rotation ceases, the particles then fall downwards through the fluid and may not report to the correct product cup since no separation force is acting.

The solution to the potential problem of pinning is to slowly decrease the rotating speed after the separation is complete before shutting off the power in order to allow pinned particles to release from the walls and report to the correct product. Also, if possible, separations should be performed on particles with a density close to the separation density to prevent excessive force on the particles and thus prevent pinning.

The standard material was separated into the following fractions: -5, 5-15, 15-25,..., 85-95, +95 vol. % borate. To ensure the accuracy of the separations, the following measures were taken:

1) The products of the first separation (rougher) were cleaned twice. Therefore, for each composition fraction, three separations were performed at both split-points of the fraction.
2) In the cleaning steps, any particles that did not re-report to their original product were removed from consideration.
3) The split-points were set 0.5 % closer to the midpoint of the fraction. For instance, for the 45-55 vol. % borate fraction, the splits points were set to 45.5 % and 54.5 vol. % borate. This leaves a 1 % gap between fractions, but this helps minimize misplaced particles.

3.3.3 Magstream separation results

The complete results of the separations are shown in Appendix 3. A summary of the final results of the separations is shown in Table 3.2.

The amount of locked material (i.e. 5-95 vol. % borate) is 86.29 mass % or 80.91 vol. % which indicates that a large proportion of the particles were locked after breakage. In this work, for the standard material, the -5 and +95 vol. % borate fractions were

considered to be free. To isolate the true free (i.e. particles containing 100% of one phase only), it would have been necessary to perform a separation at 0 and 100 vol.% borate, but this would have been difficult due to large number of near-density particles. In any case, this was not necessary, because true free particles of both phases were easily created.

Table 3.2: Results of the Magstream separations of the standard material.

Composition fraction (vol.% borate)	Magstream split-points (g/ml)	Avg. dens. (g/ml)	Mass (g)	Mass %	Vol. (ml)	Vol.%
-5	-2.719	2.611	48.83	10.48	18.71	17.05
5-15	2.719-3.152	2.936	39.38	8.46	13.42	12.23
15-25	3.152-3.585	3.369	23.00	4.94	6.83	6.22
25-35	3.585-4.018	3.802	30.81	6.62	8.10	7.39
35-45	4.018-4.451	4.235	36.60	7.86	8.64	7.88
45-55	4.451-4.884	4.668	54.16	11.63	11.60	10.58
55-65	4.884-5.317	5.101	117.98	25.33	23.13	21.08
65-75	5.317-5.750	5.534	42.37	9.10	7.66	6.98
75-85	5.750-6.183	5.967	35.55	7.63	5.96	5.43
85-95	6.183-6.616	6.400	22.00	4.72	3.44	3.13
+95	+6.616	6.725	15.05	3.23	2.24	2.04
		Total:	465.73	100.00	109.72	100.00

3.3.4 Measurement of the grade of the composition fractions

The accuracy of the composition fractions produced by the Magstream was determined by measuring the grade of the fractions. Two different methods were used: water displacement in a pycnometer and image analysis. The water pycnometer method

has been previously described (the grade as determined by the water pycnometer method will henceforth be referred to as the pycnometer grade). A 25 ml pycnometer bottle was used rather than a 100 ml bottle since the available volume of some of the composition fractions was small.

The grade as determined from image analysis (henceforth referred to as the IA grade) of the composition fractions involved the microscopic examination of the particle sections and the application of Delesse's equation [64]:

$$p_1 = \frac{A_{TI}}{A_T} \tag{3.14}$$

where p_1 = volumetric grade of phase "1" in the sample

A_{TI} = total area of phase "1" observed

A_T = total particle section area observed.

From this equation, it can be seen that the grade as measured from sectioning data is not stereologically biased. The IA grade should provide an unbiased measurement of the volumetric grade.

The IA grade was measured by taking particles from each composition fraction and mounting them in resin. A surface was cut and polished from each pellet and the polished surfaces examined by SEM. The area of the two phases were measured with the Tracor Northern 8500 image analyzer. The IA grade should be in the range of the composition fraction and close to the midpoint.

In sample preparation, the prevention of preferential settling (due to density differences between the particles) and preferential orientation (due to density differences between the phases in the locked particles) is important since this affects the IA grade. Delesse's equation is only valid for random sections. In these samples, the particles in each fraction should have very similar densities and consequently, there should be little segregation. But, regardless, precautions were taken to ensure random mounting of the particles. The sample preparation involved mixing 0.4 ml of the sample with an equal amount of a diluent material, 425-600 μm graphite particles, and placing the mixture at

the bottom of a 1¼" mold. The diluent helps to support the sample particles in space (and thus reduce preferential settling) and promotes random orientation [65]. Graphite was selected as the diluent since it has a low density and a grey level similar to the mounting medium resin when observed by backscattered electron imaging. The mounting medium that was used was Epofix resin (Struers Inc.). The resin was prepared by mixing it with the hardener in an adequate proportion and then centrifuging it at 1600 rpm for 1 minute to remove any air bubbles. A small quantity, 0.8 ml, of the resin was added to the particles in the mold and mixed. The small amount of resin helps inhibit preferential settling by restricting the space in which the particles can settle. The mold was then centrifuged at 1600 rpm for 5 minutes to remove any air bubbles that may have resulted from the mixing of the sample and resin. Afterwards, more resin was added to top off the mold.

The SEM magnification was set to 25 ×. Tests at a higher magnification, 30 ×, were performed to examine if a higher resolution provided a more accurate IA grade, but the results were very similar to those obtained at 25 ×. A low accelerating voltage and probe current, 15 keV and 1 × 10^{-8} amp, respectively, were used to reduce the halo effect. (The halo effect causes variations in grey level near interfaces of features in the sample resulting in poor definition of the section edges and interfaces. Halos are caused by the detection of signals from both sides of an interface.)

The image analyzer was programmed to automatically perform the measurements on the sections. During image analysis, a delineation filter, MIN/MAX, was applied to the primary image to sharpen the definition of the edges of the phases in the image. This reduces the halo effect. One erosion and one template dilation was performed to remove small artifacts. (An erosion refers to the removal of a single layer of pixels from all the sections in the image and a template dilation refers to the addition of a single layer of pixels to the sections (using the original image as a template) to restore the sections to their original size). The results of both the pycnometer and IA grades are shown in Table 3.3.

The data show some large discrepancies between the pycnometer grades, IA grades and the composition fraction ranges. The pycnometer grades are significantly

lower than the midpoints of the composition fractions and in some cases they are lower than the composition fraction range. On the other hand, the IA grades are mostly higher than the midpoints of the composition fractions and in some cases they are higher than the composition fraction range.

Table 3.3: Pycnometer and IA grades of the composition fractions of the standard material.

Composition fraction (vol. % borate)	Magstream split-points (g/ml)	Pycnometer density (g/ml)	Pycnometer grade (vol. % borate)	IA grade (vol. % borate)
- 5	- 2.719	2.509	0.2	0.0
5 - 15	2.719 - 3.152	2.747	5.7	8.1
15 - 25	3.152 - 3.585	3.135	14.6	20.3
25 - 35	3.585 - 4.018	3.580	24.9	33.5
35 - 45	4.018 - 4.451	3.956	33.6	42.6
45 - 55	4.451 - 4.884	4.330	42.2	53.8
55 - 65	4.884 - 5.317	4.856	54.4	63.9
65 - 75	5.317 - 5.750	5.312	64.9	79.0
75 - 85	5.750 - 6.183	5.716	74.2	87.8
85 - 95	6.183 - 6.616	6.116	83.4	97.5
+ 95	+ 6.616	6.555	93.6	99.1

There are several possible explanations for this discrepancy:

1) Magstream splits were inaccurate
2) borate or glass density measurements were inaccurate
3) some of the pycnometer measurements were not precise due to the small quantity of material available in some of the composition fractions. For an optimum pycnometer measurement, there should be enough material to fill one-third of the pycnometer bottle [66].

The third explanation is unlikely since even in the fractions where there was a sufficient amount of material to perform an optimum measurement, the pycnometer grade was still too low. In fact, there was a sufficient quantity of the 45-55 and 55-65 vol.% borate material to measure the grade using a 100 ml pycnometer. The results were in agreement with the 25 ml pycnometer.

The first and second explanations remain possible so other methods of measuring the grade of the composition fractions were examined.

3.3.5 Standard material dissolution tests

An attempt was made to measure the grade of the standard material composition fractions using atomic absorption. This required complete dissolution of the standard material. Two attempts were made at dissolving the standard material using hydrofluoric acid (HF) and aqua regia (1 part HNO_3 + 3 parts HCl):

1) HF only - 0.5 g of standard material (45-55 vol.% borate) was crushed to -38 μm. This material was placed in a plastic beaker and HF was added until the sample was completely submerged. The mixture was stirred and left overnight. The next day, some undissolved residue remained so the beakers were heated at 75°C for 1 hour. The residue still did not dissolve.
2) HF and aqua regia [67] - 0.5 g of standard material (45-55 vol.% borate) was crushed to -38 μm and immersed in a beaker containing 4 ml of aqua regia. 5 ml of HF was slowly dripped into the beaker and the beaker was heated for 3 hours at 75°C. There was partial dissolution, but there was still a significant amount of solid residue.

Since both methods failed to completely dissolve the standard material, two options remained: NaOH or peroxide fusion of the residue or fluxing the standard material to allow an XRF (X-ray fluorescence) to be performed. Fusion could not be performed at McGill University due to the lack of adequate equipment and the cost of fusion at an outside facility would have been quite high. Fluxing the sample would have been equally costly due to the necessity of acquiring a fluxing crucible.

3.3.6 Microprobe analysis of the standard material

Due to the difficulty of the dissolution of the standard material, a microprobe WDS (wavelength dispersive spectroscopy) analysis was performed. Microprobes are similar to SEMs [68] except that they can employ a higher energy electron beam. This creates more interactions with the sample which produces more signals. WDS analysis is similar to EDS analysis. WDS analysis is performed by measuring the wavelength of X-rays resulting from the interaction between an electron beam and a sample. The wavelengths are characteristic of specific elements (from which they can be identified) and from calibrations with standards, the elemental composition of the sample can be quantified. WDS is more accurate than EDS due to the increased resolution of the peaks.

Two sets of WDS analyses were performed:

1) true free particles of glass and borate (i.e. particles containing 100 % of one phase only). When these particles were created (Section 2.3.8), neither phase had been exposed to the other.
2) locked particles (55-65 vol. % borate).

The particles were mounted in resin in 1" molds and polished. The true free glass and borate particles were examined at an accelerating voltage of 15 keV. A probe diameter of 20 μm was used to determine the composition at random points in the sections. The average composition of the true free glass and borate particles is shown in Table 3.4. The precision of the microprobe analysis is 0.25 %. The emission lines and the standards that were used in all the WDS analyses in this work are presented in Appendix 4.

The data indicate that true free glass consisted mostly of SiO_2, Na_2O and CaO. True free borate consisted mostly of PbO and B_2O_3 and contained little SiO_2 or any of the other components of glass.

Table 3.4: Microprobe WDS analysis of true free glass and borate.

Oxide (wt. %)	True free glass	True free borate
Na_2O	13.20	0.01
Al_2O_3	0.10	0.04
SiO_2	72.84	0.14
MgO	3.97	0.00
K_2O	0.03	0.03
CaO	8.85	0.03
FeO	0.11	0.02
PbO	0.00	87.18
B_2O_3†	0.89	12.55
Total:	100.00	100.00

† calculated by difference

For the locked particles (55-65 vol. % borate), a series of five traverses across the interface of locked sections were performed using an accelerating voltage of 15 keV and a probe diameter of 5 μm. A smaller diameter beam was not used since this may have resulted in the migration of alkali metals in the glass [69]. The results of a typical traverse are shown in Figs. 3.8 and 3.9. Fig. 3.8 indicates that there was no diffusion of the borate into the glass; the amount of PbO in the glass phase is negligible. However, Fig. 3.9 indicates that there was some diffusion of the glass into the borate. There was $\approx$ 6.0 wt. % SiO_2 in the borate phase of this locked section. Despite this limited diffusion, the interface between the two phases remained well-defined. Backscattered electron imaging of the locked sections revealed clear, sharp interfaces in all the sections.

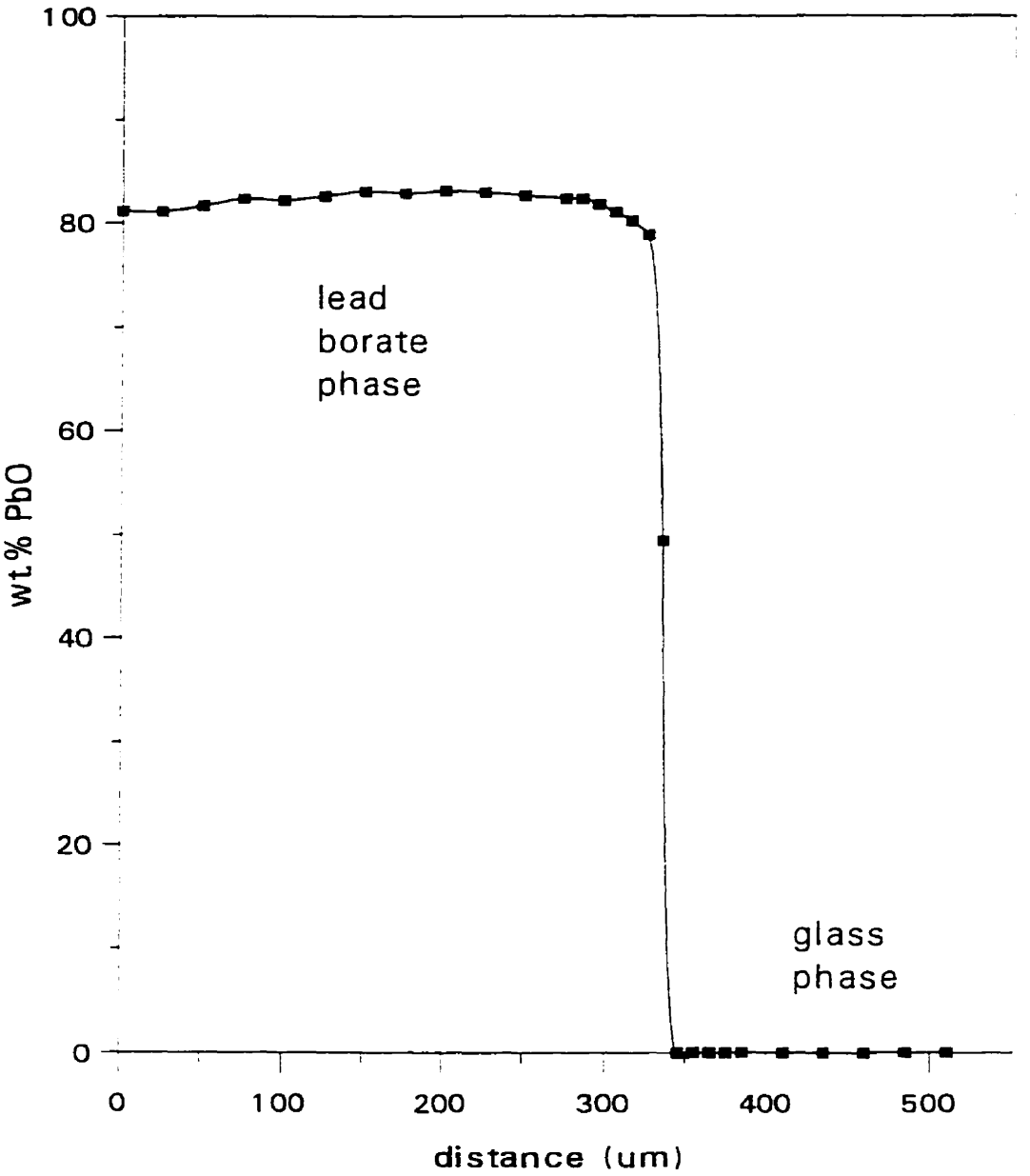

Fig. 3.8: PbO profile from a microprobe WDS traverse across a locked section.

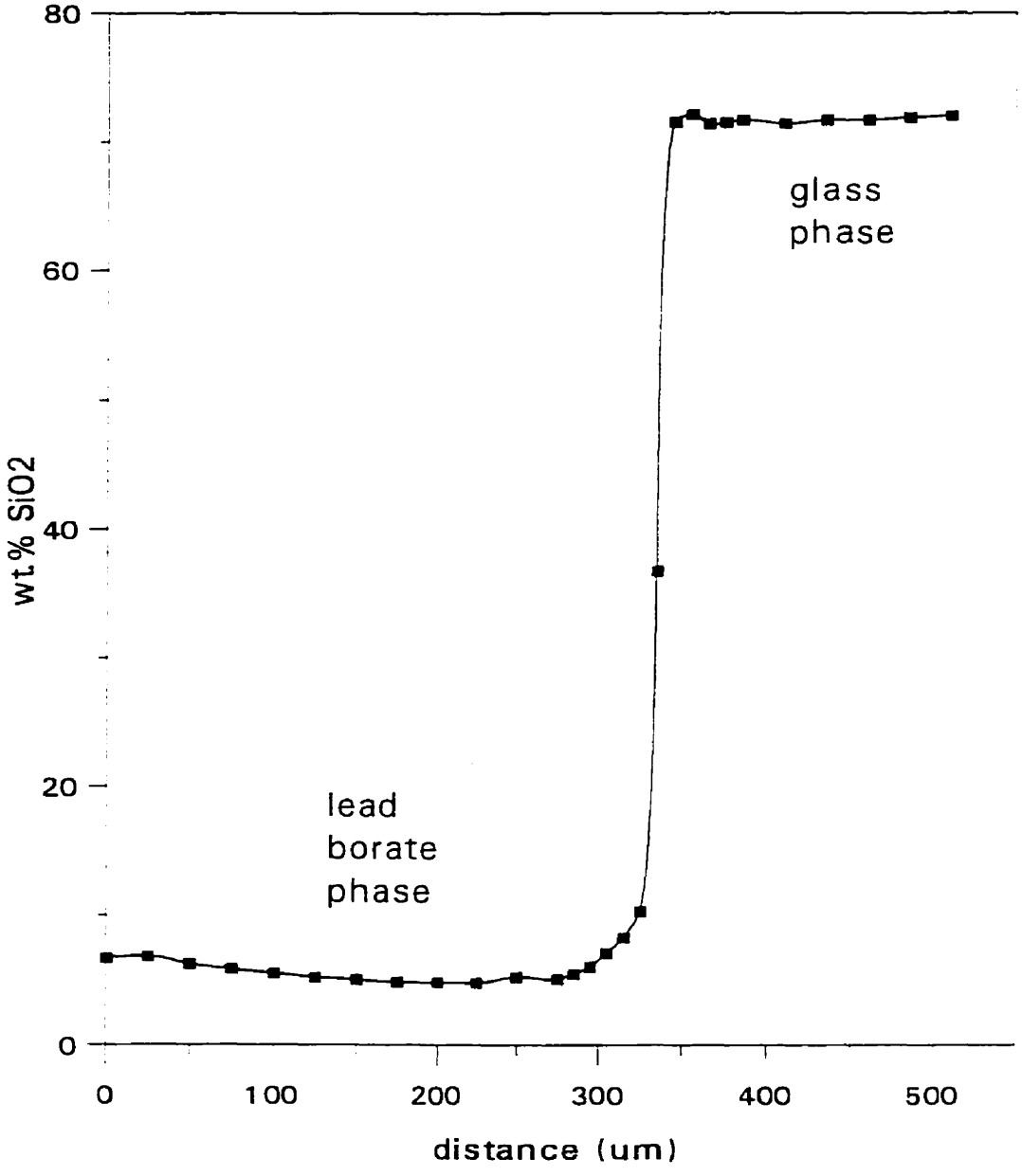

Fig. 3.9: SiO2 profile from a microprobe WDS traverse across a locked section.

The level of glass diffusion into the borate was calculated by analysing the borate phases of many locked particles. The average SiO_2 content was found to be 5.95 wt. % ($\pm$1.38%).

The diffusion of glass into the borate provides an explanation for the discrepancy between the pycnometer grades, IA grades and composition fraction ranges. To correct this, the density of the silicate-containing borate of the standard material (i.e. the density of the borate after it has been contacted with glass in the furnace) must be measured. To do this, silicate-containing borate must be created. This was accomplished by infiltrating a bath of borate with glass in the furnace and then removing the glass before the borate cooled and solidified.

A block of glass (75 mm x 25 mm x 19 mm) was inserted into a bath of borate (150 g) at 650°C. After a set period of time, the glass slides were removed and the borate was taken out of the furnace and allowed to cool. The borate was then crushed, mounted and a microprobe WDS analysis was performed to determine the degree of glass diffusion. By varying the contact time, the level of glass diffusion into the borate could be adjusted until it matched the level in the silicate-containing borate of the standard material. The results of these tests are shown in Table 3.5.

Table 3.5: Microprobe WDS analysis of silicate-containing borate created at 650°C. The contact time refers to the time that the glass was left in the borate.

Contact time (hours)	wt. % SiO_2
12	4.31
14	6.05
15	6.15
18	6.38

A 14 hour contact time was selected since it provided a glass diffusion level (6.05 % SiO_2) close to that of the silicate-containing borate of the standard material. This procedure was used to create 115 g of silicate-containing borate. The density of this material was measured using a 100 ml pycnometer to be 6.052 g/ml ($\pm$0.009). This is the value that will now be used as the density of the borate.

3.3.7 Corrected Magstream separation results

The Magstream separator was calibrated with glass, pyrite and silicate-containing borate. The previous separations were repeated using the new density split-points and the complete results are shown in Appendix 5. A summary of the results is shown in Table 3.6.

Table 3.6: Results of the corrected Magstream separations of the standard material.

Composition fraction (vol. % borate)	Magstream split-points (g/ml)	Avg. dens. (g/ml)	Mass (g)	Mass %	Vol. (ml)	Vol. %
-5	-2.680	2.591	67.99	19.66	26.24	29.16
5-15	2.680-3.035	2.858	25.64	7.41	8.97	9.97
15-25	3.035-3.390	3.213	21.94	6.34	6.83	7.59
25-35	3.390-3.745	3.568	23.07	6.67	6.47	7.19
35-45	3.745-4.100	3.923	27.66	8.00	7.05	7.84
45-55	4.100-4.455	4.278	27.60	7.98	6.45	7.17
55-65	4.455-4.810	4.633	19.07	5.51	4.12	4.57
65-75	4.810-5.165	4.988	25.08	7.25	5.03	5.59
75-85	5.165-5.520	5.343	30.52	8.82	5.71	6.35
85-95	5.520-5.875	5.698	19.08	5.52	3.35	3.72
+95	+5.875	5.964	58.26	16.84	9.77	10.86
		Total:	345.91	100.00	89.99	100.00

The amount of locked material (i.e. 5-95 vol. % borate) was 63.50 mass % or 59.98 vol. %. The high amount of locked material (considering the particle size is three Tyler size classes below the grain size) indicates that there was little breakage along the interface. The strong bonding between the two phases may be a positive side effect of the glass diffusion.

After the Magstream separations, the pycnometer and IA grades of the composition fractions were measured as before. The results are summarized in Table 3.7.

Table 3.7: Pycnometer and IA grades of the corrected composition fractions of the standard material.

Composition fraction (vol. % borate)	Magstream split-points (g/ml)	Pycnometer density (g/ml)	Pycnometer grade (vol. % borate)	IA grade (vol. % borate)
-5	-2.680	2.522	0.6	0.4
5-15	2.680-3.035	2.805	8.5	9.8
15-25	3.035-3.390	3.176	19.0	20.1
25-35	3.390-3.745	3.517	28.6	31.7
35-45	3.745-4.100	3.850	38.0	40.0
45-55	4.100-4.455	4.232	48.7	49.7
55-65	4.455-4.810	4.532	57.2	58.9
65-75	4.810-5.165	4.865	66.6	68.3
75-85	5.165-5.520	5.257	77.6	78.0
85-95	5.520-5.875	5.647	88.6	87.9
+95	+5.875	6.265	106.0	98.1

For all the fractions, both the pycnometer and IA grades fall in the composition fraction range and in most cases, they are close to the midpoint of the range. While the

IA grade is higher than the pycnometer grade in some cases, the difference is not significant.

The pycnometer grade of the +95 vol.% borate fraction was greater than 100 vol.% borate. This can be explained by considering the creation of the standard material. Although the glass is always in contact with the borate, there is a layer of borate at the bottom of the crucible (the glass grains float in the borate due to their lower density) that is at a distance from the glass grains and thus does not contain as much diffused glass. The silicate-containing borate density was calculated only for borate that had been in close contact with glass grains. The high pycnometer grade in this fraction does not present a problem since all this high density borate reports to the +95 vol.% borate fraction where it belongs.

These corrected fractions represent the standard material that was used to test the various stereological correction procedures.

3.4 Analysis of the effect of discontinuities on the sectioned distribution of the standard material

The Magstream separator is not a perfector separator so the composition fractions had to be cleaned. In the cleaning of the composition fractions, all the material which did not re-report to the original composition fraction was removed from consideration. This may lead to the preferential exclusion of particles at the ends of a composition fraction since they are the most likely to be removed by a cleaning operation. For example, in the 45-55 vol.% borate fraction, particles with a composition close to 45 or 55 vol.% borate are more likely to be removed than those particles with a composition close to 50 vol.% borate. This preferential removal of particles close to the ends of the fraction coupled with the setting of the split-points at 0.5 vol.% borate closer to the midpoint of the composition fraction (as described in Section 3.3.2) may create a discontinuity in the liberation distribution when the different composition fractions are combined together.

The effect of this type of discontinuity was examined by simulating the situation in a distribution of computer-generated spheres. These spheres were two-phase ("0" and

"1") and single-capped (the spheres are further described in the next chapter where they were used to test the stereological correction procedures). The effect of an extreme discontinuity was simulated by assuming that only particles (spheres) at the midpoint of the composition fraction remained after the cleaning of the fraction. This was compared to an even distribution of particles across the range of the composition fraction. Two sphere composition fractions were examined: 15-25 vol. % phase "1" and 45-55 vol. % phase "1". The following distributions were created and sectioned:

1(a) spheres with a composition of 20 vol. % phase "1" only

1(b) an even distribution of spheres in a composition range between 15-25 vol. % phase "1" discretized into intervals of 0.5 vol. % phases "1" (i.e. spheres with compositions of 15.0, 15.5, 16.0, 16.5, ..., 24.5, 25.0 vol. % "1" were created and it was assumed that there was an identical number of spheres at each composition)

2(a) spheres with a composition of 50 vol. % phase "1" only

2(b) an even distribution of spheres in a composition range between 45-55 vol. % phase "1" discretized into intervals of 0.5 vol. % phases "1".

The results of the sectioning of the above distributions are shown in Fig. 3.10. The results indicate that the sectioning of a single composition was very close to the sectioning of an even distribution centred on that composition. The simulated discontinuities appeared to have little effect on the sectioning data. The composition fractions appear to be quite robust with respect to discontinuities.

3.5 Analysis of the effect of misplaced material on the sectioned distribution of the standard material

The purpose of the cleaning operations is to minimize the occurrence of misplaced material. The amount of misplaced material due to non-ideal separation in a given composition fraction can be estimated by considering the relationship between a fraction and the Magstream calibration (performance) curve (Fig. 3.11).

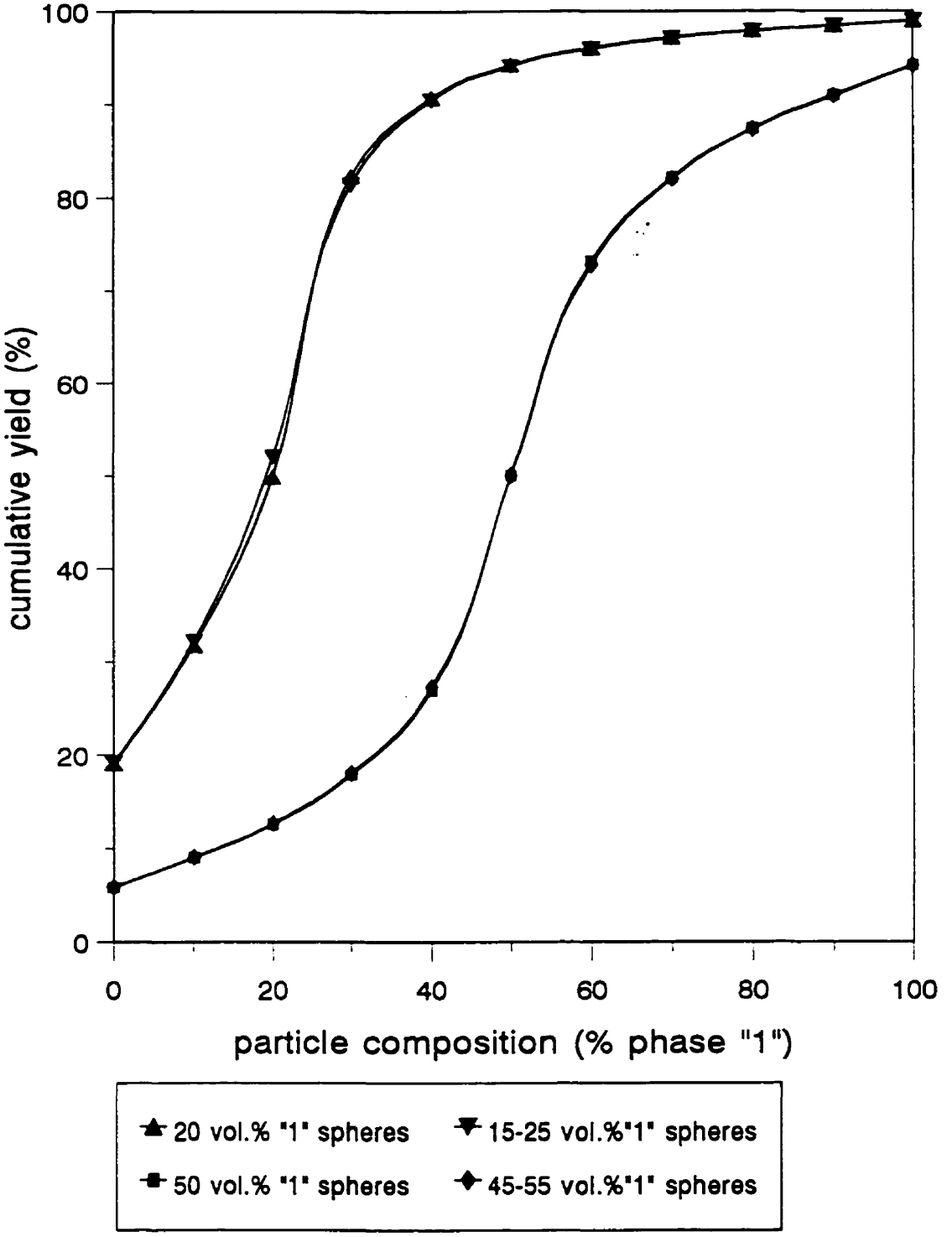

Fig. 3.10: Comparison of the sectioning of spheres of a single composition with the sectioning of spheres with an even distribution (spanning a 10 vol.% "1" interval) centred on the single composition.

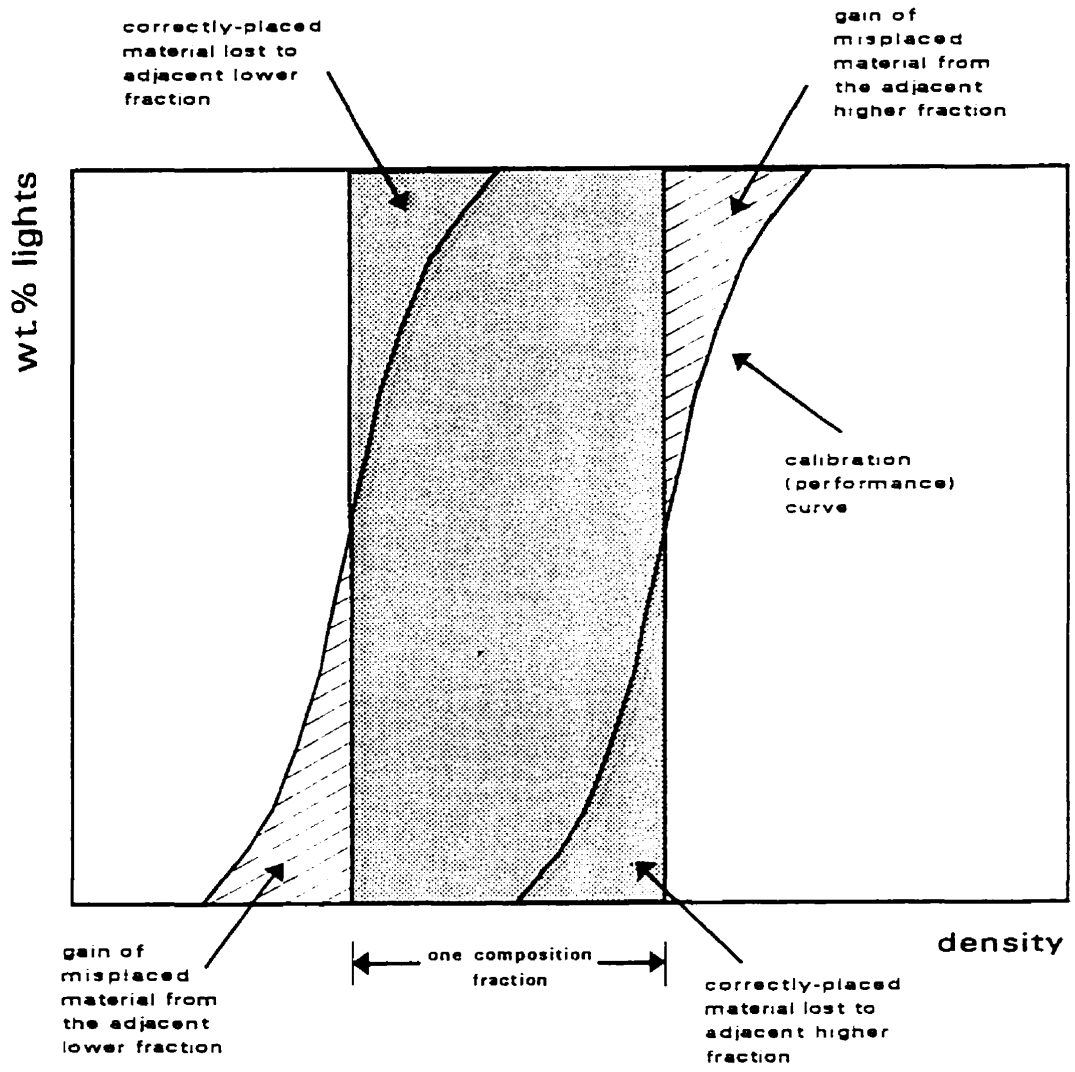

Fig. 3.11: Misplaced material lost and gained by a composition fraction.

It can be seen that the misplaced material in a given fraction originates from its two adjacent fractions. There is a corresponding loss of correctly-placed material to the adjacent fractions. If one assumes that the separator behaves in a similar manner at both split-points then the gain and loss of material is equal [70].

For each composition fraction, three separations were performed at each split-point. The first separations isolate the composition fraction and the subsequent two separations act as cleaning operations. Any material that did not re-report to its original composition fraction was removed from consideration. The mass fraction of misplaced material in a composition fraction after one Magstream separation at both split-points, γ, can be calculated by determining: [striped area]/[shaded area] (refer to Fig. 3.11). The mass fraction of correctly-placed material in a composition fraction after one Magstream separation at both split-points is defined as $1-\gamma$. Therefore, in the final product, the mass fraction of misplaced material is: $\gamma^3/(1-\gamma)^3$. The end fractions (i.e. -5 vol. % borate and +95 vol. % borate) have only one adjacent fraction and thus the amount of misplaced material in these fractions are roughly half the amount of misplaced material in the adjacent fraction.

The accuracy of the Magstream separator and the value of γ varies with density (the separator is more effective at lower densities) and, therefore, the value of γ was calculated for each of the three materials (glass, pyrite and lead borate) which were used to calibrate the Magstream. These material span the entire density range of the standard material. The calibration curves (Figs. 3.4-7) were curve-fitted and γ was found by integration. Table 3.8 tabulates the values of γ and the mass fraction of misplaced material in the final product.

It can be seen that the amount of misplaced material in the composition fractions below 5.0 g/ml was small ($<1\%$). However, at densities near 6.8 g/ml, the amount of misplaced material was significantly higher ($\approx 18\%$). It should be noted, though, that the amount of misplaced material in the high density composition fractions is lower than this for two reasons:

1) silicate-containing borate (6.052 g/ml) was the heavy phase.

2) the highest density separation was performed at 95 vol.% of the heavy phase which corresponds to 5.875 g/ml.

Table 3.8: Mass fraction of misplaced material in the final product at different densities.

Calibration material	Density (g/ml)	Mass fraction of misplaced material in a composition fraction after one separation at both split-points γ	Mass fraction of misplaced material in the final product $\gamma^3/(1-\gamma)^3$
glass (Fig. 3.4)	2.502	0.0696	0.0004
pyrite (Fig. 3.5) low density magnetic fluid	5.024	0.1646	0.0076
pyrite (Fig. 3.6) high density magnetic fluid	5.024	0.1088	0.0018
lead borate (Fig. 3.7)	6.833	0.3606	0.1794

The effect of misplaced material on the sectioning data was examined by simulating the occurrence of misplaced material in computer-generated, single-capped spheres. Two cases were examined: spheres with a composition of 20 and 50 vol.% phase "1". Two levels of misplaced material, 10 and 20%, were simulated for both cases. For example, for the case of 50 vol.% "1" spheres with 10% misplaced material, the sphere distribution consisted of:

1) 90% of the spheres with a composition of 50 vol.% phase "1"
2) 5% of the spheres with a composition of 40 vol.% phase "1"
3) 5% of the spheres with a composition of 60 vol.% phase "1".

The misplaced material was assumed to originate equally from the adjacent fractions. The sectioned distributions are plotted in Fig. 3.12. The curve for the 20 vol.% "1" spheres was nearly identical to the curves simulating 10% and 20% misplaced material; the same result was obtained for the 50 vol.% "1" spheres case. These results indicate

that up to 20 % misplaced material in a composition fraction will have little impact on the sectioning data.

Two extreme cases were also examined. Fig. 3.13 shows the results of the sectioning of the same distributions as before, but this time it was assumed that all the misplaced material originated from the adjacent higher composition fraction. Although in this extreme case, the sectioned distributions with misplaced material were further away from the sectioned distributions without misplaced material, it appears that the misplaced material did not greatly affect the sectioning data. The composition fractions appear to be quite robust with respect to misplaced material.

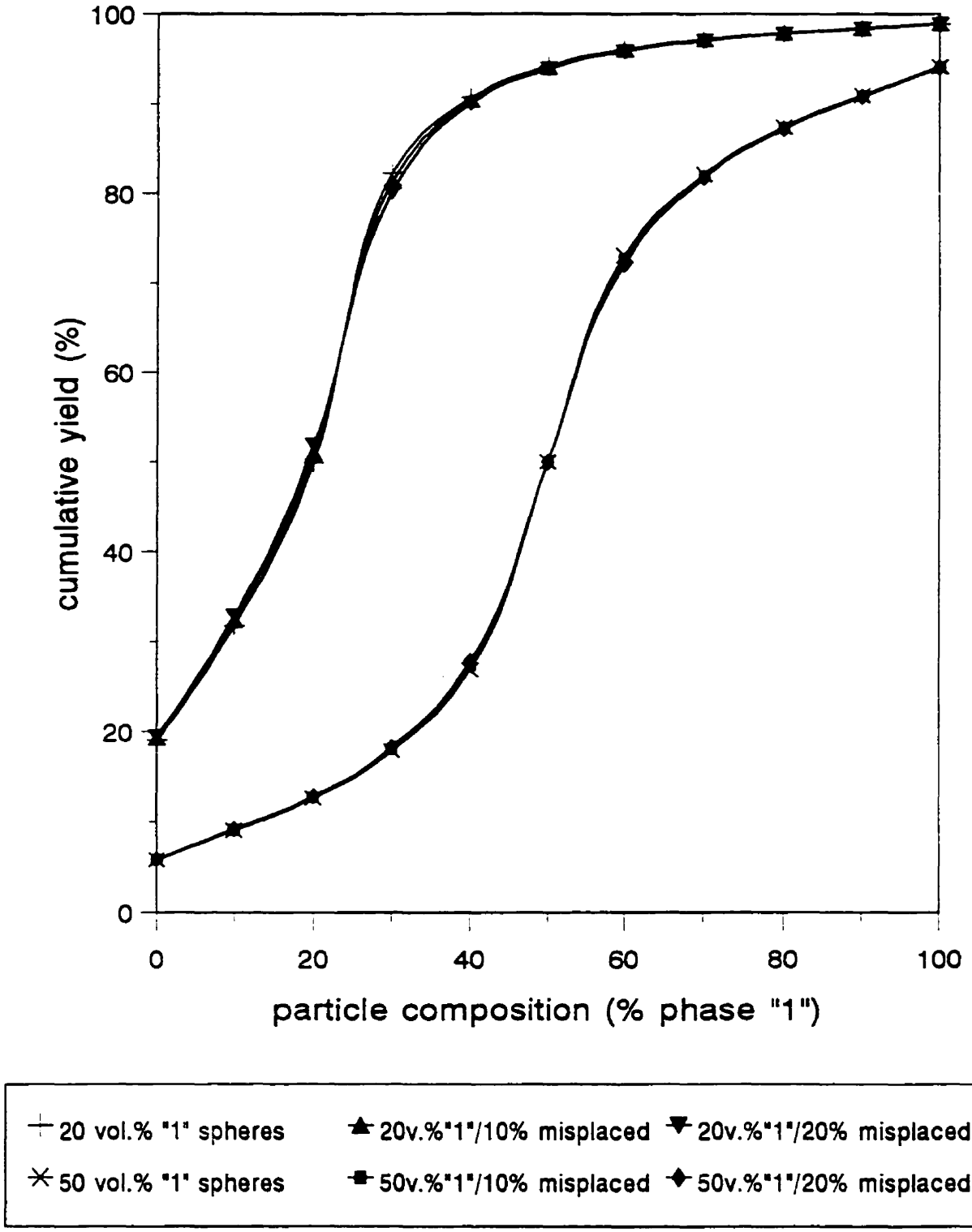

Fig. 3.12: Comparison of the sectioning of composition fractions with and without misplaced material. The misplaced material originated equally from the adjacent fractions.

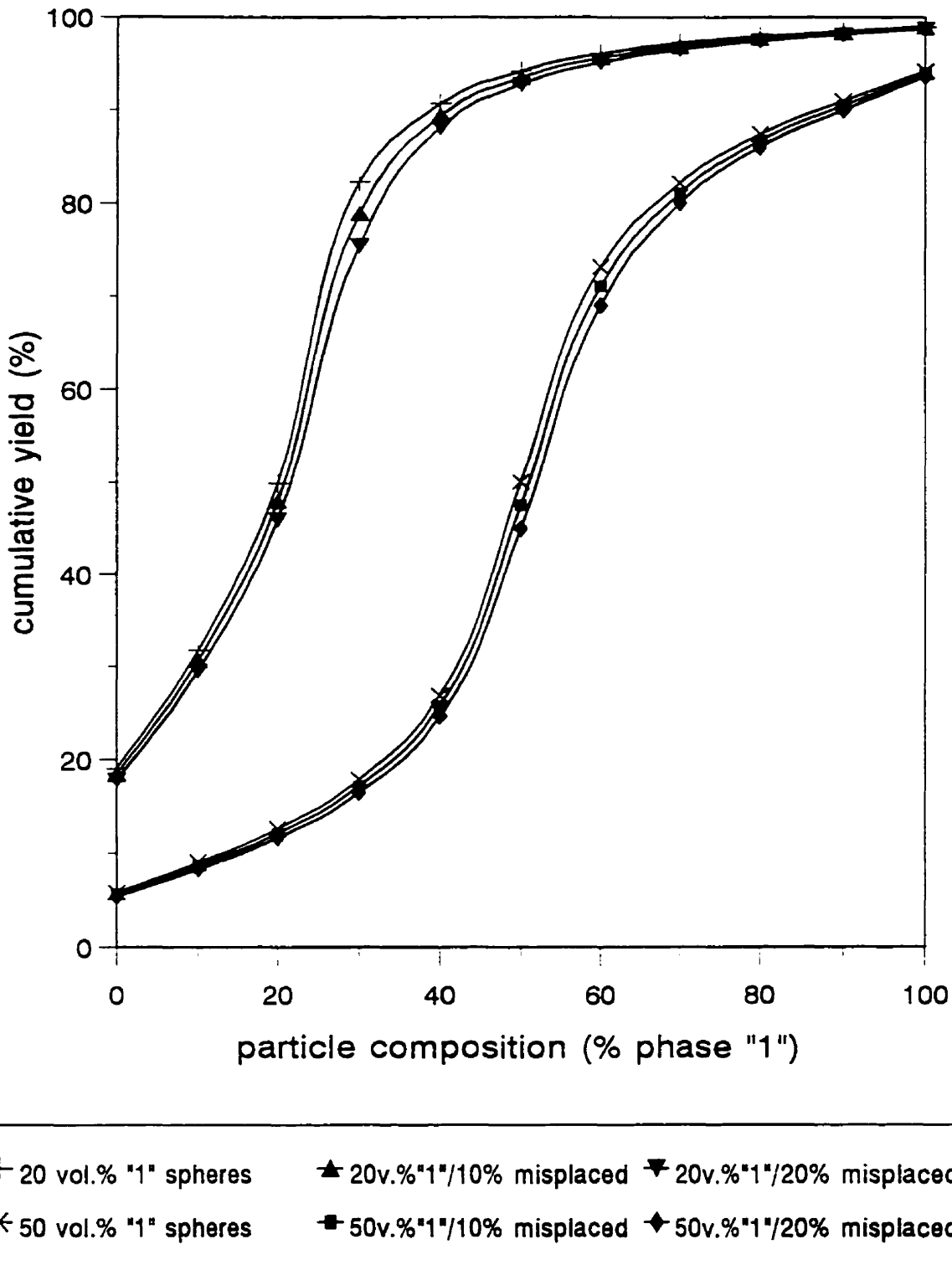

Fig. 3.13: Comparison of the sectioning of composition fractions with and without misplaced material. All the misplaced material originated from the adjacent higher fraction.

CHAPTER 4: SECTIONING AND CORRECTION OF COMPUTER-GENERATED SPHERES

4.1 Overview

The robustness of procedures that have been developed to correct stereological bias in liberation data was assessed here by examining their ability to correct sectioning data from a distribution of computer-generated spheres. The correction procedures that were examined were: large-sections correction, Hill's fast approximation, Barbery's correction and PARGEN correction.

The use of spheres to represent mineral particles has enjoyed previous applications. Jones and Horton [13], Moore and Jones [12], and Barbery et al. [9,71] have examined the sectioning of spheres with linear probes. Meloy and co-workers [72,73,74] used spheres in the development of their liberation models and theories. Gateau and Broussaud [14] used spheres with different locking textures to develop relationships between one, two and three-dimensional degrees of liberation. Hill et al. [7,8] suggested that a correction based on spheres could define an upper bound to the correction with the true liberation distribution lying between this boundary and that defined by the sectioning data. Other researchers have used the sphere model as a method of verifying correction procedures [6(pp.197-200),29,31].

In this work, assemblages of two-phase, single-capped spheres (i.e. spheres exhibiting simple locking with planar interfaces) were simulated on a computer. All the spheres were the same size to reflect the fact that liberation analyses are usually performed on a size-by-size basis. Different assemblages were created ranging from very narrow distributions to distributions representative of mineral processing. As mentioned earlier, since liberation analyses are performed one phase at a time, only two phases ("0"

and "1") need be considered - all phases other than the phase of interest can be collectively considered as the second phase.

The true liberation distribution (actual assemblage of sphere compositions) was sectioned to yield the sectioned (or observed) liberation distribution. The sectioned distribution was corrected with the various procedures to yield the corrected (or reconstructed) liberation distribution.

The advantages of using the sectioning of computer-generated, single-capped spheres to represent the real case are:

1) Simple locking with planar interfaces creates many false free sections thus exacerbating the stereological bias. This provides a severe test for the correction procedures.
2) The true and sectioned distributions are precisely and accurately known.
3) The number of particles generated can be set to meet any statistical requirement.
4) A variety of liberation distributions can be easily constructed.
5) The examination of real particles may introduce bias into the sectioning data other than stereological bias. Bias associated with sample preparation and image analysis processing may produce inaccuracies in the data for which no stereological correction procedure can compensate.

The disadvantage of using the sectioning of spheres is that real mineral particles are indeterminate in shape and locking texture. While this is a drawback, it should not obscure the purpose here which is to provide an assessment of the robustness and flexibility of the correction procedures.

The spheres were generated and sectioned using the numerical integration technique described by Hill [7] and verified by Finch et al. [10]. The software program, SECTDIST (Appendix 6), was developed for this purpose.

In the next chapter, the sectioning of standard material particles having the same distributions as the computer-generated spheres will be discussed. In order for the two sets of distributions to be identical, the average composition of the composition fractions of the spheres was set to the grade of the composition fractions of the standard material.

There were, however, two measures of the grade of the composition fractions of the standard material: the IA (image analysis) and pycnometer grades (Table 3.7). The decision was made to use the IA grade. This was done to maintain consistency since the IA grade provided a measure of the grade in the form that the liberation analysis was performed. In any case, the IA and pycnometer grades did not differ greatly.

4.2 Verification of sphere sectioning

The computer-generated spheres must be randomly sectioned to provide useful data. All correction procedures assume that sectioning data are the result of random sectioning.

To ensure the random sectioning of the spheres, the sectioning data generated by the SECTDIST software was verified using a Crofton check on the sphere volume as suggested by Barbery and Pelletier [9]. A modified form of Crofton's equation was used [15]:

$$V = \frac{256}{45\,\pi^{3/2}} \left(\frac{\overline{A^{5/2}}}{\overline{A}} \right) \tag{4.1}$$

where V = sphere volume

A = section area.

The radius of the SECTDIST computer-generated spheres is 1; therefore, the theoretical volume is 4.188790. After 100 000 spheres had been generated and sectioned, the calculated volume was 4.188793, a close match.

Two other verifications [15] of the sphere volume were also performed:

$$V = \left(\frac{6}{\pi} \right)^{1/2} \overline{A}^{\,3/2} \tag{4.2}$$

$$V = \left(\frac{35}{12\,\pi} \, \frac{\overline{A^4}}{\overline{A}} \right)^{1/2} \tag{4.3}$$

After 100 000 spheres had been generated and sectioned, Equations 4.2 and 4.3 yielded sphere volumes of 4.188869 and 4.188566, respectively. Again, both values were quite close to the theoretical volume.

The composition of the spheres generated by SECTDIST were verified as well. A range of compositions (5, 10, 15,..., 50 vol. % "1") was tested. A sphere composition of 0 vol. % "1" was not tested since this is a trivial case. Also, it was not necessary to test sphere compositions over 50 vol. % "1" due to the symmetrical nature of single-capped spheres (for example: the sectioning of 60 vol. % "1" spheres provides sections identical to the sectioning of 40 vol. % "1" spheres except that the phase labels are reversed). For each composition, 100 000 spheres were generated and sectioned. The composition was measured by applying Delesse's equation (Equation 3.14) to the sectioning data. A comparison between the true composition and the measured composition is shown in Table 4.1.

Table 4.1: True composition of the spheres compared with the composition measured using Delesse's equation.

True composition (vol. % "1")	Measured composition (vol. % "1")
5	5.00009
10	10.00017
15	15.00009
20	20.00016
25	25.00023
30	30.00037
35	35.00047
40	40.00048
45	45.00048
50	50.00045

Although the measured composition is consistently slightly higher, the data show a close match between the true and measured compositions.

4.3 Selection of the exclusion criterion for the large-sections correction

For the large-sections corrections, the exclusion criterion (the area below which a section is excluded from consideration in the liberation analysis) affects its performance. As the exclusion criterion increases (i.e. more sections are excluded), the large-sections correction becomes more effective. The relationship between the exclusion criterion and the correction effectiveness was investigated using the sectioning of single-capped spheres of a single composition.

SECTDIST was used to generate and section 100 000 spheres at three different compositions (10, 30 and 50 vol.% "1"). For each composition, the large-sections correction was applied using four exclusion criteria: sections smaller than 50, 70, 90 and 95 area % of the largest section area were excluded; this led to the exclusion of 29, 45, 68 and 78% of the sections, respectively. The results are shown in Fig. 4.1. As expected, the larger the exclusion criterion, the closer the corrected distribution is to the true distribution.

In subsequent use of the large-sections correction in this thesis, the exclusion criterion was set at 90% (i.e. all sections smaller than 90 area % of the largest section were excluded). This appears to provide an adequate compromise between the effectiveness of the correction and statistical requirements (using a 90% exclusion criterion, 68% of the sections are excluded). In computer simulations, obtaining statistically valid data is not a problem since the number of spheres generated and sectioned can be increased to satisfy any statistical demand, but it is an issue when dealing with real particles. The statistics of liberation will be discussed in the next chapter when standard material particles are used.

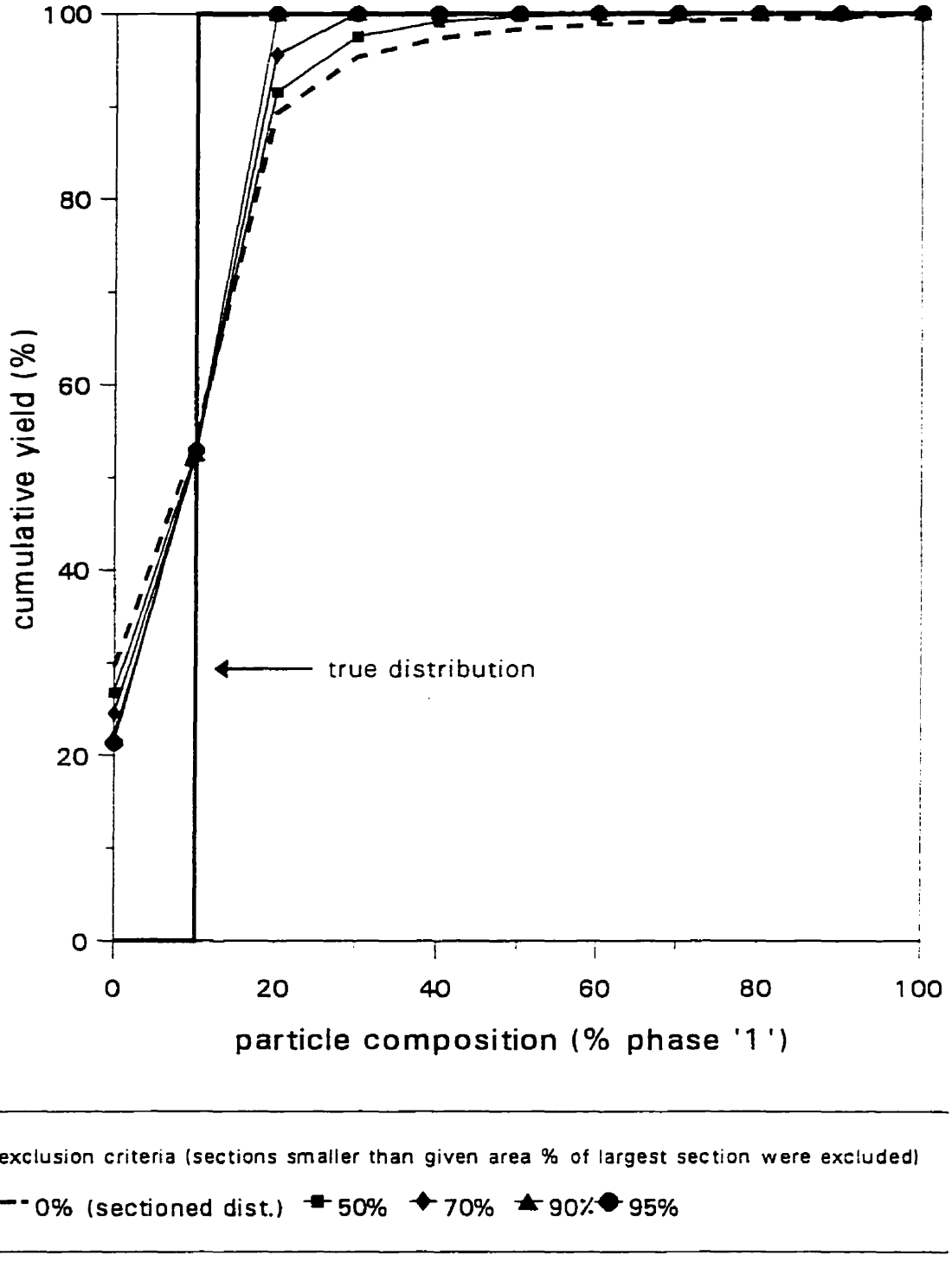

Fig. 4.1(a): Large-sections correction of the sectioning of 10 vol.% phase "1" spheres.

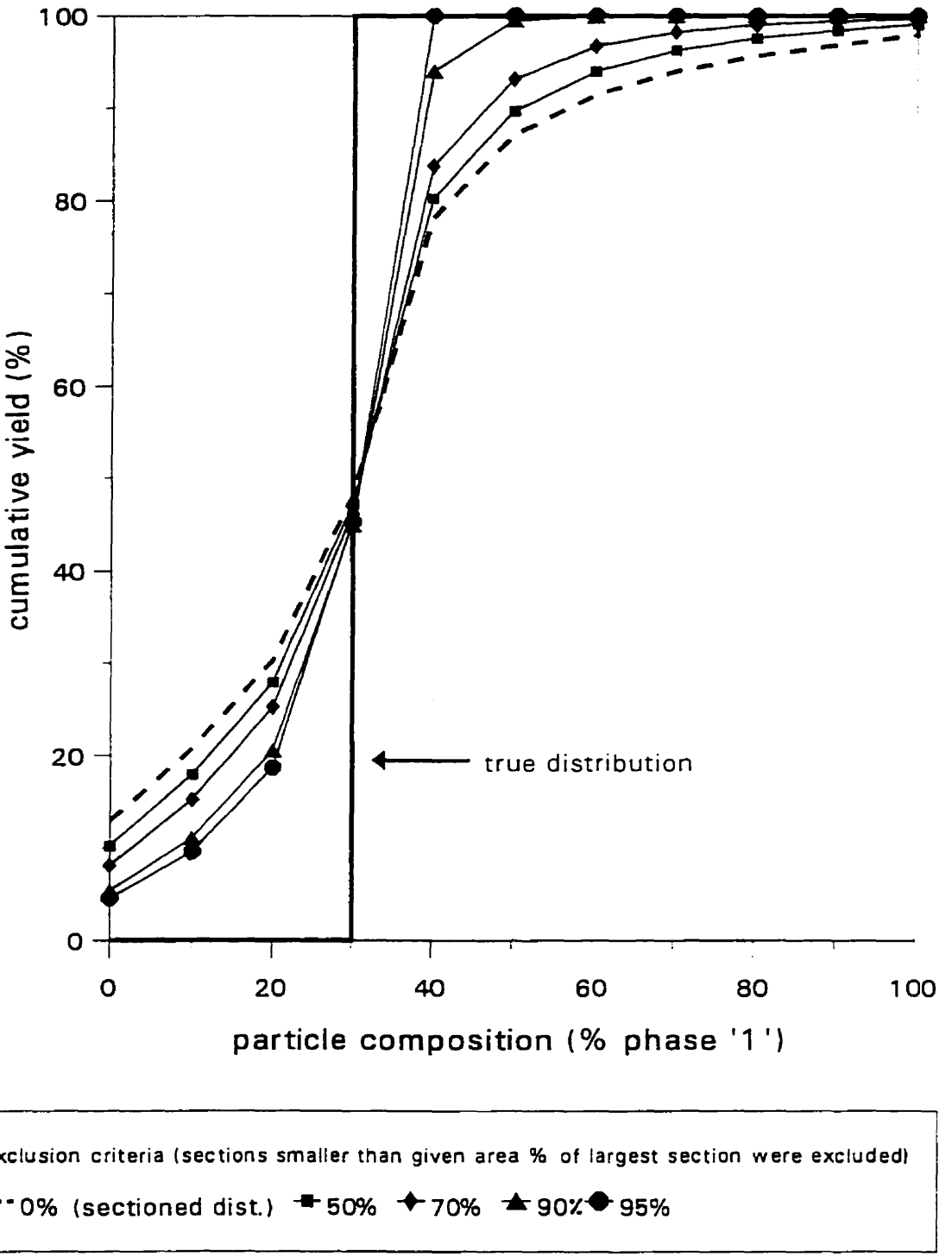

Fig. 4.1(b): Large-sections correction of the sectioning of 30 vol.% phase "1" spheres.

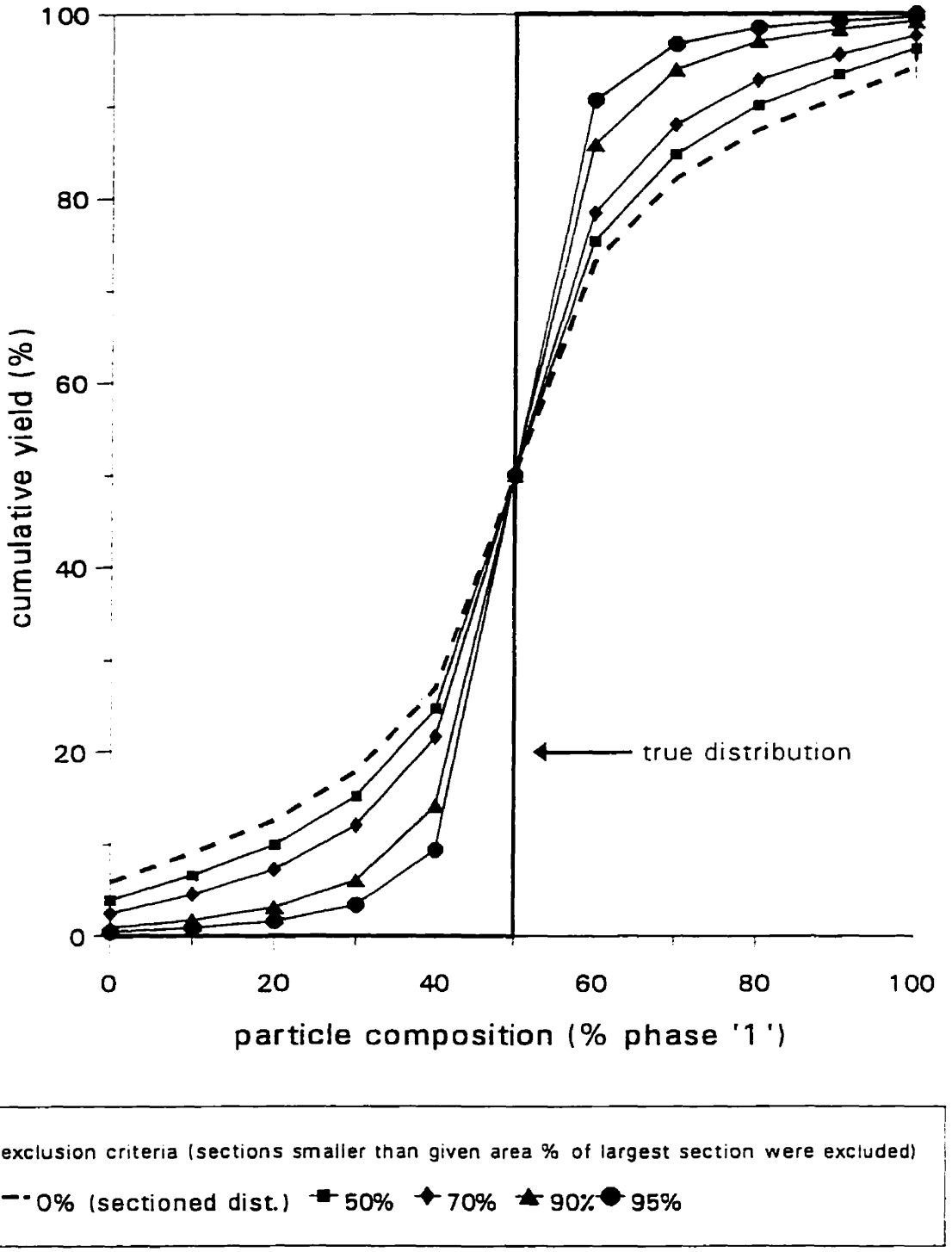

Fig. 4.1(c): Large-sections correction of the sectioning of 50 vol.% phase "1" spheres.

4.4 Results of the correction procedures

Seven cases (distributions of spheres) were created (Table 4.2). For each case, 100 000 spheres were generated and sectioned. The spheres were single-capped, two-phase (phases "0" and "1") and monosized. The spheres were generated at the IA grades of the composition fraction ranges of the standard material and they were used to represent the whole range. The sectioning data were corrected using the large-sections correction, Hill's fast approximation, Barbery's correction and PARGEN correction.

The exclusion criterion for the large-sections correction was 90%.

Hill's fast approximation was performed as described by Hill [7,8]. An example of this correction is shown in Appendix 7.

Barbery's correction was performed using the computer software, BOOKING, developed at Laval University. A boolean texture was used to model the ore texture. Phase "0" was selected as the matrix phase and phase "1", the grain phase. According to Barbery [6(pp.197-200)], neither the designation of the grain and matrix phases nor the selection of ore texture (boolean or Poisson) affect the corrected results.

The PARGEN correction was performed using the computer software, Stereological Reconstruction of Linear and Areal Grade Distributions, developed at the University of Utah. The dispersion density (dd), the number of grains per particle, was set to one. As mentioned earlier, the PARGEN correction will yield different results depending on the designation of the grain and matrix phases. Unfortunately, with single-capped spheres, the designation of the phases is not clear since either phase could be considered the grain phase. It was decided that both cases should be examined: PARGEN correction using phase "0" as the grain phase (which will be referred to as PARGEN "0") and PARGEN correction using phase "1" as the grain phase (which will be referred to as PARGEN "1").

The graphical results are presented in Fig. 4.2 which shows the cumulative yield plotted against the particle composition.

Table 4.2: The seven cases (distributions of spheres) that were computer-generated.

Composition fraction (vol. % "1")	IA grade (vol. % "1")	Volume distribution (%)						
		Case 1	Case 2	Case 3	Case 4	Case 5	Case 6	Case 7
0	0.0	0.0	0.0	20.0	80.0	5.0	0.0	0.0
0-5	0.4	0.0	0.0	10.0	1.0	10.0	5.0	0.0
5-15	9.8	0.0	0.0	8.0	1.0	45.0	5.0	50.0
15-25	20.1	0.0	0.0	6.0	1.0	15.0	5.0	0.0
25-35	31.7	0.0	10.0	3.0	2.0	15.0	10.0	0.0
35-45	40.0	0.0	20.0	2.0	3.0	10.0	15.0	0.0
45-55	49.7	100.0	40.0	2.0	3.0	0.0	15.0	40.0
55-65	58.9	0.0	20.0	2.0	2.0	0.0	10.0	0.0
65-75	68.3	0.0	10.0	3.0	1.0	0.0	5.0	0.0
75-85	78.0	0.0	0.0	6.0	1.0	0.0	5.0	0.0
85-95	87.9	0.0	0.0	8.0	1.0	0.0	5.0	0.0
95-100	98.1	0.0	0.0	10.0	1.0	0.0	5.0	10.0
100	100.0	0.0	0.0	20.0	3.0	0.0	15.0	0.0
Total vol. %		100.0	100.0	100.0	100.0	100.0	100.0	100.0
Overall grade (vol. % "1")		49.7	49.7	49.5	11.1	16.2	55.6	34.6

Case 1: single composition
Case 2: narrow composition range
Case 3: simulated primary-grinding product
Case 4: simulated concentrate or tailings (few locked particles; large amount of free "0")
Case 5: high- or low-grade middlings
Case 6: stream with no free "0" (same locked distribution as Case 4, but with the free "0" removed)
Case 7: very irregular distribution

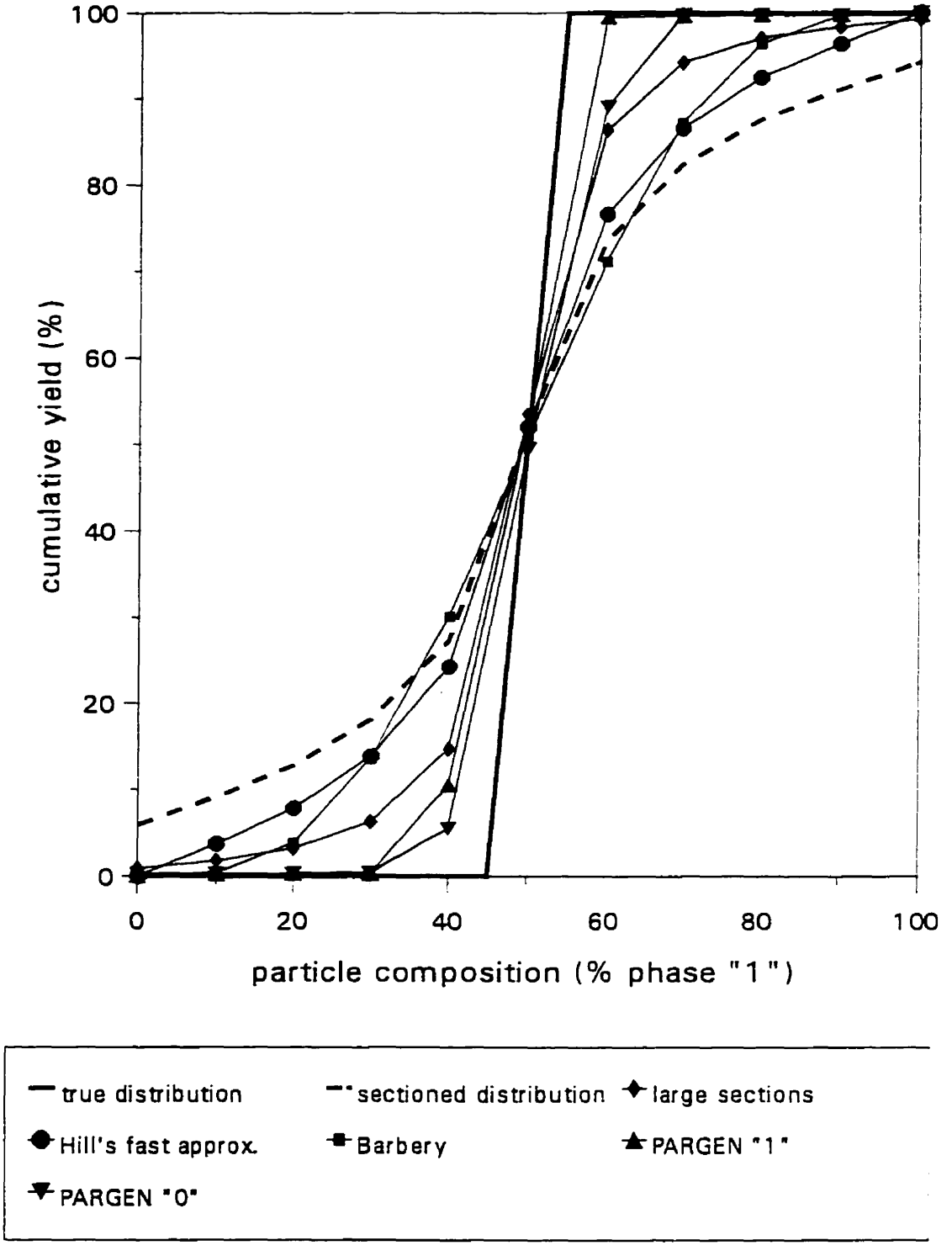

Fig. 4.2(a): Case 1, single composition.

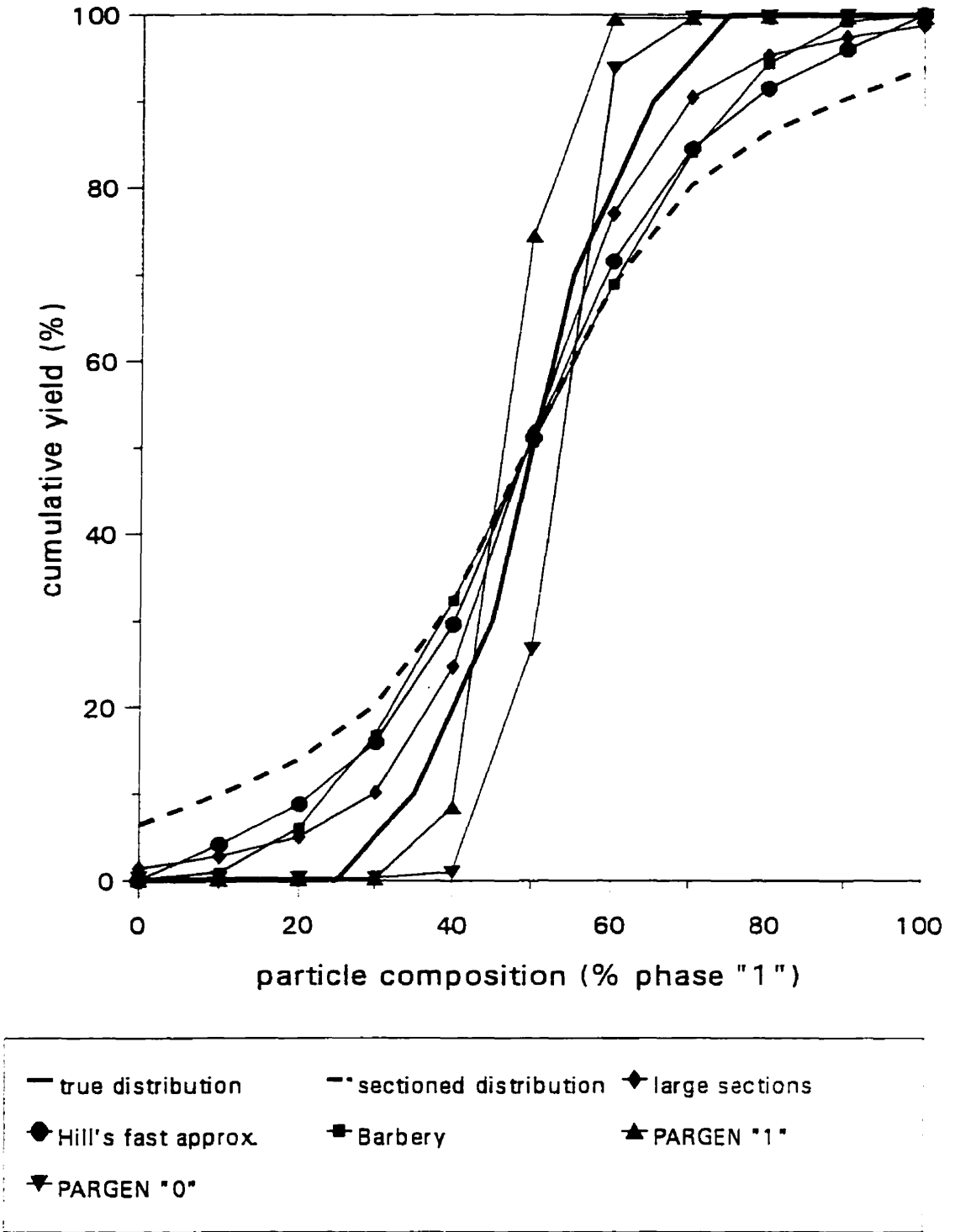

Fig. 4.2(b): Case 2, narrow composition range.

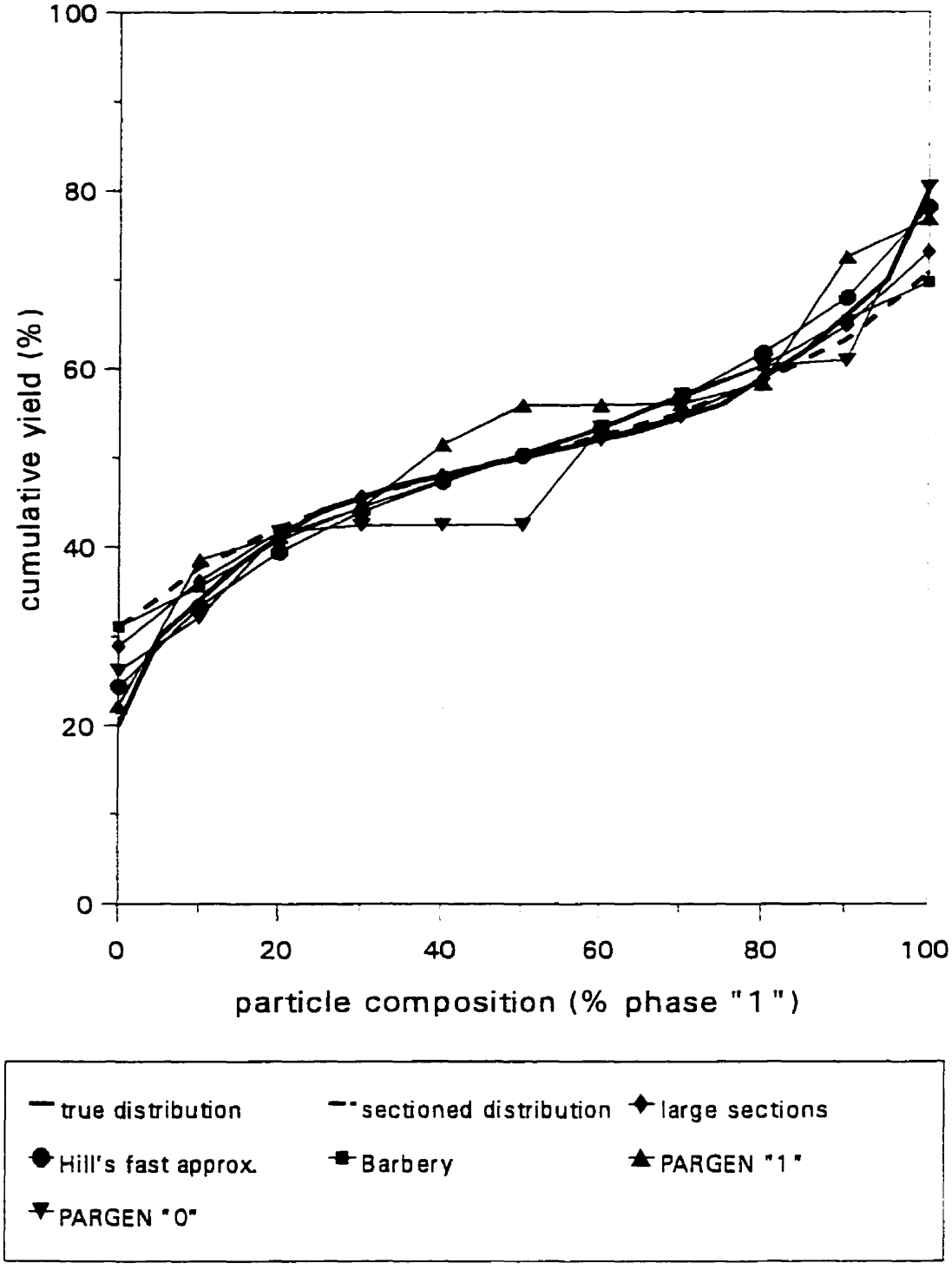

Fig. 4.2(c): Case 3, simulated primary-grinding product.

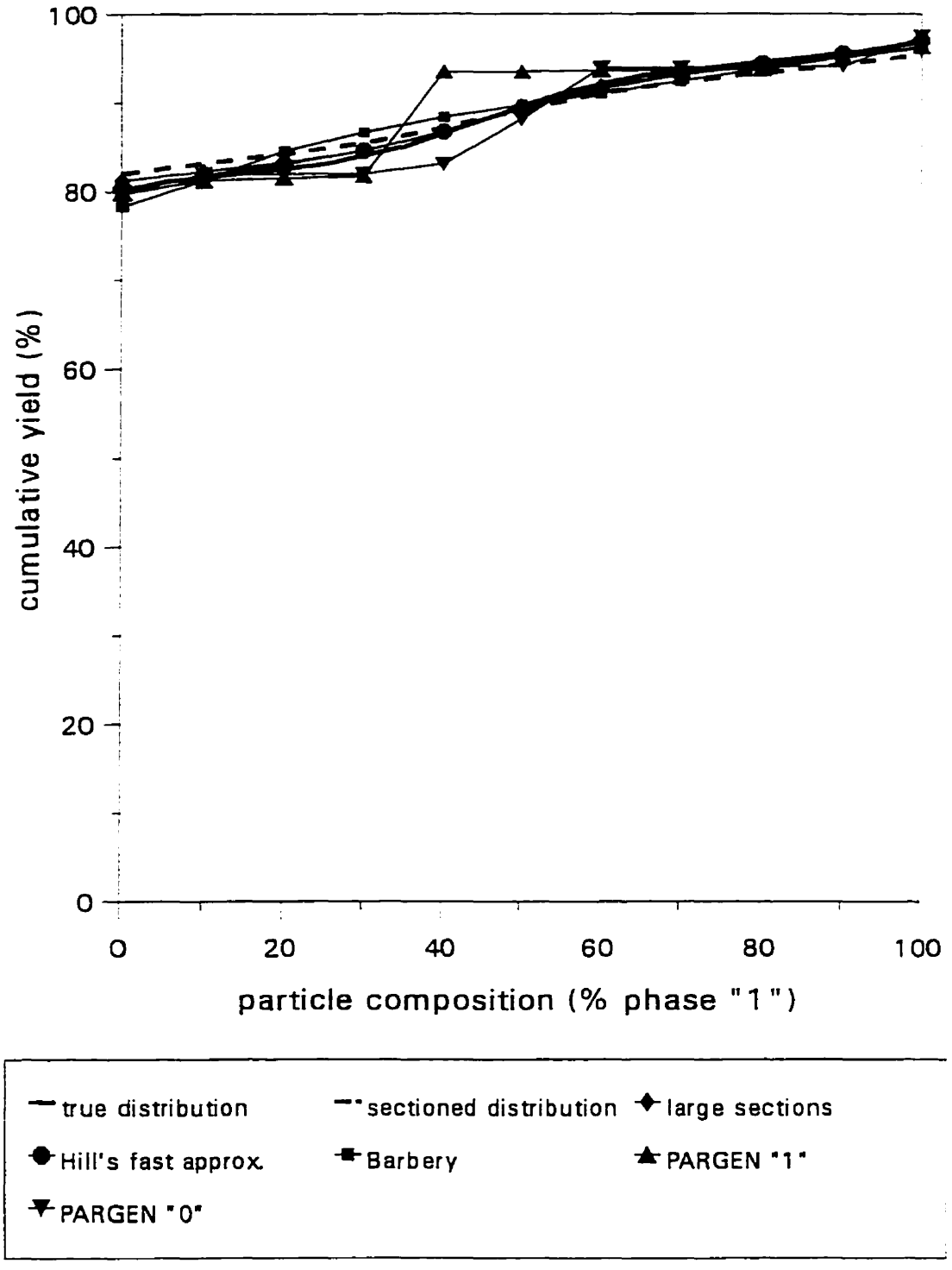

Fig. 4.2(d): Case 4, simulated concentrate or tailings.

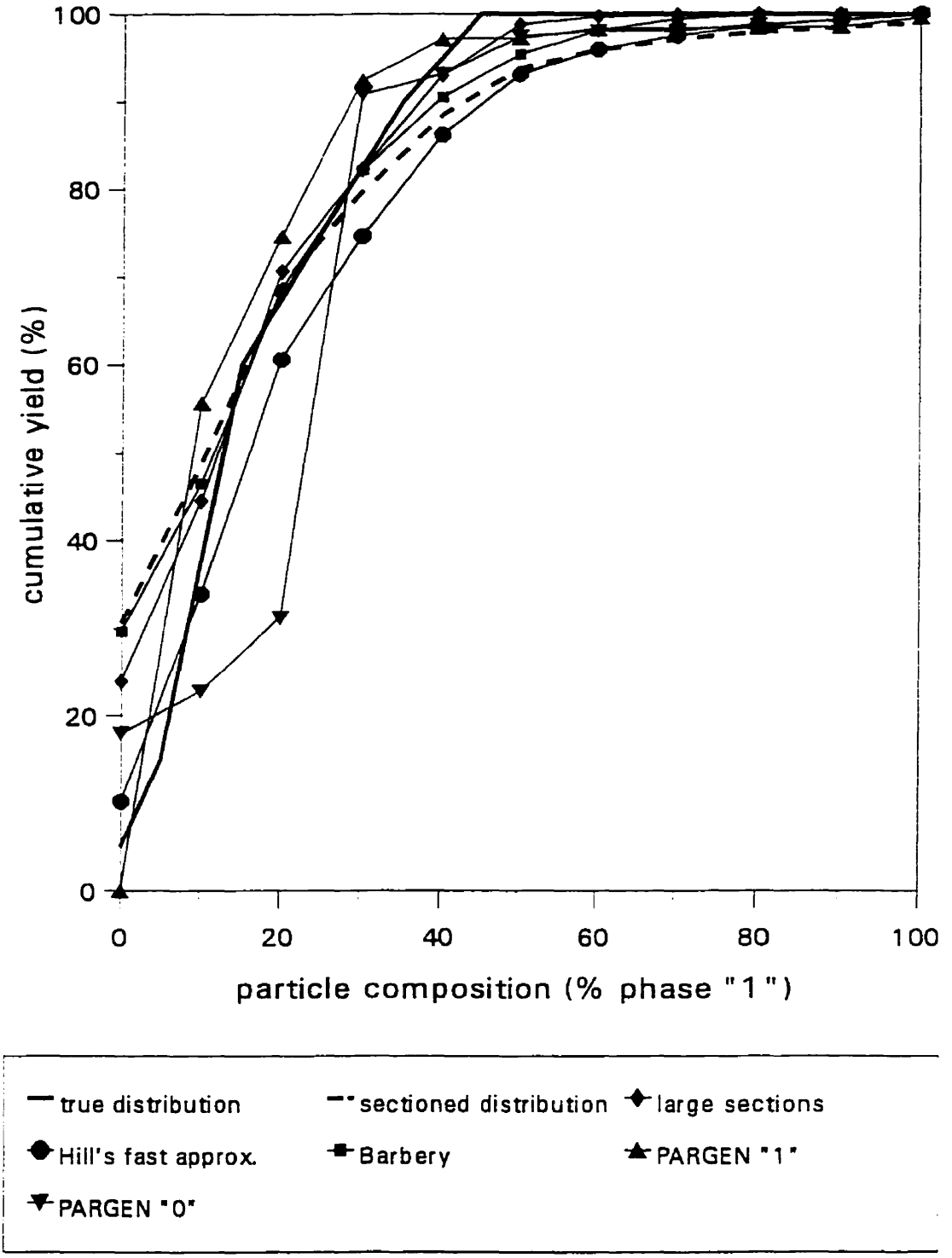

Fig. 4.2(e) Case 5, high- or low-grade middlings.

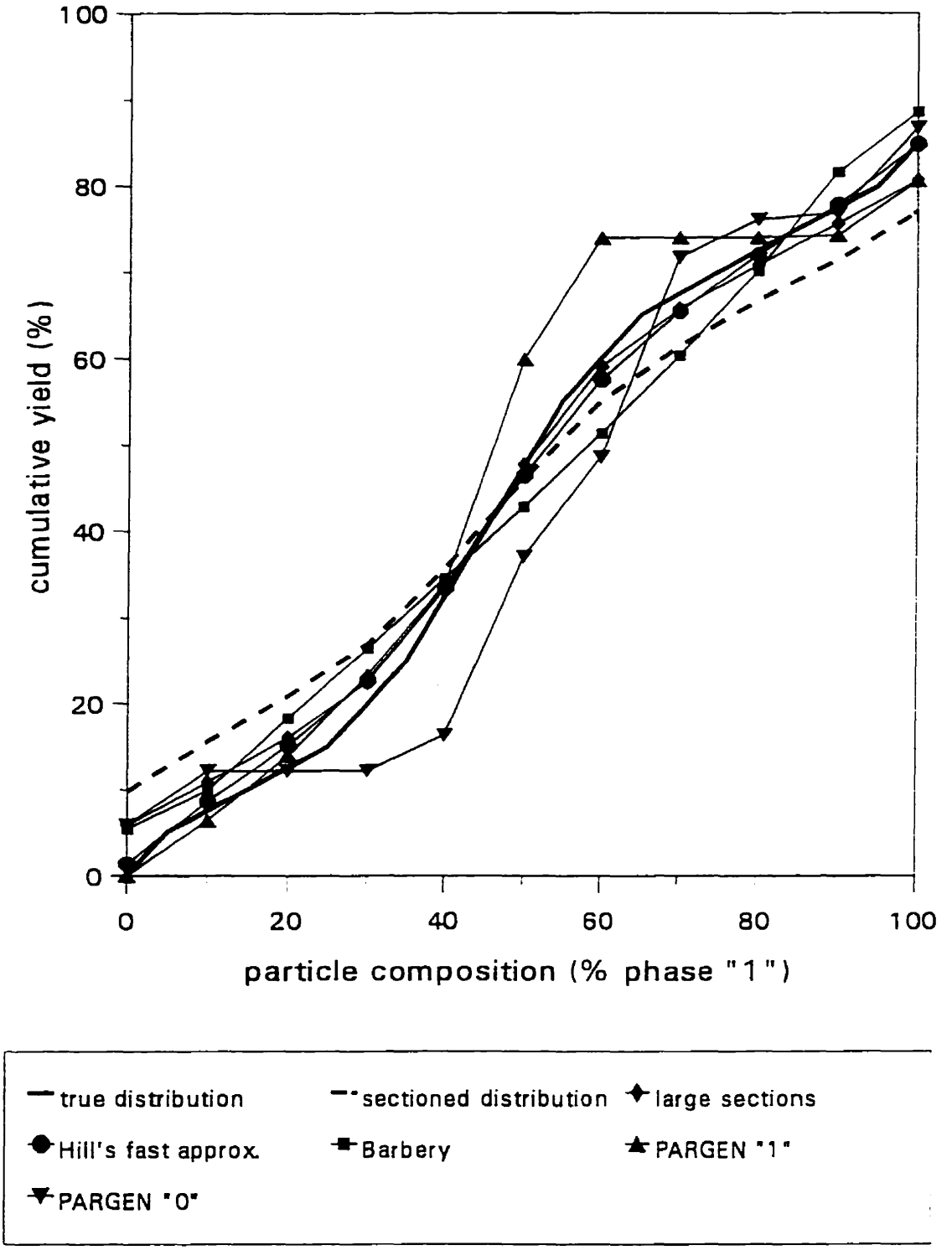

Fig. 4.2(f): Case 6, stream with no free phase "0".

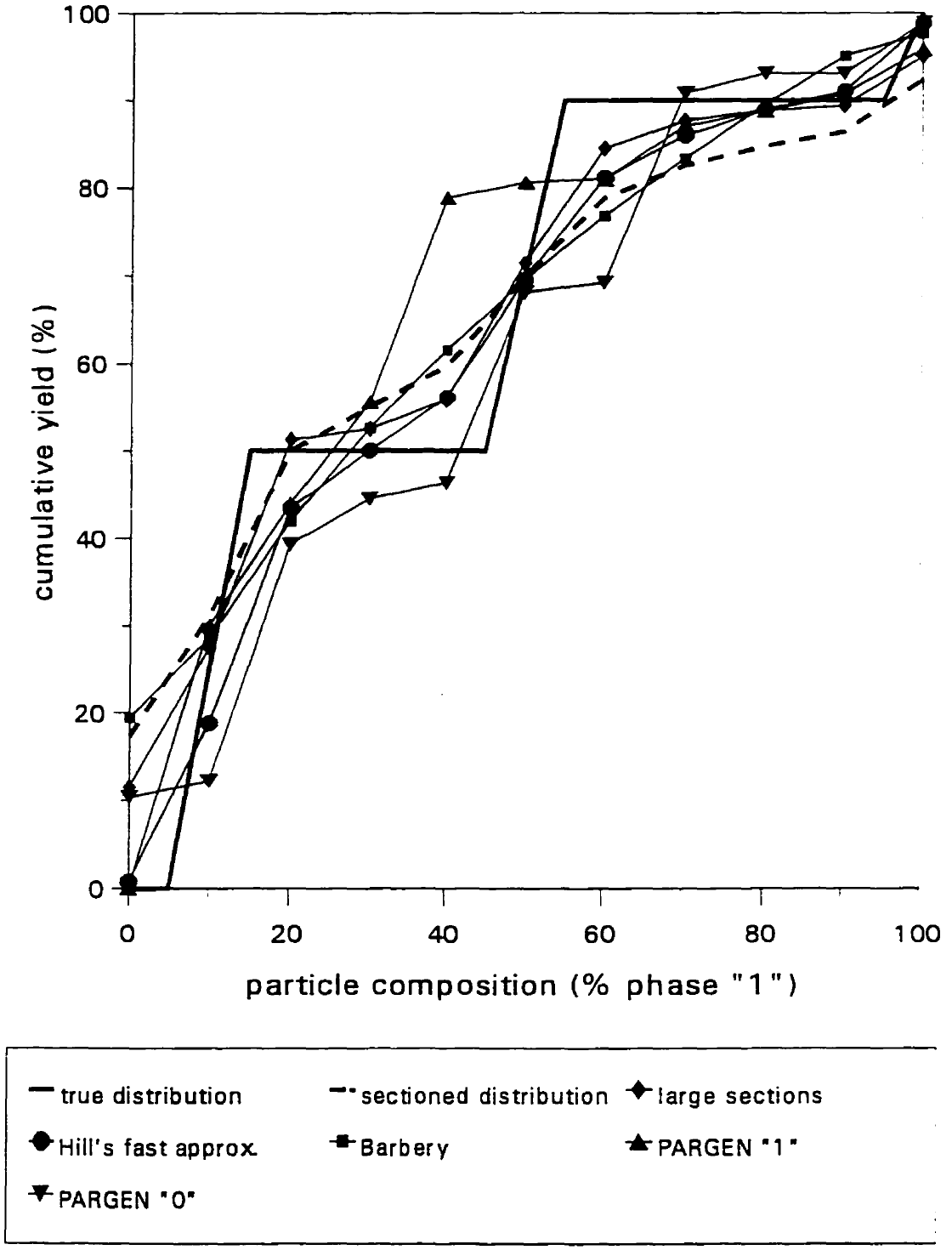

Fig. 4.2(g): Case 7, very irregular distribution.

In this work, the data are presented in cumulative form. The use of cumulative or non-cumulative data is a matter of preference (although it should be noted that they may produce slightly different results [75]). Both methods are commonly used to present liberation information.

The distribution of particles within each composition fraction is assumed to be even. This is reflected in Fig. 4.2 by the straight lines between the cumulation points. An attempt was made to curve-fit the points, but the fit supplied by mathematical software (Jandel Scientific) proved to be unsatisfactory.

Since a visual comparison of the effectiveness of the correction procedures can be subjective, an objective assessment was performed by calculating the mean difference between the true and corrected distributions (δ) and the mean square of the difference between the true and corrected distributions (Δ^2):

$$\delta = \int_0^1 | C(c) - T(c) | \, dc \tag{4.4}$$

$$\Delta^2 = \int_0^1 [C(c) - T(c)]^2 \, dc \tag{4.5}$$

where $C(c)$ = corrected distribution

$T(c)$ = true distribution

c = particle composition.

The δ value can be visualized as the fractional area between the true and corrected distributions. The Δ^2 value represents the average variance between the true and corrected.

The δ and Δ^2 values for all seven cases are tabulated in Table 4.3. The procedures were ranked in order of ascending δ and Δ^2. The values of δ and Δ^2 were also calculated for the sectioned distribution; this provides a quantification of the stereological bias. Although both measurements provide similar results, there are a few

differences between the two rankings. For the correction procedures, the closer its values of δ and Δ^2 are to zero, the more effective the correction (i.e. the closer the corrected distribution is to the true distribution). If, in a given case, either value is larger than the corresponding value for the sectioned distribution, then this indicates that the correction corrupted the sectioning data in some way.

In the calculation of δ and Δ^2, equal weighting was given to all composition fractions. At this stage, it was felt that there was no justification for preferentially weighting any composition interval, but if a certain part of the liberation distribution curve is of particular interest (for instance, the near-liberated material) then a different weighting system can be employed.

Both δ and Δ^2 were normalized with respect to the sectioned distribution:

$$normalized\ \delta = \frac{(\delta_{sectioned\ dist.} - \delta_{corrected\ dist.})}{\delta_{sectioned\ dist.}} x\ 100\,\% \qquad (4.6)$$

$$normalized\ \Delta^2 = \frac{(\Delta^2_{sectioned\ dist.} - \Delta^2_{corrected\ dist.})}{\Delta^2_{sectioned\ dist.}} x\ 100\,\% \qquad (4.7)$$

The results are shown in Table 4.4. Normalization of δ and Δ^2 provides information about the effectiveness of the correction relative to the sectioned distribution. A normalization value of 100% would indicate perfect correction. A normalization value of 0% would indicate no correction. A negative normalization value would indicate that the correction corrupted the sectioning data.

Table 4.3: Correction procedures ranked according to the mean difference and mean square of the difference between the true and corrected distributions. This data is based on the correction of computer-generated sphere sections.

Description	Correction	Mean Diff. (δ)	Correction	Mean Square of Diff. (Δ^2)
Case 1:				
single composition	PARGEN "1"	0.0380	PARGEN "1"	0.643
	PARGEN "0"	0.0432	PARGEN "0"	0.725
	Large sections (90%)	0.0759	Large sections (90%)	1.186
	Barbery	0.1185	Hill's fast approximation	2.423
	Hill's fast approximation	0.1226	Barbery	2.860
	Sectioned distribution	0.1636	Sectioned distribution	3.406
Case 2:				
narrow composition	Large sections (90%)	0.0437	Large sections (90%)	0.224
range	PARGEN "0"	0.0518	Hill's fast approximation	0.701
	PARGEN "1"	0.0523	Barbery	0.724
	Barbery	0.0696	PARGEN "0"	0.730
	Hill's fast approximation	0.0748	PARGEN "1"	0.772
	Sectioned distribution	0.1166	Sectioned distribution	1.495
Case 3:				
simulated primary-grinding product	Large sections (90%)	0.0093	Large sections (90%)	0.033
	Sectioned distribution	0.0157	Hill's fast approximation	0.034
	Hill's fast approximation	0.0163	Barbery	0.068
	Barbery	0.0171	Sectioned distribution	0.073
	PARGEN "1"	0.0265	PARGEN "1"	0.104
	PARGEN "0"	0.0268	PARGEN "0"	0.112
Case 4:				
simulated concentrate or tailings	Hill's fast approximation	0.0032	Hill's fast approximation	0.002
	Large sections (90%)	0.0046	Large sections (90%)	0.003
	PARGEN "0"	0.0102	Sectioned distribution	0.016
	Barbery	0.0108	Barbery	0.018
	Sectioned distribution	0.0120	PARGEN "0"	0.019
	PARGEN "1"	0.0158	PARGEN "1"	0.056
Case 5:				
high- or low- grade middlings	Large sections (90%)	0.0255	Large sections (90%)	0.298
	Barbery	0.0366	PARGEN "1"	0.361
	PARGEN "1"	0.0432	Hill's fast approximation	0.377
	Hill's fast approximation	0.0511	Barbery	0.493
	Sectioned distribution	0.0528	Sectioned distribution	0.645
	PARGEN "0"	0.0662	PARGEN "0"	1.373
Case 6:				
stream with no free "0"	Hill's fast approximation	0.0161	Hill's fast approximation	0.039
	Large sections (90%)	0.0228	Large sections (90%)	0.066
	PARGEN "1"	0.0452	Barbery	0.284
	Barbery	0.0478	PARGEN "1"	0.362
	PARGEN "0"	0.0585	Sectioned distribution	0.409
	Sectioned distribution	0.0601	PARGEN "0"	0.554
Case 7:				
very irregular distribution	Large sections (90%)	0.0478	Large sections (90%)	0.419
	Hill's fast approximation	0.0532	Hill's fast approximation	0.467
	Sectioned distribution	0.0757	Sectioned distribution	0.839
	PARGEN "0"	0.0764	Barbery	0.959
	PARGEN "1"	0.0786	PARGEN "0"	0.979
	Barbery	0.0794	PARGEN "1"	1.268

Table 4.4: Normalized δ and Δ^2 values for the correction procedures. This data is based on the correction of computer-generated sphere sections.

Description	Correction	Normalized δ (%)	Correction	Normalized Δ^2 (%)
Case 1:				
single composition	PARGEN "1"	76.8	PARGEN "1"	81.1
	PARGEN "0"	73.6	PARGEN "0"	78.7
	Large sections (90%)	53.6	Large sections (90%)	65.2
	Barbery	27.6	Hill's fast approximation	28.9
	Hill's fast approximation	25.1	Barbery	16.0
	Sectioned distribution	0.0	Sectioned distribution	0.0
Case 2:				
narrow composition	Large sections (90%)	62.5	Large sections (90%)	85.0
range	PARGEN "0"	55.6	Hill's fast approximation	53.1
	PARGEN "1"	55.1	Barbery	51.6
	Barbery	40.3	PARGEN "0"	51.2
	Hill's fast approximation	35.9	PARGEN "1"	48.3
	Sectioned distribution	0.0	Sectioned distribution	0.0
Case 3:				
simulated primary-	Large sections (90%)	41.0	Large sections (90%)	54.9
grinding product	Sectioned distribution	0.0	Hill's fast approximation	52.6
	Hill's fast approximation	-3.7	Barbery	6.7
	Barbery	-8.8	Sectioned distribution	0.0
	PARGEN "1"	-69.3	PARGEN "1"	-42.9
	PARGEN "0"	-71.0	PARGEN "0"	-54.0
Case 4:				
simulated concentrate	Hill's fast approximation	73.2	Hill's fast approximation	90.6
or tailings	Large sections (90%)	62.0	Large sections (90%)	83.9
	PARGEN "0"	15.0	Sectioned distribution	0.0
	Barbery	9.8	Barbery	-10.0
	Sectioned distribution	0.0	PARGEN "0"	-14.3
	PARGEN "1"	-31.7	PARGEN "1"	-240.9
Case 5:				
high- or low grade	Large sections (90%)	51.7	Large sections (90%)	53.8
middlings	Barbery	30.8	PARGEN "1"	44.0
	PARGEN "1"	18.1	Hill's fast approximation	41.5
	Hill's fast approximation	3.3	Barbery	23.6
	Sectioned distribution	0.0	Sectioned distribution	0.0
	PARGEN "0"	-25.3	PARGEN "0"	-112.8
Case 6:				
stream with no free "0"	Hill's fast approximation	73.2	Hill's fast approximation	90.6
	Large sections (90%)	62.0	Large sections (90%)	83.9
	PARGEN "1"	24.7	Barbery	30.6
	Barbery	20.5	PARGEN "1"	11.3
	PARGEN "0"	2.7	Sectioned distribution	0.0
	Sectioned distribution	0.0	PARGEN "0"	-35.5
Case 7:				
very irreguiar	Large sections (90%)	36.9	Large sections (90%)	50.0
distribution	Hill's fast approximation	29.8	Hill's fast approximation	44.3
	Sectioned distribution	0.0	Sectioned distribution	0.0
	PARGEN "0"	-1.0	Barbery	-14.3
	PARGEN "1"	-3.9	PARGEN "0"	-16.7
	Barbery	-4.9	PARGEN "1"	-51.1

Although these rankings do provide an objective measure of the correction, the results must be interpreted with care. The absolute value of the δ and Δ^2 must always be taken into consideration. For instance: in case 4, Tables 4.3 and 4.4 indicate that Hill's fast approximation was closest to the true distribution and that the PARGEN "1" correction was the farthest away, but the relatively low δ and Δ^2 values in this case (all $\delta < 0.0200$ and all $\Delta^2 < 0.060$) indicate that all the corrected distributions were close to the true distribution (as confirmed by Fig. 4.2(d)). In case 1, there was a great discrepancy between the true and corrected distributions (Fig. 4.2(a)) and this is reflected by high δ and Δ^2 values.

4.5 Discussion of the results

In general, the correction procedures were effective to some degree in nearly all the cases. The values of δ and Δ^2 of the corrected distributions were almost always smaller than the corresponding values for the sectioned distribution and this resulted in mostly positive normalized δ and Δ^2 values.

In cases 3 and 4, the sectioned distribution is quite close to the true distribution. These are the cases in which there was the largest amount of free material and consequently, the stereological bias is minor. Here, correction may not be desirable as it introduces the possibility of corrupting the sectioning data. Unfortunately, the assumption that the sectioned and true distributions are sufficiently similar cannot be generalized as demonstrated by the other cases.

Case 7, the very irregular distribution, proved to be the most difficult case to correct. The best corrected result in case 7 had the lowest normalized δ and Δ^2 values compared to the best corrected result in all the other cases.

4.5.1 Large-sections correction

The large-sections correction with a 90% exclusion criterion seemed to provide the best results of all the procedures. In cases 2,3,5 and 7, it produced the highest normalized δ and Δ^2 (and thus the lowest δ and Δ^2) and in the other cases, it produced

the second highest normalized δ and Δ^2 values. In cases 1,2,4,5 and 6, it was able to at least halve the stereological bias (i.e. its normalized δ and Δ^2 were $> 50\%$). In none of the cases, did it produce a result inferior to the sectioned distribution. The corrected yield remained largely in the range between the true and sectioned yields.

4.5.2 Hill's fast approximation

Hill's fast approximation provided some improvement over the sectioned distribution in most cases. Its normalized δ and Δ^2 values were always positive (except in case 3, but here all the δ values were small and close to each other).

Hill's fast approximation appears to have had the most difficulty in case 5 where the true distribution was narrow and concentrated in the low vol.% "1" fractions. Although it had a relatively high normalized Δ^2, its normalized δ was quite low. The correction also had trouble with the two narrowest cases (cases 1 and 2). In these cases, Hill's fast approximation produced the lowest normalized δ values of all the corrections. This is probably the result of the assumption in the procedure that the locked section and locked particle distributions are identical. In the case of narrow distributions, the locked section distribution will be significantly wider than the locked particle distribution. This forces the correction to stretch the distribution out over many composition fractions resulting in a wide corrected distribution.

Hill's fast approximation also did not perform well in the cases with discontinuities in the distribution (cases 1 and 7; note that case 1 is both narrow and discontinuous). However, in case 7, none of the corrections performed particularly well and Hill's fast approximation produced the second highest normalized δ and Δ^2. One would expect that discontinuities would cause difficulties for this correction because it always produces a continuous corrected distribution due to its use of the locked section distribution to represent the locked particle distribution. Regardless of the continuity of the true distribution, sectioning will produce a continuous locked section distribution. Discontinuities in real liberation distributions must be dealt with if a mineral steam has

been concentrated or if mineral streams of different liberation distributions have been combined.

Hill based his assumption that the locked section and locked particle distributions are identical from an examination of the sectioning of spheres similar to those used here. The similarity between these distributions can be seen clearly from an examination of Fig. 4.2. Only in cases 1 and 7 was there a significant difference between the two. The validity of this assumption is corroborated in Tables 4.4 and 4.5 where it can be seen that Hill's fast approximation performed better on a Δ^2 basis than on a δ basis. This indicates that the variances between the true and corrected were small which suggests that the corrected distribution generated by Hill's fast approximation was similar in shape to the true distribution, but consistently offset.

In most cases, this correction provided an accurate estimate of the true amount of free material. Of course, this is likely a consequence of the use of the sphere model to predict the false free sections.

(Note that the amount of free material can be easily determined from the cumulative yield graphs by the endpoints of the curve. The amount of free "0" is the cumulative yield at 0 % phase "1" and the amount of free "1" is [100% - cumulative yield at 100 % phase "1"]).

4.5.3 Barbery's correction

Barbery has used his own correction to correct the sectioning of single-capped spheres. He sectioned a distribution of spheres similar to case 3 and he obtained a result similar to that obtained here (Fig. 4.2(c) is similar to Barbery's Fig. IX.6 [6(p.200)]).

In most cases, Barbery's correction was able to improve upon the sectioned distribution, but not nearly as much as the large-sections correction. Barbery's correction had difficulty in the discontinuous cases (cases 1 and 7). In case 1, although the normalized δ value of Barbery's correction was 27.6%, this was much lower than the corresponding value for the PARGEN and large-sections corrections and its normalized Δ^2 value was the lowest of all the corrections. In case 7, both its normalized δ and Δ^2

were negative. This difficulty with the discontinuous cases can be attributed to the use of an incomplete beta function to model the corrected distribution. Although the incomplete beta function is flexible, as Barbery has pointed out [6(p.18)], there is a limit to the number of shapes the curve can adopt. It is difficult to fit an incomplete beta function to data where there are sudden, sharp changes in the distribution. In these cases, the correction tends to smooth out the data and attempts a best fit.

In case 6, Barbery's correction had normalized δ and Δ^2 values that were low relative to the other corrections. An examination of Fig. 4.2 (f) shows that the problem is that the shape of the corrected curve is not appropriate; the true distribution is S-shaped while the Barbery-corrected distribution is nearly linear.

In Barbery's correction, it is assumed that the sectioning data are the result of the breakage of a boolean or Poisson texture. This is not the case in this test, but if this correction is to be used in practice, it will have to deal with situations where the material does not conform to such textures. There is a claim [76] that there are errors in the derivation of some of Barbery's equations, specifically, in the calculation of the amount of free material generated by the random breakage of the texture models. If this is indeed the case, then this may have contributed to the poor performance of the procedure in some of the cases. In fact, its prediction of the amount of free material is inferior to that of the other corrections.

4.5.4 PARGEN correction

Both PARGEN "0" and "1" corrections provided an accurate estimation of the true amount of free material in most of the cases, but they had difficulties estimating the locked distribution. The two PARGEN corrections performed similarly to each other in terms of normalized δ and Δ^2, but there were significant differences between the shape of the two corrections as shown in Fig. 4.2 (c)-(g). It can be seen in these cases that the PARGEN "1" corrected distribution was consistently higher than the true distribution and the PARGEN "0" corrected distribution was consistently lower.

The PARGEN corrections had a tendency to create sharp increases followed by plateaus (or vice versa) in the liberation distribution. This is quite noticeable in Fig. 4.2 (d) and (f). As a consequence of this, the PARGEN correction produced inconsistent results. The PARGEN correction performed well in the cases 1 and 2 (narrow distribution cases), but not so well in cases 5, 6 and 7.

The PARGEN correction, like Hill's fast approximation, makes assumptions regarding the particle shape and particle locking texture. Hill's fast approximation partially incorporates the sphere model by using it to help calculate the amount of free material. The PARGEN correction assumes that the particles are ellipsoidal and that the particle locking texture is granular with a dispersion density of one (which corresponds to simple locking). These two procedures share the same strength: both were able to accurately predict the true amount of free material. The difference in their performance lie in their different assumptions regarding the locked particles. Although PARGEN particles are similar to single-capped spheres, they may have been sufficiently different to account for the fluctuations in the PARGEN-corrected distributions.

Gay [15(p.90)] has criticized the assumption in the PARGEN correction that the dispersion density is independent of particle composition. In the PARGEN correction, it is assumed that all particles, regardless of composition, have the same dispersion density. Gay's argument is that one would expect near-liberated particles to have a lower dispersion density than locked particles that have more-or-less equal amounts of both phases. Although this criticism may be valid in cases involving real particles, with single-capped spheres, the assumption holds true. The dispersion density is independent of particle composition.

4.6 Summary of the correction of the sphere cases

Based on the correction of computer-generated spheres, the large-sections correction (with a 90% exclusion criterion) performed the best overall. The most likely reason for this is that the large-sections correction is independent of particle shape, locking texture and the characteristics of the true distribution curve. The inconsistent

performance of the other procedures can, in many cases, be directly attributed to their assumptions. In situations where the assumptions or conditions in the correction procedure are met, the correction performed well.

Hill's fast approximation was quite good at predicting the true amount of free material, but it uses an analysis of spheres to help make this prediction. It had the most trouble with narrow and/or discontinuous distributions due to its tendency to provide a wide, continuous corrected distribution. Barbery's correction had difficulty with discontinuous distributions as well since it attempts to fit an incomplete beta distribution to the true distribution. The PARGEN correction was able to make good predictions of the true amount of free material, but the correction had difficulty predicting the locked distribution and so produced inconsistent results. It performed best with narrow distributions.

CHAPTER 5: SECTIONING AND CORRECTION OF STANDARD MATERIAL PARTICLES

5.1 Overview

The seven liberation distributions (Table 4.2) that were computer-generated in the previous chapter were re-created, this time using standard material particles developed earlier (see Chapters 2 and 3). The particles were 425-600 μm and consisted of two phases: glass and lead borate. Standard material particles from different composition fractions were carefully weighed out using an analytical balance and mixed together to produce the seven cases. The mass distribution for each case is shown in Appendix 8.

The particles were mounted in resin and a polished surface was created. A liberation analysis was performed with a microprobe and image analyzer and the sectioning data were corrected using the correction procedures examined in the previous chapter. The results of the corrections were compared to each other as before.

5.2 CANMET sample preparation and image analysis

The standard material samples were sent to CANMET (Canadian Centre for Minerals and Energy Technology) for liberation analysis. For each of the seven cases, three pellets were created. To prevent preferential settling, only a sufficient quantity of sample particles to form a single layer was placed in each mold. Thus, each pellet was prepared by mixing approximately 400 mg of sample with Araldite resin in a 1¼" mounting mold. The particles settled in a single layer and the sample and mold were centrifuged for 1 minute to remove air bubbles in the resin. The resin was allowed to harden overnight and the next day, the surface was ground down 200 μm and then polished.

The polished surfaces were examined with a JEOL 733 microprobe. For each surface, an 8 × 8 grid (64 fields-of-view) was scanned at 40 × magnification (minimum magnification of the microprobe). The fields-of-view were combined to yield four fields-of-view with an apparent magnification of 10 × which were processed by the image analyzer.

The total number of particle sections analyzed for cases 1 to 7 were 1026, 1181, 940, 1472, 1225, 1016 and 1093, respectively.

5.3 IA grade of the CANMET sectioning data

Based on the sectioning data from CANMET, the grade of each case was calculated (by applying Delesse's equation (Equation 3.14)) and compared to the theoretical grade (from Table 4.2). The results are shown in Table 5.1.

Table 5.1: Comparison of the theoretical grade and the IA grade of the CANMET-mounted samples.

Case	Theoretical grade (vol. % borate)	IA grade of CANMET-mounted samples (vol. % borate)
1	49.7	52.5
2	49.7	50.3
3	49.5	55.1
4	11.1	16.4
5	16.2	16.4
6	55.6	62.9
7	34.6	41.6

The results indicate that there were some discrepancies between the theoretical and the IA grades. This is not surprising since the purpose of liberation analysis is solely to

determine the association of the different phases in the particles. The objective of the processing filters that are applied to the images of the particle sections is to preserve and clarify structural information. Depending on the sample, this may be detrimental to the grade [7(pp.79-81)]. However, Table 5.1 shows that the IA grades were consistently higher than the theoretical grades which suggests a systematic bias. If there is a bias, then there are two possible explanations:

1) Since the density of the lead borate is greater than that of the glass, the borate appears brighter under backscattered electron imaging than the glass. Because of this, the borate may have been more clearly defined than the glass and more readily detected by the image analyzer.

2) It is possible that some preferential settling and/or orientation of the particles in the resin may have occurred. Any preferential settling or orientation would favour particles with a high vol. % borate since they would be denser and would settle faster to the bottom of the mold than other particles. The CANMET-mounted samples were mounted in a single layer to prevent preferential settling, but it is difficult to ensure that a single layer has been produced and, in any case, this does not prevent preferential orientation.

The first explanation is not likely since it would only change the IA grade slightly and it can be solved by properly adjusting the microscope brightness and contrast. The second explanation is more probable. In order to address the problems of preferential settling and orientation, the cases in which the theoretical and IA grades differed by greater than 5 % were re-mounted (i.e. cases 3,4,6 and 7). This time the samples were prepared at McGill using the mounting procedure (described in Section 3.3.4) used to mount the individual composition fractions for IA grade measurement. Again, three pellets were prepared for each case. These samples were then sent to CANMET and liberation analyses were performed. The IA grades were calculated and the results are shown in Table 5.2.

Table 5.2: IA grade of the McGill-mounted samples of cases 3,4,6 and 7.

Case	Theoretical grade (vol. % borate)	IA grade of McGill-mounted samples (vol. % borate)
3	49.5	54.1
4	11.1	11.2
6	55.6	56.8
7	34.6	34.7

With the exception of case 3, the IA grades of the McGill-mounted samples were quite close to the theoretical grades. The sectioning data from the McGill-mounted samples in cases 3, 4, 6 and 7 were used rather than the data from the corresponding CANMET-mounted samples. The number of particles analyzed in the re-analysis of cases 3, 4, 6 and 7 were 1281, 1250, 1311 and 1292, respectively.

5.4 Liberation analysis statistics

There were few concerns regarding statistics in the tests with computer-generated spheres since a large number of spheres (100 000) were examined in each case. For the tests with standard material particles, the statistical validity of the data is of some concern since significantly fewer particles are examined. This is of even greater concern in the case of the large-sections correction due its exclusion of small sections.

The statistical analysis of liberation data can be performed using a binomial distribution [7(p.86),66(p.78)]. The standard deviation, σ, of the binomial distribution is:

$$\sigma = \sqrt{\frac{pq}{n}} \tag{5.1}$$

where p = the probability of an occurrence

$q = 1 - p$

n = total number of particles examined in the sample.

The absolute error, e, at the 95% confidence level, is two standard deviations from the average. Thus,

$$e = \pm 2\sigma = \pm 2\sqrt{\frac{pq}{n}} \tag{5.2}$$

In all liberation analyses, a certain level of data reduction is required. The complete data set (i.e. the composition of all the individual sections) provides too much information to easily consider or manipulate. The data are usually discretized into a set number of composition fractions (such as was done for the computer-generated sphere distributions). For each fraction, the error can be determined by applying the binomial distribution. The value of p is unknown, but it can be estimated by:

$$\frac{\textit{number of occurrences in the fraction}}{n} \tag{5.3}$$

This permits an estimation of the standard deviation and absolute error for that fraction.

For example: if the sectioning data were discretized into 12 composition fractions (0, 0-10, 10-20, ..., 90-100 and 100 % "1") and if 231 out of 4000 examined sections were found to be 10-20 % "1" then p for this composition fraction can be estimated by 231/4000 = 0.05775 or 5.78% (thus q = 0.94225). An estimate of the standard deviation, s, can be made using Equation 5.1. In this example, s = 0.0036883. Therefore, the estimate of the absolute error, e, in this fraction is: $\pm 2s = \pm$ 0.0073766 or 0.74%. This calculation can be performed for all the fractions.

The error in the fractions can be reduced by decreasing the number of fractions. For instance, in the example above, the data could have been discretized into 7 fractions: 0, 0-20, 20-40, ..., 80-100 and 100 % "1". This would increase the number of occurrences in each fraction and thus reduce the error. The disadvantage of doing this is that this decreases the resolution of the distribution curve; there would be fewer points to define the curve. In most liberation analyses, at least 10 fractions are used.

The error in the fractions can also be reduced by increasing n, but there are practical limitations on this number. Gathering more data involves increased analysis time and cost. If the particles are large then this would also involve increased sample preparation. With large particles, many pellets of the sample may have to be created in order to provide the necessary number of sections. Most standard material particles are large due the necessity of their density fractionation (large particles facilitate more accurate density separations).

In previous studies with standard materials, the number of sections analyzed has varied greatly as shown in Table 5.3. It should be noted that in these studies, the liberation analyses were performed either on particles in a single composition fraction or on the liberation distribution of the particles after breakage. There were no attempts to construct different liberation distributions as was done in this work.

The number of sections analyzed in each case in this study ranged from 1026 to 1311. Compared with other studies performed in this field, the number of sections analyzed here is on the high side.

Table 5.3: Number of sections analyzed in previous studies of standard materials.

Study	Particle size	Number of sections analyzed per sample
AMDEL/QEM*SEM data (this data set consisted of sectioned iron ore particles similar to those of Stewart and Jones [32])	106-150 μm	504-541
Bole et al. [22]		
iron-oxide/silicate	417-595 μm	†180-200
sphalerite/dolomite	417-595 μm	not stated
Woollacott and Valenta [34]	2.5-4.0 mm	‡23-300
S. Gay [15(p.229-34)]	3.35-4.00 mm	1209
	2.36-2.80 mm	1692

† it is not clear whether this is the number of sections analyzed per sample or the number analyzed to determine the grade.
‡ the particles were used for linear analysis only.

5.5 Selection of the exclusion criterion for the large-sections correction

The sectioning data of the standard material revealed that there were some sections whose area was greater than the "theoretical" largest section (a circular section with a diameter of 600 μm). The explanation for this is that there were some large ellipsoidal particles with one of its axes greater than 600 μm. This presents a problem when the large-sections correction is applied. If the true largest section is used as the largest section and the 90% exclusion criterion is used, then nearly all the sections will be excluded since only the sections through the centre of these large particles will be left. To solve this problem, the largest section was assumed to be a circular section with a diameter of 600 μm (282 743 μm^2).

In cases 1, 2 and 5 (i.e. the CANMET-mounted cases), this resulted in the exclusion of ≈ 70 % of the sections (using an exclusion criterion of 90%). In the other cases (i.e. the McGill-mounted cases), this resulted in the exclusion of ≈ 90% of the sections. The reason for this difference lies in the mounting method. In the CANMET-mounted samples, an attempt was made to produce and section a single layer of particles. In the McGill-mounted samples, multiple layers were mounted and after sectioning, there was a wider distribution of section sizes since small sections of particles from above and below the sectioning plane were observed.

5.6 Results of the correction procedures

The graphical results of the corrections are presented in Fig. 5.1 which shows the cumulative yield plotted against the particle composition. The δ and Δ^2 values are presented in Table 5.4 and the normalized δ and Δ^2 values are presented in Table 5.5. The estimation of the statistical error in the sectioning data and the large-sections correction for all the cases is shown in Appendix 9.

The large-sections correction was applied with an exclusion criterion of 90% and it was assumed that the largest section was a circular section with a diameter of 600 μm.

Hill's fast approximation was performed as described earlier.

In Barbery's correction, the software, BOOKING, was used again. Glass was selected as the grain phase and borate was selected as the matrix phase of the boolean texture.

The PARGEN correction was performed again using the software, Stereological Reconstruction of Linear and Areal Grade Distributions. Glass was selected as the grain phase and borate was selected as the matrix phase. The selection of the dispersion density (dd) was difficult. A decision was made to perform the correction using dispersion densities from one to three. In Fig. 5.1, only the PARGEN-corrected distribution using a dispersion density of two is shown.

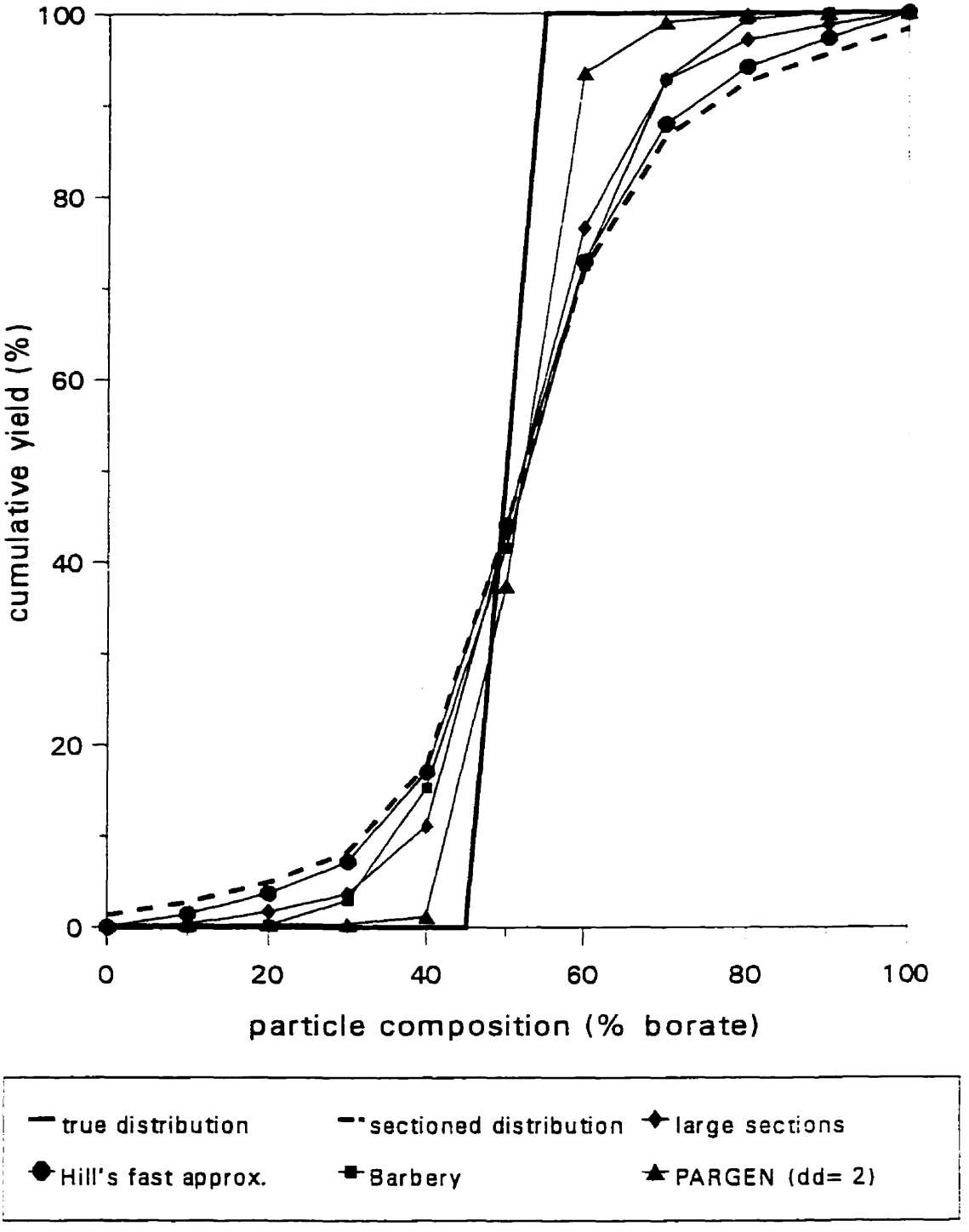

Fig. 5.1(a): Case 1, single composition.

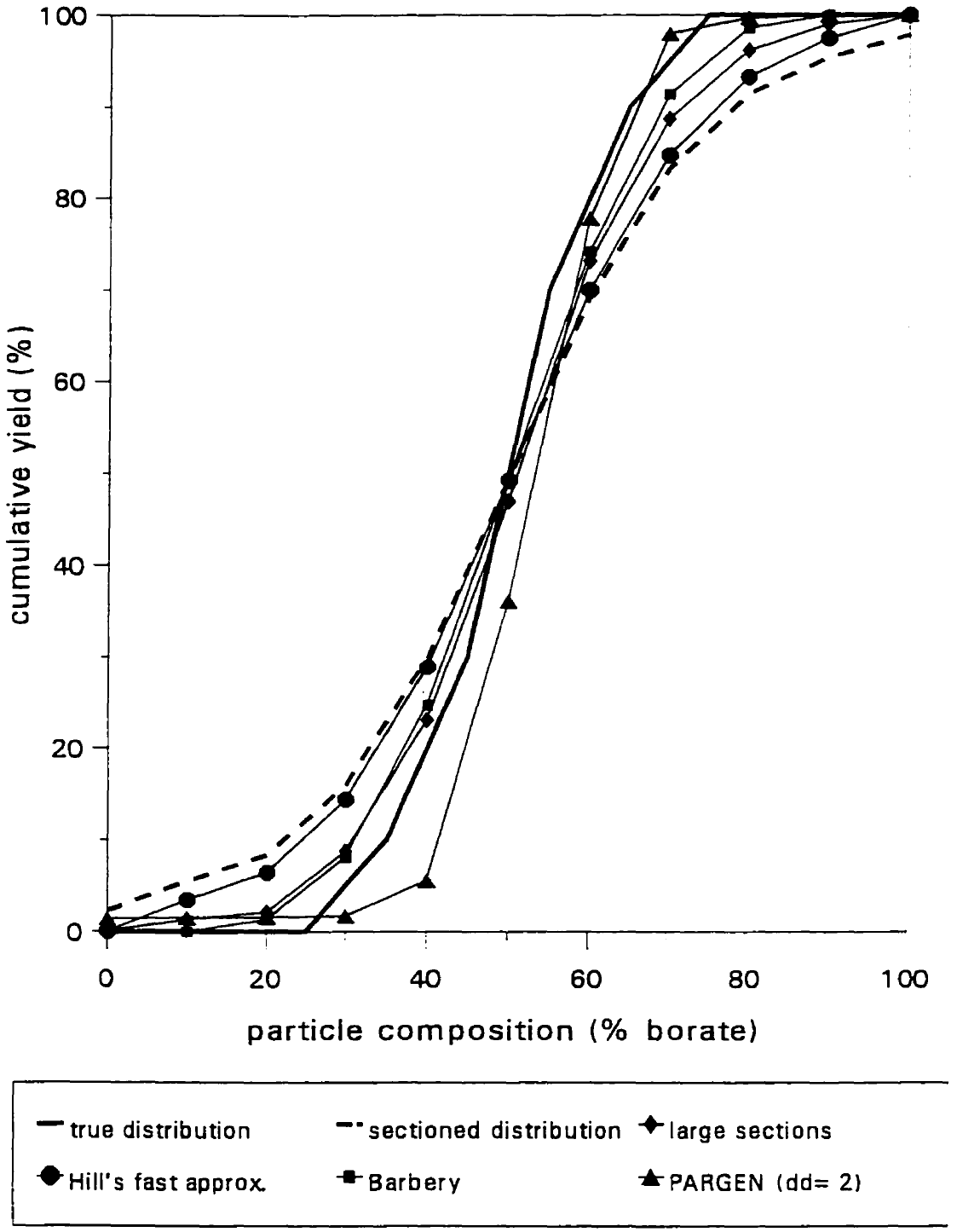

Fig. 5.1(b): Case 2, narrow composition range.

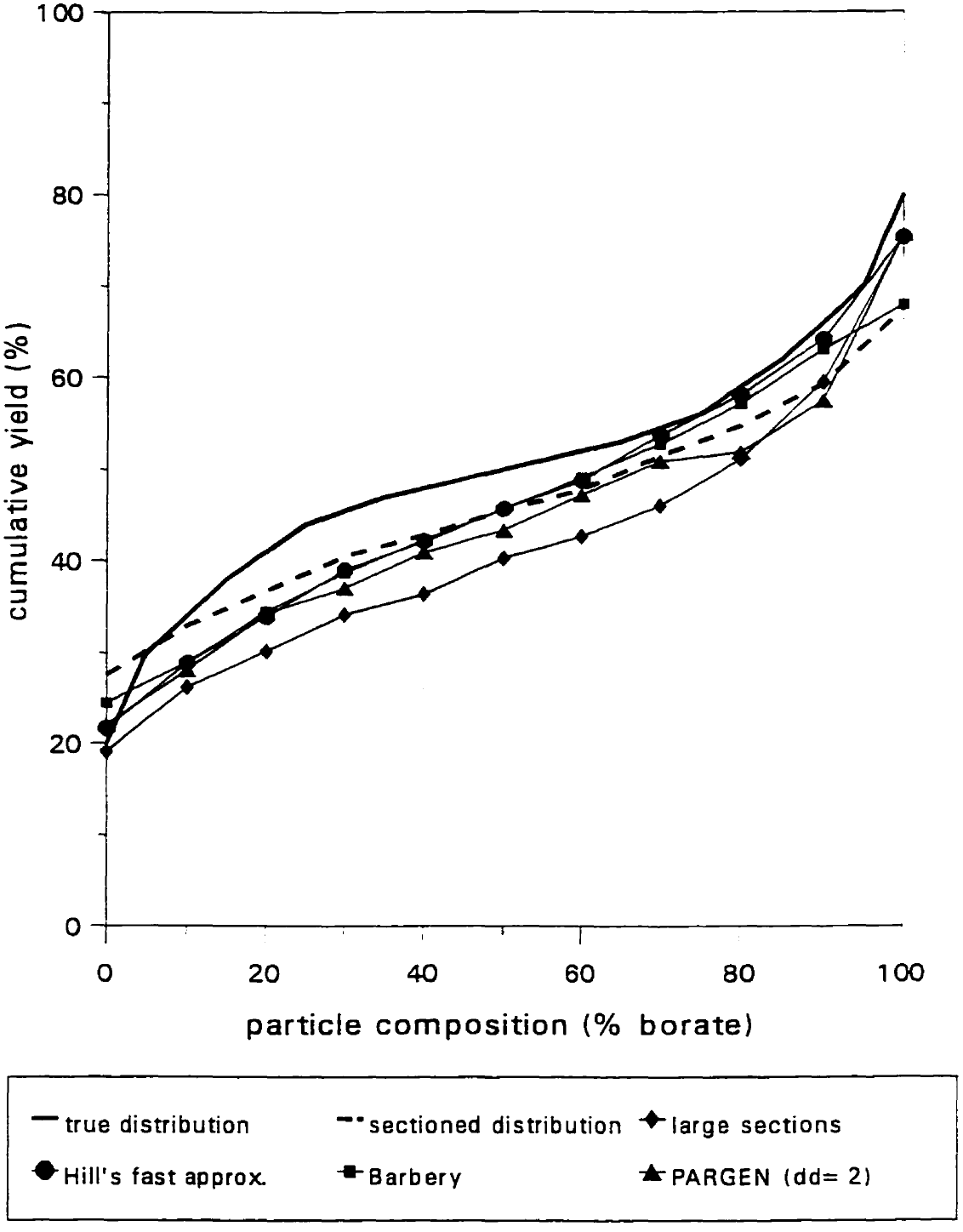

Fig. 5.1(c): Case 3, simulated primary-grinding product.

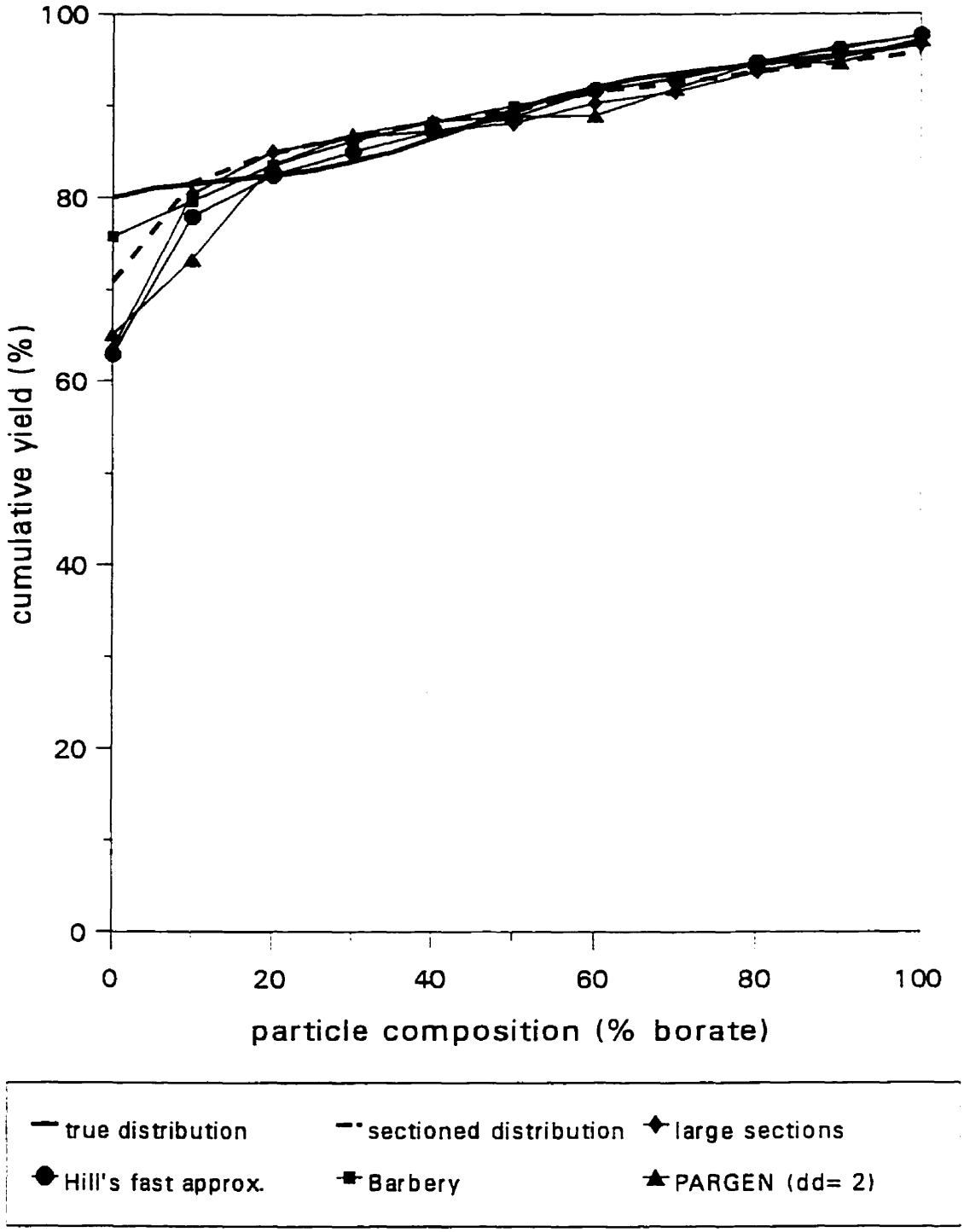

Fig. 5.1(d): Case 4, simulated concentrate or tailings.

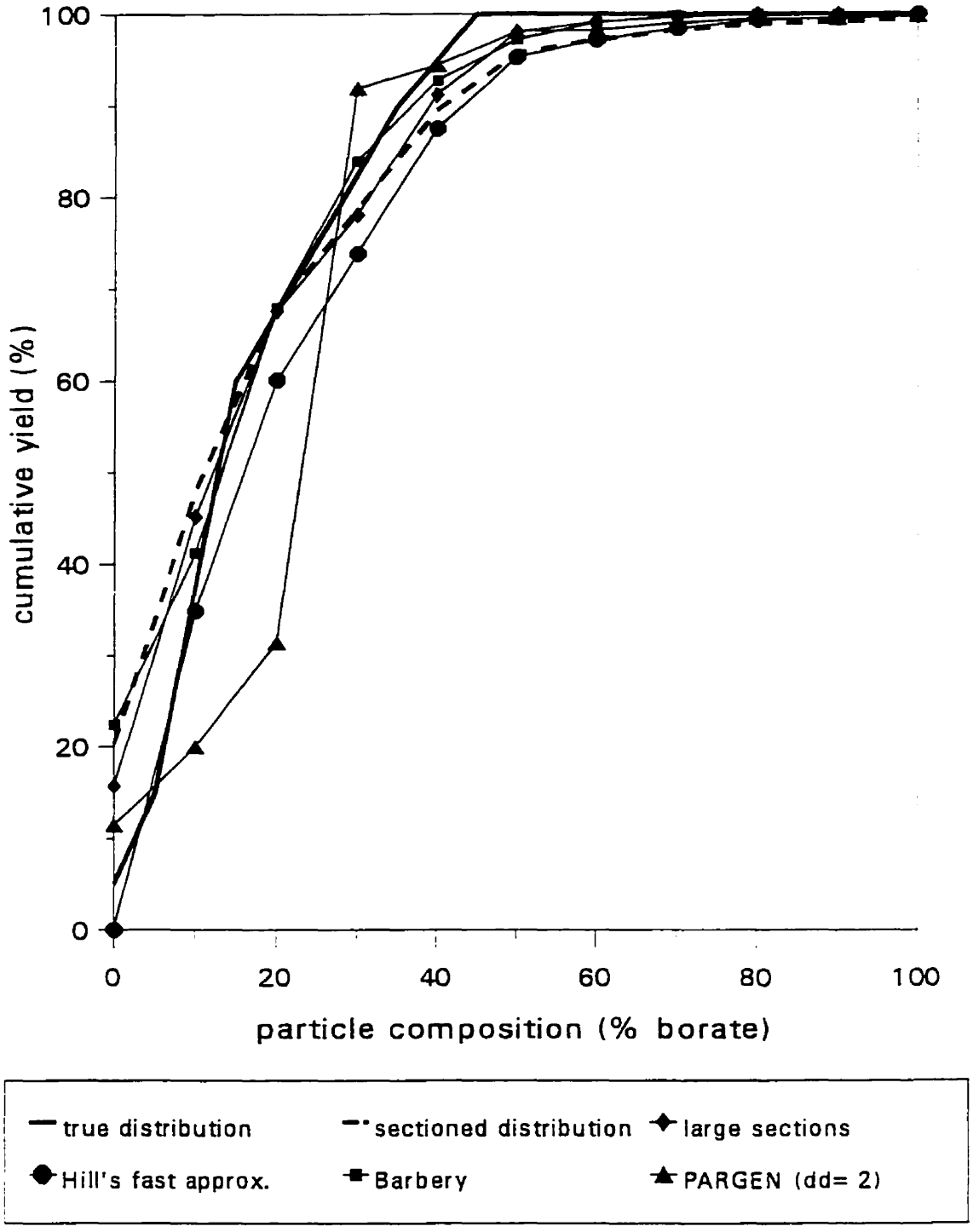

Fig. 5.1(e): Case 5, high- or low-grade middlings.

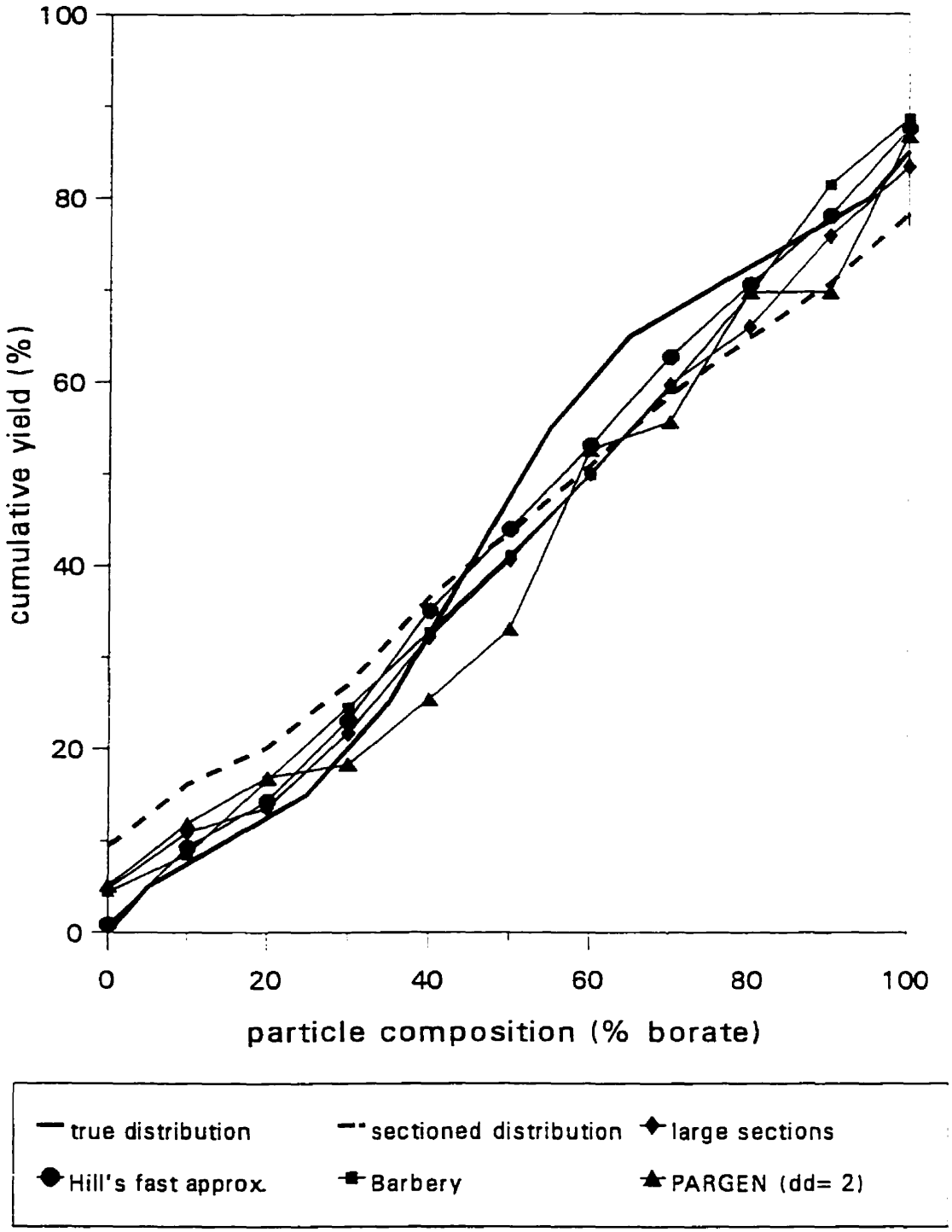

Fig. 5.1(f): Case 6, stream with no free glass.

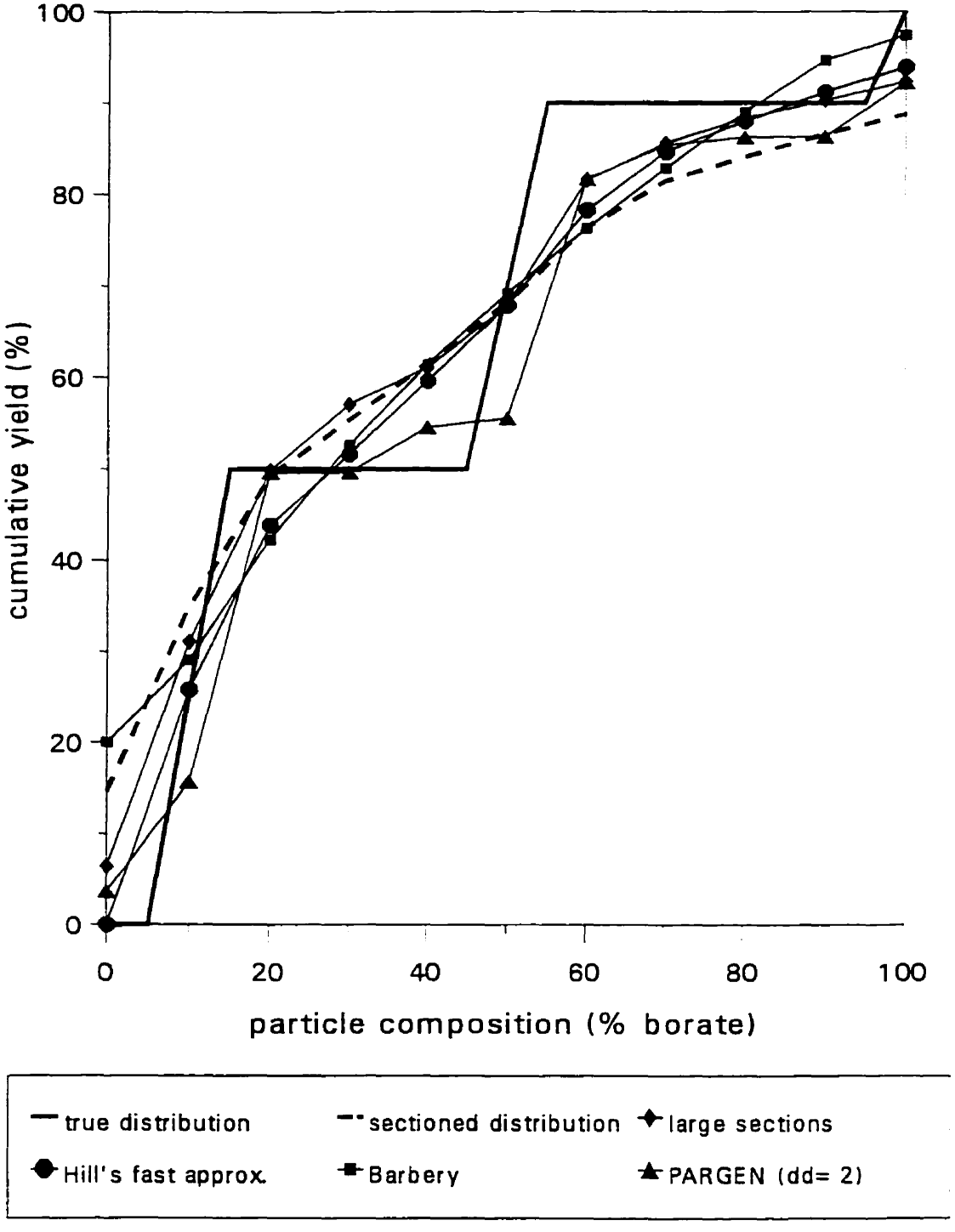

Fig. 5.1(g): Case 7, very irregular distribution.

Table 5.4: Correction procedures ranked according to the mean difference and mean square of the difference between the true and corrected distributions. This data is based on the correction of standard material particle sections.

Description	Correction	Mean Diff. (δ)	Correction	Mean Square of Diff. (Δ^2)
Case 1: single composition	PARGEN (dd=2)	0.0375	PARGEN (dd=2)	0.674
	PARGEN (dd=3)	0.0431	PARGEN (dd=3)	1.151
	Barbery	0.0717	Large-sections (90%)	1.486
	Large-sections (90%)	0.0773	Barbery	1.598
	PARGEN (dd=1)	0.0774	Hill's fast approximation	2.055
	Hill's fast approximation	0.1027	Sectioned distribution	2.253
	Sectioned distribution	0.1143	PARGEN (dd=1)	2.623
Case 2: narrow composition range	Barbery	0.0299	Barbery	0.155
	PARGEN (dd=2)	0.0372	Large-sections (90%)	0.222
	Large-sections (90%)	0.0387	PARGEN (dd=2)	0.345
	PARGEN (dd=3)	0.0537	Hill's fast approximation	0.598
	Hill's fast approximation	0.0677	PARGEN (dd=3)	0.742
	PARGEN (dd=1)	0.0691	Sectioned distribution	0.809
	Sectioned distribution	0.0827	PARGEN (dd=1)	1.702
Case 3: simulated primary-grinding product	Hill's fast approximation	0.0375	Hill's fast approximation	0.198
	Barbery	0.0429	Barbery	0.232
	Sectioned distribution	0.0446	Sectioned distribution	0.234
	PARGEN (dd=1)	0.0592	PARGEN (dd=2)	0.398
	PARGEN (dd=3)	0.0603	PARGEN (dd=3)	0.412
	PARGEN (dd=2)	0.0606	PARGEN (dd=1)	0.448
	Large-sections (90%)	0.0865	Large-sections (90%)	0.809
Case 4: simulated concentrate or tailings	Barbery	0.0114	Barbery	0.022
	Sectioned distribution	0.0157	Sectioned distribution	0.048
	Hill's fast approximation	0.0168	Large-sections (90%)	0.122
	PARGEN (dd=1)	0.0203	Hill's fast approximation	0.132
	Large-sections (90%)	0.0207	PARGEN (dd=3)	0.159
	PARGEN (dd=3)	0.0245	PARGEN (dd=1)	0.165
	PARGEN (dd=2)	0.0265	PARGEN (dd=2)	0.183
Case 5: high- or low- grade middlings	Barbery	0.0247	Large-sections (90%)	0.213
	Large-sections (90%)	0.0280	Barbery	0.236
	Sectioned distribution	0.0407	Hill's fast approximation	0.304
	Hill's fast approximation	0.0424	Sectioned distribution	0.368
	PARGEN (dd=1)	0.0571	PARGEN (dd=3)	1.137
	PARGEN (dd=3)	0.0592	PARGEN (dd=1)	1.322
	PARGEN (dd=2)	0.0630	PARGEN (dd=2)	1.411
Case 6: stream with no free glass	Hill's fast approximation	0.0291	Hill's fast approximation	0.124
	Large-sections (90%)	0.0435	Large-sections (90%)	0.287
	Barbery	0.0458	Barbery	0.293
	PARGEN (dd=2)	0.0625	PARGEN (dd=2)	0.529
	PARGEN (dd=3)	0.0632	PARGEN (dd=3)	0.547
	PARGEN (dd=1)	0.0667	Sectioned distribution	0.552
	Sectioned distribution	0.0712	PARGEN (dd=1)	0.975
Case 7: very irregular distribution	PARGEN (dd=1)	0.0544	PARGEN (dd=1)	0.523
	PARGEN (dd=3)	0.0566	PARGEN (dd=3)	0.552
	PARGEN (dd=2)	0.0587	Hill's fast approximation	0.552
	Hill's fast approximation	0.0598	Large-sections (90%)	0.586
	Large-sections (90%)	0.0615	PARGEN (dd=2)	0.596
	Barbery	0.0800	Barbery	0.985
	Sectioned distribution	0.0841	Sectioned distribution	0.997

Table 5.5: Normalized δ and Δ^2 values for the correction procedures. This data is based on the correction of standard material particle sections.

Description	Correction	Normalized δ (%)		Normalized Δ^2 (%)
Case 1:	PARGEN (dd=2)	67.2	PARGEN (dd=2)	70.1
single composition	PARGEN (dd=3)	62.3	PARGEN (dd=3)	48.9
	Barbery	37.3	Large-sections (90%)	34.1
	Large-sections (90%)	32.3	Barbery	29.1
	PARGEN (dd=1)	32.3	Hill's fast approximation	8.8
	Hill's fast approximation	10.2	Sectioned distribution	0.0
	Sectioned distribution	0.0	PARGEN (dd=1)	-16.4
Case 2:	Barbery	63.8	Barbery	80.9
narrow composition	PARGEN (dd=2)	55.0	Large-sections (90%)	72.5
range	Large-sections (90%)	53.3	PARGEN (dd=2)	57.3
	PARGEN (dd=3)	35.1	Hill's fast approximation	26.0
	Hill's fast approximation	18.2	PARGEN (dd=3)	8.2
	PARGEN (dd=1)	16.5	Sectioned distribution	0.0
	Sectioned distribution	0.0	PARGEN (dd=1)	-110.4
Case 3:	Hill's fast approximation	16.0	Hill's fast approximation	15.4
simulated primary-	Barbery	3.7	Barbery	0.9
grinding product	Sectioned distribution	0.0	Sectioned distribution	0.0
	PARGEN (dd=1)	-32.8	PARGEN (dd=2)	-69.9
	PARGEN (dd=3)	-35.2	PARGEN (dd=3)	-76.2
	PARGEN (dd=2)	-35.9	PARGEN (dd=1)	-91.5
	Large-sections (90%)	-93.8	Large-sections (90%)	-245.7
Case 4:	Barbery	27.5	Barbery	53.5
simulated concentrate	Sectioned distribution	0.0	Sectioned distribution	0.0
or tailings	Hill's fast approximation	-6.9	Large-sections (90%)	-155.7
	PARGEN (dd=1)	-28.9	Hill's fast approximation	-176.9
	Large-sections (90%)	-32.0	PARGEN (dd=3)	-231.9
	PARGEN (dd=3)	-55.7	PARGEN (dd=1)	-244.8
	PARGEN (dd=2)	-68.9	PARGEN (dd=2)	-283.4
Case 5:	Barbery	39.4	Large-sections (90%)	42.0
high- or low grade	Large-sections (90%)	31.3	Barbery	35.8
middlings	Sectioned distribution	0.0	Hill's fast approximation	17.2
	Hill's fast approximation	-4.1	Sectioned distribution	0.0
	PARGEN (dd=1)	-40.4	PARGEN (dd=3)	-209.3
	PARGEN (dd=3)	-45.4	PARGEN (dd=1)	-259.6
	PARGEN (dd=2)	-54.9	PARGEN (dd=2)	-283.8
Case 6:	Hill's fast approximation	59.1	Hill's fast approximation	77.5
stream with no free glass	Large-sections (90%)	38.9	Large-sections (90%)	48.0
	Barbery	35.6	Barbery	47.9
	PARGEN (dd=2)	12.2	PARGEN (dd=2)	4.1
	PARGEN (dd=3)	11.3	PARGEN (dd=3)	0.9
	PARGEN (dd=1)	6.3	Sectioned distribution	0.0
	Sectioned distribution	0.0	PARGEN (dd=1)	-76.8
Case 7:	PARGEN (dd=1)	35.3	PARGEN (dd=1)	47.6
very irregular	PARGEN (dd=3)	32.7	PARGEN (dd=3)	44.6
distribution	PARGEN (dd=2)	30.3	Hill's fast approximation	44.6
	Hill's fast approximation	29.0	Large-sections (90%)	41.2
	Large-sections (90%)	26.9	PARGEN (dd=2)	40.3
	Barbery	4.9	Barbery	1.2
	Sectioned distribution	0.0	Sectioned distribution	0.0

5.7 Discussion of the results

A case-by-case visual comparison of the sphere cases (Fig. 4.2) and the standard material cases (Fig. 5.1) shows that the sectioned distributions had similar shapes. The main difference between the curves of these two sets of sectioned distributions lie in the amount of free material. The sectioned distributions in the standard material cases provided a lower estimation of the amount of free material than the sphere cases. This, of course, was expected since the sectioning of single-capped spheres produces a large stereological bias. There was one exception, case 7, but the measured amount of free borate in standard material case 7 (Fig. 5.1(g)) was only slightly higher than that of the corresponding sphere case (Fig. 4.2(g)).

In standard material case 4 (Fig. 5.1(d)), it was found that the amount of free glass sections was lower than the amount of free glass particles. This is surprising since one would expect the stereological bias to increase the observation of free material. This may have been a result of some scratches that were later discovered on the polished surface of the pellets of this case. In any event, the correction procedures proved to be quite robust; they may have had a problem estimating the true amount of free glass, but from 10 vol.% borate and higher, all the corrected distributions were close to the true distribution. This is confirmed in Table 5.4 by the small δ and Δ^2 values for case 4. Of all the cases, this case produced the least stereological bias and the sectioned distribution itself is quite close to the true. A similar observation was made in the corresponding sphere case.

Case 3 proved to be a problematic case. In the other cases, the relationship between the true and sectioned distributions in the standard material cases was similar to the relationship between the true and sectioned distributions in the sphere cases (this is confirmed by a visual comparison of Figs. 4.2 and 5.1). However, an examination of Fig. 5.1(c) reveals that the sectioned distribution was considerably lower than the true distribution compared with the corresponding sphere case (Fig. 4.2(c)). This observation combined with fact that the IA grade of case 3 was $\approx$ 5 vol.% borate (absolute) higher than the theoretical grade makes the sectioning data of this case extremely suspect. It

appears that preferential settling during sample preparation may have biased the data. This is supported by the fact that case 3, of all the standard material cases, contained the largest amount of high vol.% borate particles. Since denser particles settle the most rapidly in the mounting medium, they will be over-represented in the polished surface.

Due to the poor sectioning data in case 3, it is not included in the discussion of performance of the correction procedures. Regardless, the δ and Δ^2 values and their normalized values were calculated and are included in Tables 5.4 and 5.5. It is instructive to note that all the corrections perform rather poorly, even the large-sections correction, which performed the best in corresponding sphere case. This serves to illustrate the importance of gathering accurate sectioning data. Large experimental errors in the sectioning data may cause stereological correction procedures to perform erratically.

A comparison of Tables 4.4 and 5.5 shows that, in general, the correction procedures produced less correction in the standard material cases than in the sphere cases. Also, there were more instances where the correction procedures yielded results that were farther from the true distribution than the sectioning data. This may be due in part to the larger statistical error in the standard material sectioning data.

The statistical error in the sectioned distribution and the large-sections correction (Appendix 9) was estimated using the binomial distribution as explained in Section 5.4. The absolute statistical error in the sectioned distribution varied depending on the case and the composition fraction, but rarely exceeded 3.0%. The absolute statistical error in the large-sections correction was larger due to the exclusion of small sections. It varied greatly; in some cases, it was as high as 8.5%. The statistical error in Hill's fast approximation, Barbery's correction and PARGEN correction are difficult to calculate due to the transformations that are performed on the sectioning data, but one would expect that the statistical error in these corrections to be similar to the statistical error in the sectioned distribution.

5.7.1 Large-sections correction

In the standard material cases, the large-sections correction (with an exclusion criterion of 90%) performed reasonably well and there was only one case (case 4) where the large-sections correction corrupted the sectioning data. In this case, Table 5.5 indicates that both the normalized δ and Δ^2 values for large-sections corrections are negative, but as mentioned earlier, the true and all the corrected distributions are quite close together. Although it did not perform the best in any given case (in contrast to its performance in the sphere cases), its normalized δ and Δ^2 values were greater than 25% in all the cases other than case 4.

5.7.2 Hill's fast approximation

Hill's fast approximation proved to be most effective in cases 6 and 7 where both its normalized δ and Δ^2 values were greater than 25%. In case 6, Hill's fast approximation provided the best corrected result. In case 7, Hill's fast approximation provided the second best corrected result.

Hill's fast approximation had difficulty with the narrowest distribution, (i.e. cases 1, 2 and 5) and in fact, in case 5, its normalized δ value was slightly negative. The same observation was made in the sphere cases; the difficulty Hill's fast approximation has with narrow distributions can be attributable to the fact that it will always provide a wide corrected distribution.

An examination of Fig. 5.1 shows that the locked section and locked particle distributions are similar except for cases 1 and 7, the discontinuous cases. This lends support to the assumption in Hill's fast approximation that they are identical.

Although Hill's fast approximation uses an analysis of spheres to help predict the true amount of free material, it still provided a good estimate in the standard material cases. The explanation for this is that the standard material particles were designed to exhibit a large degree of simple locking and, as a result, may have produced sectioning results roughly similar to those for single-capped spheres. Hill's fast approximation did overcorrect in some instances (for example, the amount of free glass in case 5 (see Fig.

5.1 (e)), but it was better at predicting the free material than either Barbery's correction or the large-sections correction.

5.7.3 Barbery's correction

Barbery's correction performed quite well in the standard material cases. Of all the corrections examined, it did not corrupt the sectioning data in any of cases. It was quite effective in cases 1, 2, 5 and 6 where both its normalized δ and Δ^2 values were greater than 30%.

In the sphere cases, Barbery's correction had some difficulty with discontinuous cases (cases 1 and 7) and case 6. In standard material case 7 (the very irregular distribution), it again had difficulties. Both its normalized δ and Δ^2 values were below 5%. In standard material case 1, it managed a slightly improved performance (in terms of normalized δ and Δ^2) over sphere case 1. In sphere case 6, Barbery's correction had difficulties since an appropriate incomplete beta function could not be found to fit the true distribution. In standard material case 6, Barbery's correction performs better, in spite of the fact that the shape of the incomplete beta function is still nearly linear while the true distribution is S-shaped.

Barbery's correction proved to be more effective in the standard material cases than in the sphere cases (compare Tables 4.3 and 4.4 with Tables 5.4 and 5.5.). The improvement in performance of this procedure in the standard material cases may be attributable to the change in texture. The spheres were obviously not the product of a boolean (or Poisson, for that matter) texture. It may be that the texture of the standard material is boolean or near-boolean. Although this is not necessarily a condition for the application of this procedure, this would certainly enhance its performance. The determination of whether a texture is boolean or not is difficult based solely on particle sections. The original texture of the standard material (i.e. the locked blocks) was somewhat boolean (grains in a continuous matrix), but the particles were subjected to numerous density separations and then re-combined together. This may render the original texture irrelevant.

5.7.4 PARGEN correction

In the sphere cases, the selection of the grain phase and the matrix phase for the PARGEN correction was difficult since either phase "0" or "1" could be considered the grain phase because the particles were single-capped spheres. With the standard material particles, the designation of the phase labels was easier. Clearly, the glass was the grain phase and the borate was the matrix phase.

In the sphere cases, the dispersion density was obvious: it was set to one since the spheres were simple-locked. In the standard material cases, the selection of the dispersion density is much less clear. If the selection of the dispersion density is based on an inspection of the original texture, then a dispersion density of one would be selected since for the standard material, the grain size was larger than the particle size (the grain size of the glass was 1180-1700 μm and the particle size was 425-600 μm). If the selection is based on an inspection of the particle sections, then the dispersion density could have a value ranging from one to three (most of the particle sections had either one or two grains, but there were a few sections with three grains). The selection is further complicated by the fact that the dispersion density must be an integer [77] and thus, fractional values could not be used. Since a single dispersion density could not be chosen, the PARGEN correction was performed three times (using dispersion densities of one, two and three) for each case.

An examination of Tables 5.4 and 5.5 shows that the PARGEN correction using the three dispersion densities provided similar results in most of the cases. There were, however, two exceptions: cases 1 and 2. In these cases, the PARGEN correction with a dispersion density of two was superior. This appeared to be the most appropriate dispersion density and so in Fig. 5.1, only the PARGEN-corrected distribution using a dispersion density of two was plotted.

As in the sphere cases, the PARGEN correction proved to be most effective with narrow distributions (cases 1 and 2). The PARGEN correction also performed well in case 7 where it provided the best correction of all the procedures, but it was less effective in case 6 and was found to corrupt the sectioning data in case 5.

The strength of the PARGEN correction was its ability to predict the true amount of free material. In the standard material cases as in the sphere cases, the PARGEN correction was able to provide a good estimate of the amount of free material. The weakness of the PARGEN was its ability to predict the locked particle distribution. In the sphere cases, the PARGEN-corrected distribution was subject to sharp increases and plateaus. In the standard material cases, this problem also occurs, but to a lesser degree.

It is somewhat surprising that the PARGEN correction did not perform significantly better in the standard material cases than in the sphere cases. The standard material particles are much more similar to PARGEN particles than single-capped spheres. The glass/borate particles were ellipsoidal and possessed a granular texture. This is quite similar to the description of PARGEN particles. There are two possible explanations for this:

1) Grain position. The textural dependence of the PARGEN correction has been commented upon in the work of Woollacott and Valenta [34] in studies on synthetic ore particles. They found that the linear liberation distributions of their particles were significantly different from those of PARGEN particles. They attributed this difference to the position of the grains in the particle (i.e. whether they were on the surface or completely occluded). This is supported by the work of Jones and Horton [13]. In their linear sectioning of computer-generated spheres and cubes, they demonstrated that the sectioned distribution was different depending upon the position of the grain in the particle shape. For example, there was a significant difference between the linear liberation distributions of a single-capped sphere and a sphere with the grain completely occluded. It should be noted that these two studies considered only linear sectioning. The effect of the grain position would be less pronounced if areal sectioning had been used since areal sectioning always provides sectioning data with less bias than linear sectioning.

2) Variation in the dispersion density. As mentioned earlier, Gay [15(p.90)] has criticized the assumption in the PARGEN correction procedure that all the

particles, regardless of particle composition, have the same dispersion density. He suggests that one would expect near-liberated particles to have a lower dispersion density than locked particles that have more equal amounts of both phases. It was difficult to determine if this is the case with the standard material particles. A comparison of a SEM examination of the near-liberated fractions (-5 vol.% borate and +95 vol.% borate) with the 45-55 vol.% borate fraction showed that nearly all the locking in near-liberated particles was simple locking whereas there were significantly more instances of complex locking in the 45-55 vol.% borate fraction. This is not conclusive since particle locking texture is subject to stereological bias and complex locking in near-liberated particles is difficult to observe since the grains are so small.

5.8 Summary of the correction of the standard material cases

There appeared to be a serious problem with the sectioning data in case 3. Preferential settling of the higher density (high vol.% borate) particles over the lower density particles appears to have significantly biased the data in this case. This is reflected in the high IA grade ($\approx$ 5 vol.% borate (absolute) greater than the theoretical grade) and the significant difference between the standard material sectioned distribution and corresponding sphere case sectioned distribution. All the correction procedures performed poorly in this case which clearly demonstrates the importance of gathering accurate sectioning data, particularly if a stereological correction procedure is to be used. Errors in the sectioning data may lead to unpredictable results when correction is applied.

The large-sections correction proved to be generally applicable. Although it was not the most effective in any of the standard material cases, it did provide a consistent level of correction.

Hill's fast approximation produced varying results. It had difficulty dealing with narrow distributions, but it was able to provide a good estimate of the true amount of free material in most of the cases. The standard material sectioned distributions

supported the assumption in this correction that the locked section and locked particle distributions are identical.

Barbery's correction performed very well. Its performance was a definite improvement over its performance in the sphere cases. It only had difficulty with the very irregular distribution.

The PARGEN correction proved to be most effective with narrow distributions and discontinuous distributions and it was also able to provide a good estimate of the true amount of free material. The correction had difficulty re-creating the true locked distribution and as a result, produced some inconsistent results. The selection of the dispersion density had an affect upon the performance of the PARGEN correction, especially in the case of the narrow distributions. A standard method of selecting the dispersion density must be established as this parameter appears to have a significant effect on the corrected distribution. In the standard material cases, the true distribution is known and the appropriate dispersion density can selected based on the δ and Δ^2 information, but obviously, this cannot be done in a real situation.

CHAPTER 6: CONCLUSIONS

6.1 Standard material

A two-phase (glass/lead borate) standard material was successfully created. It was produced with two types of textures: granular and layered. The granular texture was achieved by embedding glass particles into a lead borate matrix. The layered texture was achieved by embedding parallel glass slides separated by a set distance into a bath of lead borate. Blocks of these materials were crushed to produce locked particles.

The complexity of the locking of these particles can be varied by changing the particle/grain size relationship of the granular-texture material or by changing the thickness of the layers of the layered-texture material. Locked particles exhibiting only simple locking were generated by creating blocks of layered-texture material and crushing them until the particle size was smaller than the thickness of the layers. The composition of the locked particles was determined by density fractionation using the Magstream separator (a centrifugal magnetogravimetric separator). In this work, the granular-texture standard material was used to test various stereological correction procedures.

There are two possible future applications of the standard material:

1) The standard material could be used to assess liberation models. So-called "size reduction" models attempt to predict liberation by assuming that there is little breakage along the interfaces. Since the bonding between the glass and lead borate is quite strong, the standard material can be used to evaluate the accuracy of these models.

2) The standard material could be used as a basis for a stereological correction procedure. Standard materials could be created so that the locking texture and complexity of locking varies. By sectioning the composition fractions of these materials, a series of kernel matrices can be produced which can be used for

stereological correction. The difficulty with this approach (as with all corrections that use kernel matrices) lies with the quantification of the texture and the selection of the appropriate kernel matrix. One would have to categorize the different types of particle locking textures (such as granular, banded locking, etc.) [78] or to quantify the locking texture using stochastic geometry [6,15,31,79,80]. If the texture of the sample can be quantified using only one or two parameters, then the appropriate kernel matrix could be applied.

6.2 Sectioning and correction of computer-generated spheres

Computer software was used to create seven different liberation distributions of single-capped spheres. The spheres were sectioned and the sectioning data corrected using four stereological correction procedures: large-sections correction, Hill's fast approximation, Barbery's correction and PARGEN correction. The effectiveness of each correction was quantified by determining the mean difference and mean square of the difference between the true and corrected distributions. The large-sections correction with a 90% exclusion criterion performed the best in these cases.

6.3 Sectioning and correction of standard material particles

Standard material particles were used to re-create the seven liberation distributions that were computer-generated. These particles were mounted in resin and a polished surface was created. The sectioning data were measured using the microprobe and image analyzer at CANMET. The same four corrections were performed on these sectioning data. Barbery's correction appeared to provide the most consistent results in these cases.

6.4 Summary of correction procedure performance

Many of the observations made in the sphere cases were mirrored in the standard material cases. In general, most corrections provided corrected distributions that were superior to the sectioned distribution. There were only a few cases where the sectioning data were significantly corrupted.

In one of the standard material cases (case 3), the sectioning data were biased probably due to preferential settling during sample preparation and all the corrections performed poorly. It is important that the sectioning data be as error-free as possible since stereological correction may exacerbate the error.

The recommendation of a single stereological correction procedure is difficult since all the corrections have both strengths and weaknesses. The limitations of each correction should be considered before it is applied.

In some situations, the most important requirement for the selection of a stereological correction is that the correction not corrupt the sectioning data. If this is of great concern then the large-sections correction should be used since it appears to be the most generally applicable and can be safely used in a variety of cases. If the requirement is that the true amount of free material be accurately predicted then the choice is either the PARGEN correction or Hill's fast approximation (if the locking is predominantly simple). If the requirement is that the locked particle distribution be accurately predicted then Barbery's correction or Hill's fast approximation should be considered. The large-sections correction was also able to predict the locked distribution quite well. The strengths, weaknesses and applicability of the correction procedures are summarized below.

6.4.1 Large-sections correction

There are two drawbacks to the large-sections correction:

1) many polished surfaces may have to be prepared in order to yield a sufficient number of large sections
2) the correction can never provide a complete correction regardless of the number of small sections excluded.

The strength of the procedure lies in its ability to provide a simple, uncorrupted correction. The large-sections correction is independent of particle shape, locking texture and the characteristics of the true distribution curve. It performed the best in the sphere cases and although it did not perform the best in any of the standard material cases, it

did provide a consistent correction. If the large-sections correction is to be used, it should be applied using the same exclusion criterion on all the data in a liberation study. If different exclusion criteria are used for different samples in a study then the degree of correction will vary and a comparison of the samples will be difficult.

6.4.2 Hill's fast approximation

Hill's fast approximation is based on two assumptions:

1) the locked section distribution is identical to the locked particle distribution
2) the amount of false free sections generated can be predicted using an analysis of single-capped spheres.

The standard material cases provided evidence that appeared to justify these two assumptions: the locked section and locked particle distributions were similar (except in the narrow or discontinuous cases) and the correction did well in estimating the amount of free material, but this second observation may have followed because there was a large degree of simple locking in the standard material particles.

Both the standard material and sphere cases showed that Hill's fast approximation performed well except in the narrow distribution cases. The correction is most applicable in cases where the liberation distribution is reasonably wide.

6.4.3 Barbery's correction

From a theoretical perspective, Barbery's correction may encounter problems in the following situations:

1) there is a large amount of preferential breakage in the ore
2) the sample has been concentrated or mixed with other streams.

Barbery's correction did not fare well in the sphere cases, but there was a noticeable improvement in its performance in the standard material cases. The correction should perform well as long as the true distribution is relatively continuous and can be modelled with an incomplete beta distribution.

6.4.4 PARGEN correction

The PARGEN correction assumes that the particles possess a granular texture and ellipsoidal shape. This was not appropriate in the sphere cases, but in the standard material cases, the particles were ellipsoidal and granular-textured. In both sets of data, the correction performed inconsistently. It appeared to be most effective with narrow liberation distributions. The strength of the PARGEN correction lies in its ability to provide a good estimate of the true amount of free material.

6.5 Suggestions for future work

Preferential settling in the sample preparation of one of the standard material cases led to poor sectioning data. Measures were taken to prevent preferential settling, but they were insufficient in this one case. The standard material, besides providing a stereological challenge, also provides a sample preparation challenge. The standard material particles have a wide density range and are quite coarse. A sample preparation technique should be developed to prevent any preferential settling or orientation. The use of a large amount of diluent material may reduce preferential settling (some researchers have used volumetric ratios of up to 10:1 (diluent material:sample material) [3]), but this reduces the number of sections visible per polished surface and may necessitate the preparation of an increased number of pellets.

There are certain aspects of the different correction procedures that need further investigation.

1) Large-sections correction - Further work should be conducted to study the trade-off between the exclusion of small sections and the generation of statistically valid data. At present, the large-sections correction can be practically applied by gathering as much data as possible and then excluding as many small sections as statistics will permit. Further work should also be conducted examining the effect of the exclusion criterion on the effectiveness of this correction.

2) Hill's fast approximation - Further work should be performed to examine if the sphere model can provide or can be modified to provide an adequate prediction of the false free sections in real particle assemblages. The sphere model does

tend to overcorrect [8], but if there is a large degree of simple locking, this may not be a problem. If the sphere model is found to be unsuitable, then a more accurate method of estimating the true amount of free material could be substituted. The PARGEN estimation could possibly be used.

3) Barbery's correction - Barbery's correction was very inconsistent at predicting the true amount of free material. There has been a claim that there are derivation errors in Barbery's equations [76] specifically regarding the estimation of the amount of free material. If these suspected errors are substantiated, the procedure should be re-assessed.

4) PARGEN correction - If the dispersion density is to be a useful parameter, a standard method should be established for its determination. Also, it should be allowed to take on fractional values. This correction procedure has undergone many changes and appears still to be under development. The latest change may be a move toward using kernel matrices from real particle systems [81]. Although this would improve the performance for particles having a similar shape and locking characteristics, it would limit the applicability of the correction to specific systems.

REFERENCES

1. Gabriel B.L. *SEM: A user's manual for materials science* (Metals Park, Ohio: American Society for Metals, 1985), 53-78.

2. Heinrich K.F.J. *Electron beam x-ray microanalysis* (Toronto: Van Nostrand Reinhold Co., 1981), 99-186.

3. Reid A.F., Gottlieb P., MacDonald K.J. and Miller P.R. QEM*SEM image analysis of ore minerals: volume fraction, liberation and observational variances. *Applied Mineralogy*, Park W.C., Hausen D.M and Hagni R.D. eds. (New York: AIME, 1984), 191-204.

4. Sutherland D.N. and Gottlieb P. Application of automated quantitative mineralogy in mineral processing. *Minerals Engineering*, **4(7-11)**, 1991, 753-62.

5. Gaudin A.M. *Principles of mineral dressing* (New York: McGraw-Hill, 1939), 87-9.

6. Barbery G. *Mineral liberation: measurement, simulation, and practical use in mineral processing* (Quebec: Les Editions GB, 1991), 351 p.

7. Hill G.S. Applications of two-dimensional image analysis to mineral liberation studies. Ph.D. thesis, McGill University, 1990.

8. Hill G.S., Rowlands N. and Finch J.A. Data correction in two-dimensional liberation studies. *Process Mineralogy VII*, Vassiliou A., Hausen D. and Carbon D. eds. (Warrendale, PA: The Metallurgical Society of AIME, 1987), 617-32.

9. Barbery G. and Pelletier R. Simulation techniques in mineral liberation analysis. *Proc. 1st Canadian Conference on Computer Applications in the Mineral Industry, Québec 1988*, Fytas K., Collins J.L. and Singal R.K. eds. (Rotterdam: Balkema, 1988), 251-6.

10. Finch J.A., Hill G.S. and Rowlands N. Verification of a particle sectioning model. *Can. Metall. Q.*, **29**, no. 3, 1990, 239-41.

11. Moore S.W. and Jones M.P. Mathematical methods for estimating particle compositions from the results of image analysis. *XV Int. Mineral Process. Congress, Cannes*, **1**, 1985, 3-11.

12. Moore S.W. and Jones M.P. Random linear probes through composite spheres that have multiple planar boundaries. *Trans. Instn. Min. Metall. (Sect. C: Mineral Process. Extr. Metall.)*, **89**, 1980, C190-3.

13. Jones M.P. and Horton R. Recent developments in the stereological assessment of composite (middling) particles by linear measurements. *Proc. 11th Commonwealth Min. Metall. Congress, Hong Kong* Jones, M.P. ed. (London: I.M.M., 1978), 113-22.

14. Gateau C. and Broussaud A. New approaches to the interpretation of one and two dimensional measurements of mineral liberation. *Acta Stereologica*, **5**, no. 2, 1986, 397-402.

15. Gay S.L. Liberation modelling using particle sections. Ph.D. thesis, University of Queensland, 1996.

16. Sepulveda J.E., Miller J.D. and Lin C.L. Generation of irregularly shaped multiphase particles for liberation analysis. *XV Int. Mineral Process. Congress, Cannes*, **1**, 1985, 120-32.

17. Baba K., Miller J.D. and Herbst J.A. A general transformation function for the prediction of volumetric abundance from linear grade distributions. *Annual AIME meeting*, New York, 1985.

18. Lin C.L., Miller, J.D. and King R.P. The validity of the PARGEN simulation for mineral liberation analysis. *Powder Technol.*, **58**, 1989, 231-3.

19. Miller J.D. and Lin C.L. Treatment of polished section data for detailed liberation analysis. *Int. J. Mineral Process.*, **22**, 1988, 41-58.

20. Lin C.L., Miller J.D. and Herbst J.A. Solutions to the transformation equations for volumetric grade distribution from linear and/or areal grade distributions. *Powder Technol.*, **50**, 1987, 55-63.

21. Schneider C.L., Lin C.L., King R.P. and Miller J.D. Improved transformation technique for the prediction of liberation by a random fracture model. *Powder Technol.*, **67**, 1991, 103-11.

22. Bole J., Lin C.L. and Miller J.D. Experimental verification of the PARGEN simulator for liberation analysis. *Int. J. Mineral Process.*, **37**, 1993, 209-21.

23. Barbery G. Random sets and integral geometry in comminution and liberation of minerals. *Mineral and Metall. Eng.*, **4**, 1987, 96-102.

24. Barbery G. and Leroux D. Prediction of particle composition distribution after fragmentation of heterogeneous materials. *Int. J. Mineral Process.*, **22**, 1988, 9-24.

25. Barbery G. Liberation 1,2,3: theoretical analysis of the effect of space dimension on mineral liberation by size reduction. *Minerals Engineering*, **5(2)**, 1992, 123-41.

26. King R.P. Determination of the distribution of size of irregularly shaped particles from measurements on sections or projected areas. *Powder Technol.*, **32**, 1982, 87-100.

27. King R.P. Measurement of particle size distribution by image analyzer. *Powder Technol.*, **39**, 1984, 279-89.

28. Leroux D. Développement et calibration de modèles stéréostochastiques de libération. M.Sc. thesis, Laval University, 1988, 122.

29. Lin D., Gomez C.O. and Finch J.A. Test of Barbery's liberation correction procedure. *Trans. Instn. Min. Metall. (Sect C: Mineral Process Extr. Metall.)*, **103**, 1994, C91-6.

30. Gay S.L. and Lyman G.J. Stereological error in particle sections - the solution. *Proc. 25th Conf. APCOM, Brisbane, Qld., Australia*, 1995, 313-7.

31. Gay S.L. Stereological equations for phases within particles. *J. Microscopy*, **179(3)**, 1995, 297-305.

32. Stewart P.S.B. and Jones M.P. Determining the amounts and the compositions of composite (middling) particles. *Proc. 12th Int. Mineral Process. Congress, Sao Paulo*, 1977, Meeting B, paper 4.

33. Bagga P.S. Simulation of the liberation phenomena in mineral systems. Ph.D. thesis, Pennsylvania State University, 1983.

34. Woollacott L.C. and Valenta M. Use of synthetic ore particles to test a transformation function in liberation analysis. *Minerals Engineering*, **9(10)**, 1996, 1017-32.

35. Lin D. The production of a standard material for liberation analysis. M.Eng. thesis, McGill University, 1991.

36. Lin D., Finch J.A., Gomez C.O. and Rowlands N. An artificial standard material for liberation analysis. *Powder Technol.*, **72**, 1992, 131-8.

37. Gomez C.O., research associate, McGill University, personal communication, 1993.

38. Weast R.C., ed. *CRC handbook of chemistry and physics* (Boca Raton, Florida: CRC Press Inc, 1981).

39. Wills B.A. *Mineral processing technology, 3rd edition* (Oxford: Pergamon Press, 1985), 342-75.

40. Kelly E.G. and Spottiswood D.J. *Introduction to mineral processing* (New York: John Wiley & Sons, 1982), 243-9.

41. Rhodes D., Hall S.T. and Miles N.J. Density separations in heavy inorganic liquid suspensions. *XVIII Int. Mineral Process. Congress, Sydney*, 1993.

42. Miehe M., Sometu Inc., personal communication, 1993.

43. Andres U. Magnetohydrodynamic and magnetohydrostatic separation - a new prospect for mineral separation in the magnetic field. *Miner. Sci. Eng.*, 7(2), 1975, 99-109.

44. Khalafalla S.E. Magnetic separation of the second kind: magnetogravimetric, magnetohydrostatic and magnetohydrodynamic separations. *IEEE Trans. Magn.*, **MAG-12**(5), 1976, 455-62.

45. Andres U. *Magnetohydrodynamic and magnetohydrostatic methods of mineral separation* (New York: John Wiley and Sons, 1976), 224 p.

46. Neuringer J.L. and Rosensweig R.E. Ferrohydrodynamics. *Phys. Fluids*, 7(12), 1964, 1927-37.

47. Andres U., Bunin G.M. and Gil B.B. Magnetohydrostatic separation. *J. Appl. Mech. Tech. Phys.*, 7(3), 1966, 109-112.

48. Rosensweig R.E. Fluidmagnetic buoyancy. *AIAA J.*, **4**(10), 1966, 1751-8.

49. Parsonage P. Small-scale separation of minerals by use of paramagnetic liquids. *Trans. Instn Min. Metall. (Sect B.)*, **86**, 1977, B43-6.

50. Rosensweig R.E. *Ferrohydrodynamics*. (Cambridge: Cambridge University Press, 1985), 344 p.

51. Gubarevich V.N. and Vidsota S.V. Theoretical principles, present status and prospects for development of material separation in magnetic fluids. *Mag. Electr. Sep.*, **5**(3), 1994, 169-92.

52. Tremblay R. Étude du procédé magnétohydrostatique. *Le Centre Recherches Minérales report*, Sainte-Foy, Québec, May 1983.

53. Lin D., Leroux M. and Finch J.A. Batch magnetohydrostatic separations with a modified Frantz separator. *Minerals Engineering*, **8(3)**, 1995, 283-292.

54. Walker M.S., Devernoe A.L., Stuart R.W., Urbanski W.S. and Andres U. A new method for the commercial separation of particles of differing densities using magnetic fluids - the MC process. *Proc. XV Int. Mineral Process. Congress, Cannes*, 307-16, 1985.

55. Walker M.S., Devernoe A.L. and Urbanski W.S. Separation of non-magnetic minerals using magnetic fluids in a flow-through MHS rotor. *Miner. Metall. Process.*, **7(4)**, 1990, 209-14.

56. Walker M.S., Devernoe A.L., Urbanski W.S. and Morrow G.R. Mainly "gravity" separations using magnetic fluids under rotation. *Proc. XVII Int. Mineral Process. Congress, Dresden*, Vol. III, 1991, 105-16.

57. Walker M.S. and Devernoe A.L. Mineral separations using rotating magnetic fluids. *Int. J. Mineral Process.*, **31**, 195-216, 1991.

58. Bunge R.C. and Fuerstenau D.W. Mineral separations with a magnetogravimetric separator. *SME pre-print 90-192*, Salt Lake City, 1990.

59. Bunge R.C. and Fuerstenau D.W. Separation characteristics of a magnetogravimetric separator. *Proc. XVII Int. Mineral Process. Congress, Dresden*, 1991, 31-42.

60. Bunge R.C. and Fuerstenau D.W. Magnetogravimetric separation in a rotational device. *Mag. Electr. Sep.*, **7(3)**, 1996, 163-84.

61. Svoboda J. A contribution to the theory of separation in a rotating ferrofluid. *Minerals Engineering*, **9(7)**, 1996, 743-52.

62. Intermagnetics General Corporation. Operating instructions for the Magstream Model 100 Laboratory Separator. Guilderland, NY.

63. Hess H.H. Notes on operation of Frantz isodynamic magnetic separator. S.G. Frantz Co.

64. Delesse A. Procédé mécanique pour déterminer la composition des roches. *Annales des Mines*, **13**, 1848, 379-88.

65. Gomez C.O., Rowlands N., Finch J.A. and Wilhelmy, J.-F. A specimen preparation procedure for automated image analysis. *Process Mineralogy VIII*, Carson D. and Vassiliou A., eds. (TMS-AIME, 1988), 359-67.

66. Jones M.P. *Applied mineralogy* (Oxford: Graham and Trotman Ltd., 1987), 260 p.

67. Ahmedali T. Geochemistry Dept., McGill University, personal communication, 1995.

68. Goldstein J.I. et al. *Scanning electron microscopy and x-ray microanalysis* (New York: Plenum Press, 1992), 1-19.

69. Poirier G., McGill University, personal communication, 1996.

70. Adorjan L.A. Accumulation of errors in float and sink analysis. *XVI Int. Mineral Process. Congress, Cagliari, Italy*, 1988, 1633-44.

71. Barbery G. and Huyet G. Mineral liberation analysis: theoretical study and computer simulation. *SME-AIME pre-print 77-B-80*, Atlanta, 1977.

72. Meloy T.P. Liberation theory - eight, modern, usable theorems. *Int. J. Mineral Process.*, **13**, 1984, 313-24.

73. Meloy T.P. and Gotoh K. Liberation in a homogeneous two-phase ore. *Int. J. Mineral Process.*, **14**, 1985, 45-55.

74. Ferrara G., Preti U. and Bevilacqua, P. State-of-the-art and new developments in the modelling of mineral liberation using the Meloy approach. *Comminution - Theory and Practice*, Kawatra S. ed. (Littleton, CO: SME, Inc., 1992), 53-68.

75. Lin D., Gomez C.O. and Finch J.A. Comparison of stereological correction procedures for liberation measurements. *Trans. Instn Min. Metall. (Sect. C: Mineral Process. Extr. Metall.)*, **104**, 1995, C155-61.

76. Leigh G.M., Lyman G.J. and Gottlieb P. Stereological estimates of liberation from mineral section measurements: a rederivation of Barbery's formulae with extensions. *Powder Technol.*, **87**, 1996, 141-52.

77. Schneider, C.L. Documentation with the computer software program: *Stereological reconstruction of linear and areal grade distributions*, 1993.

78. Ferrara G., Preti U. and Meloy T.P. Inclusion shape, mineral texture and liberation. *Int. J. Mineral Process.*, **27**, 1989, 295-308.

79. Miles R.E. and Davy P.J. Precise and general conditions for the validity of a comprehensive set of stereological fundamental formulae. *J. Microscopy*, **107**, no. 3, 1976, 211-26.

80. Davy, P.J. Probability models for liberation. *J. Appl. Prob.*, **21**, 1984, 260-9.

81. King, R.P. Comminution and liberation of minerals. *Minerals Engineering*, **7(2/3)**, 1994, 129-40.

APPENDICES

APPENDIX 1: GLASS MATRIX STANDARD MATERIAL TESTS

This appendix describes the series of tests performed to determine the best materials and conditions for the creation of the standard material with a glass matrix. For each test, the grain material and matrix material were mixed together and placed in a furnace pre-heated to a set temperature. After a set period of time, the furnace was shut off and the material was allowed to cooled to room temperature. The next day, the block of material was removed from the furnace and crushed to various sizes.

The following variables were examined:

1) grain material - Four materials were tested: TiO_2, unchlorinated TiO_2, Al_2O_3 and ZrO_2.
2) matrix material - Two materials were tested: glass and borosilicate glass. The size of the matrix material was -38 µm, but this was inconsequential since the matrix material completely melted in all the tests.
3) particle/grain size relationship - Various combinations of particle and grain size were examined.
4) furnace type - Three types were tested: vacuum, gas and induction. The gas furnace used natural gas. The maximum temperatures of the vacuum, gas and induction furnaces are 1600, 1100 and 1300°C, respectively.
5) crucible - Two types were tested: slip-cast alumina and refractory (A.P. Green Refractories Ltd.). Refractory crucibles were used in the majority of the tests because the alumina crucibles occasionally cracked and broke in the furnace due to thermal shock.
6) vol.% matrix material: 60 to 80%

The particles were mounted in resin from which a polished surface was created and examined by SEM. In some cases, the block of material before breakage was polished and examined. The comments are based on a visual inspection of the particle sections. It was impossible to obtain a quantitative measure the occurrence of voids or the amount of grain fragmentation.

Vacuum furnace tests

Test 11-4-3

grain material:	300-425 μm TiO_2
matrix material:	glass
vol.% matrix:	60
furnace:	vacuum furnace
temperature:	1000°C for 3 hours at high vacuum (40 mTorr)

comments: The mixture was drawn right out of the crucible by the vacuum. It was not possible to examine the sample.

Test 11-26-3

grain material:	300-425 μm TiO_2
matrix material:	glass
vol.% matrix:	60
furnace:	vacuum furnace
temperature:	1500°C for 10 minutes at low vacuum (110 mTorr)

comments: A slip-cast alumina crucible was used in this test. The sample became fused to it and was very difficult to remove. A surface of the block of material was examined. There were few small (<10μm) voids in the glass, but there were many large (>50 μm) voids. Some TiO_2 grains had fragmented into 10 μm droplets.

Test 12-23-3

grain material:	300-425 μm TiO_2
matrix material:	borosilicate glass
vol.% matrix:	80
furnace:	vacuum furnace
temperature:	950°C for 1 hour at low vacuum (110 mTorr)

comments: The sample contained many voids, both large (>50 μm) and small (<10 μm).

Test 12-15-3b

grain material:	300-425 μm TiO_2
matrix material:	borosilicate glass
vol.% matrix:	80
furnace:	vacuum furnace
temperature:	950°C for 2 hours at low vacuum (110 mTorr)

comments: A visual inspection of the block of material showed that it contained many voids. SEM examination of the surface revealed that most of the voids were large (>50 μm). The block was crushed to 212-300 μm and re-examined. Most of the large voids had disappeared due to the breakage, but approximately 10% of the borosilicate glass sections contained 10-20 μm voids.

Gas furnace tests

Test 12-16-3

grain material:	300-425 μm TiO_2
matrix material:	glass
vol.% matrix:	60
furnace:	gas furnace
temperature:	1100°C for 1 hour

comments: The gas furnace was very difficult to control. The temperature fluctuated by up to 30°C during the test. The sample was crushed to 150-212 μm. SEM examination revealed that there were some small (< 10 μm) voids in the glass and that glass had infiltrated the pores (1-2 μm voids) in the TiO_2. SEM EDS analysis of the glass near the glass/TiO_2 interface yielded a small Ti peak indicating that a small amount of TiO_2 may have diffused into the glass.

Test 12-17-3

grain material:	300-425 μm TiO_2
matrix material:	borosilicate glass
vol.% matrix:	60
furnace:	gas furnace
temperature:	950°C for 25 minutes

comments: Again, there was difficulty controlling the temperature of the gas furnace; the temperature fluctuated by up to 30°C. The block of material was mounted and examined by SEM. There was a large number of voids, both large and small.

Test 12-17-3b

grain material:	300-425 μm TiO_2
matrix material:	borosilicate glass
vol.% matrix:	60
furnace:	gas furnace
temperature:	950°C for 2 hours

comments: Same comment as above Test 12-17-3.

Induction furnace tests

Test 11-4-3b

grain material:	300-425 μm TiO_2
matrix material:	glass
vol.% matrix:	60
furnace:	induction (Thermolyne)
temperature:	800°C for 3 hours

comments: The sample was crushed to 150-212, 212-425 and 425-600 μm. In all the size fractions, there were many locked sections, but there were also many small (<10 μm) voids in the glass. There was little glass infiltration of TiO_2 pores.

Test 12-9-3b

grain material:	300-425 µm TiO_2
matrix material:	borosilicate glass
vol.% matrix:	60
furnace:	induction (Thermolyne)
temperature:	900°C for 4 hours

comments: The sample was crushed to 212-300 µm and 150-212 µm. In both size fractions, there were many locked particles, but there were also many large and small voids in the borosilicate glass sections. SEM EDS analysis revealed that there was slight diffusion of TiO_2 into the borosilicate glass.

Test 12-9-3c

grain material:	300-425 µm TiO_2
matrix material:	borosilicate glass
vol.% matrix:	80
furnace:	induction (Thermolyne)
temperature:	900°C for 4 hours

comments: Same comments as Test 12-9-3b except that SEM EDS analysis revealed no diffusion of TiO_2 into the borosilicate glass near their interface.

Test 5-29-6

grain material:	300-425 µm TiO_2
matrix material:	borosilicate glass
vol.% matrix:	60
furnace:	induction (Lindberg)
temperature:	1050°C for 1 hour

comments: The sample was crushed to 212-300 µm. SEM examination revealed that there were many locked sections, but there were many 10-30 µm voids in the borosilicate glass.

Test 12-15-3

grain material:	300-425 μm TiO_2
matrix material:	borosilicate glass (grain and matrix material were pressed into a pellet)
vol.% matrix:	80
furnace:	induction (Thermolyne)
temperature:	room temperature to 800°C

comments: The pellet was placed in the furnace at room temperature and was observed as the furnace was heated to 800°C. The pellet started to lose shape at about 700°C; by 750°C, the pellet had shortened and flattened. At 800°C, the pellet had nearly collapsed and the furnace was shut off. After it had cooled, the pellet was crushed and examined. The borosilicate glass contained many small (<10 μm) voids.

Test 12-22-3d

grain material:	none
matrix material:	borosilicate glass
vol.% matrix:	100
furnace:	induction (Lindberg)
temperature:	1200°C for 90 minutes

comments: There were some voids in the borosilicate glass, but all of them were large (>50 μm).

Test 5-29-6b

grain material:	300-425 μm TiO_2
matrix material:	borosilicate glass
vol.% matrix:	60
furnace:	induction (Lindberg)
temperature:	1275°C for 30 minutes

comments: The sample was crushed to 212-300 μm. SEM examination revealed that there were few voids, but there was a large amount of TiO_2 fragmentation.

Test 12-9-3

grain material:	300-425 μm TiO_2
matrix material:	borosilicate glass
vol.% matrix:	60
furnace:	induction (Blue M)
temperature:	1200°C for 30 minutes

comments: A visual inspection of the block of material indicated that it was very porous. There were many large (>50 μm) voids in the borosilicate glass. The block was crushed to 150-212 μm and examined by SEM. There were some small (<10 μm) voids in the borosilicate glass, but the large voids had disappeared due to the breakage.

Test 12-20-3

grain material:	300-425 μm TiO_2
matrix material:	borosilicate glass
vol.% matrix:	60
furnace:	induction (Lindberg)
temperature:	1200°C for 20 minutes

comments: An examination of the block of material revealed a moderate number of small (<10 μm) voids. There was infiltration of the TiO_2 pores by borosilicate glass. SEM EDS analysis showed that some TiO_2 had diffused into the borosilicate glass. No TiO_2 fragmentation was observed.

Test 12-20-3b

grain material:	300-425 μm TiO_2
matrix material:	borosilicate glass
vol.% matrix:	60
furnace:	induction (Lindberg)
temperature:	1200°C for 1 hour

comments: The block of material was examined; the majority of the voids were large (>50 μm) and there were only a few small (<10 μm) voids, but there was evidence of TiO_2 fragmentation.

Test 12-22-3b

grain material:	300-425 µm TiO_2
matrix material:	borosilicate glass
vol.% matrix:	80
furnace:	induction (Lindberg)
temperature:	1200°C for 90 minutes

comments: The sample was crushed to 150-212 µm. An examination showed that were few small voids in the borosilicate sections. There were many locked particles; about half of them seemed to be simple-locked. There appeared to be slightly more simple locking in this sample than in previous tests due to the increased vol.% matrix material. TiO_2 fragmentation was observed.

Test 1-9-4

grain material:	300-425 µm TiO_2
matrix material:	borosilicate glass
vol.% matrix:	80
furnace:	induction (Lindberg)
temperature:	1200°C for 45 minutes

comments: The sample was crushed to 150-212 µm. Many locked sections were observed. There were few small voids in the borosilicate glass, but there were signs of TiO_2 fragmentation.

Test 1-9-4b

grain material:	106-150 µm TiO_2
matrix material:	borosilicate glass
vol.% matrix:	80
furnace:	induction (Lindberg)
temperature:	1200°C for 45 minutes

comments: The sample was crushed to 75-106 µm. Same observations as Test 1-9-4.

Test 12-22-3e

grain material:	300-425 Al_2O_3
matrix material:	borosilicate glass
vol.% matrix:	60
furnace:	induction (Lindberg)
temperature:	1200°C for 90 minutes

comments: The block of material was very difficult to crush due to the hardness of the Al_2O_3. The borosilicate glass broke preferentially and this resulted in most locked sections containing a large proportion of Al_2O_3. There were few small voids in the borosilicate glass and the Al_2O_3 displayed no signs of fragmentation.

Test 1-11-4

grain material:	106-150 µm naturally-occurring ZrO_2 (Zirconia Sales Inc.)
matrix material:	borosilicate glass
vol.% matrix:	80
furnace:	induction (Lindberg)
temperature:	1200°C for 45 minutes

comments: The sample was crushed to 75-106 µm and 150-212 µm and examined. There were many locked sections, the majority of which were complex-locked. There were few small voids in the borosilicate glass sections. The ZrO_2 did not exhibit any sign of fragmentation.

Test 2-11-4

grain material:	212-425 µm naturally-occurring ZrO_2 (Zirconia Sales Inc.)
matrix material:	borosilicate glass
vol.% matrix:	80
furnace:	induction (Lindberg)
temperature:	1200°C for 45 minutes

comments: The sample was crushed to 75-106 µm and 150-212 µm. There was more simple locking than in Test 1-11-4. Again, there were few small voids and the ZrO_2 showed no signs of fragmentation.

Test 7-24-4

grain material:	+1700 µm synthetic ZrO_2 (Norton Zirconia Inc.)
matrix material:	borosilicate glass
vol.% matrix:	80
furnace:	induction (Lindberg)
temperature:	1200°C for 40 minutes

comments: The sample was crushed to 600-850 µm and 425-600 µm. The synthetic ZrO_2 was very hard and the borosilicate glass broke preferentially. As a result, most locked sections contained a large proportion of ZrO_2.

Test 1-18-4b

grain material:	300-425 µm unchlorinated TiO_2
matrix material:	borosilicate glass
vol.% matrix:	80
furnace:	induction (Lindberg)
temperature:	1200°C for 40 minutes

comments: The sample was crushed to 150-212 µm. There were few small voids in the borosilicate glass and there was a large amount of locking with about half of locked material exhibiting simple locking. The unchlorinated TiO_2 showed only a few signs of fragmentation. A SEM EDS analysis revealed that were some 1 µm occurrences in the borosilicate glass that yielded a very high iron peak. It is likely that these occurrences originate from the unchlorinated TiO_2.

Test 2-14-4

grain material:	600-850 µm unchlorinated TiO_2
matrix material:	borosilicate glass
vol.% matrix:	70
furnace:	induction (Lindberg)
temperature:	1200°C for 45 minutes

comments: The material was crushed to 425-600 µm and 300-425 µm. There were many locked particles. The unchlorinated TiO_2 showed few signs of fragmentation and there were few small voids in the borosilicate glass. There were some 1 µm iron occurrences in the borosilicate glass.

Test 12-22-3c

grain material:	300-425 µm unchlorinated TiO_2
matrix material:	borosilicate glass
vol.% matrix:	60
furnace:	induction (Lindberg)
temperature:	1200°C for 90 minutes

comments: The block was crushed to 150-212 µm. There were few small voids in the borosilicate glass and many locked sections. The unchlorinated TiO_2 showed definite signs of fragmentation.

APPENDIX 2 : The following paper was published in Minerals Engineering (Vol. 8, No. 3, pp. 283-292, 1995).

BATCH MAGNETOHYDROSTATIC SEPARATIONS WITH A MODIFIED FRANTZ SEPARATOR

D. LIN[§], M. LEROUX[†] and J.A. FINCH[§]

§ Department of Mining and Metallurgical Engineering, McGill University, Montreal, Quebec, Canada

† Leroux Mineral Processing Laboratory Inc., Boucherville, Quebec, Canada

ABSTRACT

The difficulty of density separations at high specific gravities (> 3 g/mL) with conventional heavy liquids has led to the development and refinement of magnetohydrostatic separators. Magnetohydrostatic separation involves the separation of particles on the basis of their relative density (and magnetic susceptibility) in a magnetic fluid acted on by a magnetic field. Most of the research in this area has been concentrated on the development of continuous separators for industrial use. The work in this paper describes the creation of a batch laboratory separator through modifications to a Frantz isodynamic magnetic separator. The separator allowed the rapid separation of coarse (600–850 μm) particles based on relative density. It may find application in "heavy liquid" analysis to characterize materials.

Keywords
Density separation, Frantz, magnetic fluid, magnetohydrostatic separator

INTRODUCTION

Over the past three decades, the behaviour of magnetic fluids in magnetic fields has been extensively studied [1,2,3,4,5]. These magnetic fluids are either paramagnetic salt solutions or stabilized suspensions of colloidal ferromagnetic particles. Magnetic fluids have a Newtonian nature and retain their fluidity in the presence of a magnetic field. Magnetohydrostatic separations are based on the principle that these magnetic fluids can be made to behave like heavy liquids when subjected to a controlled magnetic field [6,7]. Most separators utilizing this principle were designed for continuous operation [8,9,10,11,12].

Previous work has been conducted using the Frantz isodynamic magnetic separator to supply the magnetic force in magnetohydrostatic separations [9,12]. The Frantz is a convenient instrument for use in small-scale magnetohydrostatic separations because it is a common laboratory instrument for the magnetic separation of solids.

The main advantages of magnetohydrostatic separators are that they can reach densities much greater than 3 g/mL and they are much safer and more convenient to use than conventional high-density heavy liquids. The main disadvantages are that they are best used with non-magnetic materials (if separation only on the basis of density is desired) and that the particle size be relatively coarse [11] if centrifugal force [13] is not applied to accelerate the separation. (Even using centrifugal force, separation efficiency still decreases markedly with particle size [14].)

In this work, a Frantz isodynamic magnetic separator was modified to perform magnetohydrostatic separations in batch mode. The batch operation provided fast separations of 600–850 μm particles with one cleaning operation.

THEORY

The net force acting on a magnetic fluid, F_f, in a magnetic field is the sum of the gravitational force (F_g) and magnetic force (F_m):

$$F_f = F_g + F_m \tag{1}$$

The gravitational force on a volume of the magnetic fluid, V, is:

$$F_g = V \rho_f g \tag{2}$$

where ρ_f is the fluid density and g is gravitational acceleration. The magnetic force on the fluid is:

$$F_m = V \kappa_f \left(\frac{B}{\mu_o}\right) \frac{dB}{dx} \tag{3}$$

where κ_f is the magnetic susceptibility of the fluid (dimensionless in SI units), μ_o is the permeability of free space ($4\pi \times 10^{-7}$ Tesla-metre/Ampere), B is the magnetic flux density (Tesla) and x is the distance perpendicular to the lines of flux of the magnetic field (metre). Thus, the net force on the fluid is:

$$F_f = V \rho_{fa} g = V \rho_f g + V \kappa_f \left(\frac{B}{\mu_o}\right) \frac{dB}{dx} \tag{4}$$

where ρ_{fa} is the apparent density of the fluid. The apparent density can be solved for and expressed as:

$$\rho_{fa} = \rho_f + \frac{\kappa_f}{g} \left(\frac{B}{\mu_o}\right) \frac{dB}{dx} \tag{5}$$

Note that the apparent density is a function of $B \cdot dB/dx$, the force factor, which can be adjusted by changing B or dB/dx, the latter being a function of pole geometry.

EXPERIMENTAL WORK AND DISCUSSION

Experimental Setup

The magnetohydrostatic separator developed here was based on the separator developed at le Centre de Recherches Minérales (CRM) [12]. There, a Frantz was modified by rotating the magnetic coils until the gap between the pole pieces was at the top and by replacing the Frantz pole pieces with two trapezoidal-shaped pole pieces (Figure 1). This arrangement yielded a V-shaped notch between the pole pieces in which a separation cell was placed. Because this setup was designed for continuous operation, the coils were sloped forward so that lights (floating particles) would flow out of the top chute of the separation cell and the heavies (sinks) would leave via the bottom chute.

The CRM separator was modified for batch operation simply by:

1) moving the coils so that they do not slope forward

2) using a plastic, wedged-shaped, separation cell without a top or bottom chute — the lights would be removed using a scoop made from 65 mesh screen material.

An iron oxide colloidal suspension from Intermagnetics General Corporation (IGC) was used as the magnetic fluid rather than the kerosene-based fluid used by CRM since the IGC fluid is water soluble which allowed easy cleaning of the particles.

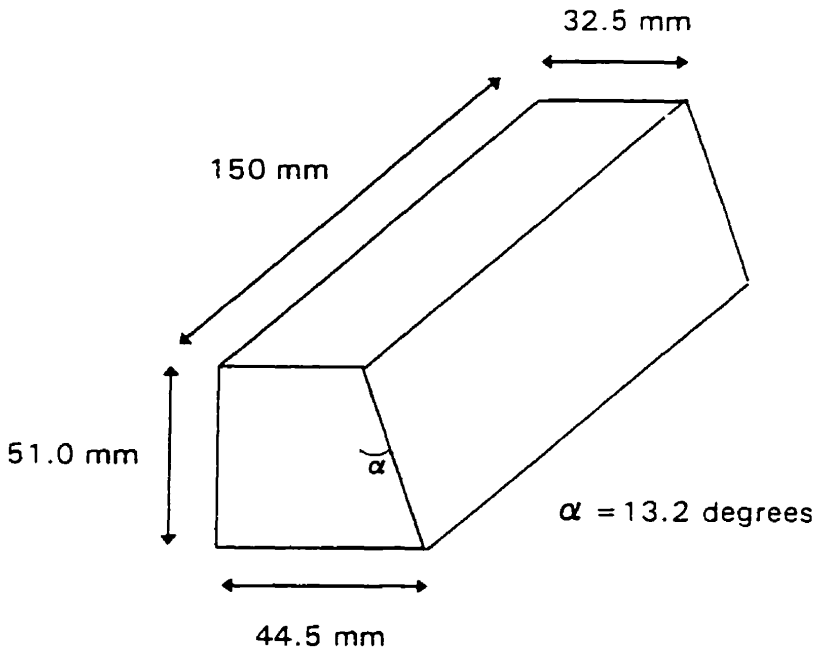

Fig.1 CRM pole piece for magnetohydrostatic separation

Magnetic Field Measurements

Magnetic field measurements were made with a gaussmeter to profile the flux density and force factor between the pole pieces. The measurements were made at three different current settings (as measured with a digital multimeter) at three longitudinal (i.e. parallel to the pole pieces) positions at various depths. The results are shown in Table 1. There are three features of note: the force factor (and hence fluid apparent density) increases with depth; at a given depth, the force factor is nearly constant at the three longitudinal positions; and there is no discernible edge effect (change in magnetic field near the edges of the pole pieces). A corollary of the constant force factor at any given depth is that to maintain a constant apparent density at the fluid surface, the fluid level must remain constant during a test. The apparent density at the surface of the magnetic fluid will change during a test if the fluid level is lowered by the removal of an excessive amount of magnetic fluid with the lights. It is also important that the fluid level during a test be the same as it was during calibration. In this work, the level was kept constant by placing an exact amount (70 mL) of magnetic fluid in the cell for all calibrations and tests.

The increasing force factor from the top to the bottom of the pole pieces indicates that the apparent density at the bottom is greater than that at the top. This creates an upward force on lights particles in the magnetic fluid, thus accelerating the separation.

The fluid level should not be higher than the pole pieces, otherwise the fluid surface takes on a convex shape and the lights would be forced to the sides of the cell and be difficult to remove. If the fluid level is kept below the level of the pole pieces then the fluid surface is concave. This creates a trough in which the lights can collect and be easily removed. This trough does not affect the apparent density of separation because the lights near the edge of the cell will slide down to the centre and be separated there. The concave shape occurs because the field is stronger where the fluid is close to the pole pieces and weaker at a distance from them (i.e. in the centre of gap) in the area just below the top of the pole pieces. When

the fluid level is raised above the level of the pole pieces, the fluid at the edges are in an area where the magnetic field is relatively weak and this results in the convex surface. This was confirmed by additional magnetic field measurements.

TABLE 1 Magnetic flux densities and force factors between the CRM pole pieces at different current settings

Current (Amp)	Dist. from bottom of the pole pieces (cm)	Magnetic Flux Density, B (Tesla)			Force Factor † (Tesla²/m)		
		Dist. from far edge of the pole pieces			Dist. from far edge of the pole pieces		
		2 cm	7.5 cm	13 cm	2 cm	7.5 cm	13 cm
0.700	6	0.060	0.060	0.060			
	5	0.100	0.100	0.100	0.400	0.375	0.375
	4	0.140	0.135	0.135	0.490	0.473	0.439
	3	0.170	0.170	0.165	0.638	0.680	0.660
	2	0.215	0.215	0.215	1.344	1.290	1.344
	1	0.295	0.290	0.290	3.024	2.973	2.973
	0	0.420	0.420	0.420			
1.100	6	0.100	0.100	0.100			
	5	0.165	0.165	0.160	0.990	0.990	0.960
	4	0.220	0.220	0.220	1.210	1.210	1.265
	3	0.275	0.275	0.275	1.788	1.788	1.788
	2	0.350	0.350	0.350	3.413	3.413	3.413
	1	0.470	0.470	0.470	7.755	7.520	7.520
	0	0.680	0.670	0.670			
1.500	6	0.145	0.150	0.145			
	5	0.225	0.230	0.230	1.856	1.898	1.898
	4	0.310	0.315	0.310	2.480	2.520	2.325
	3	0.385	0.390	0.380	3.561	3.413	3.325
	2	0.495	0.490	0.485	6.806	6.738	6.548
	1	0.660	0.665	0.650	14.685	14.298	14.138
	0	0.940	0.920	0.920			

† force factor = $B \cdot dB/dx$ where dB/dx is approximated by $\Delta B/\Delta x$.

Separator Calibration

The separator was calibrated with standard floats (floats of known density) from R.P. Cargille Laboratories Inc. In a conventional heavy liquid, the liquid is assumed to have the same density as the standard float when the float neither moves up nor down in the liquid bulk. Since the magnetic fluid is opaque, it was assumed that the apparent density of the magnetic fluid had the same density as the standard float when it just sank below the fluid surface.

The apparent density was calibrated with the current of the electromagnet. The calibration was performed with 70 mL of magnetic fluid in the separation cell. The results are shown in Figure 2. Although the relationship is nearly linear, there is some deviation. This can be attributable to the different shapes and sizes of the standard floats which made it difficult to determine exactly when a float just sank. Also, since there is a gradient in the apparent density in the separation cell, the standard float is an indicator of the average apparent density in the fluid near the surface over the length of the float, not the apparent density at the surface.

The apparent density was calibrated up to 5.00 g/mL which is near the maximum apparent density possible with this setup. If a higher apparent density is required, a fluid of higher magnetic susceptibility must be substituted or the pole pieces re-designed.

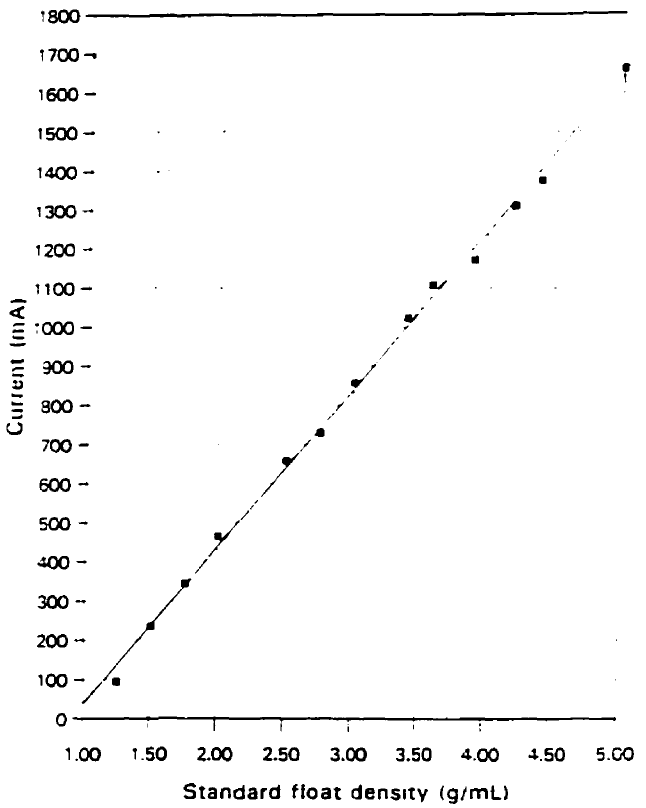

Fig.2 Calibration of magnetohydrostatic separator

TiO_2 and SiO_2 Separations

The first tests of the separator were performed using SiO_2 (silica) and TiO_2, two materials with very low magnetic susceptibilities. Although there were some density variations in the materials due to impurities, the density of SiO_2, 2.62 g/mL, is sufficiently different from that of TiO_2, 3.96 g/mL, that the separation

should have been straightforward. The difference in colour between the two (the TiO_2 is orange and the SiO_2 is a translucent white) allowed an easy visual assessment of the effectiveness of the separation. The particle size in all the tests was 600–850 μm (−20+28 mesh).

The following procedure was used:

1) the fluid in the separation cell was calibrated with a standard float
2) the current was switched off
3) the feed particles were placed in the fluid and manually stirred until all the particles were wetted
4) the current was increased to the target on the calibration and the fluid was stirred
5) using the mesh scoop, the lights were scooped out, making sure not to scoop too deeply and not to remove too much magnetic fluid
6) the fluid was stirred again
7) steps 5 and 6 were repeated two more times

A long separation time was not necessary, the separations occurring quickly.

Four separations of mixtures of SiO_2 and TiO_2 were performed. The separation densities (2.50, 2.85, 3.80 and 4.20 g/mL) were near the densities of the SiO_2 and TiO_2 in order to examine the sharpness of the separations. In most tests, the separation was repeated on one product (i.e. a cleaning operation). The results are shown in Tables 2a–d.

TABLE 2a Magnetohydrostatic separation of SiO_2 and TiO_2 at 2.50 g/mL

Feed	Apparent Density (g/mL)	Product Weight	Comment
2.00 g SiO_2 2.00 g TiO_2	2.50	lights: 0.04 g	- all SiO_2 except 1 particle of TiO_2
		heavies: 3.96 g	- mixture of SiO_2 and TiO_2
lights of above test	2.50	lights: 0.00 g	- only a few particles of SiO_2
		heavies: 0.04 g	- all SiO_2 except 1 particle of TiO_2

TABLE 2b Magnetohydrostatic separation of SiO_2 and TiO_2 at 2.85 g/mL

Feed	Apparent Density (g/mL)	Product Weight	Comment
2.00 g SiO_2 2.00 g TiO_2	2.85	lights: 2.00 g	- all SiO_2
		heavies: 2.00 g	- all TiO_2 except for 5 particles of SiO_2

TABLE 2c Magnetohydrostatic separation of SiO_2 and TiO_2 at 3.80 g/mL

Feed	Apparent Density (g/mL)	Product Weight	Comment
2.00 g SiO_2 2.00 g TiO_2	3.80	lights: 2.06 g	- mostly SiO_2 with some TiO_2 particles
		heavies: 1.94 g	- all TiO_2 except for 1 particle of SiO_2
lights of above test	3.80	lights: 2.02 g	- mostly SiO_2 with some TiO_2 particles
		heavies: 0.04 g	- all TiO_2 except for 2 particles of SiO_2

TABLE 2d Magnetohydrostatic separation of SiO_2 and TiO_2 at 4.20 g/mL

Feed	Apparent Density (g/mL)	Product Weight	Comment
2.01 g SiO_2	4.20	lights: 3.83 g	- mixture of SiO_2 and TiO_2
2.01 g TiO_2		heavies: 0.19 g	- all TiO_2 except 2 particles of SiO_2
heavies of above test	4.20	lights: 0.13 g	- all TiO_2 except 1 particle of SiO_2
		heavies: 0.06 g	- all TiO_2 except 1 particle of SiO_2

Overall, the separations were quite sharp. The cleaning operations were found to improve the overall separation. Although the separations were good, a test of the accuracy of separation was performed.

Magnetohydrostatic Separator Accuracy

A 600–850 μm synthetic, two-phase material (borosilicate glass — TiO_2) of varying particle composition was separated using both the magnetohydrostatic separator and a conventional heavy liquid (sodium polytungstate (SPT)). Two grams of the synthetic material were separated with the magnetohydrostatic separator (as calibrated with a standard float) at 2.96 g/mL. A cleaning operation was performed on both products of the initial separation. The results are shown in Tables 3a–c.

TABLE 3a Magnetohydrostatic separation of 2.00 g of synthetic material at 2.96 g/mL (rougher)

$\rho < 2.96$	0.91 g
$\rho > 2.96$	1.07 g

TABLE 3b Magnetohydrostatic separation at 2.96 g/mL (lights cleaner)

$\rho < 2.96$	0.89 g
$\rho > 2.96$	0.02 g

TABLE 3c Magnetohydrostatic separation at 2.96 g/mL (heavies cleaner)

$\rho < 2.96$	0.00 g
$\rho > 2.96$	1.06 g

The lights of the lights cleaner and the heavies of the heavies cleaner were separated in SPT at 2.96 g/mL (as measured with a 100 mL pycnometer bottle). The results are shown in Tables 4a and b.

The results indicated that the magnetohydrostatic separation came close to agreeing with the separation in SPT, but there were some misplaced particles. This could be due to either some inaccuracy in the calibration of the magnetohydrostatic separator as explained earlier or the presence of a large quantity of near density particles.

TABLE 4a SPT separation of the lights of the magnetohydrostatic lights cleaner

$\rho < 2.96$	0.82 g
$\rho > 2.96$	0.07 g

TABLE 4b SPT separation of the heavies of the magnetohydrostatic heavies cleaner

$\rho < 2.96$	0.07 g
$\rho > 2.96$	0.99 g

Pole Piece Design

The change in the force factor in the CRM pole pieces is very large from bottom to top (Table 1) so new pole pieces were designed in an attempt to generate a more uniform apparent density. Pole pieces similar to the CRM pole pieces (Figure 1), but with different slopes (α values of 0°, 5° and 10°) were tested. It was found that these pole pieces were ineffective for magnetohydrostatic separations. The magnetic fluid could not be made to float most of the standard floats even with the current turned to maximum. This result was explained by magnetic field measurements of the new pole pieces (the field measurements for $\alpha = 5°$ are shown in Table 5). Although the magnetic flux density increased from top to bottom, the force factor decreased. This created layers of lower apparent density underneath layers of higher apparent density. This caused material that fell below the layer of higher density to be either trapped underneath this layer or to continue falling to the bottom of the cell.

With $\alpha = 10°$ and a decreased interpolar distance, a more uniform apparent density was achieved but, if anything, separation efficiency declined. Software (Infolytica Inc.) is available to design pole pieces of given magnetic fields and force factors. At present, however, there appears little incentive to change the original CRM pole piece design. The large change in force factor with depth may accelerate and sharpen the separation.

CONCLUSIONS

The magnetohydrostatic separator described here allowed rapid batch separations utilizing one cleaning operation of coarse (600–850 μm) particles based on density. Further work should be conducted to determine the minimum particle size and the maximum sample volume that can be processed. A decrease in particle size beyond a certain point or a very large volume of feed to the separation cell could result in imprecise separations.

ACKNOWLEDGEMENTS

The authors are grateful to CRM for the loan of their equipment. Thanks are due in particular to Diane Gagné Gilbert and Denis Cotnoir for demonstrating the CRM separator. Funding for this research was provided by Inco Ltd. and the Natural Sciences and Engineering Research of Canada through the INCO-NSERC Chair in Mineral Processing and the Department of Energy, Mines and Resources, Canada.

TABLE 5 Magnetic flux densities and force factors between the modified (α=5°) pole pieces at different current settings

Current (Amp)	Dist. from bottom of the pole pieces (cm)	Magnetic Flux Density, B (Tesla)			Force Factor † (Tesla²/m)		
		Dist. from far edge of the pole pieces			Dist. from far edge of the pole pieces		
		2 cm	7.5 cm	13 cm	2 cm	7.5 cm	13 cm
0.700	6	0.070	0.070	0.070			
	5	0.105	0.105	0.105	0.315	0.341	0.315
	4	0.130	0.135	0.130	0.293	0.304	0.293
	3	0.150	0.150	0.150	0.225	0.150	0.188
	2	0.160	0.155	0.155	0.160	0.116	0.155
	1	0.170	0.165	0.170	0.043	0.041	0.043
	0	0.165	0.160	0.160			
1.100	6	0.115	0.115	0.115			
	5	0.165	0.165	0.165	0.784	0.784	0.784
	4	0.210	0.210	0.210	0.683	0.683	0.683
	3	0.230	0.230	0.230	0.460	0.460	0.460
	2	0.250	0.250	0.250	0.438	0.375	0.375
	1	0.265	0.260	0.260	0.066	0.065	0.065
	0	0.255	0.255	0.255			
1.500	6	0.160	0.160	0.160			
	5	0.210	0.210	0.210	1.155	1.103	1.103
	4	0.270	0.265	0.265	1.215	1.060	1.060
	3	0.300	0.290	0.290	0.750	0.725	0.725
	2	0.320	0.315	0.315	0.640	0.709	0.709
	1	0.340	0.335	0.335	0.085	0.084	0.084
	0	0.325	0.320	0.320			

† force factor = $B \cdot dB/dx$ where dB/dx is approximated by $\Delta B/\Delta x$.

REFERENCES

1. Neuringer, J.L. & Rosensweig R.E., Ferrohydrodynamics. *Phys. Fluids* 7(12), 1927 (1964).
2. Andres, U., Bunin, G.M. & Gil, B.B., Magnetohydrostatic separation. *J. Appl. Mech. Tech. Phys.* 7(3), 109 (1966).
3. Rosensweig, R.E., Fluidmagnetic buoyancy. *AIAA J.* 4(10), 1751 (1966).
4. Rosensweig, R.E., Ferrohydrodynamics. Cambridge University Press, Cambridge (1985).

5. Gubarevich, V.N. & Vidsota, S.V., Theoretical principles, present status and prospects for development of material separation in magnetic fluids. *Mag. Electr. Sep.* **5**(3), 169 (1994).
6. Andres, U., Magnetohydrodynamic and magnetohydrostatic separation — a new prospect for mineral separation in the magnetic field. *Miner. Sci. Eng.* 7(2), 99 (1975).
7. Khalafalla, S.E., Magnetic separation of the second kind: magnetogravimetric, magnetohydrostatic and magnetohydrodynamic separations. *IEEE Trans. Magn.* **MAG-12**(5), 455 (1976).
8. Reimers, G.W., Rholl, S.A. & Khalafalla, S.E., Device and process for magneto-gravimetric particle separation using non-vertical levitation forces. *United States Patent 3,788,465*, (1974).
9. Parsonage, P., Small-scale separation of minerals by use of paramagnetic liquids. *Trans. Instn. Min. Metall.*, Sect. B, **86**, B43 (1977).
10. Shimoiizaka, J., Nakatsuka, K., Fujita, T. & Kounosu, A., Sink-float separators using permanent magnets and water based magnetic fluid. *IEEE Trans. Magn.* **MAG-16**(2), 368 (1980).
11. Parsonage, P., Factors that influence performance of pilot-plant paramagnetic liquid separator for dense particle fractionation. *Trans. Instn. Min. Metall.*, Sect. C, **89**, C166 (1980).
12. Tremblay, R., Etude du procédé magnétohydrostatique. *Le Centre Recherches Minérales report*, Sainte-Foy, Québec, (May 1983).
13. Walker, M.S. & Devernoe, A.L., Mineral separations using rotating magnetic fluids. *Int. J. Min. Proc.* **31**, 195 (1991).
14. Bunge, R.C. & Fuerstenau, D.W., Mineral separations with a magnetogravimetric separator. *SME pre-print 90–192*, Salt Lake City (1990).

APPENDIX 3: RESULTS OF THE FIRST MAGSTREAM FRACTIONATION OF THE GLASS/BORATE STANDARD MATERIAL

This appendix details the results of the first Magstream fractionation of the glass/borate standard material. The first separations of the standard material were the rougher separations. They started at the lowest vol.% borate split-points and worked upwards (i.e. a split was made at 5 vol.% borate, then 15, 25...etc.). The particle composition and the corresponding Magstream split-point are shown in Table A3.1.

Each composition fraction was cleaned at least twice. For example: the 15-25 vol.% borate fraction was isolated by rougher separations at 3.152 and 3.585 g/ml. Thus, the fraction consisted of the 3.152 heavy product and the 3.585 light product. This fraction was then re-processed at 3.152 g/ml resulting in two products: [3.152 heavy heavy] and [3.152 heavy light]. The [3.152 heavy light] was removed from consideration and the [3.152 heavy heavy] fraction was re-processed at 3.152 g/ml again. This resulted in two fractions: [3.152 heavy heavy heavy] and [3.152 heavy heavy light]. The [3.152 heavy heavy light] was removed from consideration. The [3.152 heavy heavy heavy] was similarly re-processed twice at 3.585 g/ml. This produced the final clean 15-25 vol.% borate fraction.

Table A3.1: Particle composition and the corresponding Magstream split-point.

Particle composition (vol.% borate)	Magstream split-point (g/ml)
5	2.719
15	3.152
25	3.585
35	4.018
45	4.451
55	4.884
65	5.317
75	5.750
85	6.183
95	6.616

Results of the first Magstream fractionation (all data in grams)

5-15 vol.% borate fraction

2.719 heavy light	4.08
2.719 heavy heavy light	1.12
3.152 light heavy	11.74
3.152 light light heavy	0.52
2.719-3.152 final product	40.23

15-25 vol.% borate fraction

3.152 heavy light	6.62
3.152 heavy heavy light	1.07
3.585 light heavy	5.24
3.585 light light heavy	0.28
3.152-3.585 final product	23.62

25-35 vol.% borate fraction

3.585 heavy light	11.03
3.585 heavy heavy light	1.21
4.018 light heavy	5.27
4.018 light light heavy	2.15
3.585-4.018 final product	31.89

35-45 vol.% borate fraction

4.018 heavy light	1.31
4.018 heavy heavy light	0.52
4.451 light heavy	3.23
4.451 light light heavy	3.00
4.018-4.451 final product	37.45

45-55 vol.% borate fraction

4.451 heavy light	6.19
4.451 heavy heavy light	2.15
4.884 light heavy	3.36
4.884 light light heavy	3.19
4.451-4.884 final product	55.50

55-65 vol.% borate fraction

4.884 heavy light	10.54
4.884 heavy heavy light	5.70
5.317 light heavy	5.61
5.317 light light heavy	3.73
5.317 light light light heavy	2.58
4.884-5.317 final product	121.06

65-75 vol.% borate fraction

5.317 heavy light	3.56
5.317 heavy heavy light	2.01
5.317 heavy heavy heavy light	1.79
5.750 light heavy	12.50
5.750 light light heavy	7.63
5.317-5.750 final product	43.61

75-85 vol.% borate fraction

5.750 heavy light	11.32
5.750 heavy heavy light	3.67
5.750 heavy heavy heavy light	4.40
6.183 light heavy	15.95
6.183 light light heavy	7.71
5.750-6.183 final product	37.29

85-95 vol.% borate fraction

6.183 heavy light	3.93
6.183 heavy heavy light	1.86
6.183 heavy heavy heavy light	2.39
6.616 light heavy	7.68
6.616 light light heavy	7.13
6.183-6.616 final product	24.38

APPENDIX 4: EMISSION LINES AND STANDARDS USED IN WDS ANALYSES

The emission lines and standards that were used in the identification of the oxides in the standard material are shown in Table A4.1. The composition of the standards are shown in Table A4.2-4.

Table A4.1: Emission lines and standards used in the identification of the oxides in WDS analyses.

Oxide	Emission line	Emission line energy (keV)	Standard
Na_2O	k-alpha	1.041	NBS 620
Al_2O_3	k-alpha	1.487	BMAK
SiO_2	k-alpha	1.740	NBS 620
MgO	k-alpha	1.254	NBS 620
K_2O	k-alpha	3.313	OBS 1
CaO	k-alpha	3.691	NBS 620
FeO	k-alpha	6.403	BMAK
PbO	m-alpha	2.346	pure galena (PbS)
B_2O_3	calculated by difference		

Table A4.2: Composition of NBS 620.

Oxide	wt.%
SiO_2	72.08
TiO_2	0.02
Al_2O_3	0.02
FeO	0.04
MgO	3.69
CaO	7.11
Na_2O	14.39
K_2O	0.41
SO_3	0.11
Cl_2O	0.02
Total:	99.67

Table A4.3: Composition of BMAK.

Oxide	wt.%
SiO_2	50.94
TiO_2	4.06
Al_2O_3	12.49
FeO	13.30
MnO	0.15
CaO	9.30
Na_2O	2.66
K_2O	0.82
P_2O_5	0.38
MgO	5.08
Total:	99.18

Table A4.4: Composition of OBS 1.

Oxide	wt.%
SiO_2	73.44
TiO_2	0.31
Al_2O_3	13.93
FeO	1.80
MnO	0.04
MgO	0.33
CaO	1.22
Na_2O	4.19
K_2O	4.34
H_2O	0.41
Total:	100.01

APPENDIX 5: RESULTS OF THE SECOND (CORRECTED) MAGSTREAM FRACTIONATION OF THE GLASS/BORATE STANDARD MATERIAL

This appendix details the results of the second (corrected) Magstream fractionation of the glass/borate standard material. The first separations of the standard material were the rougher separations. They started at the highest vol.% borate split-points and worked downwards (i.e. a split was made at 95 vol.% borate, then 85, 75...etc.). The particle composition and the corresponding Magstream split-point are shown in Table A5.1.

Each fraction was cleaned at least twice. For example: the 15-25 vol.% borate fraction was isolated by rougher separations at 3.035 and 3.390 g/ml. Thus, the fraction consisted of the 3.035 heavy product and the 3.390 light product. This fraction was then re-processed at 3.035 g/ml resulting in two products: [3.035 heavy heavy] and [3.035 heavy light]. The [3.035 heavy light] was removed from consideration and the [3.035 heavy heavy] fraction was re-processed at 3.035 g/ml again. This resulted in two fractions: [3.035 heavy heavy heavy] and [3.035 heavy heavy light]. The [3.035 heavy heavy light] was removed from consideration. The [3.035 heavy heavy heavy] was similarly re-processed twice at 3.390 g/ml. This produced the final clean 15-25 vol.% borate fraction.

Table A5.1: Particle composition and the corresponding Magstream split-point.

Particle composition (vol.% borate)	Magstream split-point (g/ml)
5	2.680
15	3.035
25	3.390
35	3.745
45	4.100
55	4.455
65	4.810
75	5.165
85	5.520
95	5.875

Results of the second (corrected) Magstream fractionation (all data in grams)

+95 vol.% borate fraction

5.875 heavy light	5.26
5.875 heavy heavy light	4.14
5.875 heavy heavy heavy (final product)	58.26

85-95 vol.% borate fraction

5.520 heavy light	6.00
5.520 heavy heavy light	5.88
5.875 heavy	14.85
5.875 light heavy	4.36
5.875 light light heavy	2.31
5.520-5.875 final product	19.08

75-85 vol.% borate fraction

5.165 heavy light	8.93
5.165 heavy heavy light	4.65
5.520 heavy	16.16
5.520 light heavy	5.19
5.520 light light heavy	2.89
5.165-5.520 final product	30.52

65-75 vol.% borate fraction

4.810 heavy light	3.59
4.810 heavy heavy light	1.84
5.165 heavy	14.42
5.165 light heavy	1.21
5.165 light light heavy	0.83
4.810-5.165 final product	25.08

55-65 vol.% borate fraction

4.455 heavy light	9.24
4.455 heavy heavy light	3.38
4.810 heavy	14.42
4.810 light heavy	4.18
4.810 light light heavy	1.68
4.455-4.810 final product	19.07

45-55 vol.% borate fraction

4.100 heavy light	3.54
4.100 heavy heavy light	3.60
4.455 heavy	9.30
4.455 light heavy	4.61
4.455 light light heavy	2.29
4.100-4.455 final product	27.60

35-45 vol.% borate fraction

3.745 heavy light	2.18
3.745 heavy heavy light	1.14
4.100 heavy	14.99
4.100 light heavy	3.08
4.100 light light heavy	1.76
3.745-4.100 final product	27.66

25-35 vol.% borate fraction

3.390 heavy light	2.38
3.390 heavy heavy light	1.16
3.745 heavy	9.28
3.745 light heavy	1.61
3.745 light light heavy	0.89
3.390-3.745 final product	23.07

15-25 vol.% borate fraction

3.035 heavy light	1.34
3.035 heavy heavy light	1.57
3.390 heavy	20.19
3.390 light heavy	1.89
3.390 light light heavy	0.50
3.035-3.390 final product	21.94

5-15 vol.% borate fraction

2.680 light	n/a
2.680 heavy light	1.31
2.680 heavy heavy light	1.84
3.035 heavy	5.96
3.035 light heavy	1.52
3.035 light light heavy	1.11
2.680-3.035 final product	25.64

-5 vol.% borate fraction

2.680 heavy	9.38
2.680 light heavy	2.68
2.680 light light heavy	1.58
2.680 light light light (final product)	67.99

APPENDIX 6: SPHERE SECTIONING PROGRAM

The following is the Microsoft QuickBASIC 4.5 code for the computer software program SECTDIST.

```
'SECTDIST.BAS

'SECTDIST is a BASIC program that performs the sectioning of two-phase
'(A and B) spheres. The spheres are single-capped and the sphere diameter
'is 2. 100 000 sections are generated for each sphere composition.
'This simulation is based on the numerical integration technique as described
'by G.S. Hill in his doctorate thesis (McGill University, 1990).

'The interval between the composition of the spheres to be sectioned
'is input by the user. The exclusion criterion (for the large-sections
'correction) is also input by the user.
'The output is the sectioned distribution (discretized into the following
'intervals: 0, 0-10, 10-20, 20-30, . . .90-100, 100%).
'The variables required for Barbery's correction (i.e. E(S), E(S^2), Var(S)
'and E(SA*SB)) are also calculated.
'This program uses Crofton's equation as a check on the sphere volume.

'Variable definition
'i = distance from sphere centre to middle of A/B interface plane
'i ranges from -1 to 0, i.e. 0 to 50% B
'd = distance from sphere centre to middle of section plane
'd ranges from 0 to 1, i.e. from sphere surface to the middle of sphere
'H = perpendicular distance from the plane through the centre of the sphere
'    to a point on the sphere surface where the line from the sphere centre
'    through the section plane intersects the sphere surface
'H ranges from -1 to 1
'thetai = angle between a line from the sphere centre to the middle of
'  the plane of the A/B interface and a line from the sphere centre to
'  the middle of the section plane
'thetad = angle between a line from the sphere centre to the edge of
'  the section plane and a line from the sphere centre to the middle of
'  of the section plane
'thetar = angle between a line from the sphere centre to the middle of
'  the plane of the A/B interface and a line from the sphere centre to
'  the edge of the plane of the A/B interface
'AreaFractA = fraction of section area consisting of phase A
```

```
'AreaFractB = fraction of section area consisting of phase B
'SectionArea = area of the section
'TotalSectionArea = sum of all the section areas
'SectionRadius = radius of the section
'NumSection = number of sections generated
'AvgS = average section area
'VarS = variation of the section area
'CrossProduct = average product of section area 'A' and section area 'B'
'AvgSsquared = average square of the section area
'TotalSsquared = sum of the squares of the section areas
'bin(12) = array of the sectioning distribution
'freq(12) = array of the frequency of the sectioning distribution
'label(12) = name of the composition interval

DIM d, H, thetar, thetad, thetai, yes, st AS SINGLE
DIM AreaFractA, AreaFractB, mu, x, z AS SINGLE
DIM SectionRadius, NumSection, TotalAreaB, largest AS SINGLE
DIM CalcVolumeB, AvgS, AvgSsquared, TotalSsquared AS SINGLE
DIM VarS, CP, CrossProduct, CheckArea AS SINGLE
DIM bin(0 TO 12) AS DOUBLE
DIM freq(0 TO 12) AS SINGLE
DIM label(0 TO 12)  AS STRING
DIM TotalSectionArea AS DOUBLE
DIM SectionArea AS DOUBLE
DIM i AS DOUBLE
DIM k AS DOUBLE
DIM temp AS DOUBLE
DIM VolumeB AS DOUBLE

CONST pi = 3.1415926536#

CLS

'Save results to a file?
yes = 0
PRINT
PRINT "This program sections two-phase (phases A and B) spheres and calculates"
PRINT "the sectioned distribution.  The results can be saved in a file."
INPUT "Would you like to save the information to a file "; yn$
IF yn$ = "y" OR yn$ = "Y" OR yn$ = "yes" OR yn$ = "YES" THEN
    INPUT "Please enter the name of the file "; filname$
    OPEN filname$ FOR OUTPUT AS #1
    CLOSE #1
```

```
        PRINT filname$; " has been created."
        yes = 1
END IF
PRINT

'Enter the step interval
15 PRINT "Please select the interval between the sphere compositions."
PRINT "The spheres will be sectioned at intervals between 0 and 50% phase B."
PRINT "If, for example, an interval of 5% is selected, spheres with a composition"
PRINT "of 5, 15, 25, ... 50% phase B will be sectioned.  The interval must be"
PRINT "between 0 and 50%."
INPUT "Enter the interval [%] "; st
IF st <= 0 THEN GOTO 15
PRINT "The interval you have selected is "; st; "%."
PRINT
PRINT "Enter the exclusion criterion (area % below which sections are excluded"
INPUT "from analysis). (0 = consider all sections) [%] "; largest
PRINT "All sections smaller than "; largest; "% of the largest section will be excluded."
PRINT

label$(0) = "   0"
label$(1) = "0-10"
label$(2) = "10-20"
label$(3) = "20-30"
label$(4) = "30-40"
label$(5) = "40-50"
label$(6) = "50-60"
label$(7) = "60-70"
label$(8) = "70-80"
label$(9) = "80-90"
label$(10) = "90-100"
label$(11) = " 100"

'********************* MAIN LOOP ******************

'Volume Fraction of B ranges from 0 to 0.5

FOR v% = st * 100 TO 50 * 100 STEP st * 100

VolumeB = v% / 10000

'Variable initiation
TotalSectionArea = 0
```

```
TotalAreaB = 0
SectionArea = 0
NumSection = 0
CalcVolumeB = 0
TotalSsquared = 0
VarS = 0
CP = 0
CrossProduct = 0
CheckArea = 0
d = 0
FOR j% = 0 TO 12
      bin(j%) = 0
      freq(j%) = 0
NEXT j%

'Iterative calculation of i
i = .5
k = .001
FOR j% = 1 TO 13
10     temp = (i ^ 3 - 3 * i + 2) / 4
      IF temp > VolumeB THEN i = i + k
      IF temp < VolumeB THEN i = i - k
      IF ABS(temp - VolumeB) > k THEN 10
      k = k / 10
NEXT j%

i = ABS(i) * -1

VolumeB = (ABS(i) ^ 3 - 3 * ABS(i) + 2) / 4

'**************** CALCULATION LOOP ***************
'100 000 sections will be generated

FOR dd% = 5 TO 995 STEP 10

      d = dd% / 1000
      PRINT "d="; d

FOR HH% = -999 TO 999 STEP 2

      H = HH% / 1000

      thetar = ATN(H / SQR(-H * H + 1)) + pi / 2
```

```
thetai = ATN(i / SQR(-i * i + 1)) + pi / 2
thetad = ATN(SQR(1 - d ^ 2) / d)

SectionArea = pi * (1 - d ^ 2)

IF (SectionArea / pi) < (largest / 100) THEN GOTO 20

SectionRadius = SQR(1 - d ^ 2)
TotalSectionArea = TotalSectionArea + SectionArea
NumSection = NumSection + 1


IF d > ABS(i) AND thetar < (thetai - thetad) THEN
      bin(11) = bin(11) + SectionArea
      freq(11) = freq(11) + 1
      AreaFractB = 1
END IF

IF ABS(i) > d AND thetar < (thetad - thetai) THEN
      bin(0) = bin(0) + SectionArea
      freq(0) = freq(0) + 1
      AreaFractB = 0
END IF

IF thetar > (thetai + thetad) THEN
      bin(0) = bin(0) + SectionArea
      freq(0) = freq(0) + 1
      AreaFractB = 0
END IF

IF thetar > ABS(thetai - thetad) AND thetar < (thetai + thetad) THEN
     'Locked Particle

     IF -i < d * COS(thetar) THEN
           x = (i + d * COS(thetar)) / SIN(thetar)
           mu = x / SectionRadius
           z = SQR(1 - mu ^ 2)
           AreaFractA = 1 - (mu * z + pi - ATN(z / mu)) / pi
      ELSE
           x = (-i - d * COS(thetar)) / SIN(thetar)
           mu = x / SectionRadius
           z = SQR(1 - mu ^ 2)
           AreaFractA = (mu * z + pi - ATN(z / mu)) / pi
```

```
            END IF

            AreaFractB = 1 - AreaFractA
            IF AreaFractB < .1 THEN comp% = 1
            IF AreaFractB >= .1 AND AreaFractB < .2 THEN comp% = 2
            IF AreaFractB >= .2 AND AreaFractB < .3 THEN comp% = 3
            IF AreaFractB >= .3 AND AreaFractB < .4 THEN comp% = 4
            IF AreaFractB >= .4 AND AreaFractB < .5 THEN comp% = 5
            IF AreaFractB >= .5 AND AreaFractB < .6 THEN comp% = 6
            IF AreaFractB >= .6 AND AreaFractB < .7 THEN comp% = 7
            IF AreaFractB >= .7 AND AreaFractB < .8 THEN comp% = 8
            IF AreaFractB >= .8 AND AreaFractB < .9 THEN comp% = 9
            IF AreaFractB >= .9 THEN comp% = 10
            bin(comp%) = bin(comp%) + SectionArea
            freq(comp%) = freq(comp%) + 1
        END IF

        CheckArea = CheckArea + SectionArea ^ (5 / 2)
        TotalAreaB = TotalAreaB + AreaFractB * SectionArea
        TotalSsquared = TotalSsquared + SectionArea ^ 2
        AreaFractA = 1 - AreaFractB
        CP = CP + (AreaFractB * SectionArea) * (AreaFractA * SectionArea)

20 NEXT HH%
NEXT dd%

CalcVolumeB = TotalAreaB / TotalSectionArea
AvgS = TotalSectionArea / NumSection
AvgSsquared = TotalSsquared / NumSection
VarS = AvgSsquared - AvgS ^ 2
CrossProduct = CP / NumSection
CalcSphereVol = 256 / 45 / pi ^ (3 / 2) * (CheckArea / NumSection) / AvgS

'****************** END OF CALCULATION LOOP ***************

'Save results in a file
IF yes = 1 THEN
    OPEN filname$ FOR APPEND AS #1
    WRITE #1,
    WRITE #1, CalcVolumeB * 100
    WRITE #1,
    FOR j% = 0 TO 11
        WRITE #1, bin(j%) / TotalSectionArea * 100
```

```
    NEXT j%
    WRITE #1,
    WRITE #1, "E(S)=", AvgS
    WRITE #1, "E(S^2)=", AvgSsquared
    WRITE #1, "Var(S)=", VarS
    WRITE #1, "E(SA*SB)=", CrossProduct
    WRITE #1,
    WRITE #1, 100 - (CalcVolumeB * 100)
    WRITE #1,
    FOR j% = 11 TO 0 STEP -1
        WRITE #1, bin(j%) / TotalSectionArea * 100
    NEXT j%
    CLOSE #1
END IF

'Print results to screen
PRINT "Volume % B (input) ="; VolumeB * 100; "    ";
PRINT "Volume % B (calculated) ="; CalcVolumeB * 100
PRINT "Check: Theoret. Sphere Vol.= 4.188790     Calc. Vol.="; CalcSphereVol
PRINT
PRINT "SECTION %B          AREA %          FREQ. % "
xsum = 0
FOR j% = 0 TO 11
    xsum = xsum + bin(j%)
    PRINT label$(j%), bin(j%) / TotalSectionArea * 100, freq(j%) / NumSection * 100
NEXT j%
PRINT
PRINT "Number of sections analyzed ="; NumSection
PRINT "E(S) ="; AvgS
PRINT "E(S^2) ="; AvgSsquared
PRINT "Var(S) ="; VarS
PRINT "E(SA*SB) ="; CrossProduct
PRINT

INPUT "Press ENTER to continue "; pause$

NEXT v%

'***************** END OF MAIN LOOP *****************
```

APPENDIX 7: HILL'S FAST APPROXIMATION

An example of Hill's fast approximation is shown in the table below. The correction is easily performed on a spreadsheet. The input is the sectioned distribution (Column C). The formulas are displayed below.

	A	B	C	D	E	F	G	H	I
	Comp. Fract. (%"1")	Avg. Comp. (%"1")	Sect. Dist.	Lock Sect. Dist.	Free "1"	Loc-ked	Free "0"	Scaled Dist.	Corr. Dist.
1	0	0	5.89					-2.03	0.00
2	0-10	5	3.26	3.26	0.02	1.95	1.30	3.84	3.69
3	10-20	15	3.62	3.62	0.04	2.68	0.91	4.27	4.10
4	20-30	25	5.34	5.34	0.08	4.41	0.84	6.29	6.04
5	30-40	35	9.19	9.19	0.23	8.05	0.92	10.82	10.40
6	40-50	45	24.50	24.50	0.97	21.99	1.54	28.84	27.73
7	50-60	55	21.73	21.73	1.37	19.50	0.86	25.57	24.59
8	60-70	65	8.85	8.85	0.88	7.74	0.22	10.41	10.01
9	70-80	75	5.18	5.18	0.82	4.28	0.08	6.10	5.87
10	80-90	85	3.51	3.51	0.88	2.59	0.03	4.13	3.97
11	90-100	95	3.17	3.17	1.26	1.89	0.02	3.73	3.59
12	100	100	5.75					-1.97	0.00
13		Sum	100.0	88.36	6.55	75.08	6.73	100.0	100.0
14		Scale-up:		1.18	7.71	88.36	7.92	103.99	

Free "1": E = 10 ^ (2 * (B/100) - 2) / 2 * D
Locked : F = D - (E + G)
Free "0": G = 10 ^ (-2 * (B/100)) / 2 * D

Scale-up factor: D14 = D13 / F13
Scaled Free "1": E14 = E13 * D14
Scaled Locked: F14 = F13 * D14
Scaled Free "0": G14 = G13 * D14

Scaled distribution (Column H)
H1 = C1 - G14
H2 to 11 = D * D14
H12 = C12 - E14
H14 = sum (H2 to H11)

For the corrected distribution (Column I), I1 and I12 are set to zero if their corresponding scaled value (in Column H) is negative. Column I is then scaled so the distribution totals 100.

APPENDIX 8: MASS DISTRIBUTION OF THE STANDARD MATERIAL CASES

Table A8.1 shows the mass distribution of the seven cases that were created using the glass/borate standard material and sent to CANMET for liberation analysis. The mass in each composition fraction was carefully weighed out on an analytical balance with four decimal place accuracy.

In cases 1, 2 and 5, the samples were mounted at CANMET and the sample mass was 1.8 grams which was divided amongst three pellets. In cases 3, 4, 6 and 7, the samples were mounted at McGill and the sample volume per pellet was 0.4 ml.

Note that the density of the +95 vol.% borate composition fraction is 6.265 g/ml. This is the pycnometer-measured density of this fraction, not the density based on the IA grade. This was done since the calculation of the mass distribution required the true density of the composition fraction. In this one instance, the pycnometer-measured density is much closer to the true density than the density based on the IA grade.

Table A8.1(a): Case 1: single composition.

average sample density = 4.266 g/ml sample volume = 0.4219 ml						
Compos i-tion fraction (vol.% borate)	IA grade (vol.% borate)	Volume fraction	Density (g/ml)	Mass units	Volume (ml)	Mass (g)
0	0.0	0.00	2.502	0.000	0.0000	0.0000
-5	0.4	0.00	2.516	0.000	0.0000	0.0000
5-15	9.8	0.00	2.850	0.000	0.0000	0.0000
15-25	20.1	0.00	3.216	0.000	0.0000	0.0000
25-35	31.7	0.00	3.627	0.000	0.0000	0.0000
35-45	40.0	0.00	3.922	0.000	0.0000	0.0000
45-55	49.7	1.00	4.266	4.266	0.4219	1.8000
55-65	58.9	0.00	4.593	0.000	0.0000	0.0000
65-75	68.3	0.00	4.927	0.000	0.0000	0.0000
75-85	78.0	0.00	5.271	0.000	0.0000	0.0000
85-95	87.9	0.00	5.622	0.000	0.0000	0.0000
+95	-	0.00	6.265	0.000	0.0000	0.0000
100	100.0	0.00	6.052	0.000	0.0000	0.0000
		1.00			0.4219	1.8000

Table A8.1(b): Case 2: narrow composition range.

average sample density = 4.265 g/ml sample volume = 0.4220 ml						
Compos i-tion fraction (vol.% borate)	IA grade (vol.% borate)	Volume fraction	Density (g/ml)	Mass units	Volume (ml)	Mass (g)
0	0.0	0.00	2.502	0.000	0.0000	0.0000
-5	0.4	0.00	2.516	0.000	0.0000	0.0000
5-15	9.8	0.00	2.850	0.000	0.0000	0.0000
15-25	20.1	0.00	3.216	0.000	0.0000	0.0000
25-35	31.7	0.10	3.627	0.363	0.0422	0.1531
35-45	40.0	0.20	3.922	0.784	0.0844	0.3311
45-55	49.7	0.40	4.266	1.707	0.1688	0.7202
55-65	58.9	0.20	4.593	0.919	0.0844	0.3877
65-75	68.3	0.10	4.927	0.493	0.0422	0.2079
75-85	78.0	0.00	5.271	0.000	0.0000	0.0000
85-95	87.9	0.00	5.622	0.000	0.0000	0.0000
+95	-	0.00	6.265	0.000	0.0000	0.0000
100	100.0	0.00	6.052	0.000	0.0000	0.0000
		1.00			0.4220	1.8000

Table A8.1(c): Case 3: simulated primary grinding product.

sample volume = 0.4000 ml					
Compos i-tion fraction (vol.% borate)	IA grade (vol.% borate)	Volume Fraction	Density (g/ml)	Volume (ml)	Mass (g)
0	0.0	0.20	2.502	0.0800	0.2002
-5	0.4	0.10	2.516	0.0400	0.1006
5-15	9.8	0.08	2.850	0.0320	0.0912
15-25	20.1	0.06	3.216	0.0240	0.0772
25-35	31.7	0.03	3.627	0.0120	0.0435
35-45	40.0	0.02	3.922	0.0080	0.0314
45-55	49.7	0.02	4.266	0.0080	0.0341
55-65	58.9	0.02	4.593	0.0080	0.0367
65-75	68.3	0.03	4.927	0.0120	0.0591
75-85	78.0	0.06	5.271	0.0240	0.1265
85-95	87.9	0.08	5.622	0.0320	0.1799
+95	-	0.10	6.265	0.0400	0.2506
100	100.0	0.20	6.052	0.0800	0.4842
		1.00		0.4000	1.7153

Table A8.1(d): Case 4: simulated concentrate or tailings (few locked particles; large amount of free glass).

sample volume = 0.4000 ml					
Compos i-tion fraction (vol.% borate)	IA grade (vol.% borate)	Volume Fraction	Density (g/ml)	Volume (ml)	Mass (g)
0	0.0	0.80	2.502	0.3200	0.8006
-5	0.4	0.01	2.516	0.0040	0.0101
5-15	9.8	0.01	2.850	0.0040	0.0114
15-25	20.1	0.01	3.216	0.0040	0.0129
25-35	31.7	0.02	3.627	0.0080	0.0290
35-45	40.0	0.03	3.922	0.0120	0.0471
45-55	49.7	0.03	4.266	0.0120	0.0512
55-65	58.9	0.02	4.593	0.0080	0.0367
65-75	68.3	0.01	4.927	0.0040	0.0197
75-85	78.0	0.01	5.271	0.0040	0.0211
85-95	87.9	0.01	5.622	0.0040	0.0225
+95	-	0.01	6.265	0.0040	0.0251
100	100.0	0.03	6.052	0.0120	0.0726
		1.00		0.4000	1.1600

Table A8.1(e): Case 5: high or low grade middlings.

average sample density = 3.078 g/ml sample volume = 0.5848 ml						
Compos i-tion fraction (vol.% borate)	IA grade (vol.% borate)	Volume fraction	Density (g/ml)	Mass units	Volume (ml)	Mass (g)
0	0.0	0.05	2.502	0.125	0.0292	0.0732
-5	0.4	0.10	2.516	0.252	0.0585	0.1472
5-15	9.8	0.45	2.850	1.282	0.2632	0.7500
15-25	20.1	0.15	3.216	0.482	0.0877	0.2821
25-35	31.7	0.15	3.627	0.544	0.0877	0.3182
35-45	40.0	0.10	3.922	0.392	0.0585	0.2294
45-55	49.7	0.00	4.266	0.000	0.0000	0.0000
55-65	58.9	0.00	4.593	0.000	0.0000	0.0000
65-75	68.3	0.00	4.927	0.000	0.0000	0.0000
75-85	78.0	0.00	5.271	0.000	0.0000	0.0000
85-95	87.9	0.00	5.622	0.000	0.0000	0.0000
+95	-	0.00	6.265	0.000	0.0000	0.0000
100	100.0	0.00	6.052	0.000	0.0000	0.0000
		1.00			0.5848	1.8000

Table A8.1(f): Case 6: stream with no free glass (same locked distribution as Case 4, but with the free glass removed).

sample volume = 0.4000 ml					
Compos i-tion fraction (vol.% borate)	IA grade (vol.% borate)	Volume Fraction	Density (g/ml)	Volume (ml)	Mass (g)
0	0.0	0.00	2.502	0.0000	0.0000
-5	0.4	0.05	2.516	0.0200	0.0503
5-15	9.8	0.05	2.850	0.0200	0.0570
15-25	20.1	0.05	3.216	0.0200	0.0643
25-35	31.7	0.10	3.627	0.0400	0.1451
35-45	40.0	0.15	3.922	0.0600	0.2353
45-55	49.7	0.15	4.266	0.0600	0.2560
55-65	58.9	0.10	4.593	0.0400	0.1837
65-75	68.3	0.05	4.927	0.0200	0.0985
75-85	78.0	0.05	5.271	0.0200	0.1054
85-95	87.9	0.05	5.622	0.0200	0.1124
+95	-	0.05	6.265	0.0200	0.1253
100	100.0	0.15	6.052	0.0600	0.3631
		1.00		0.4000	1.7966

Table A8.1(g): Case 7: very irregular distribution.

sample volume = 0.4000 ml					
Compos i-tion fraction (vol.% borate)	IA grade (vol.% borate)	Volume Fraction	Density (g/ml)	Volume (ml)	Mass (g)
0	0.0	0.00	2.502	0.0000	0.0000
-5	0.4	0.00	2.516	0.0000	0.0000
5-15	9.8	0.50	2.850	0.2000	0.5700
15-25	20.1	0.00	3.216	0.0000	0.0000
25-35	31.7	0.00	3.627	0.0000	0.0000
35-45	40.0	0.00	3.922	0.0000	0.0000
45-55	49.7	0.40	4.266	0.1600	0.6826
55-65	58.9	0.00	4.593	0.0000	0.0000
65-75	68.3	0.00	4.927	0.0000	0.0000
75-85	78.0	0.00	5.271	0.0000	0.0000
85-95	87.9	0.00	5.622	0.0000	0.0000
+95	-	0.10	6.265	0.0400	0.2506
100	100.0	0.00	6.052	0.0000	0.0000
		1.00		0.4000	1.5032

APPENDIX 9: ESTIMATION OF THE STATISTICAL ERROR IN THE SECTIONING DATA OF THE STANDARD MATERIAL PARTICLES AND THE LARGE-SECTIONS CORRECTION

The statistical error in the sectioning data and in the large-sections correction for each of the seven standard material cases was estimated using the binomial distribution. The absolute error (95% confidence interval) in the cumulative yield of each composition fraction, e, was estimated thus:

$$e = \pm 2\sigma = \pm 2\sqrt{\frac{pq}{n}} \qquad \text{(A8.1)}$$

where p = probability of an occurrence, $q = 1 - p$ and n = total number of particles examined in the given case. All the data are tabulated in Table A9.1.

Table A9.1: Statistical error in the sectioning data of the standard material particles and the large-sections correction in the seven cases.

composition fraction (vol. % borate)	Case 1: single composition									
	sectioning data					large-sections correction				
	no. of obs.	cum. no. of obs.	cum. freq., p (fract.)	abs. error (fract.)	abs. error, e (%)	no. of obs.	cum. no. of obs.	cum. freq., p (fract.)	abs. error (fract.)	abs. error, e (%)
0	74	74	0.07	0.016	1.6	0	0	0.00	0.000	0.0
0-10	27	101	0.10	0.019	1.9	1	1	0.00	0.007	0.7
10-20	32	133	0.13	0.021	2.1	4	5	0.02	0.015	1.5
20-30	36	169	0.16	0.023	2.3	6	11	0.04	0.022	2.2
30-40	91	260	0.25	0.027	2.7	22	33	0.11	0.036	3.6
40-50	208	468	0.46	0.031	3.1	96	129	0.43	0.057	5.7
50-60	219	687	0.67	0.029	2.9	100	229	0.76	0.049	4.9
60-70	121	808	0.79	0.026	2.6	48	277	0.92	0.031	3.1
70-80	64	872	0.85	0.022	2.2	14	291	0.97	0.020	2.0
80-90	35	907	0.88	0.020	2.0	5	296	0.99	0.013	1.3
90-100	33	940	0.92	0.017	1.7	4	300	1.00	0.000	0.0
100	86	1026	1.00	0.000	0.0	0	300	1.00	0.000	0.0
	1026					300				

composition fraction (vol. % borate)	Case 2: narrow composition range									
	sectioning data					large-sections correction				
	no. of obs.	cum. no. of obs.	cum. freq., p (fract.)	abs. error (fract.)	abs. error, ϵ (%)	no. of obs.	cum. no. of obs.	cum. freq., p (fract.)	abs. error (fract.)	abs. error, ϵ (%)
0	117	117	0.10	0.017	1.7	0	0	0.00	0.000	0.0
0-10	47	164	0.14	0.020	2.0	4	4	0.01	0.013	1.3
10-20	43	207	0.18	0.022	2.2	3	7	0.02	0.017	1.7
20-30	82	289	0.24	0.025	2.5	21	28	0.09	0.033	3.3
30-40	131	420	0.36	0.028	2.8	42	70	0.23	0.048	4.8
40-50	176	596	0.50	0.029	2.9	75	145	0.47	0.057	5.7
50-60	169	765	0.65	0.028	2.8	77	222	0.73	0.051	5.1
60-70	139	904	0.77	0.025	2.5	48	270	0.88	0.037	3.7
70-80	86	990	0.84	0.021	2.1	24	294	0.96	0.022	2.2
80-90	47	1037	0.88	0.019	1.9	9	303	0.99	0.011	1.1
90-100	35	1072	0.91	0.017	1.7	3	306	1.00	0.000	0.0
100	109	1181	1.00	0.000	0.0	0	306	1.00	0.000	0.0
	1181					306				

composition fraction (vol. % borate)	Case 3: simulated primary grinding product									
	sectioning data					large-sections correction				
	no. of obs.	cum. no. of obs.	cum. freq., p (fract.)	abs. error (fract.)	abs. error, ϵ (%)	no. of obs.	cum. no. of obs.	cum. freq., p (fract.)	abs. error (fract.)	abs. error, ϵ (%)
0	443	443	0.35	0.027	2.7	27	27	0.19	0.067	6.7
0-10	49	492	0.38	0.027	2.7	9	36	0.26	0.074	7.4
10-20	37	529	0.41	0.028	2.8	5	41	0.29	0.077	7.7
20-30	37	566	0.44	0.028	2.8	6	47	0.34	0.080	8.0
30-40	27	593	0.46	0.028	2.8	3	50	0.36	0.081	8.1
40-50	27	620	0.48	0.028	2.8	5	55	0.40	0.083	8.3
50-60	25	645	0.50	0.028	2.8	4	59	0.42	0.084	8.4
60-70	32	677	0.53	0.028	2.8	5	64	0.46	0.085	8.5
70-80	29	706	0.55	0.028	2.8	7	71	0.51	0.085	8.5
80-90	33	739	0.58	0.028	2.8	12	83	0.60	0.083	8.3
90-100	62	801	0.63	0.027	2.7	22	105	0.76	0.073	7.3
100	480	1281	1.00	0.000	0.0	34	139	1.00	0.000	0.0
	1281					139				

composition fraction (vol. % borate)	Case 4: simulated concentrate or tailings									
	sectioning data					large-sections correction				
	no. of obs.	cum. no. of obs.	cum. freq., p (fract.)	abs. error (fract.)	abs. error, e (%)	no. of obs.	cum. no. of obs.	cum. freq., p (fract.)	abs. error (fract.)	abs. error, e (%)
0	979	979	0.78	0.023	2.3	78	78	0.62	0.087	8.7
0-10	72	1051	0.84	0.021	2.1	22	100	0.79	0.072	7.2
10-20	26	1077	0.86	0.020	2.0	6	106	0.84	0.065	6.5
20-30	19	1096	0.88	0.019	1.9	2	108	0.86	0.062	6.2
30-40	17	1113	0.89	0.018	1.8	1	109	0.87	0.061	6.1
40-50	10	1123	0.90	0.017	1.7	1	110	0.87	0.059	5.9
50-60	15	1138	0.91	0.016	1.6	3	113	0.90	0.054	5.4
60-70	7	1145	0.92	0.016	1.6	2	115	0.91	0.050	5.0
70-80	11	1156	0.92	0.015	1.5	3	118	0.94	0.043	4.3
80-90	7	1163	0.93	0.014	1.4	2	120	0.95	0.038	3.8
90-100	8	1171	0.94	0.014	1.4	2	122	0.97	0.031	3.1
100	79	1250	1.00	0.000	0.0	4	126	1.00	0.000	0.0
	1250					126				

composition fraction (vol. % borate)	Case 5: high or low grade middlings									
	sectioning data					large-sections correction				
	no. of obs.	cum. no. of obs.	cum. freq., p (fract.)	abs. error (fract.)	abs. error, e (%)	no. of obs.	cum. no. of obs.	cum. freq., p (fract.)	abs. error (fract.)	abs. error, e (%)
0	361	361	0.29	0.026	2.6	62	62	0.16	0.037	3.7
0-10	271	632	0.52	0.029	2.9	112	174	0.45	0.050	5.0
10-20	196	828	0.68	0.027	2.7	88	262	0.67	0.048	4.8
20-30	119	947	0.77	0.024	2.4	42	304	0.78	0.042	4.2
30-40	103	1050	0.86	0.020	2.0	52	356	0.91	0.029	2.9
40-50	63	1113	0.91	0.016	1.6	27	383	0.98	0.014	1.4
50-60	16	1129	0.92	0.015	1.5	4	387	0.99	0.010	1.0
60-70	17	1146	0.94	0.014	1.4	2	389	0.99	0.007	0.7
70-80	11	1157	0.94	0.013	1.3	2	391	1.00	0.000	0.0
80-90	6	1163	0.95	0.013	1.3	0	391	1.00	0.000	0.0
90-100	8	1171	0.96	0.012	1.2	0	391	1.00	0.000	0.0
100	54	1225	1.00	0.000	0.0	0	391	1.00	0.000	0.0
	1225					391				

composition fraction (vol. % borate)	Case 6: stream with no free glass									
	sectioning data					large-sections correction				
	no. of obs.	cum. no. of obs.	cum. freq., p (fract.)	abs. error (fract.)	abs. error, e (%)	no. of obs.	cum. no. of obs.	cum. freq., p (fract.)	abs. error (fract.)	abs. error, e (%)
0	293	293	0.22	0.023	2.3	7	7	0.05	0.036	3.6
0-10	75	368	0.28	0.025	2.5	9	16	0.11	0.053	5.3
10-20	46	414	0.32	0.026	2.6	4	20	0.14	0.058	5.8
20-30	66	480	0.37	0.027	2.7	12	32	0.22	0.070	7.0
30-40	83	563	0.43	0.027	2.7	16	48	0.34	0.079	7.9
40-50	59	622	0.47	0.028	2.8	12	60	0.42	0.083	8.3
50-60	66	688	0.52	0.028	2.8	13	73	0.51	0.084	8.4
60-70	63	751	0.57	0.027	2.7	14	87	0.61	0.082	8.2
70-80	60	811	0.62	0.027	2.7	9	96	0.67	0.079	7.9
80-90	46	857	0.65	0.026	2.6	13	109	0.76	0.071	7.1
90-100	70	927	0.71	0.025	2.5	10	119	0.83	0.063	6.3
100	384	1311	1.00	0.000	0.0	24	143	1.00	0.000	0.0
	1311					143				

composition fraction (vol. % borate)	Case 7: very irregular distribution									
	sectioning data					large-sections correction				
	no. of obs.	cum. no. of obs.	cum. freq., p (fract.)	abs. error (fract.)	abs. error, e (%)	no. of obs.	cum. no. of obs.	cum. freq., p (fract.)	abs. error (fract.)	abs. error, e (%)
0	381	381	0.29	0.025	2.5	9	9	0.06	0.040	4.0
0-10	169	550	0.43	0.028	2.8	36	45	0.31	0.077	7.7
10-20	130	680	0.53	0.028	2.8	27	72	0.50	0.083	8.3
20-30	63	743	0.58	0.028	2.8	11	83	0.58	0.082	8.2
30-40	67	810	0.63	0.027	2.7	5	88	0.61	0.081	8.1
40-50	57	867	0.67	0.026	2.6	9	97	0.67	0.078	7.8
50-60	68	935	0.72	0.025	2.5	20	117	0.81	0.065	6.5
60-70	53	988	0.76	0.024	2.4	6	123	0.85	0.059	5.9
70-80	27	1015	0.79	0.023	2.3	4	127	0.88	0.054	5.4
80-90	31	1046	0.81	0.022	2.2	3	130	0.90	0.049	4.9
90-100	25	1071	0.83	0.021	2.1	3	133	0.92	0.044	4.4
100	221	1292	1.00	0.000	0.0	11	144	1.00	0.000	0.0
	1292					144				

IMAGE EVALUATION TEST TARGET (QA-3)

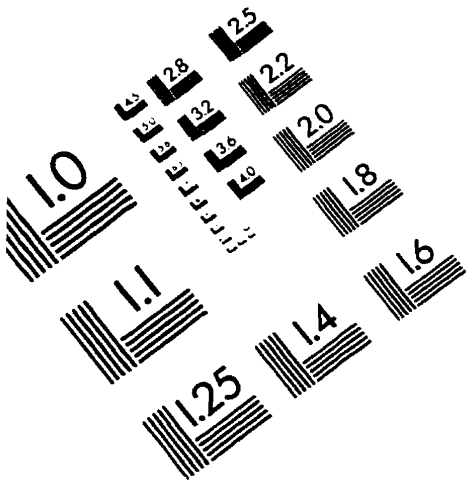

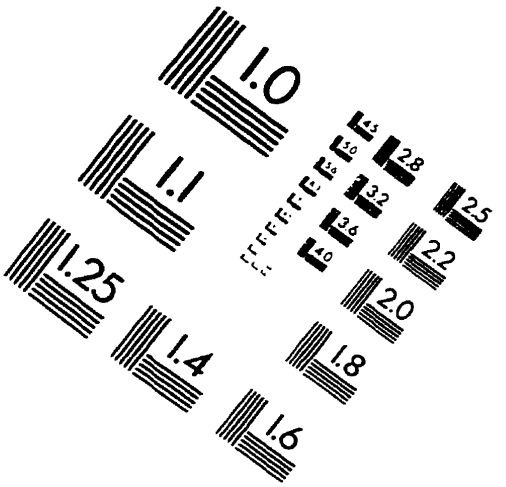

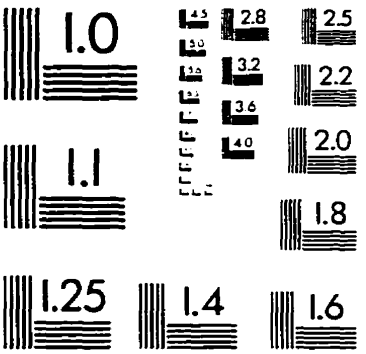

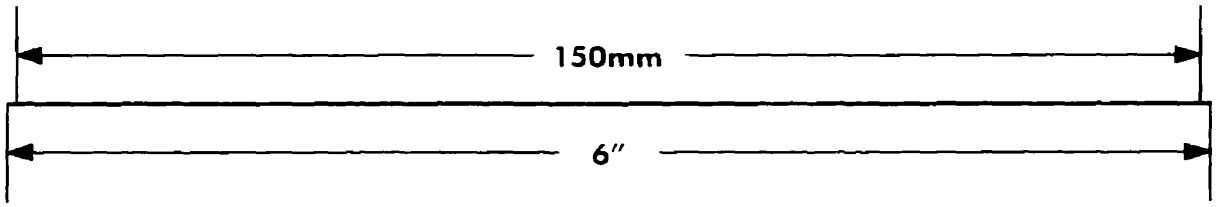

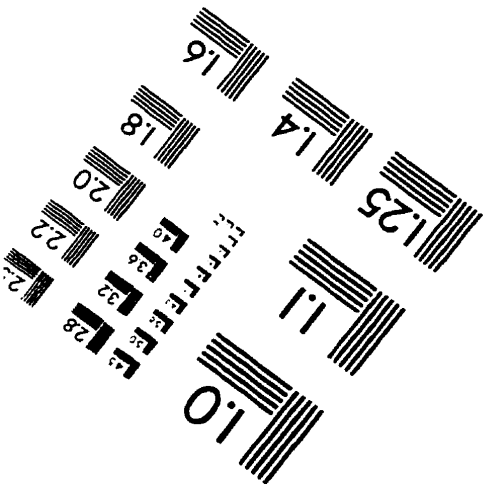

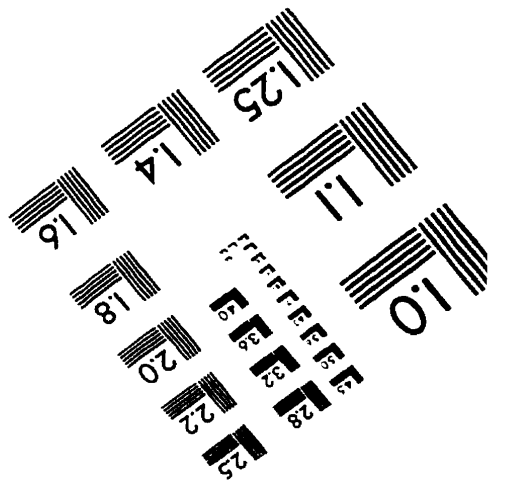

APPLIED IMAGE, Inc
1653 East Main Street
Rochester, NY 14609 USA
Phone: 716/482-0300
Fax: 716/288-5989